Proceedings of the

9th International Ship Stability Workshop

Hamburg, Germany, August 30 – 31, 2007

Germanischer Lloyd

OPERATING 24/7

Preface

On behalf of the Local Organizing Committee of the 9th International Stability Workshop, I warmly welcome all the participants of the workshop to Hamburg. The workshop is being organized by Germanischer Lloyd, the well known classification society, with the support of the International Standing Committee of the International Ship Stability Conference.

Former Stability Workshops have contributed greatly to the advancement of scientific treatment of ship safety in all its forms. The main aim of this workshop is to promote a full exchange of ideas, techniques, methodologies and best practice by providing a forum for the maritime profession to meet and discuss the stability of ships and ocean vehicles, seeking ways for improving maritime safety.

We would like to thank our sponsor BMVBS, the German Ministry of Transport for their support. Additionally we would like to thank all the presenters, authors and participants, from all continents, for their contributions to this workshop.

Hendrik Bruhns

Chairman of the Local Organizing Committee of the
9th International Ship Stability Workshop

International Standing Committee Members

Dr. Vadim Belenky
Mr. Hendrik Bruhns
Prof. Alberto Francescutto
Mr. Rob Gehling
Dr. Stefan Grochowalski
Prof. Yoshibo Ikeda
Dr. Jan-Otto de Kat (Chairman)
Prof. Marcelo A.S. Neves
Prof. Apostolos Papanikolaou
Prof. Maciej Pawlowski
Prof. Luis Perez-Rojas
Prof. Kostas J. Spyrou
Mr. Robert Tagg
Prof. Naoya Umeda
Prof. Dracos Vassalos

The International Ship Stability Workshop

This is the 9th Workshop of series after

Istanbul	(Turkey)
Shanghai	(China)
New York	(USA)
Trieste	(Italy)
St. Johns	(Canada)
Hersonissos	(Greece)
Osaka	(Japan)
Strathclyde	(UK)

Special thanks to the Session Chairman of the 9th International Workshop

R.Gehling and A. Francescutto:	*Probabilistic assessment of intact stability*
J.O.de Kat and D.Vassalos:	*Progressive flooding prediction*
A.Jost and A. Papanikolaou:	*Investigation on Severe Stability Incidents*
N.Umeda and V.Belenky:	*Simulation of Parametric Rolling*
S.Grochowalski and K.Spyrou:	*Surf-riding, broaching and capsizing in following/quartering seas*
Y.Ikeda and M. Neves:	*Numerical prediction of intact stability*
H.Bruhns and P. Sames:	*Probabilistic approach to damage stability and survivability assessment*
A.J.Peters and L. Perez-Rojas:	*Intact capsize investigations*

Local Organizing Committee

Mr. Hendrik Bruhns, Germanischer Lloyd AG, (Chairman)
Mr. Ould El Moctar, Germanischer Lloyd AG
Ms. Gundula Grzybowski, Germanischer Lloyd AG
Dr. Thomas Schellin, Germanischer Lloyd AG
Mr. Jan Schuer, Germanischer Lloyd AG
Mr. Vladimir Shigunov, Germanischer Lloyd AG
Ms. Ana Vanessa Vieira Belchior, Germanischer Lloyd AG
Ms. Simone Vogel, Germanischer Lloyd AG

Contents

Session 5: Surf-riding, broaching and capsizing in following/quartering seas

Session Chairman: Prof. St. Grochowalski Prof. K.J. Spyrou

1) N. Umeda, M. Shuto, A. Maki: "Theoretical Prediction of Broaching Probability for a Ship in Irregular Astern Seas"
2) A.Matsuda, H. Hashimoto, T. Momoki: "Non-linear Hydrodinamic Force Measurement System in Heavy Seas for Broaching Prediction"
3) F.Kluwe, St.Krüger: "Using Full-Scale Capsizing Accidents for the Validation of Numerical Seakeeping Simulations"

Session 6: Numerical prediction of intact stability

Session Chairman: Prof. Y.Ikeda Prof. M. Neves

1) O. M. El Moctar: "Prediction of Extreme Ship Responses Using Potential Flow and RANSE Codes"
2) L. Mc Cue, B.Campbell: "Approximation of ship equations of motion from time series data"
3) T. Katayama, M. Kotaki, Y. Ikeda: "A Study on the Characteristics of Roll Damping of Multi-hull Vessels"
4) Ch. Bassler, B.Campbell, W. Belknap, L. Mc Cue: "Dynamic Stability of Flared and Tumblehome Hull Forms in Waves"

Session 7: Probabilistic approach to damage stability and survivability assessmen(9)

Session Chairman: H. Bruhns Dr. P. Sames

1) M. Gerigk: "Model of identification of events and accident scenarios for a method of risk and safety assessment of ships in damaged conditions"
2) M.Schreuder "HASARD Holistic Assessment of Ships Survivability and Risk after Damage"
3) A. Jasionowski, D. Vassalos: "SOLAS 2009 – Raising the Alarm"

Session 8: Intact capsize investigations

Session Chairman: A. Peters Prof. Perez-Rojas

1) L. Perez-Rojas, C. Lopez Pavon, F. Perez Arribas, A. Martin Landaluce: "On the Experimental Investigation on the Capsizing of Small Fishing Vessels"
4) Y. I. Nechaev, O. N. Petrov: "Control of Functioning Regimes of On-Board Intelligence Systems of Safety Monitoring"
5) A. B. Degtyyarev, Y. I. Nechaev: "Virtual Testbed for Marine Objects Behaviour Investigation"

Session 1: Probabilistic assessment of intact stability

Session Chairman: R. Gehling ***Prof. A. Francescutto***

1) L. Kobylinski:

   "Goal-based stability standards"

2) N.Umeda, S.Koga, J.Ueda, E.Maeda, I. Tsukamoto, D.Paroka:

   "Methodology for Calculating Capsizing Probability for a Ship under Dead Ship Condition"

3) K.J. Spyrou, N. Themelis, S.Niotis:

   "Probabilistic Assessment of Parametric Rolling: Comparative Study of Detailed and Simplified Models"

Goal-based stability standards

Lech Kobyliński

Foundation for Safety of Navigation and Environment Protection

ABSTRACT

Goal based standards is a concept that was introduced in IMO work at 89th session of the Maritime Safety Committee. The concept of goal based standard that includes holistic approach and involving risk analysis is an alternative to prescriptive standards widely used in regulatory work.

The author briefly considers how to apply risk analysis to system of safety against capsizing with more detailed consideration of different steps of the procedure and specifically proposing identification system of hazards and methodology of risk assessment.

KEYWORDS

Stability of ships; risk analysis; ship's safety.

INTRODUCTION

At 50th session of the IMO SLF Subcommittee completed the task of revision of the Intact Stability Code. The Code was divided in two parts, the first of which will be made compulsory by the reference in the 1974 SOLAS Convention and 1988 LL Protocol, the other will remain as recommendation (IMO 2006). With this decision the first stage of work towards improved stability criteria was completed (IMO 2007). But this is not the final solution. From time to time stability casualties happen in spite of the fact that ships meet all IMO criteria. The existing criteria may be also not applicable to some types of modern ships incorporating novel design features. There is no previous experience in relation to safety and stability of those ships and to satisfy existing criteria may not assure required level of safety. Due to this, the IMO Maritime Safety Committee has recently included in its work programme the development of performance-oriented criteria for ships of novel ship type.

The author is of the opinion, that with the completion of the work on revision of the basic stability requirements included in the IS Code, it is now time to consider a holistic and risk based approach to stability standards as an alternative to the existing prescriptive criteria. This has to be done in order to enhance safety and not to hinder the development of novel ships types.

CURRENT SITUATION REGARDING STABILITY CRITERIA

The compulsory part of the revised IS Code contains basic stability criteria, virtually unchanged from those in resolution A.167(ES.IV) adopted by the IMO assembly in 1968 and weather criterion adopted by resolution A.562(14) adopted in 1987. In spite of the fact, that some ships satisfying those criteria capsized, the wide experience with application of those criteria, including weather criterion, justifies the general opinion that the great majority of conventional ships that meet the criteria are reasonably safe.

Advent of very large and sophisticated ships some of them revealing novel design features causes, however, that those criteria may be inadequate. Therefore IMO meetings consider possible ways of development of improved

criteria. It seems that the opinion of the majority of participants is that the future "improved" stability criteria should be performance-oriented. The understanding of the idea behind the performance-oriented criteria is not, however, clear and the way that such criteria might be developed is now under discussion.

It seems that the merit of the majority of proposals related to the possible methods of developing performance oriented criteria consist of consideration of some phenomena occurring when the ship is sailing amongst the waves, namely parametric resonance in following and head seas, loss of stability in wave crest and broaching to. In fact those are dangerous situations well recognized 25 years ago, when the SLF Subcommittee at its 29th and following sessions recognized those situations as those that need further consideration leading possibly to development of some safety criteria (IMO 1984). The problem was at that time apparently too difficult to solve and the idea was ultimately abandoned. With much better tools (computer codes) available now, the idea of developing criteria taking into consideration those situations came back to life again and the possibility of developing non-structural formulae as a basis for the new criteria was advanced. In the opinion of the author there is a merit in consideration of the dangerous situations mentioned above, but the possibility to develop comparatively simple non-structural formulae that could be used as criteria is doubtful.

PRESCIPTIVE CRITERIA, SYSTEM APPROACH AND RISK ANALYSIS

The existing criteria are design oriented and their essence consists of specification of critical values of some stability parameters, therefore they could be classified as prescriptive criteria. Prescriptive regulations have many advantages. They are formulated in a simple language, which is easily understood by everybody, they are easy in application, they also make checking adherence to the requirements easy. The main shortcoming of prescriptive regulations is that they are bounding designers and they do not allow introduction of novel design solutions. They are based on experience gained with existing objects and they are not suitable for novel types. Mostly, they were amended after serious casualties happened. The risk involved with the application of prescriptive regulations is not known.

At the opposite side of the prescriptive regulations, there is risk-based approach. In the risk-based approach the regulations do not require meeting certain specific measures, they are based on assessment of risk involved that may or may not be accepted. The advantages of risk-based approach are obvious. They give free hand for the designer to develop new solutions, they actually allow taking optimal decisions from the point of view of economy and safety and the risk to the public and to the environment is assessed and accepted.

As mentioned above, existing criteria are design criteria intended to be applied during the design stage of a ship. However, even the preliminary analysis of stability casualties shows, that design features of the ship are neither the most important nor most often cause of casualty. Casualty – it will be in the following called LOSA (loss of stability accident) - (Kobyliński 2006), is usually the result of a sequence of events that involve environmental conditions, ship loading condition, ship handling aspects and human factor in general. Therefore, system approach to stability safety should be adopted.

Ship stability system is rather complicated. However, in most cases it could be considered as consisting of four basic elements: ship, environment, cargo and operation (fig.1, Kastner 2003). The Venn diagram in this figure stresses strong interactions between the four elements. The author proposed the use of the system approach to stability criteria quite long time ago (Kobyliński 1984). It was also partly applied in development of the Intact Stability Code but in general until this day stability requirements remain basically design oriented.

Analysis of LOSA casualties reveals that the causes of casualty may be attributed to:

- functional aspects resulting from reliability characteristics of the technical system, therefore stability characteristics of the ship

- operational aspects resulting from action of the personnel handling the system, therefore crew members but also ship management, cargo handling, marine administration and owners company organisation

- external causes resulting from factors independent from designers builders and operators of the technical system therefore ship environment and climatology (Cleary 1975, Erickson et al 1997)

- cargo related aspect resulting from characteristics of cargo and its way of transporting

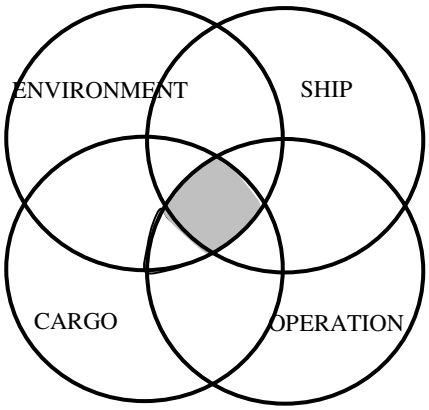

Fig.1. Four-fold Venn diagram for ship stability system

Human factor plays an important part in all four elements of the system. Human and organisational errors, HOE, according to some authors, are responsible for approximately 80% of all marine casualties (Manum 1990), other sources definitely stated that this percentage is 80% (US Coast Guard 1995). In order to achieve sufficient level of safety with respect of stability, all elements creating stability system have to be taken into account. Taking into account the fact, that less than 20% of all casualties are caused by faulty or bad design of the ship, the existing safety requirements that refer mainly to design features of the ship can not insure sufficient level of safety, in particular with regard to ships having novel design features.

CONCEPT AF SAFETY

The oldest concept of safety regulations consists of specifying hull scantlings considered as assuring safety. Krappinger (1967) defined this concept of safety as the assignment of hardware and this concept is often used as a basis of simple safety requirements up to this day.

A more advanced concept of safety does not include assignment of dimensions or proportions of an object, but assignment of its physical properties or performance characteristics. In respect to stability, in a simple case this means, for example, assignment of critical values of metacentric height or of the righting arms at various angles of heel. In a more advanced case, it may mean the assignment of a probability of capsizing in certain assumed situation. In all cases the resulting criteria are prescriptive criteria.

The most recent concept of safety regulations is goal-based standards. Goal based regulations do not specify the means of achieving compliance but set goals that allow alternative ways of achieving compliance (Hoppe 2006). Goal-based standards are being considered at IMO for some time and appraised by some authors (Vassalos 2002, Chantelauve 2005), and they were introduced in some areas, albeit not in the systematic manner. The IMO Marine Safety Committee commenced in 2004 at MSCC 78 its work on goal-based standards in relation to ship construction adopting five-tier system (Table 1).

IMO MSC committee agreed in principle on the following tier I goals to be met in order to build and operate safe and environmentally friendly ships: “Ships are to be designed and constructed for a specific design life to be safe and environmentally friendly, when properly operated and maintained under specified

operating and environmental conditions, in intact and specified damage conditions, throughout their life".

Table 1. Five-tier system for goal-based requirements

Tier I:	Goals
Tier II:	Functional requirements
Tier III:	Verification criteria of compliance
Tier IV	Technical procedures and guidelines, classification rules and industry standards
Tier V	Codes of practice and safety and quality systems for shipbuilding, ship operation, maintenance, training etc

It seems that the future alternative criteria should be based on the above principle. With this in mind, the system of stability requirements proposed may be as shown in fig.2 and in Table 2. Left hand side of the diagram in fig.2 refers to conventional ships, whether the right hand part refers to non-conventional ships. Shaded part is actually completed and the practical problem consists of how to develop requirements for non-conventional ships. The diagram shows, that it could be done using SOLAS clause allowing using alternative means of assuring safety.

Table 2. Methods of safety assurance

Ships	Method of stability safety assessment
Conventional, not sophisticated	Prescriptive criteria as in the IS Code
Novel types, large sophisticated ships	Risk analysis under the provision allowing application of alternative means of assuring safety

Clarification is needed regarding the definition of conventional and non-conventional ships. Traditionally under the term "non-conventional ships", ships revealing novel design features are understood. However this is a very vague definition and the major difficulty is which features may be classified as "novel". It seems that the best way to classify ships as non-conventional would be to include in this category all ships to which requirements of the existing IS Code are considered non applicable in the view of designers, ship owners or administrations.

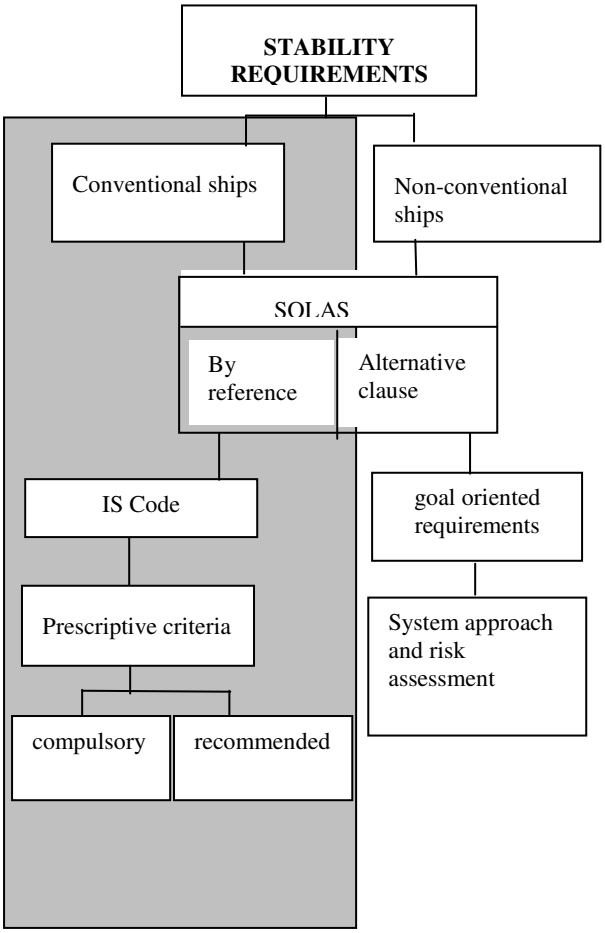

Fig.2. System of stability requirements as proposed

GOAL ORIENTED REQUIREMENTS

With relation to stability goal oriented requirements should be based on risk analysis, because the final stage of risk analysis is assessment of safety measured by risk involved. Risk is a measure of safety and risk estimated has to be accepted; if not accepted risk control measures must be applied including putting some barriers with the result to reduce risk to such level that can be accepted.

Risk-based approach according to IMO recommendation is formalized and includes the following steps:

1. Identification of hazards

2. Risk assessment
3. Risk control options
4. Cost-benefit assessment, and
5. Recommendations for decision making

It is rather obvious that application of risk assessment methodology is a tedious and time-consuming task, but in principle it is feasible. It would be not practical to apply this method to conventional ships that are reasonably safe, but it could be effectively applied to important and large ships of non-conventional design. Risk analysis may, therefore, be recommended as an alternative to existing prescriptive criteria subject to the discretion of the Maritime Administrations involved. The general procedure for application of system and risk approach is shown in fig.3.

HAZARD IDENTIFICATION

The crucial problem in safety assessment analysis is proper identification of various hazards to which a ship may be subjected. According to the definition, hazard is *"a potential to threaten human life, health, property or the environment*" (IMO 2002). In the goal oriented approach and when performing risk analysis all relevant types of hazards must be taken into consideration – environmental, technical, operational and managerial. And the frequency (probability) of occurrence of those hazards should be assessed. Human factor must be taken also into consideration. Belenky et al (2007) proposed to apply "vulnerability criteria" within the system of future criteria. Those criteria are, in fact, hazards. However, the vulnerability criteria are meant as considered in a binary mode, whether hazards are inherently connected with probability.

Hazard identification is carried-out using hazard identification and ranking procedure (HAZID). Hazards could be identified using several different methods.

IMO resolution included general guidance on the methodology of hazard identification. With respect to stability, hazard identification could be achieved using standard methods involving evaluation of available data in the context of functions and systems relevant to the type of ship and mode of its operation. Stability

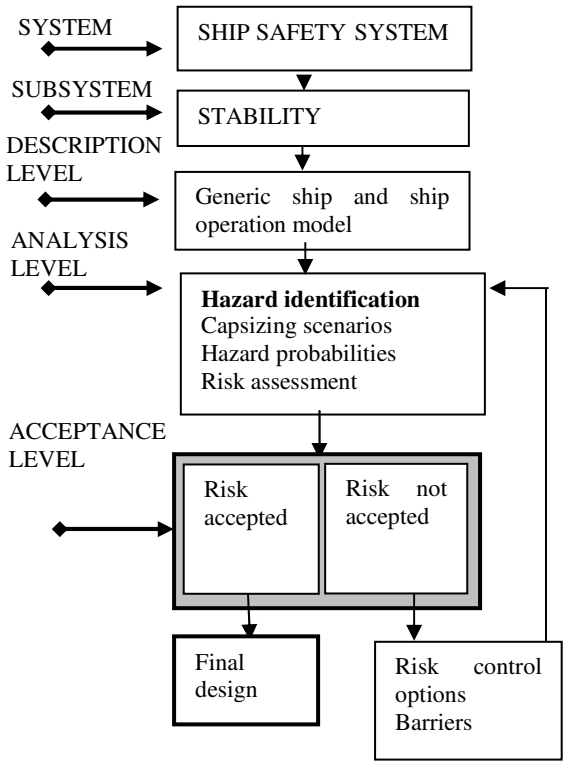

Fig.3. Block diagram of risk analysis

is considered assuming that the ship is intact and accident evaluated is called LOSA (loss of stability accident). LOSA is a new definition covering capsizing, that means taking by the ship position upside down, but also covering a situation where amplitudes of rolling motion or heel exceed a limit that makes operation or handling the ship impossible for various reasons –e.g. loss of power, loss of manoeuvrability, necessity to abandon the ship etc. It does not necessary mean the total loss of the ship. (Kobyliński 2006).

According to general recommendation, the method of hazard identification comprised mixture of creative and analytical techniques. Creative element was necessary in order to ascertain that the process is proactive and is not limited to hazards that happened in the past.

In general HAZID involves several possibilities used separately or in combination:

- statistical data concerning causes of accidents
- historical data including detailed description of accidents
- conclusions resulting from model tests of ships in waves
- conclusions resulting from computer simulation of capsizing
- event and fault trees method
- analysis of accidents scenarios using (e.g. TRIPOD method (ter Bekke et al 2006))
- organized opinions of experts (e.g. according to DELPHI method)

As an example of application of this methodology, the list of hazards in respect of stability is shown in fig. 4. The list was prepared on the basis of evaluation of data for approximately 350 stability casualties, of detailed analysis of several LOSA accidents and of evaluation of results of opinion of experts organized by DELPFI method.

In this example, ranking of hazards is not shown. Furthermore, the sketch could be considered as the first level of the fault tree leading to LOSA. Hazards identified as relevant to safety against LOSA are all strongly interconnected, moreover, human factor understood as performance of an individual (in most cases the master), plays an important part in each case. Hazards identified should be further decomposed preferably using fault trees and/or events trees reproducing various scenarios of LOSA casualty. The set and combination of fault trees and event trees as developed for all hazards identified and all scenarios (defined as risk contribution trees – RCT) is a basis for HAZOP (hazard and operability study) procedure that allows also assessment of frequencies (probabilities) of hazards required for risk assessment. This is rather tedious task bearing in mind the multitude of possible scenarios. This problem, however, is not discussed here.

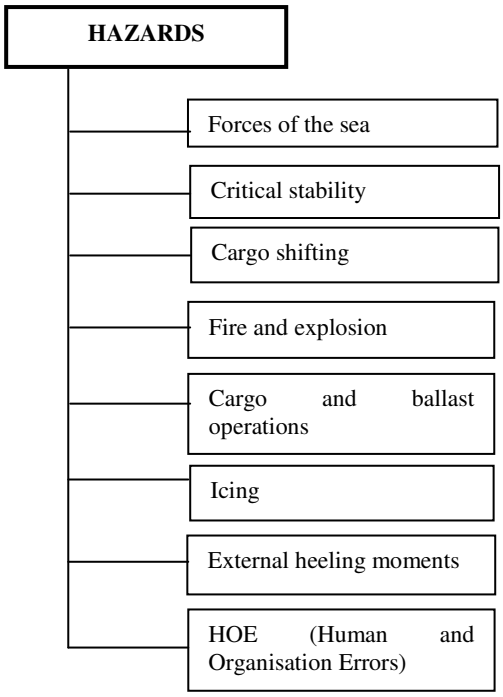

Fig. 4: Basic hazards to stability

Further decomposition of the basic hazards listed in fig.4 leads to hazardous situations and finally, to possible capsizing scenarios. This provides quite a large number of different scenarios for consideration. However, in reality the number of scenarios that need to be considered in a particular case could be substantially reduced, due to their very low probability.

CONCLUSION

In order to proceed with the development of performance based criteria provision allowing for alternative design and arrangements included in the SOLAS convention could be used. Within this provision goal oriented approach may be recommended as an alternative to prescriptive standards. Risk assessment and analysis may be the proper method to achieve the goal, which is the safety of the ship.

List of References

Belenky V., de Kat J.O., Umeda N. (2007): Towartds performance-based criteria for intact stability. To be published in Marine Technology.

Cleary W.A.(1975): Marine stability criteria. Proceedings of the 1st International Conference on Stability of Ships and Ocean Vehicles**,** Glasgow.

Chantelauve, G. (2005): *On the use of risk analysis in maritime certification and classification.* Advances in Safety and Reliability ESREL 2005, Vol. I p.329.

Erickson, A., Person, J., Rutgerson, O., (1997): On the use of formal safety assessment when analysing the risk for cargo shift in rough seas**.** International Conference on Design and Operation in Abnormal Conditions, Proceedings, Glasgow.

Hoppe H. (2006) Goal based standards – a new approach to the international regulation of ship construction. IMO News, Issue 1.

IMO (1984): Intact Stability. Report of the ad hoc working group. Doc. SLF29/WP.7.

IMO (2002): Guidelines for Formal Safety Assessment (FSA) for use in the IMO rule-making process. Doc. MSC/Circ.1023; MEPC/Circ.392.

IMO (2006): Revised Intact Stability Code Prepared by the Intersessional Correspondence Group. Submitted by Germany. Doc. SLF 49/5.

IMO (2007): Subcommittee on Stability, subdivision and Safety of Fishing Vessels, Report of the 50th session. Doc.SLF 50/WP.6.

Kastner S. (2003): Safety and Stability of Ships, Vol.1, Elsevier

Kobyliński L. (1984): Philosophishe und Hydrodynamische Probleme der Internationalen Kenterkriterien von Schiffen. Intern. Schiffstechnische Symposium, Rostock.

Manum I.A. (1990): What have guided international activities on intact stability so far? 4th STAB Conference, Naples.

ter Bekke E.C.A., van Daalen E.F.G., Willeboordse E.J., Boonstra H., Keizer E.W.H., Ale, B. (2006): Integrated safety assessment of small container ships. 8th Intern. Conference on Probabilistic Safety Assessment and Management, New Orleans.

U.S.Coast Guard (1995): Prevention through people. Quality Action Team Report.

Vassalos D. (2002): Total ship safety – a life-cycle risk-based DOR for safety. The Stability Research Centre, NAME, Universities of Glasgow and Strathclyde, May 2002.

Methodology for Calculating Capsizing Probability for a Ship under Dead Ship Condition

Naoya Umeda, Sadaharu Koga, Junpei Ueda, Eri Maeda, Izumi Tsukamoto and Daeng Paroka

Osaka University, JAPAN

ABSTRACT

Stability under dead ship condition is one of the major scenarios to be dealt with for performance-based intact stability criteria at the IMO. Since the criteria are to be based on a risk analysis, capsizing probability should be calculated. For this purpose, we propose a methodology for calculating capsizing probability under dead ship condition. Firstly, the drifting attitude and velocity is determined by solving an equilibrium equation. Secondly, effective wave slope coefficient is estimated experimentally and theoretically. Thirdly, the capsizing probability is calculated with a piece-wise linear restoring arm. Finally, annual capsizing probability is estimated with wave statistics and operational practice.

KEYWORDS

Dead ship condition; the effective wave slope coefficient; capsizing probability; risk analysis

INTRODUCTION

At the International Maritime Organization (IMO) revision of the Intact Stability Code (IS Code) started in 2002 and, other than that of its prescriptive criteria, performance-based criteria are requested to be developed by 2010. (IMO, 2007) This new criteria should cover three major capsizing scenarios: restoring variation problems such as parametric rolling, stability under dead ship condition and manoeuvring-related problems such as broaching. It was expected to be a probabilistic stability assessment based on physics by utilising first principle tools. This is due to the fact that probabilistic approach can be linked with a risk analysis and dynamic-based approach enables us to deal with new ship-types without experience. Here it is important to establish a method for evaluating capsizing probability under dead ship condition because its safety level could be a base for other capsizing scenarios. In case of the dead ship condition, under which the main propulsion plant, boilers and auxiliaries are not in operation due to absence of power, a shipmaster cannot do any operational actions. This means that operational factors are not relevant to safety level evaluation. Since some operational actions such as high-speed running in following waves can decrease safety level against capsizing (Umeda and Yamakoshi, 1994), the safety level under dead ship condition can be regarded as that with ideal operational practice.

For this dead ship condition, the weather criterion is currently implemented in the IS Code and provides a semi-empirical criterion for preventing capsizing in beam wind and waves. The dead ship condition, however, does not always mean beam wind and waves. If a ship has a longitudinally asymmetric hull form, ship may drift to leeward with a certain heading angle. Thus, it is important to estimate the drifting attitude of a ship and to evaluate its effect on capsizing probability. It is also widely known that empirical estimation of effective

wave slope coefficient in the weather criterion is often difficult to be applied to modern ship-types such as a RoPax ferry. Thus, the IMO (2006) recently allows us to use model experiments for this purpose although it is not always feasible. A simplified prediction method is still desirable if accurate enough.

Based on the above situation, the authors propose a methodology for calculating capsizing probability of a ship under dead ship condition. First, we estimate drifting velocity and attitude by a local stability analysis. Second, we estimate the effective wave slope and roll damping coefficients with or without model experiment. Third, capsizing probability is calculated with a piece-wise linear approach under the estimated drifting attitude and then risk is also examined. In this paper, we summarise this methodology and present an example of the application of this methodology to a RoPax ferry.

SUBJECT SHIP

For ships having large windage area, the weather criterion or its alternative could be dominant. Among them, a RoPax ferry is selected here as a subject ship. Her principal dimensions, body plan are shown in Table 1 and Fig. 1, respectively, the restoring arm curve is given in Fig. 2.

Table 1: Principal dimension of the car carrier

Length between perpendiculars	170 (m)
Breadth	25.0 (m)
Depth	14.8 (m)
Draught	6.06 (m)
Block coefficient	0.521
Area of bilge keels	61.38 (m^2)
Vertical position of centre of gravity above keel line	10.63 (m)
Metacentric height	1.41 (m)
Down flooding angle	39.5 (degrees)
Natural roll period	17.90 (s)
Lateral projected area	3433.0 (m^2)
Height centre of lateral windage area above water line	9.71 (m)

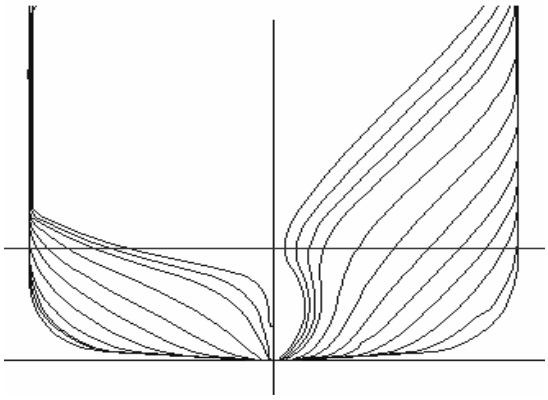

Fig 1: Body plan of the car carrier

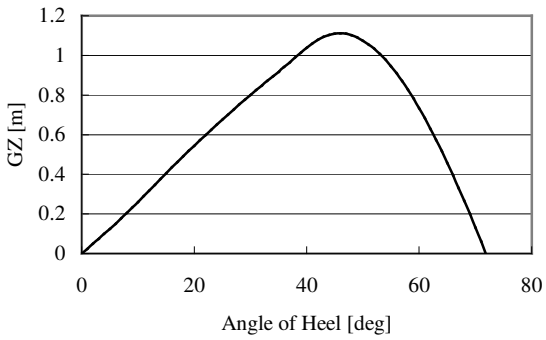

Fig 2: Curve of righting arm of the car carrier

ESTIMATION OF DRIFTING ATTITUDE UNDER DEAD SHIP CONDITION

For estimating drifting velocity and attitude of a ship in regular waves and steady wind, we propose a method for identifying fixed points of a surge-sway-yaw-roll model and for examining its local stability. (Umeda, Koga et al., 2005)

Fixed points can be estimated by solving 4-DOF non-linear equations as shown in the following co-ordinate systems. (Fig 3);

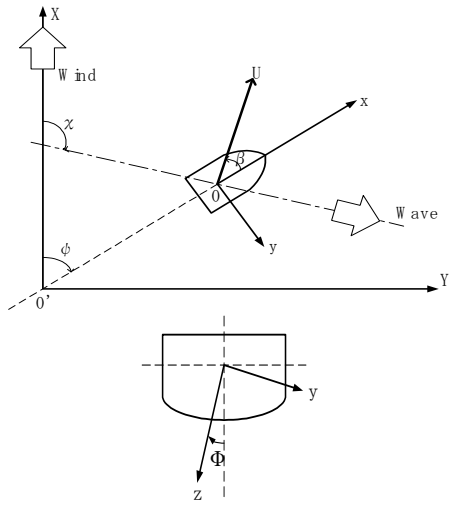

Fig 3: Co-ordinate systems

$$\left(m+m_x\right)\dot{u}-\left(m+m_y\right)vr=X_H+X_A+X_W \tag{1}$$

$$\left(m+m_y\right)\dot{v}+\left(m+m_x\right)ur-m_y l_y\ddot{\phi}=Y_H+Y_A+Y_W \tag{2}$$

$$\left(I_z+J_z\right)\ddot{\psi}=N_H+N_A+N_W \tag{3}$$

$$\left(I_x+J_x\right)\ddot{\phi}-m_y l_y\dot{v}-m_x l_x ur+2\mu\dot{\phi}+W\overline{GM}\phi=K_H+K_A \tag{4}$$

where,

u, v ; ship speed in x,y-axis

ψ, ϕ ; yaw,roll angle

m ; ship mass

W ; displacement

GM ; metacentric height

m_x, m_y ; added mass in x,y-axis

I_x, I_z ; morment of inertia around x,z-axis

J_x, J_z ; added morment of inertia around x,z-axis

l_x, l_y ; z-direction of centre of m_x, m_y

X, Y ; force in x,y-axis

N, K ; yaw,roll morment

Here the subscript H, A and W means hydrodynamic force/moment, wind force/moment and wave-induced drifting force/moment.

In this model, a mathematical model for hydrodynamic forces under low speed manoeuvring motion (Yoshimura, 1988), an empirical method for wind forces (Fujiwara, 2001), and a potential theory for wave-induced drifting forces (Kashiwagi, 2003) are used.

The stability of equilibrium is evaluated by calculating the eigenvalues of the Jacobean matrix in the locally linearised system around equilibrium. The Newton method was used to solve the equations and we assume that wind speed is 26 m/s, wave amplitude is 2.85m and wave length to ship length ratio is 2.94. As an initial input, the equilibria in the beam wind and waves from starboard and those from port side are calculated. And then, equilibria for different angle between the wind and waves, χ, are calculated. The calculation are done in two ways: the first one is that χ changes from 0 degrees to 180 degrees (forward) with the wind direction fixed, and the second is that χ changes from 180 degrees to 0 degrees (backward). The results are shown in Fig 4-7.

These figures indicate that when the relative angle between wind and waves is 0 degrees, ship is drifting leeward in beam wind and wave. Having the relative angle between wind and waves larger from 0 degrees, the heading angle gradually increases from the beam wind

condition. And the relative angle is close to 90 deg, the equilibrium becomes unstable in almost head wind and becomes stable in almost following wind.

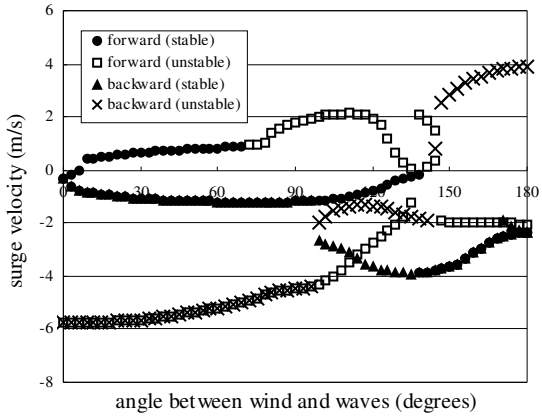

Fig 4: Surge velocity of fixed points as a function of relative angle between wind and waves

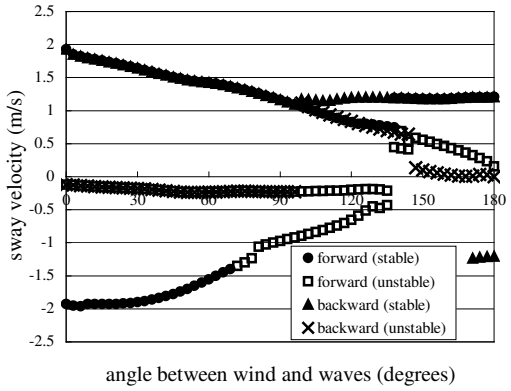

Fig 5: Sway velocity of fixed points as a function of relative angle between wind and waves

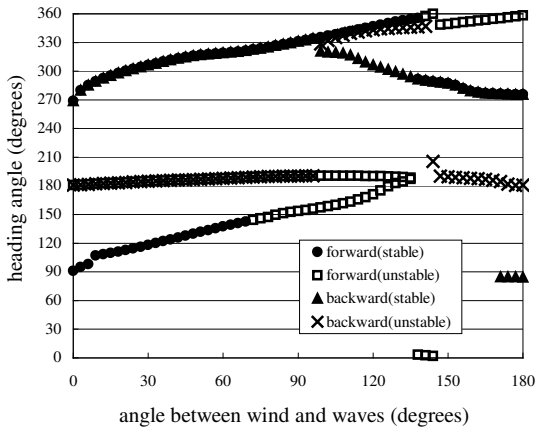

Fig 6: Heading angle of fixed points as a function of relative angle between wind and waves

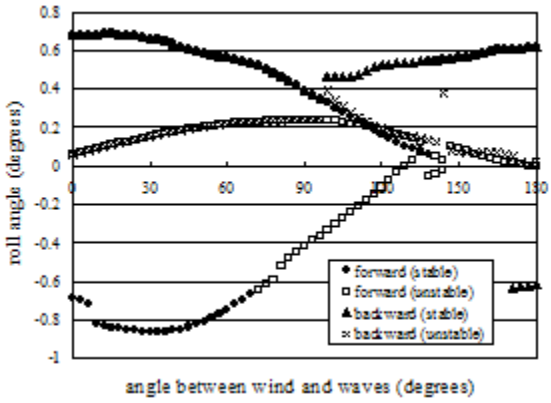

Fig 7: Roll angle of fixed points as a function of relative angle between wind and waves

It is noteworthy here that all fixed points have complex eigenvalues. This suggests that limit cycle around the fixed point may exist when the fixed point is unstable. In addition, an unstable solution with about 0 degrees of yaw angle at 0 degrees of the relative angle between wind and waves may exist but the Newton method here fails to detect it. Further researches for these points are now under way.

ESTIMATION OF EFFECTIVE WAVE SLOPE COEFFICIENT

Since recently, the IMO allows us to estimate the effective wave slope and damping coefficients as well as heeling lever due to beam wind by model experiments with the interim guidelines. The authors applied this model test approach to the RoPax ferry for investigating its feasibility. (Umeda, Ueda et al., 2005) Based on the interim guidelines, the model experiments were executed with three different constraints: a guide rope method, a looped wire system and a mechanical guide method. The guide rope method means that the model was controlled by guide ropes. The looped wire system means that, by utilizing a looped wire attached to a towing carriage, the yaw motion of the model is fixed but the sway, heave and roll motions are allowed. The mechanical guide is the combination of a sub-carriage, a heaving rod and gimbals. Among them, as shown in Fig.8, the looped wire system is less accurate because natural roll period and damping was slightly changed owing to a looped wire. In case the yaw angle increases with larger wave steepness, the guide rope method has inherent difficulty for keeping a beam wave condition. The guideline allows the three different methods for determining the roll angle from the experiment: the direct method, the three step method and the parameter identification. As shown in Fig 9, the difference between the three methods is negligibly small. In conclusion, the interim guidelines can guarantee reasonable accuracy if appropriate constraint is used.

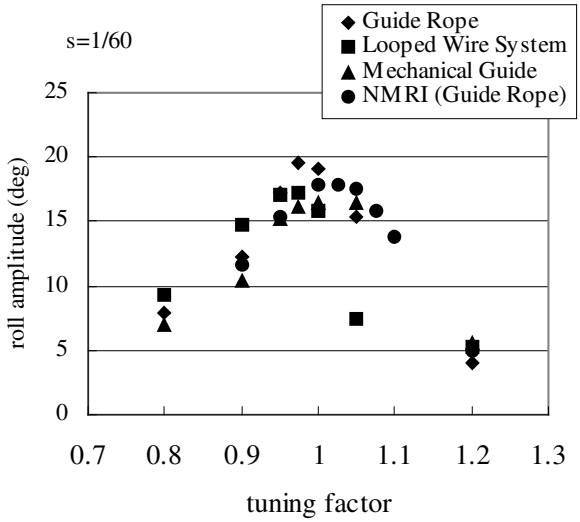

Fig 8: Roll amplitude in regular beam waves with three different constraints as well as the experiment at NMRI (Taguchi et al., 2005).

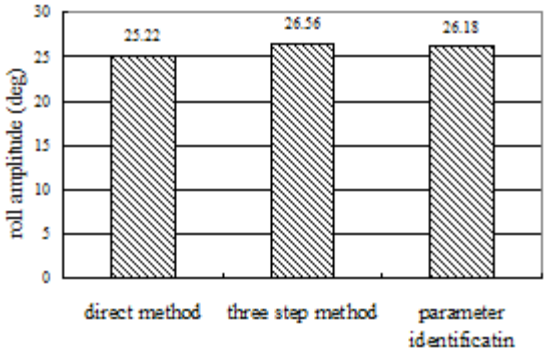

Fig 9: Comparison in estimated roll amplitude of three different estimation methods

The model tests can provide accurate estimation of the coefficients for a given ship but it could be impractical due to cost and time for model testing. Thus, it is desirable to develop an empirical or theoretical method to accurately predict obtained results from the model test. The measured roll damping coefficient from the model tests for the RoPax ferry was 0.0121, while the estimated with the Ikeda's semi-empirical method (Ikeda, 2004) was 0.0134. Thus, Ikeda's method can well predict for roll damping coefficient and it is

well known that a strip theory can explain the effective wave slope coefficient. Since a strip theory requires numerical solution of simultaneous equation for determining two dimensional coefficients, however, a further simplified theoretical method is expected to be developed.

For this purpose, the authors (Umeda, Tsukamoto, et al., 2007) investigated several possible simplified versions of theoretical methods and finally proposed to calculate the effective roll coefficient of the rectangular sections only with the Froude-Krylov component on its own. Here the local breath and area of the rectangular section should be the same as those of original transverse ship sections. As shown in Fig. 10, this simplified method agrees well with the experiment and the strip theory. This is mainly because the diffraction component can almost cancel out the radiation due to sway. It is recommended to use this simplified approach for regulatory purpose.

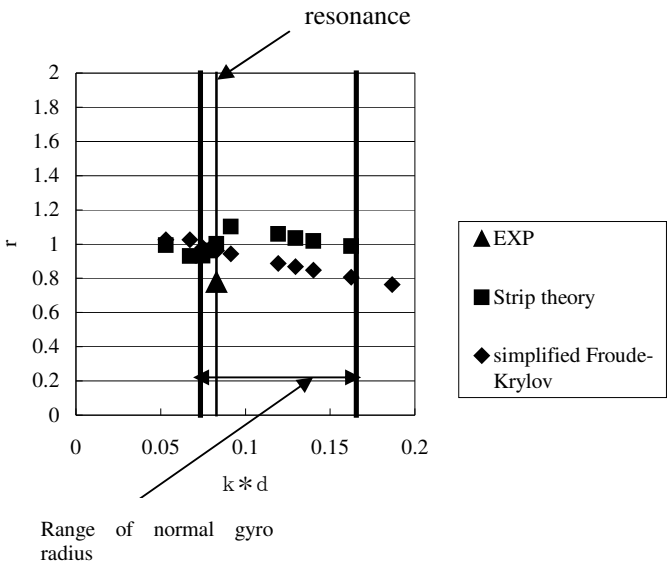

Fig 10: Effective wave slope coefficient, r, of Ro-Pax fery . Here k is the wave number and d is the ship draught.

CAPSIZING PROBABILITY

Capsizing probability in irregular beam wind and waves can be analytically calculated with piece-wise linear restoring moment. This approach was originally developed by Belenky (1993), corrected by Paroka et al. (2006) and verified by Paroka and Umeda (2006a). Here the capsizing probability in a stationary sea state is calculated as the product of the probability exceeding the threshold and the probability of diverging behaviour in the range of negative restoring slope. If necessary, the probability exceeding the down-flooding angle or cargo-shift angle can be taken into account. (Paroka and Umeda, 2006b) Then the annual capsizing probability can be calculated with wave statistics. (Paroka and Umeda, 2006c) Furthermore, the effect of water on deck can be evaluated. (Paroka and Umeda, 2006c) The details of this method is available in these literatures.

In case of dead ship condition, the drifting velocity and attitude should be taken into account. Umeda, Koga et al. (2006) evaluated the effect of drifting velocity by changing the external frequency and the effect of drifting attitude by changing both the windage area and the effective wave slope coefficient.

The results are shown in Fig 11 where the two coexisting stable steady attitudes are investigated. Here the wind velocity is 26 m/s and the duration is one hour. The fully developed wind waves under this wind velocity are assumed. In this calculation, the heeling lever due to drift are estimated with the model tests by Taniguchi et al. (2005)

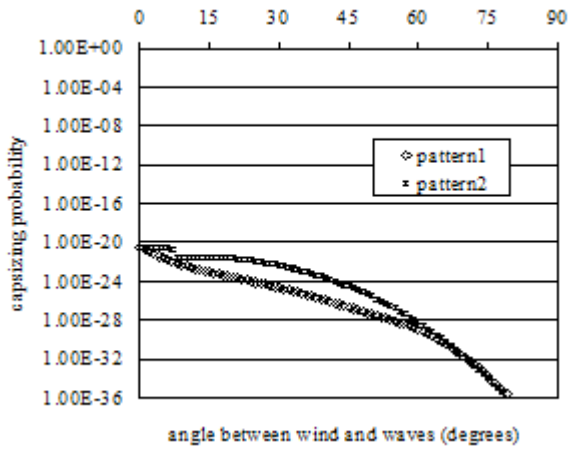

Fig 11: Capsizing probability of the RoPax ferry under the dead ship condition as a function of the relative angle between wind and waves.

From this figure, it is confirmed that the most dangerous condition for this particular ship is beam wind and waves, i.e. χ is 0 degrees. Obviously it depends on underwater and above-water ship geometry.

The authors also investigate the effect of estimation methods of the effective wave slope coefficient on capsizing probabilities for one hour of the duration. As shown in Fig. 12, the simplified estimation method of the effective wave slope coefficient can improve the result with the empirical formula in the current weather criterion and can provide good agreement with the outcomes with the measured coefficient with the interim guidelines or the calculated one with a strip theory. Here the heeling lever due to drift is calculated with the formula in the weather criterion.

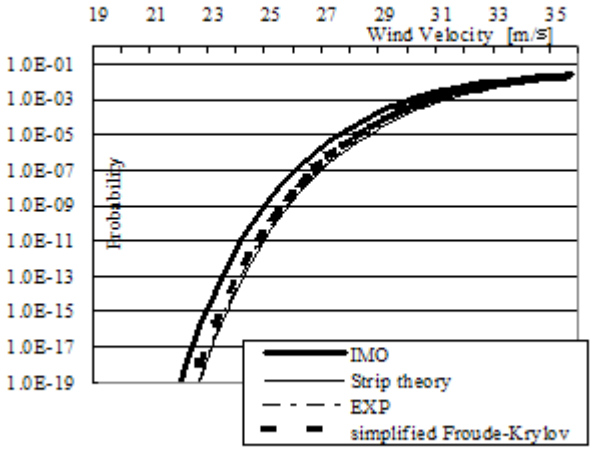

Fig 12: Capsizing probability of the RoPax ferry in stationary beam wind and waves.

RISK ANALYSIS

Finally the authors attempted to evaluate the safety levels of four merchant ships by utilising the above mentioned capsizing probability calculation. (Umeda, Maeda et al., 2007) The annual capsizing probabilities are plotted on a FN diagram as shown in Fig. 13. Here the annual capsizing probabilities, as the ordinate of the FN diagram, are calculated for a car carrier, a container ship, a cruise ship and the RoPax ferry with optimal operational practice, which means a beam wind and waves condition. The operational area for the RoPax ferry is the limited greater coastal area of Japan and those for other three ships are the North Atlantic. The metacentric height and freeboard are adjusted to be each designed condition. The number of people onboard, as the abscissa of the FN diagram, is regarded as the consequence because capsize of intact ship normally does not provide a chance for people onboard to survive. The acceptance criteria of this FN diagram are taken from the IMO document submitted by Japan (2002) in trial and are required further discussion.

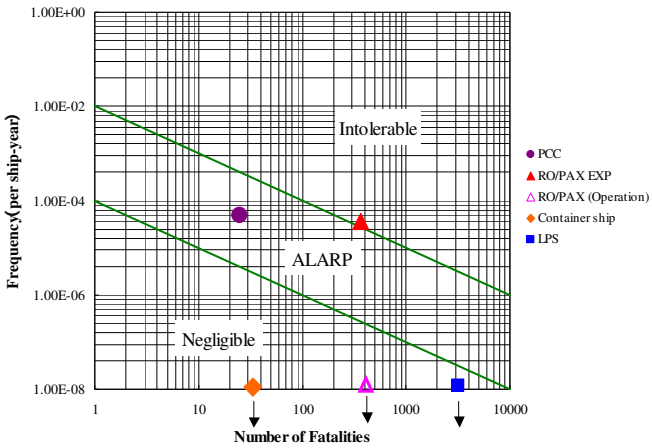

Fig 13: Risk level for ships under designed condition.

This FN diagram suggests that the risk levels against intact capsizing with good operational practice of the containership and the large cruise ship are negligibly small. The risk level

of the RoPax ferry exists between the border between the "intolerable" and "ALARP (As Low As Reasonably Practicable)" regions. If we introduce the operational limit, i.e. no operation with 10 m of the significant wave height or over, however, the risk level of the RoPax ferry is moved to the "negligible" region. This operational limitation nearly coincides with actual practice of this ship type. For the RoPax ferry, the heeling lever due to drift are estimated with the model test. The risk level of the car carrier exists in the "ALARP" region so that shift of the down-flooding point upwards should be considered as a cost-effective risk control option.

This methodology proposed in this paper can provide the safety level of these conventional ships. Thus, it is possible that, with this methodology utilizing the same risk levels of conventional ships, stability of unconventional ships can be evaluated.

CONCLUSIONS

The authors proposed a methodology for calculating capsizing probability under dead ship condition. This was extended to risk analysis. The authors believe that this methodology can be utilised as a part of the performance-based intact stability criteria for unconventional vessels.

ACKNOWLEDMENTS

This research was supported by a Grants-in Aid for Scientific Research of the Japan Society for promotion of Science (No. 18360415). It was partly carried out as a research activity of SPL project of Japan Ship Technology Research Association in the fiscal years of 2005 and 2006, funded by the Nippon Foundation. The authors express their sincere gratitude to the above organizations. The authors thank Drs. Y. Ogawa and G. Bulian for providing the calculated data of the wave drifting forces and the computer program of parameter identification technique, respectively. The data and scaled model of the RoPax ferry was kindly provided by the National Maritime Research Institute.

REFERENCES

Belenky, V.L., A Capsizing Probability Computation Method, Journal of Ship Research, Vol. 37, pp.200-207, 1993

Fujiwara, T., An Estimation Method of Wind Forces and Moments Acting on Ships, Mini Symposium on Prediction of Ship Manoeuvring Performance, Mini Symposium on Prediction of Ship Manoeuvring Performance, 2001

Ikeda, Y., Prediction Method of roll Damping of Ships and Its Application to determine optimal stabilization devices, Marine Technology, Vol. 41, pp. 89-93, 2004

IMO, Interim Guidelines for Alternative Assessment of the Weather Criterion, MSC.1/Circ. 1200, 2006

IMO, Report of the Working Group (Part 1), SLF 50/WP.2, 2007

Japan. Report on FSA Study on Bulk Carrier Safety , MSC75/5/2, IMO, 2002

Kashiwagi, M and T. Ikebuchi, Performance Prediction System by Means of a Linear Calculation Method, Proceedings of the 4th JTTC Symposium on Ship Performance at Sea (In Japanese), The Society of Naval Architects of Japan, pp.43-59, 2003

Paroka, D., Y. Ohkura and N. Umeda, Analytical Prediction of Capsizing Probability of a Ship in Beam Wind and Waves, Journal of Ship Research, Vol. 50, No.2, pp. 187-195, 2006

Paroka, D. and N. Umeda, Capsizing Probability Prediction for a Large Passenger Ship in Irregular Beam Wind and Waves, Journal of Ship Research, Vol. 50, No. 4, pp.371-377, 2006a

Paroka, D. and N. Umeda, Piece-wise Linear Approach for Calculating Probability of Roll Angle Exceeding Critical Value in Beam Seas, Conference Proceedings of the Japan Society of Naval Architects and Ocean Engineers, Vol. 3, pp. 181-184, 2006b

Paroka, D. and N. Umeda, Prediction of Capsizing Probability for a Ship with Trapped Water on Deck, Journal of Marine Science and Technology, Vol. 11, No. 4, pp. 237-244, 2006c

Taguchi, H. , Ishida, S. and Sawada, H. : A Trial Experiment on the IMO Draft Guidelines for Alternative Assessment of the Weather Criterion, Proceeding of the 8th International Ship Stability Workshop , Istanbul , 2005

Umeda, N., J. Ueda, D. Paroka, G. Bulian and H. Hashimoto, Examination of Experiment-Supported Weather Criterion with a RoPax Ferry Model, Conference Proceedings of the Japan Society of Naval Architects and Ocean Engineers, Vol. 2K, pp. 5-8, 2006

Umeda, N., S. Koga, Y. Ogawa and D. Paroka, Stability Assessment of a (in Japanese), Conference Proceedings of the Japan Society of Naval Architects and Ocean Engineers, Vol. 3, pp. 185-188, 2006

Umeda, N., E. Maeda and D. Paroka, Risk Level of Ship Capsizing in Beam Wind and Waves (in Japanese), Conference Proceedings of the Japan Society of Naval Architects and Ocean Engineers, Vol. 4, pp. 163-166, 2007

Umeda, N., I. Tsukamoto and D. Paroka, Simplified Estimation of Effective Wave Slope Coefficient and Its Effect on Capsizing Probability (in Japanese), Conference Proceedings of the Japan Society of Naval Architects and Ocean Engineers, (to appear), 2007

Umeda,N. and Y. Yamakoshi : Probability of Ship Capsizing due to Pure Loss of Stability in Quartering Seas, Naval Architecture and Ocean Engineering, Vol.30, pp.73-85, 1994

Yoshimura, Y., Mathematical Model for the Manoeuvring Ship Motion in Shallow Water (2nd Report) (in Japanese), Journal of the Kansai Society of Naval Architects, Japan Vol.210, pp.77-84, 1988

Probabilistic Assessment of Parametric Rolling: Comparative Study of Detailed and Simplified Models

K.J. Spyrou, N. Themelis & S. Niotis

National Technical University of Athens, Greece

ABSTRACT

Current capability in predicting the occurrence of parametric rolling is explored by comparing results obtained by a well-known panel code against predictions obtained by a simple analytical criterion of parametric roll growth in the principal region, deriving from a classical Mathieu-type model. A modern post - panamax containership has been selected as basis of this investigation, that was known to exhibit head-seas parametric rolling at low speed. Recorded discrepancies in stability boundary predictions were converted into quantitative differences in the probability of realising parametric rolling in a realistic seaway.

KEYWORDS

Ship; stability; probability; risk; parametric; roll; capsize.

INTRODUCTION

In their bare essence or as backbone of reliability and risk analysis, probabilistic methods receive positive regard in engineering. In the field of ship stability, the debate on probabilistic methods of assessment has been running for long; yet the current regulatory framework, and notwithstanding recent amendments, reflects little of this. Current international activity makes one feel however that developments are forthcoming (see for example IMO 2007).

The probabilistic properties of a Gaussian sea can be accounted by a number of parametric models of sea waves. However, the serious setback towards the quantitative prediction of the probabilistic properties of extreme ship responses comes from the intricacies of mathematical models of ship motions, especially at condition far from the upright equilibrium, combined with the deficiency of current probabilistic methods to handle such complex models of ship dynamics. In the domain between rudimentary idealized modeling that is amenable to some analytical processing and brute force simulation, several approaches can be (and have been) devised, each with distinctive strengths and weaknesses.

A new method of probabilistic assessment of intact stability was developed recently, described in two deliverables of the Safedor integrated project of the European Commission (see Spyrou and Themelis 2006 for the theory; and Themelis et al. 2007 for the implementation). The method targets capsize modes in an individual basis and thus their probability of occurrence can be distinguished. Moreover, spatial variation of the probability along a ship route or in an area of operation can be produced, a feature that should constitute a useful aid to weather routing. The method exploits the tendency for groupiness of high waves which implies approximate periodicity

within the run length of the group that produces the excitation to the ship.

As is obvious, a critical contributor to any probabilistic assessment that exploits numerical predictions of ship dynamics is the quality of these predictions and although we are still far from being content with the state-of-the-art in this field it would be useful to know at least how different tools perform against each other. In the current paper the focus is on a comparison of calculated capsize probabilities using, on the one hand, a simplified model of ship dynamics; and on the other, a detailed panel code that, to our knowledge, has not been used before for the prediction of ship instability. The phenomenon of parametric rolling has been set as the focal point of interest and the investigated ship was a modern post - panamax containership.

The paper is structured as follows: In the next section are presented some basic facts about parametric rolling and a simple analytical criterion is summarised for the growth of roll in the so-called principal region of parametric instability. In the ensuing section is described briefly the panel code that has been used in the current comparative study. Moreover, simulations are presented that verify the capability of this software to capture parametric rolling. Comparisons of critical wave group predictions then follow between the simplified and the detail model. Lastly, the reflections of the findings by these two methods, in terms of the probability of exhibiting parametric instability, are determined.

BOUNDARIES OF PARAMETRIC ROLLING

The region that is customarily identified with principal parametric resonance is in the hollow part of curves (a) and (b) in Fig. 1. This boundary is in fact a bifurcation locus (types shown on the figure) where loss of stability of the upright position equilibrium is generated. Depending on the initially hardening (case shown) or softening character of the restoring curve, the marked bifurcation types are interchanged. Whilst analytical or numerical prediction methods usually target this linear boundary, in reality roll oscillations can be realized also to its exterior. Underneath (b) exists the locus of folding of the oscillation amplitude [curve (c)] that is a boundary resulting purely from the nonlinearity system. Notably, between (b) and (c) the upright equilibrium coexists with the oscillatory response; as a matter of fact, parametric rolling could arise there only by a discontinuous transition; for example invoked by a sudden gust or impulsive wave effect.

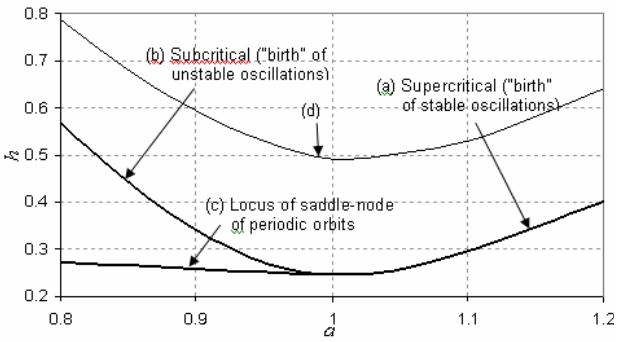

Fig. 1: Region of principal parametric instability of damped nonlinear Mathieu-type system ($a = 4\omega_0^2/\omega_e^2$ and h is representative of the intensity of fluctuation of the restoring).

These boundaries refer to long-term dynamic behaviour which is unlikely to be reached in a realistic seaway. Thus they are not a convenient interface with the probabilistic wave group analysis. The true technical question is not whether parametric instability can be exhibited 'after' an infinite number of wave encounters, but rather whether roll oscillations can grow to a dangerous level within a few waves. Therefore, transient response boundaries should be sought, like the curve (d) which has been drawn in a qualitative sense in Fig. 1, and that normally lie higher than the boundary curves obtained through the customary stability analysis of steady-states. To determine such 'transient' boundaries entails some understanding of the mechanism of parametric roll growth, i.e. of the law of transient response. A closed form expression could be sought if the permissible roll angle is not set too high (which however leaves out the

nonlinear oscillations that exist in the high amplitude region), as follows:

Assume a Mathieu-type equation as a fundamental level model for parametric rolling:

$$\ddot{\varphi} + 2k\dot{\varphi} + \omega_0^2\left[1 - h\cos\left(\omega_e t\right)\right]\varphi = 0 \qquad (1)$$

k is the linear 'half-dimensional' roll damping, h is the parametric excitation amplitude and ω_e, ω_0 are respectively the encounter frequency and the natural roll frequency (undamped). Then, it can be shown that at exact principal resonance the unstable motion builds-up according to the following approximate general rule (Spyrou 2005):

$$\varphi\left(pT_0\right) \approx e^{-\frac{2p\pi k}{\omega_0}}\left(\frac{e^{\frac{p\pi h}{2}} + e^{-\frac{p\pi h}{2}}}{2}\right)\varphi \qquad (2)$$

To realize a q-fold increase in roll amplitude within p roll cycles from some initial roll angle φ_0 the following condition should hold according to our approximate theory:

$$\ln q = \ln\frac{\varphi}{\varphi_0} \approx -\frac{2p\pi k}{\omega_0} + \ln\left(\frac{e^{\frac{p\pi h}{2}} + e^{-\frac{p\pi h}{2}}}{2}\right) \qquad (3)$$

As the dominant exponential term is the one with positive sign, the following expression delineates the necessary parametric excitation h for achieving q-fold growth:

$$h \approx \frac{4k}{\omega_0} + \frac{0.693 + \ln q}{1.571\,p} \qquad (4)$$

The above expression may be generalised for non-perfect tuning. This extended version will be used in fact in the later sections of this paper but, for the sake of brevity, its exact form is omitted.

SWAN2: A NUMERICAL CODE FOR TIME DOMAIN SIMULATIONS

SWAN2 is a numerical time-domain code for the analysis of the steady and unsteady free surface flows past ships which are stationary or cruising in water of infinite or finite depth or in a channel (SWAN2 2002). This software will be used for predicting parametric rolling in the time domain. *SWAN2* solves the steady and unsteady free-surface potential flow problems around ships using a three-dimensional Rankine Panel Method in the time domain using a distribution of quadrilateral panels over the ship hull and the free surface. The developers of the software argue that the numerical solution algorithms lead to convergent, accurate and efficient wave flow simulations without problems related with numerical dissipation. The ship hull input to *SWAN2* is in the form of standard Computer Aided Design (CAD) generated offsets. Moreover, the creation of the panel mesh over the ship hull and the free surface is performed internally by suitable routines of the program.

Water depth may be either infinite or finite with uniform depth. Mono-hulls, catamarans, trimarans and SES are supported. A mono-hull is supposed to be longitudinally symmetric with cruiser or transom stern. The free-surface flows are solved about the reference coordinate system fixed at the ship's mean position while a uniform stream with velocity U flows in the negative x-direction. A selection between linear and nonlinear Froude-Krylov forces should be made.

Two input files are necessary; a hull offset file and a job control parameters file that contains mainly sea wave characteristics (wave height and period) and operational information (ship mass, speed and etc). In terms of the output files, the grid information on the computational mesh, the principal ship hydrostatic particulars and inertial properties are included. Other ouput files concern the time history of the motions as well as of the forces and moments acting on the body.

Numerical constraints and stability problems have been identified as in the case of large panel aspect ratio where the discrete solution of the wave flow may become unstable which affects negatively the accuracy of the solution. Numerical convergence studies have been performed by the developers of the software in order to ensure that such errors are negligible.

THE INVESATIGATED CONTAINERSHIP

A modern post panamax containership has been selected as a basis for the investigation. This ship had been known to exhibit parametric instability in head seas and at low speed. Her basic particulars are collected in Table 1.

Table 1: Ship particulars

L_{BP} *(length)*	288.87 m	Δ (disp/ment)	11395 t
B *(beam)*	42.80 m	T_0 (natural roll period)	30.26 s
D *(depth to upper deck)*	24.40 m	KG (vertical position of centre of gravity above keel)	18.83 m
T_d *(mean draught)*	14.00 m	GM (metacentric height)	1.08 m

The hull geometry of the ship was introduced into *Maxsurf* 11.03 which is a well-known commercial ship design software. In Figure 2 is shown a rendered view of the modelled hull. This software has been utilised in the context of application of the analytical criterion, in order to determine the amplitude of parametric excitation incurred by restoring's variation.

Moreover, to predict her motions in the time domain the ship has been modelled also with the program *SWAN2*. In Figure 3 can be seen a characteristic 3D plot mesh generation of the containership, as obtained with *SWAN2*.

Fig.2: Rendered hull of containership exported from Maxsurf.

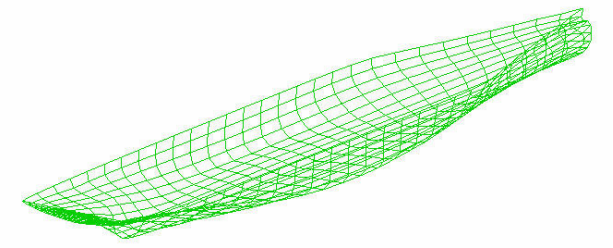

Fig.3: 3D plot mesh generation of containership by SWAN2.

CONTAINERSHIP DYNAMICS ACCORDING TO ALTERNATIVE TOOLS

At first, the critical wave groups that are predicted by each tool to be capable of generating parametric rolling will be contrasted against each other. The calculation of the respective probabilities of encountering these critical wave groups will follow in the final stage as a case study.

Speeds hosting tendency for parametric rolling

It was confirmed by both methods that the ship is liable to head seas parametric rolling at the low speed range. In Figure 4 are shown the critical combinations of ship speed and wavelength where head-sea parametric rolling should be observed when an exact tuning condition has been realised (in mathematical terms when $\alpha \doteq 4\omega_0^2 / \omega_e^2 = 1$). However, as said earlier, critical combinations of speed and wavelength covering a broad range around $\alpha = 1$ will be taken into account.

Estimation of damping

Roll damping plays an important role for the growth of parametric rolling and, as a matter of fact, in the specification of critical wave groups. In the analytical criterion the damping has been calculated by a method described in Themelis and Spyrou (2006).

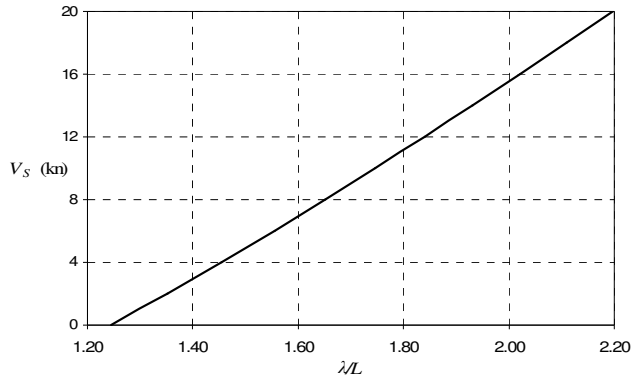

Fig. 4: Critical combinations of speed and wavelength for head seas paramedic rolling ($a = 1$).

Specifically, the viscous part of the damping is estimated by taking into account the skin friction, eddy making and the drag force from appendages (e.g. bilge keel) due to rolling motion. An equivalent linear damping coefficient has been estimated around natural roll frequency, with no forward speed, which is subsequently introduced into the analytical criterion (Eq. 4). The ship has been examined without bilge keels and the value of equivalent linear 'half-dimensional' damping k was determined as 0.0129 s^{-1}. As the speed effect was not taken into account in this calculation method, the roll damping coefficient that appears in the application of the analytical criterion is essentially a constant.

On the other hand, numerical decay tests at various speeds have been carried out with SWAN2. Roll damping calculation in SWAN2 follows the well-known method of Ikeda (1978) and Himeno (1981). Corrections due to forward ship speed are taken into account as lifting effects influence significantly roll damping (Sclavounos 1996). In Figures 5 and 6 are shown two decay tests of the investigated containership; the first with no forward speed and the second with moderate speed. In Figure 7 is compared the calculated linear damping coefficient as function of speed, against the constant damping coefficient obtained from the alternative "in-house" method. The two methods produce identical values at a speed around $V_S = 13$ kn.

Specification of critical wave groups

To ensure that the analytical criterion is applicable with reasonable accuracy, a roll angle of 15^0 has been set as the limiting inclination whose exceedance should be avoided. An uncertain heel disturbance that is necessary for the growth of roll amplitude up to the specified limit is considered, distributed in the range $\varphi_0 = 0^0 - 6^0$. Similarly, a probabilistic speed distributed in the range $V_S = 0 - 20$ kn has been considered.

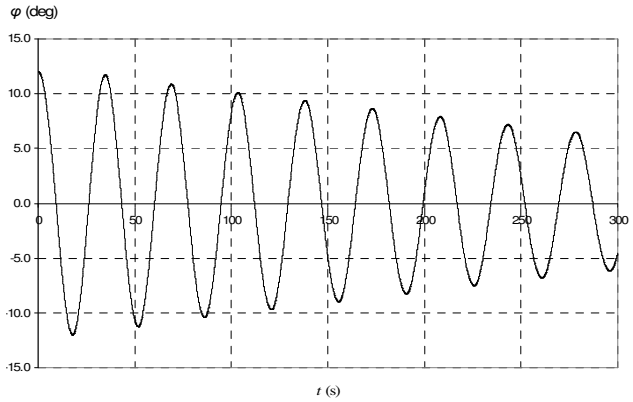

Fig. 5: Roll decay with no forward speed.

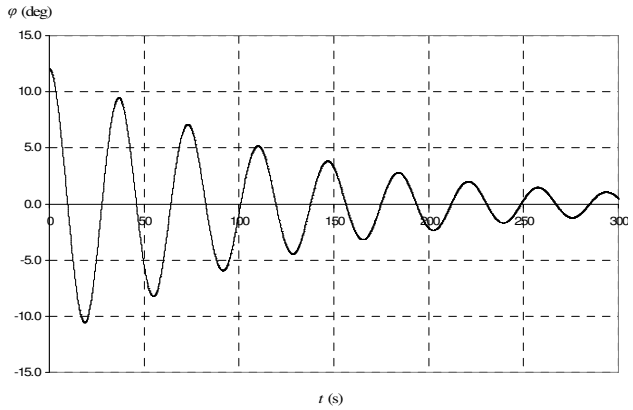

Fig. 6: Roll decay with forward speed $V_S = 18$ kn.

Analytical criterion

As already explained, the criterion targets the critical magnitude of parametric excitation h_{cr} that is necessary for realising a q-fold increase from some initial roll disturbance, within a limited number (say p) of roll cycles. At condition of exact principal resonance, $2p$

wave encounters are required for p parametric roll cycles. In Figure 8 one observes the critical parametric amplitudes which correspond to $a=1$, for three different initial conditions, each assumed to be the representative of a narrow range of initial roll angles. Up to 8 waves in a group have been considered because a larger number corresponds to trivially low probability of encounter.

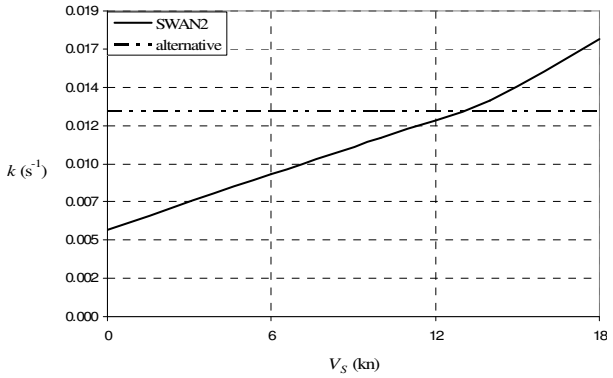

Fig. 7: Comparison of damping coefficients at various speeds.

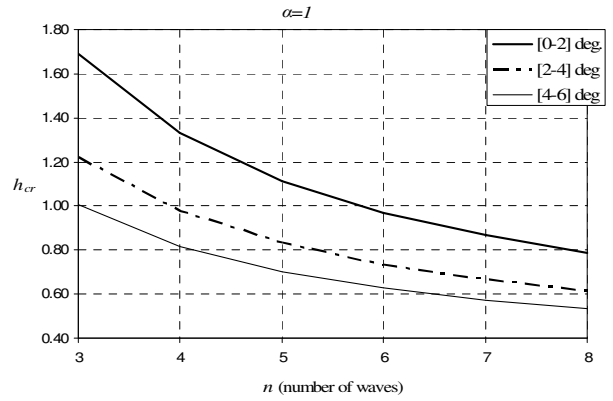

Fig. 8: Critical parametric amplitudes for $a=1$.

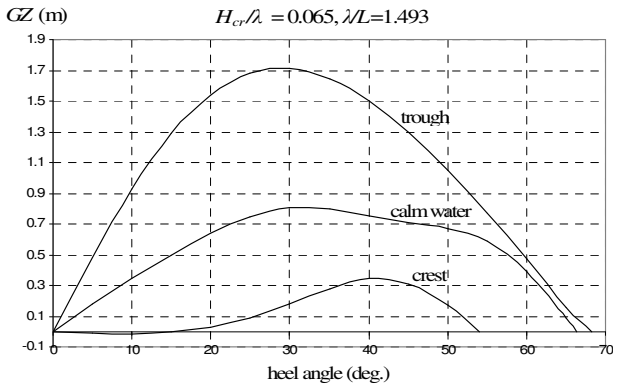

Fig. 9: Characteristic GZ variation.

Critical parametric excitation amplitudes should be transformed into critical wave heights by taking into account the geometry of the submerged hull. Thus the variation of restoring between wave crests and troughs needs to be calculated for a range of wavelengths that are near to satisfying the condition $a=1$. In Figure 9 is shown a characteristic GZ variation that corresponds to one of the identified critical wave group specifications.

Numerical simulations

Critical wave group characteristics are identified on the basis of a campaign of numerical simulations, with occasional recording of the occurrence of growth of the roll amplitude to 15^0 within the allowed number of wave encounters. Nonlinear Froude-Krylov force calculation was selected. As manifested by the characteristic time-histories shown in Figures 10 to 12 referring to the principal instability regime, SWAN2 can capture parametric rolling.

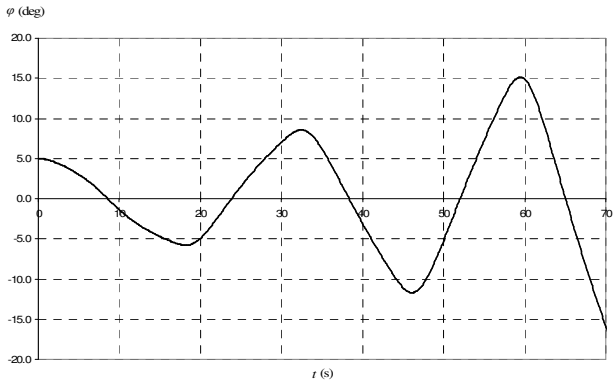

Fig. 10: Roll response in head waves ($a=0.8$, $H=9.9$ m).

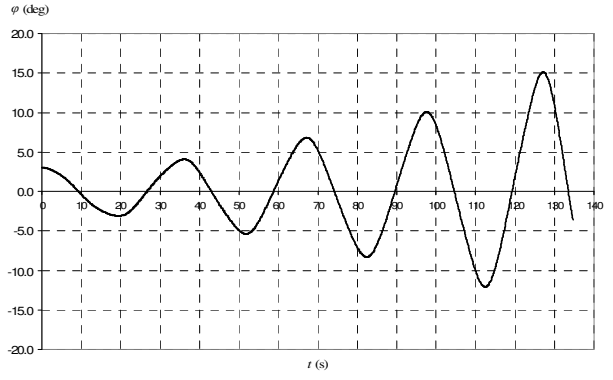

Fig. 11: Roll response in head waves ($a=1$, $H=7$ m).

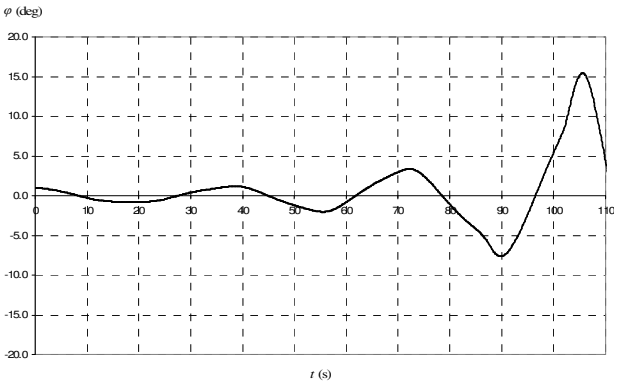

Fig. 12: Roll response in head waves ($a = 1.2$, $H = 10.4$ m).

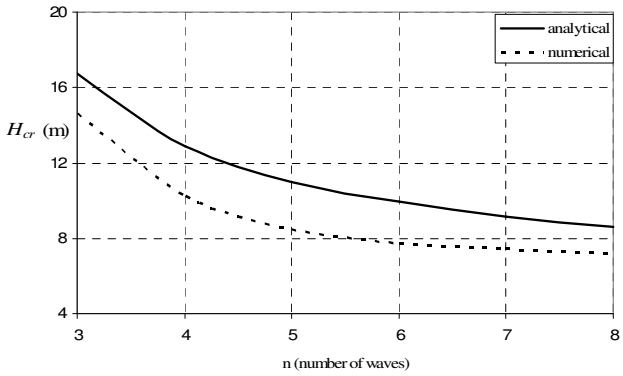

Fig. 13: Critical wave height as function of run length ($a = 1$, $V_S = 14$ kn , $\varphi_0 = 5^0$).

COMPARISON OF CRITICAL WAVES

The comparison between analytical and numerical predictions was focused on differences of wave height with all other parameters kept identical. The critical wave heights as calculated by the two prediction techniques are illustrated in Figure 13. Despite the fact that, according to Figure 7, for the selected speed of 14 kn higher roll damping was present in the numerical simulation model than the one inserted in the analytical criterion, the critical wave heights predicted by the numerical tool turned out to be lower. This could possibly be attributed to effects incurred by the heave and pitch motions.

Next, the critical wave heights that generate 5-fold increase in roll amplitude within $n = 3, 4, ..., 8$ wave encounters have been compared for various speeds. The results are shown in Figures 14 to 19, varying from one figure to the next the wave group run length n. A trend of wave height increase is noted as the speed is raised, that follows a similar pattern for both prediction methods. In the case of the *SWAN2* simulations one could also notice that, despite its increase with speed, roll damping does not seem to affect substantially the critical wave heights. Therefore, the augmentative trend in wave height should be attributed mainly to an increase of the required wavelength; in its turn owed to the higher speed required for achieving frequency tuning at $a = 1$.

An alternative option is to fix the speed, determine those wave lengths that are eligible to incur head-seas parametric rolling when a obtains a value around 1, and then determine the critical wave heights according to the wave group run length. Such diagrams are collected in the set of Figures 20 to 24, covering a wide range of speeds.

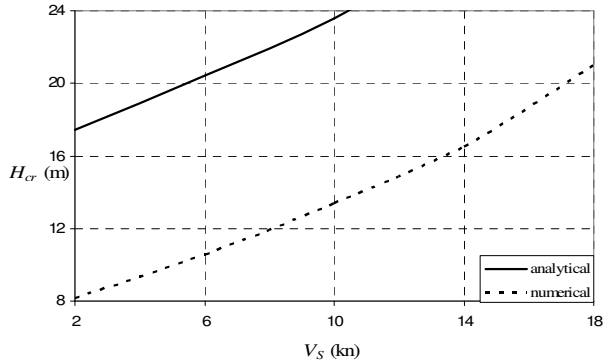

Fig. 14: Critical wave height as function of speed ($a = 1$, $q = 5$ and $n = 3$ wave encounters).

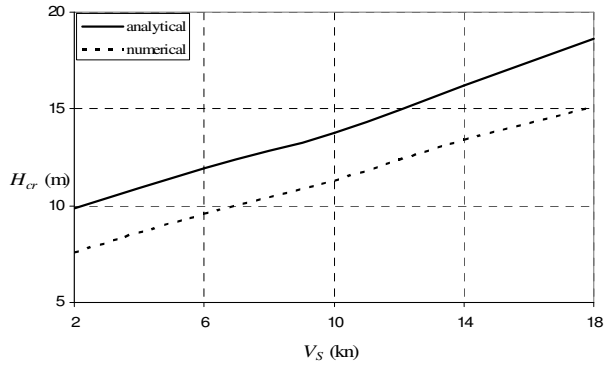

Fig. 15: Critical wave heights ($a = 1$, $q = 5$ and $n = 4$).

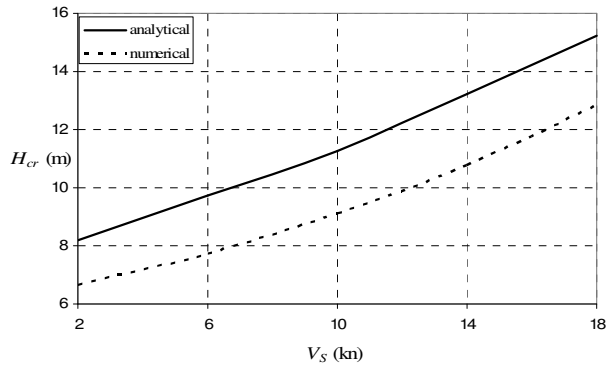

Fig. 16: Critical wave heights ($a = 1,\ \ q = 5$ and $n = 5$).

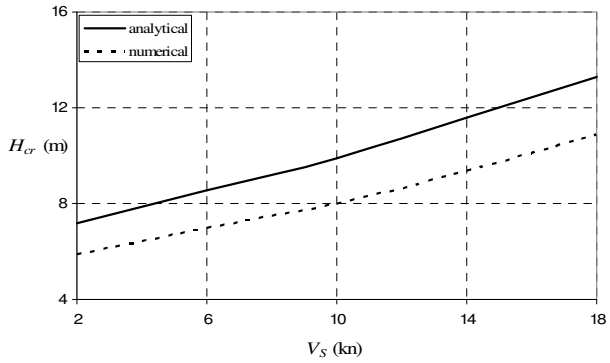

Fig. 17: Critical wave heights ($a = 1,\ \ q = 5$ and $n = 6$).

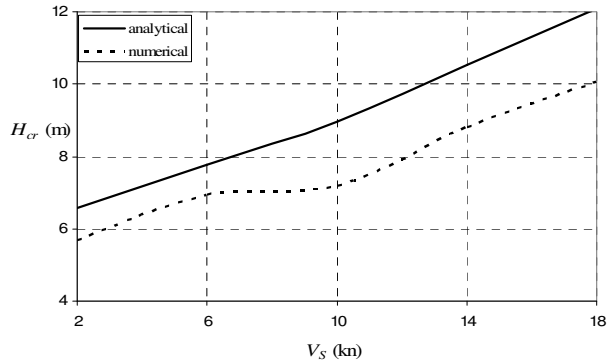

Fig. 18: Critical wave heights ($a = 1,\ \ q = 5$ and $n = 7$).

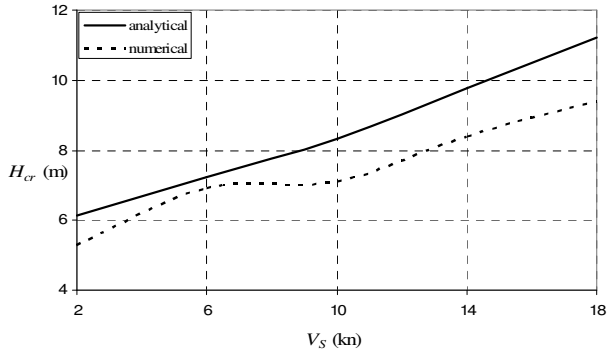

Fig. 19: Critical wave heights for $a = 1,\ \ q = 5$ and $n = 8$).

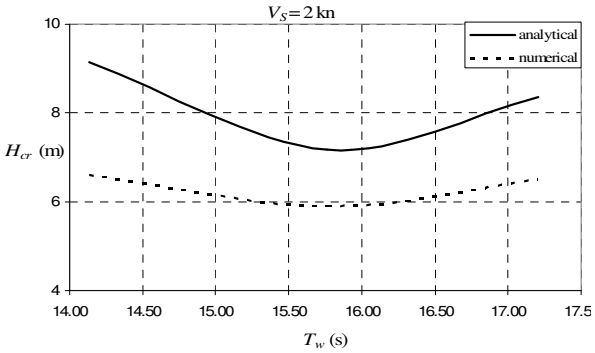

Fig. 20: Critical wave height as function of wave period ($q = 5$, $V_S = 2$ kn and $n = 6$).

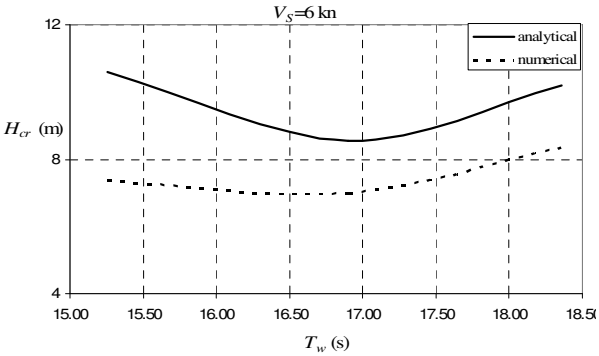

Fig. 21: Critical wave heights ($q = 5$, $V_S = 6$ kn and $n = 6$).

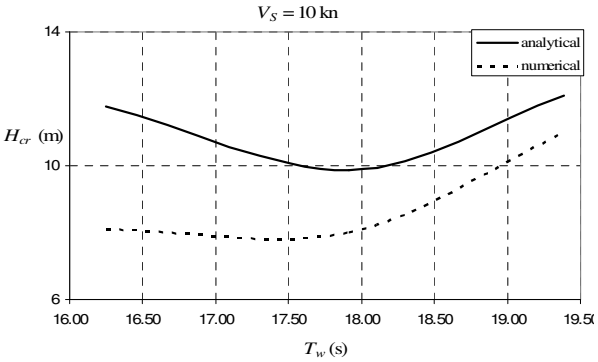

Fig. 22: Critical wave heights ($q = 5$, $V_S = 10$ kn and $n = 6$).

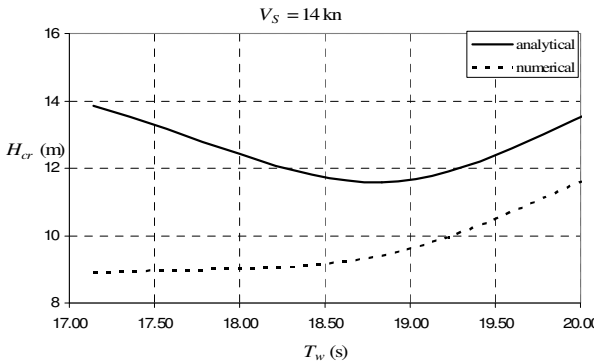

Fig. 23: Critical wave heights ($q = 5$, $V_S = 14$ kn and $n = 6$).

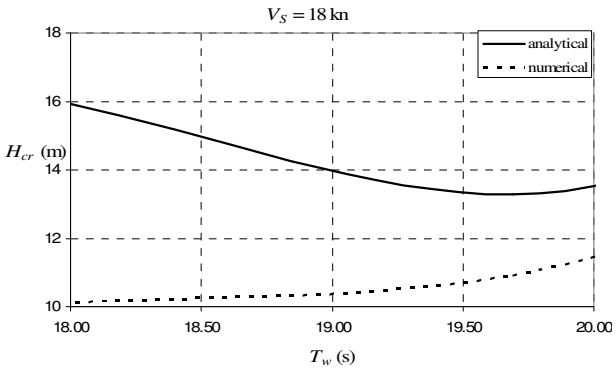

Fig. 24: Critical wave heights ($q = 5$, $V_S = 18$ kn and $n = 6$).

CALCULATION OF PROBABILITIES

Probabilities to encounter the wave groups specified in the previous paragraphs, given a selection of sea state, have been calculated. A comprehensive discussion on the joint and marginal probability density functions that are necessary for such a calculation are given in Themelis and Spyrou (2006). Very briefly, the underlying theory of the current probabilistic wave group analysis is based on a modification of Kimura's (1980) approach, developed by Battjes & Van Vledder (1984). Assumption of the Markov chain property is made for the successive waves in the group. Adding to the versatility of the methodology, necessary probability calculations exploit spectral information of the wave field; i.e. there is no need of using direct time-series results.

A sea state with $H_S = 7.6\ m$ and $T_P = 16.4$ s has been picked out of the set of results of a hindcast study which addressed the North Atlantic region (Behrens 2006). Such weather could have prevailed at location 59.5^0N - 7^0W, with a few hours duration on January 14th, 1991. The JONSWAP spectrum was assumed in order to expedite the calculation procedure (Hasselmann 1973). The peakness parameter of this spectrum was determined as recommended in DnV (2002).

The obtained probability values are illustrated in Figure 25 as functions of speed. Concerning initial condition, the assumption was made of some uncertain heel disturbance with the following distribution: 50% to lie within $0^0 - 2^0$, 30% in $2^0 - 4^0$ and 20% in $4^0 - 6^0$. Lastly, the overall probability values are shown in Table 2. To this, the speed was treated as a probabilistic parameter obtaining values in the range 0 – 20 kn. Five successive sub-ranges with length 4 kn were then considered and probabilities were attributed as follows: 30% for the middle sub range and 20% for each one of the others.

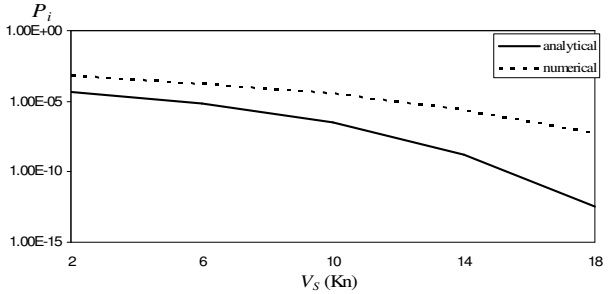

Fig. 25: Probabilities of encountering the critical wave groups in terms of ship speed.

Table 2: Total probabilities

Analytical criterion	1.047×10^{-5}
Numerical simulations	1.663×10^{-5}

CONCLUDING REMARKS

The results of a comparative study between a well-known panel code and a simple analytical criterion have been presented, in terms of the boundary of instability of parametric rolling of a post-panamax containership. Transient growth at the initial phase of the occurrence of the phenomenon has been targeted by the two methods. The critical wave heights obtained by the analytical criterion were in every case higher than those obtained by the panel code, even when the damping was higher. This could reflect the effect of pitch and heave motions in a way aggravating the effect of restoring variation. Reasonable coincidence of predictions was found at frequency tuning

about $a = 1.2$. Despite the grave differences in the modelled physics between the two models, one should regard these predictions, as well as others that are presented in the open literature from time to time, with caution and should not rush to consider as more correct those produced by the detailed tool.

REFERENCES

Battjes, J.A & van Vledder, G.Ph., 1984, "Verification of Kimura's theory for wave group statistics", In Proc. 10th ICCE, pp. 642- 648.

Behrens, A., 2006, "Environmental data: Inventory and new data sets", Safedor S.P. 2.3.2 Deliverable Report.

Det Norske Veritas, 2002, "DNV MaxWave", Report No. 2001 – 1491.

Hasselmann, K., 1973, "Measurements of wind - wave growth and swell decay during the Joint North Sea Wave Project (JONSWAP)", Dt. Hydrogr. Z. Reihe A (8) 12.

Himeno, Y., 1981, "Prediction of ship roll damping- State of Art", Department of Naval Architecture and marine Engineering, University of Michigan, Ann Arbor, MI, Report No. 239.

IMO, 2007, IMO SLF 50 report on the 50th session of IMO Sub – Committee on Stability and Load Lines and on Fishing Vessel Safety.

Ikeda, Y., Himeno, Y., and Tanaka, N., 1978, "A prediction method for ship roll damping, Report No. 00405 of Department of Naval |Architecture, University of Osaka Prefecture.

Kimura, A., 1980, "Statistical properties of random wave groups", Proceedings of the 17th International Conference on Coastal Conference, Sydney, Australia, pp. 2955 – 73.

Sclavounos, P., 1996, "Computations of wave ship interactions", Advances in Marine Hydrodynamics, Computational Mechanics Publications, 1996.

Spyrou, K.J., 2005, "Design criteria for parametric rolling", Oceanic Engineering International, Vol. 9, pp. 11-27.

Spyrou, K. & Themelis, N. 2006, "Development of probabilistic procedures and validation – Alternative 2: Capsize mode analysis", Safedor S.P. 2.3.5 Deliverable Report.

SWAN2, 2002, Boston Marine Consulting, Ship Flow Simulation in Calm Water and in Waves. User Manual.

Themelis, N, Spyrou, K. & Niotis, S. 2007, "Implementation and application of probabilistic procedures", Safedor S.P. 2.3.6 Deliverable Report.

Themelis, N. & Spyrou, K., 2005, "Probabilistic Assessment of Resonant Instability", Proceedings of 9th International Conference on Stability of Ships and Ocean Vehicles, (STAB 2006), Rio de Janeiro, September 2006.

Session 2: Progressive flooding prediction

Session Chairman: Dr. J.-O. de Kat Prof. D. Vassalos

1) F. van Walree, A. Papanikolaou:

   "Benchmark study of numerical codes for the prediction of time to flood of ships: Phase I"

2) D. Spanos, A. Papanikolaou:

   "On the Time to Capsize of a Damaged RoRo/Passenger Ship in Waves"

3) P. Ruponen:

   "Extensions to a Pressure-Correction Method for Simulation of Progressive Flooding"

4) P.Ruponen, A.-L. Routi:

   "Time Domain Simulation of Cross-Flooding for Air Pipe Dimensioning"

Benchmark study of numerical codes for the prediction of time to flood of ships: Phase I

F. van Walree

Maritime Research Institute Netherlands (MARIN), the Netherlands

A. Papanikolaou

National Technical University of Athens (NTUA), Greece

ABSTRACT

This paper provides a summary of the progress of an ITTC benchmark study on numerical codes for the prediction of time-to-flood of damaged passenger ships. Simulation data for the flooding of a barge like ship has been provided by developers of several numerical codes and compared with relevant model experimental data. Overall it can be stated that the steady state flooding condition is reasonably well predicted by the codes. However, the prediction of the flooding rates and transient phenomena is less satisfactory and urges for increased research effort in this area in the future.

INTRODUCTION

On request of the 48th IMO-SLF Committee, The Sub-Committee on Ship Stability in Waves (SiW) of the ITTC has agreed to carry out a systematic benchmark study of numerical codes that are currently in use for the prediction of the damaged stability of ships in waves. The development of a "structured approach" to benchmark testing is a key feature of the current effort. Several comparisons of predictions for time-to-flood and motions at calm water and in waves, obtained from running the participating numerical codes, shall be reported for progressively more complex ship motion and flooding scenarios.

The initial intention was to carry out benchmark studies for a cruiser ship. Unfortunately, the data for a realistic cruiser ship with a complex internal geometry were not readily available to the ITTC-SiW committee. Therefore it has been decided to split the work in two phases as follows:

I. Benchmark based on a box-shaped barge for which detailed model test data are available;
II. Benchmark based on a realistic passenger ship with complex internal geometry.

The present paper describes the benchmark work for the first phase.

OBJECTIVE

The objective of the herein reported benchmark study is to establish current capability and weaknesses in predicting, qualitatively and quantitatively, the time-to-flood for a simple configuration of compartments in a barge-like hull form. Besides time-to-flood, related quantities as motions and flooding volumes in compartments will be compared with experimental results.

BACKGROUND

The barge that is taken as the basis for the study has been tested recently at the Helsinki University of Technology (TKK, formerly HUT), see Ruponen [1]. The model is box

shaped with tapered bow, stern and bilges, see Figure 1. The model scale was 1:10 while the model length was 4 m. The main particulars are shown in Table 1. The model was instrumented with water level sensors in the eight floodable compartments as to obtain detailed information on the flooding process. Two pressure sensors were located in the two lower double bottom compartments. The floodable compartments are located somewhat forward of midship as to introduce a trim angle and thereby progressive flooding, see Figures 2 and 3.

Length over all	4.000 m
Breadth	0.800 m
Height	0.800 m
Design draft	0.500 m
Block coefficient	0.906
Volume of buoyancy	1.450 m^3

Table 1 Main particulars barge

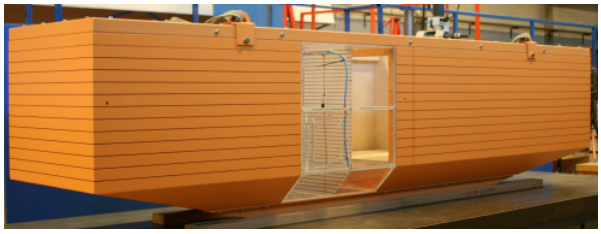

Figure 1 Barge model at TKK

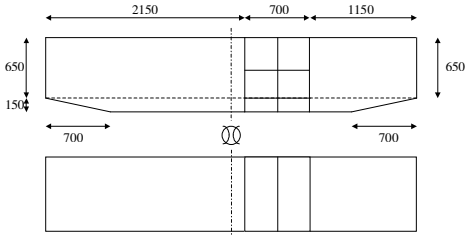

Figure 2 Compartment arrangement-1

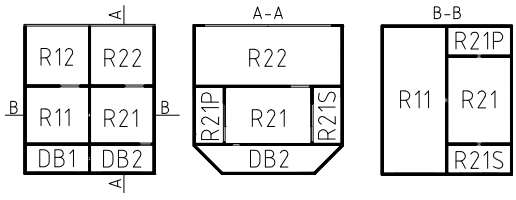

Figure 3 Compartment arrangement-2

Six damage cases have been tested of which four have been selected for benchmarking. Two cases are discussed herein as follows:

Test03 – Down Flooding

- Damage hole (25 mm x 25 mm) in the bottom of the forward double bottom compartment (DB2).
- The door on the upper deck is closed.
- The door, connecting R12 and R22, is open, allowing down-flooding from R12 to R11.

Test06 – Side Damage

- Damage hole (40 mm x 60 mm) is in the side of the forward compartment (R21S).
- The door on the upper deck is closed.
- The double bottom (DB1 and DB2) remains dry, i.e. the opening between R21 and DB2 is closed.

A comprehensive report about all benchmark tests may be found in Ref. [2].

PARTICIPATION

The following organisations participated in phase I of the benchmark study:

- Safety at Sea (S@S), United Kingdom.
- Helsinki University of Technology (TKK), Finland.
- Maritime Research Institute Netherlands (MARIN), The Netherlands
- Maritime and Ocean Engineering Research Institute (MOERI), Korea
- National Technical University of Athens (NTUA), Greece.

In the presentation of results the numerical simulation results from the participants are referenced to anonymously as C1 to C5.

TYPES OF NUMERICAL MODELS

All codes incorporate time domain simulation methods and can predict motions in six degrees of freedom. The codes are applied to mono-hulls at zero or normal operating speeds although some have been applied also to (high speed) multi-hulls in the past.

Froude-Krylov and restoring forces are based on integration of undisturbed wave pressures over the instantaneously submerged hull and superstructure portions. Radiation and diffraction forces are generally based on strip theory or a 3D frequency domain panel method. This frequency domain information is used in the time domain by means of convolution integrals (retardation forces). The hydrodynamic force components that are influenced significantly by viscosity are corrected semi-empirically.

The employed flooding methods use relatively simple hydraulic models, although the implementation of more advanced CFD methods is currently investigated by some participants. A modified Bernoulli equation is used to determine the water ingress through damage openings. The flow rate through an opening is related to a pressure head and a semi-empirical discharge coefficients. This approach is also applied to the progressive flooding between ship compartments through open doors, ducts, collapsed bulkheads, etc. Some of the codes may take into account sloshing effects, if occurring. The flooded compartment water surface is either assumed to be horizontal at all times, or movable due to the coupling with the ship motion, but still plane.

More detailed:

S@S's code has also evolved from a manoeuvring model following the "modular" MMG philosophy, based on detailed models of hull, propeller and rudder plus their interactions. Wave effect is added by calculating the Froude-Krylov force up to the instantaneous free surface, use of strip theory for the radiating wave forces and slender body theory for wave diffraction. Appendage hydrodynamics are calculated from their geometry. A PD autopilot is used. Flooding is determined by means of Bernoulli type equations.

TKK's code is based on a two-stage approach where loading and responses are decomposed into a linear approximation and a nonlinear part. Linear responses are obtained from linear transfer functions while the loads are determined from strip theory. The nonlinear part is composed of cross coupling terms of body dynamics and the nonlinear part of the Froude-Krylov force. Wave radiation forces appear as convolution integrals. Flooding is determined by means of Bernoulli type equations in combination with a pressure correction method.

MARIN's code FREDYN can deal with large angles in roll and yaw. Wave pressure is calculated up to the instantaneous free surface. The memory effect is taken into account through convolution integrals accounting for the radiation forces. Wave orbital velocities are taken into account in the calculation of drag forces. Flooding is determined by means of Bernoulli type equations which are solved in the time domain in a quasi-steady manner.

MOERI's code also can deal with large motions. It considers gravity, buoyancy, propulsion, steering, wind, manoeuvring and viscous (roll damping) force components. Wave excitation (diffraction and Froude-Krylov) and radiation forces are accounted for. With respect to flooding, the method is much the same as described above in the general part.

NTUA's code CAPSIM is a non-linear time domain numerical method, which is based on linear potential theory with respect to the basic hydrodynamics of the problem and considers a variety of non-linear terms of ship's equations of motions, like the excitation by large amplitude regular or irregular waves, the exact body geometry below and above the still waterline and its impact on ship's restoring and semi-empirical nonlinear viscous damping. The flooding rate through the openings is governed by the Bernoulli equation modified with the discharge coefficient to account for the effects of the openings.

RESULTS

Graphs showing comparisons between the experimental (Test) and simulation results (C1 through C5) are shown in Figures 4 through 24. Water level heights in compartments are denoted by H-x where x stands for the compartment identification shown in Figure 2. The pressure in double

bottom compartment DB1 is denoted by P-DB1. Sinkage, trim and heel are denoted by heave, pitch and roll respectively.

Water level results from Code C1 are only defined between the instants that the level starts to rise and that the compartment is filled. Otherwise a zero value is given.

In Code C2 a too low atmospheric pressure is present since this method can not be applied at model scale and the ambient air pressure is fixed in the code. Therefore, the effects of air compressibility are likely to be underestimated.

Codes C3 and C4 results do not include pressures as air compressibility is not taken into account, for the present case. The compartments are assumed to be fully ventilated.

In Code C5 individual compartments have been grouped into larger compartments as follows:

- Test 03: DB1+DB2 and R21+R21S+R21P
- Test 06: R21+R21P

Results for grouped compartments can not be compared directly to the results for the individual compartments.

In some of the codes it was possible to use the experimentally determined discharge coefficients, in other codes a fixed discharge coefficient has been used.

Test 03

This condition allows for progressive down flooding.

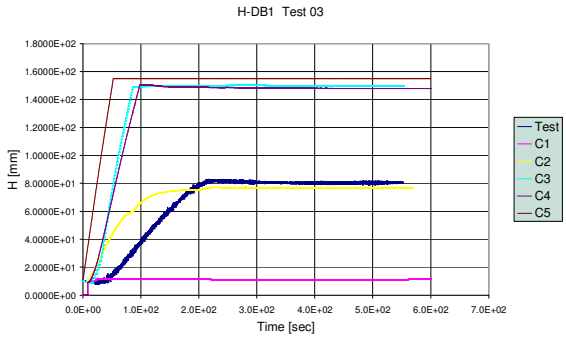

Figure 4 H-DB1 versus time

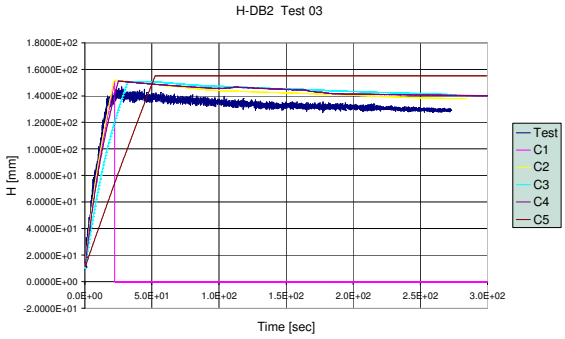

Figure 5 H-DB2 versus time

For the non-ventilated compartment DB1 the results are such that Code C1 overestimates the air pressure effect, C3 and C4 do not to account for air pressure while the Code C2 result is closest to the experimental flooding rate. For the ventilated compartment DB2 the agreement is better. Code C3 results lags behind a bit, but Code C4 results are reasonably good.

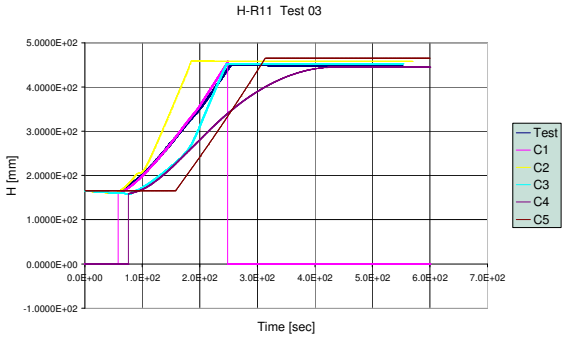

Figure 6 H-R11 versus time

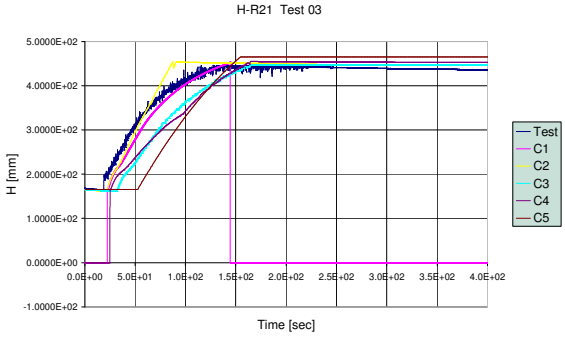

Figure 7 H-R21 versus time

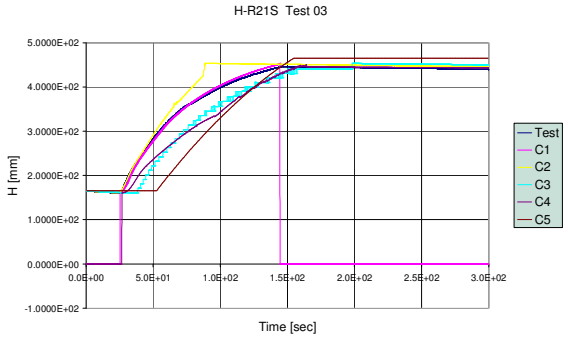

Figure 8 H-R21S versus time

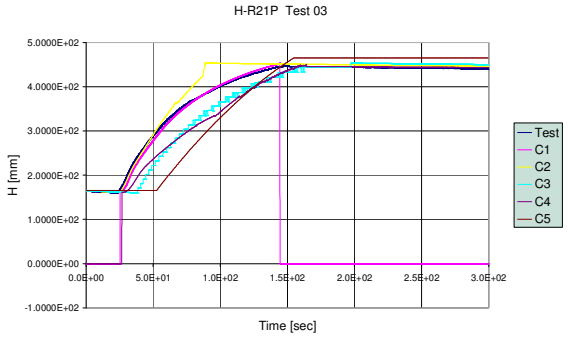

Figure 9 H-R21P versus time

For the R11, R21, R21S and R21P compartments located on top of the double bottom, the Code C1 result is about right, C2 shows a too high flooding rate while the flooding for C3, C4 and C5 lags behind in time.

For the top compartments R12 and R22, Code C2 results show a too early flooding, C1 and C3 results are close to the experimental values. Code C4 predicts no flooding in these compartments. C5 lags behind for R12 and R22.

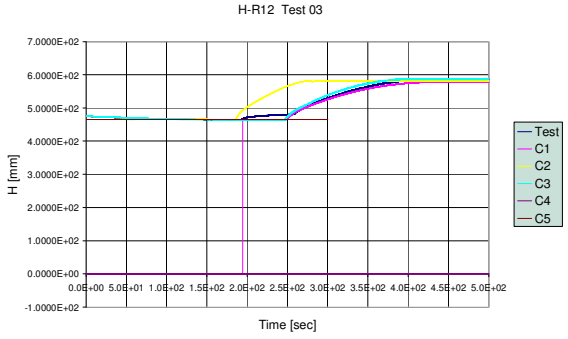

Figure 10 H-R12 versus time

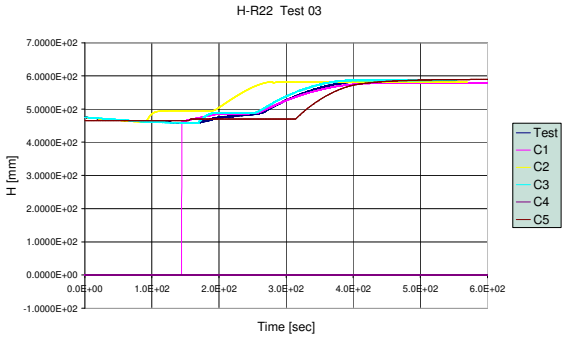

Figure 11 H-R22 versus time

The pressures in compartment DB1 are quite well predicted by Code C1, while C2 shows a too steep pressure rise. It seems strange that the pressure for compartment DB1 is well predicted by Code C1 while the water level is significantly off, see Figure 4. For compartment DB2, C1 does not provide the pressure while that of Code C2 is reasonable.

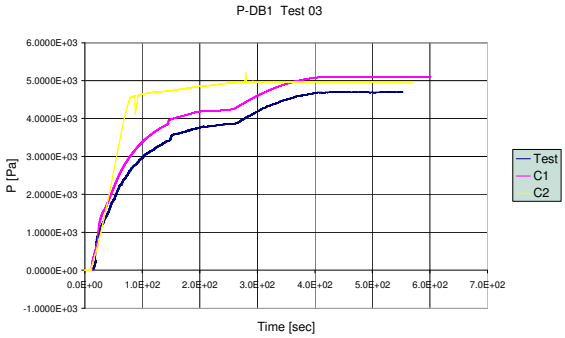

Figure 12 P-DB1 versus time

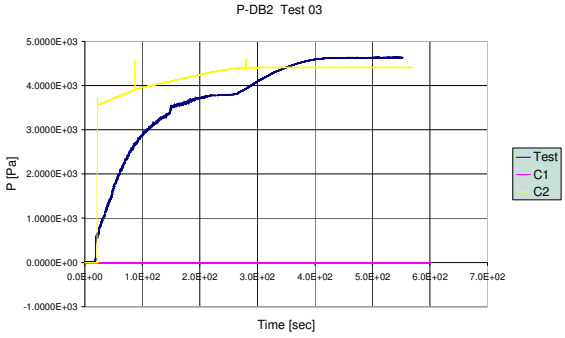

Figure 13 P-DB2 versus time

The results for the water level comparison are also reflected in the heave and pitch curves: the heave and pitch rates for C2 are too high but the steady values are well predicted. Code C1 results are close to the experimental values while C3 results also

show too high heave and pitch rates and somewhat too high steady values. This is in contradiction with the general under prediction of flooding rates for C3. For Code C4 both heave and trim are under predicted which is in agreement with the general under prediction of flooding rates. Code C5 finally predicts the heave quite well while the pitch is somewhat underestimated.

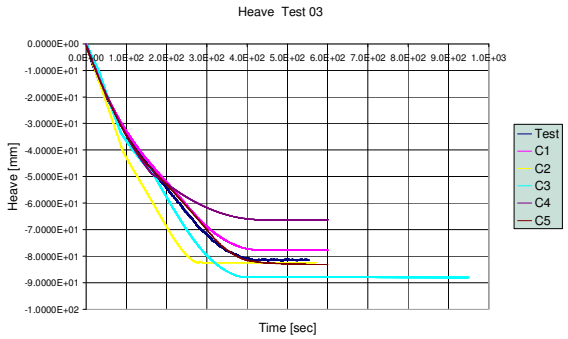

Figure 14 Sinkage versus time

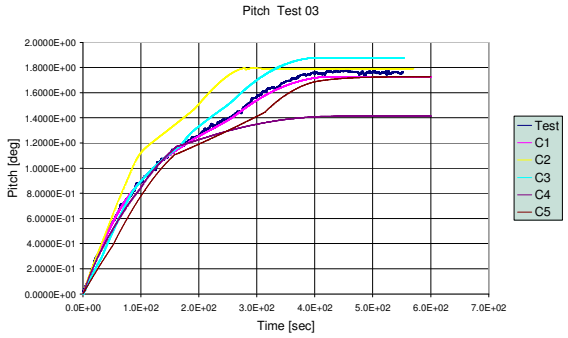

Figure 15 Trim versus time

Test 06

Test 06 shows a case with side damage in the starboard compartment R21S. The double bottom compartments DB1 and DB2 remain dry, therefore no results for these are included here.

Flow rates for compartment R11 are correctly predicted by Code C1 while C3, C4, C5 and especially C2 predict too low flow rates.

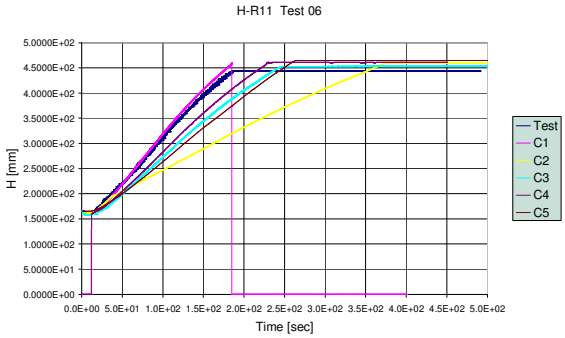

Figure 16 H-R11 versus time

For compartment R21, adjacent to the damaged compartment R21S, differences are smaller and most predictions are close to the experimental values. Code C5 predicts a too high flow rate. For the damaged compartment R21S itself, all codes over predict the initial inflow, furthermore code C5 does not predict well the reduction in flow rate at 50 seconds. This should have an effect on the roll angle shown later. For the port side compartment R21P, predictions are reasonably correct, but C5 again seriously over predicts the flow rate.

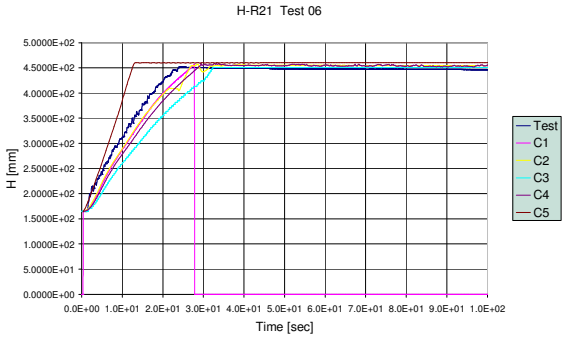

Figure 17 H-R21 versus time

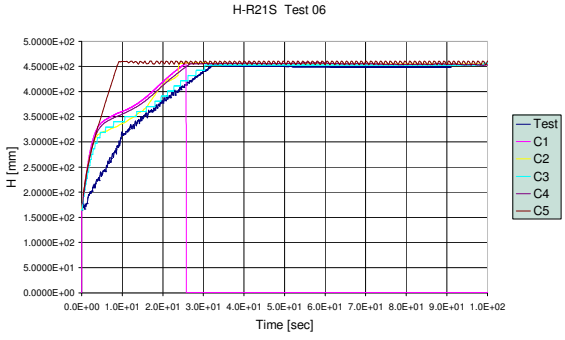

Figure 18 H-R21S versus time

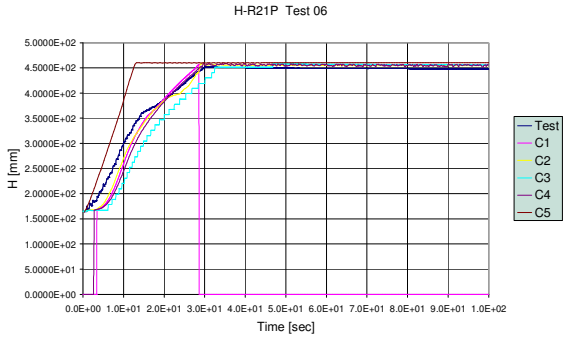

Figure 19 H-R21P versus time

For the top compartments R12 and R22, the predicted rise of the water level in time is generally acceptable, but Code C3 and especially C2, C4 and C5 lag behind for R12. Code C1 results are close to the experimental values.

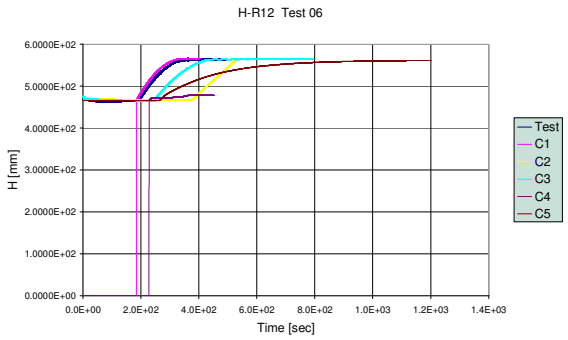

Figure 20 H-R12 versus time

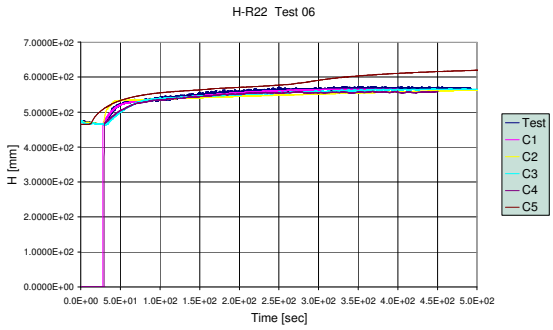

Figure 21 H-R22 versus time

Heave and pitch curves are well predicted by Code C1 while C2, C3 and C5 show deviating results. Code C4 shows again an underestimation of the equilibrium heave and pitch values.

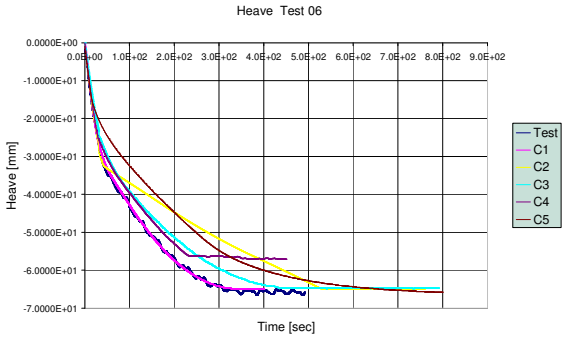

Figure 22 Sinkage versus time

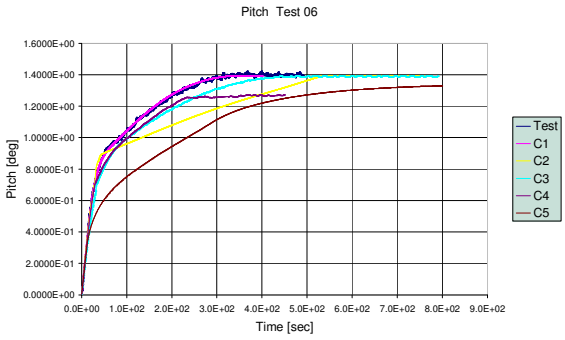

Figure 23 Trim versus time

All codes except C5 over predict the transient roll peak angle in a similar way, but also show upright conditions at approximately the same time instant as the experiments. The over prediction of the roll peak is probably due to neglecting the jet-like properties of the inflow and/or underestimating the roll damping. Interestingly, the roll time trace from Code C1, C4 and C5 are relatively smooth, while these from Codes C2 and C3 are irregular, similar to the experimental result.

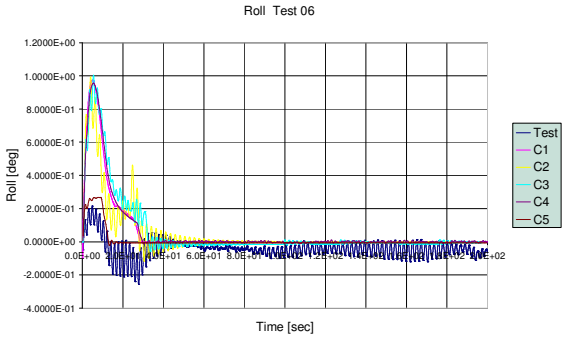

Figure 24 Heel versus time

CONCLUSIONS

On the basis of the above analysis, the following conclusions are drawn:
Code C1 produces results that are generally close to the experimental values. This code seems to have problems only with the non-ventilated double bottom compartment DB1 for Test 03.

Code C2 predicts generally the right trends but may show either too high flow rates for lightly ventilated compartments and/or irregularities in the water level and pressure signals. It is recommended to take into account the correct atmospheric pressure.

The over predictions in flow rates for Code C2 probably result in too steep heave and pitch rates. However, the steady state heave and pitch values are well predicted.

Code C3 and C4 predict generally the right trends but often predict too low flow rates while all compartments seem to be fully ventilated. This is inconsistent.

Heave and pitch predictions by Code C3 may either be somewhat under- or over-predicted. Code C4 generally under predicts the equilibrium sinkage and trim.

Results from Code C5 can be compared with the other data for a limited number of compartments only. Flow rates from Code C5 show the right trends, but are often too low or too high. Air pressure effects seem not to be taken in to account. Heave and trim predictions are reasonable to good.

The initial heel peak angle in the side damage case is over predicted by all codes, except for Code C5. This may be due to the simplifications made in the flooding method and an underestimation of roll damping. It should be noted that the experimental initial heel peak has a magnitude of 0.20 degree only. The steady state roll angle is correctly predicted by all codes.

Overall it can be stated that the steady state condition of all tests is reasonably well predicted by the codes. The prediction of the flooding rates and transient phenomena is less satisfactory. As such, reasonable time to sink predictions appear feasible by the present codes, at least for ships having a relatively simple internal geometry and interrelation between flooded compartments under calm water conditions. How this will work out for ships having a more complex geometry in calm water and for seaway conditions (including wave excited ship motions) remains to be seen in later stages of the present benchmarking work.

References

Ruponen, P., 'Model Tests for the Progressive Flooding of a Box-Shaped Barge', HUT Ship Laboratory Report M-292, 88 p., 2006.

Walree F. van, 'Benchmark Study of Numerical Codes for the Prediction of Time to Flood of Ships: Phase I', ITTC-SiW report, July 2007.

On The Time to Capsize of a Damaged RoRo/Passenger Ship in Waves

Dimitris Spanos

National Technical University of Athens – Ship Design Laboratory

Apostolos Papanikolaou

National Technical University of Athens – Ship Design Laboratory

ABSTRACT

The time to capsize of a damaged RoRo/Passenger ship in waves has been analysed by a numerical simulation procedure, consisting of a nonlinear hydrodynamic method for the simulation of motion and flooding and a statistical simulation method to account for the variability and uncertainty of the various parameters affecting the complex behaviour of the damaged and flooded ship in waves. The probability distribution for the time to capsize has been derived. It is shown that there appears to be no practical time margins for the safe evacuation of RoRo-Passenger ships in the determined non-survival conditions. The results also suggest that the ship, which is complying with current damage stability requirements (SOLAS 90), will always capsize in the presence of waves, which are higher than a critical wave height, the so-called *survive limit*, and her overall survival time is determined by her *survive boundary*.

KEYWORDS

Time-to-capsize; Time-to-flood; damaged ship; survivability; numerical simulation; passenger ship safety

INTRODUCTORY INFORMATION FOR AUTHORS

Dimitris Spanos

is naval architect and marine engineer; he graduated from NTUA and is working as post-doctoral senior researcher at NTUA-SDL. He is developer of theoretical models and computer codes for the prediction of the seakeeping behaviour of ships, both in intact and damaged conditions, which are employed in the prediction and assessment of the dynamic ship stability, the design verification and the operability assessment of ships and floating structures.

Apostolos Papanikolaou

is Professor of Ship Design and Director of the Ship Design Laboratory at the School of Naval Architecture and Marine Engineering, National Technical University of Athens (NTUA-SDL). His educational, research and professional activities cover a broad area of Naval Architecture and Ocean Engineering. He was and is Principal Investigator of a large variety of funded research work regarding the design and optimisation of conventional and unconventional vessels, the hydrodynamic analysis and assessment of calm water performance and seakeeping behaviour of ships and floating structures, the stability and safety of ships and regulatory developments of the International Maritime Organization (IMO).

INTRODUCTION

In case of ship accidents resulting to sinking, the survivability of people onboard depends on the time required and being available for their

safe evacuation and abandonment. The required time is determined by the duration of the evacuation and abandonment, which is affected by a variety of factors, like the number of people onboard, the internal ship arrangements and ways to muster stations, the ship motions, the live saving equipment, the visibility conditions (day or night) etc. The available time corresponds to the time until the ship loss, which reflects the resistance of the ship to capsize/sink, and is a property of the principal ship geometry mass and stability characteristics, her watertight subdivision and the environmental conditions.

A straightforward *assessment of the risk* of people onboard (in case of loss of watertight integrity) is based on the comparison of the time required for the people to safe evacuate and the time available up to the ship loss for a range of possible damage scenarios. Differently, estimating the time for the people to safely evacuate (by a proper evacuation study) and setting it as a requirement, then the time for the ship loss could be controlled by appropriate *risk based design measures* (and possibly additional operational measures), namely by minimizing the related risk, *Vassalos et. al* (2000).

In this context, IMO, *MSC.78* (2004), has introduced performance based criteria for the safety of the 'large' passenger ships, namely that of three (3) hours over which the ship is required to "remain habitable" after damage or safe return to the port under her own power. The explicit timeframe for habitability has been later revised, *MSC.80* (2005), to the "required time for safe evacuation and orderly abandonment" to better reflect the particulars of each vessel. These criteria determine the casualty thresholds, namely the extent of damage that a ship could sustain and they are being used by IMO in the development of appropriate requirements. Such developments imply the capability of managing the time for the ship loss after damage, which is an area of current and future intensive research that still needs time to become part of a standard design practice and eventually form a mature regulatory component.

In the framework of a holistic risk-based design procedure, as currently studied in the research project *SAFEDOR* (2005-2007), focused research on methods for the estimation of the time to capsize of passenger ships and the assessment of related risk has been conducted by the authors and some fundamental results of the related investigations are herein presented and discussed.

These results regard the time to capsize of a damaged RoRo/Passenger ship in irregular seaways due to flooding. The effect of the random waves on the time to capsize and its dispersion has been investigated on the basis of systematic numerical simulations of the ship in critical stability conditions. The criterion of three (3) hours habitability has been used as a reference time for the evaluation of the ship's capability to remain afloat and upright after damage. In the sense of IMO regulations, the study ship cannot be considered a 'large' passenger by size (Lpp=170 m); however, recent discussions at IMO, *MSC.82* (2006), have extended the safe return to port considerations to smaller passenger ships, hence relevant considerations apply also to the present one.

SHIP LOSS DUE TO FLOODING

The various flooding stages of the ship, which may lead to the physical or conventional loss of ship, are briefly revisited in order to facilitate the subsequent discussion.

Conventional and physical ship loss

Assuming a ship complying with current SOLAS damage stability requirements (SOLAS 90), the loss of her watertight integrity due to collision, and the damage extent within the range of current regulations, leads to the flooding of ship's internal spaces and the development of a new equilibrium, in principle with reduced transverse stability and floatability. Thereafter and in presence of waves, the ship may loose her transverse stability or floatability due to further accumulation of seawater and to capsize or sink. The latter process might last for a long

time or lead to a fast ship loss depending on the ship however the prevailing wave conditions.

The damaged ship is said to be lost when it first loses her *floatability* or *stability,* and the corresponding time is the *time to ship loss*.

The *loss of floatability* occurs when the total floodwater mass, which entered the ship through any opening on her shell, equals the residual buoyancy related to the ship's loading condition in question. Apparently, loss of floatability does not mean concurrent full submergence of the ship. A delay will result due to the time required to flood the superstructures. So, *sink* is considered as the disappearance of the ship from the sea surface.

The *loss of stability* occurs when the ship first fails to comply with the transverse stability requirements, whereas it may physically *capsize* on a later time. For the present investigation the *capsize* event has been literally considered as the ship turn over.

Subjective time to ship loss

Theoretically the available time for evacuation of the people on board would be equal to the time to ship loss. However, in reality, the available time for evacuation is considerably reduced, because of the subjective perception of the passengers on the remaining time until the physical loss. This is rather evident in the sink of the RoRo/passenger ferry EXPRESS SAMINA, as noted by *Papanikolaou et. al* (2003), where the survivors testified as time to sink a considerably varying time between 20 and 45 min. In that accident the flooding caused rapidly a large heeling, hence most of the passengers tried (and many managed) to abandon the ship at the very early stage, though the disappearance of the ship from the sea surface happened about 50 minutes after the damage.

Flooding stages

In the ship flooding, two mechanisms can be identified that of the flooding due to hydrostatic head difference at the damage opening(s), which dominates the *flooding in calm water*, and that of flooding due to waves and ship motion, called *flooding in waves*. In terms of timing, both mechanisms start developing simultaneously after the damage incidence, hence, complicating the distinction of their impact on the stability of the ship.

It is used to refer to the flooding in calm water as *transient flooding,* while any stage between the start and the completion of transient flooding as *intermediate stage* of flooding. When the transient flooding has been completed, namely the damaged spaces have been fully flooded, the ship might continue be flooded due to waves action. This flooding stage is called *steady state* in order to distinguish against transient flooding.

Progressive flooding, namely the sequential flooding of adjacent spaces, is encountered during the otherwise transient flooding of multi-spaces. Progressive flooding could be triggered even in steady state flooding, due to the wave-induced and the floodwater-induced motion of the ship. In cases of highly compartmented internal arrangements, like passenger and cruiser ships, and in absence of wide spaces, like the car deck, the progressive flooding is governed by the hydrostatic flooding in calm water, whereas the waves' effect is limited, especially when the damage opening is limited too, *Papanikolaou et al* (2003).

The variety of the flooding stages of a damaged ship is illustrated in Figure 1.

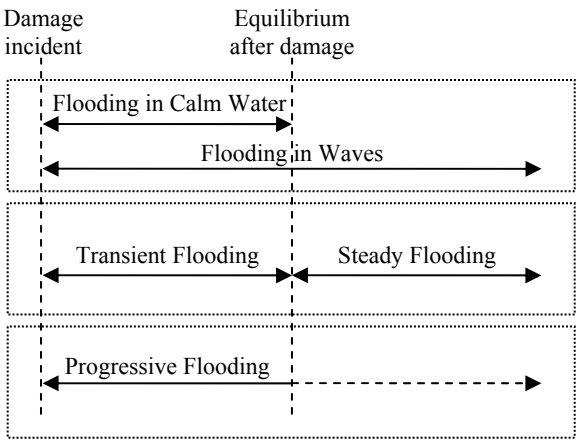

Figure 1 Flooding stages of the damaged ship

NUMERICAL SIMULATION PROCEDURE

Numerical Statistics

The time to capsize is a probabilistic quantity depending on several random variables that affect the flooding of the damaged ship in waves. The environmental conditions, waves and wind, the ship loading, the damage size, shape and location of the damage opening, the compartmentation and the status of the interconnecting openings (namely open or closed water-, weather- or splash-tight doors etc), all define a wide set of random variables and uncertain parameters that characterize the probabilistic nature of the flooding and the related time of specific events, like capsize.

To deal with above randomness the statistical method of Monte Carlo combined with a deterministic numerical hydrodynamic simulation for the ship motion and flooding is applied. The numerical hydrodynamic simulation program runs for a set of ship and environmental data, which have been specified randomly, to produce a single realization, a numerical test, of the damaged ship's flooding. The conducted numerical test may or may not result to capsize. The maximum time for the simulation has been set to three (3) hours in ship scale. For the next test, the simulation parameters are randomly updated by a Monte Carlo controller and the simulation process is repeated. The procedure keeps on until a sufficient number of numerical statistics has been gathered (convergence of statistical results) enabling a statistically reliable assessment. These statistics practically define the basis of the present investigation and reveal the nature of the time to flood/capsize problem.

Time domain simulation method

The numerical simulation method applied herein for the calculation of the time to capsize of the damaged ship is a nonlinear time domain numerical method for the coupled problem of the motion and flooding of the damaged ship in waves. The motion is defined with six (6) degrees of freedom. The hydrodynamics of the problem are based on a linear potential theory, whereas a variety of important non-linear terms of ship's equations of motions are considered, like the excitation by large amplitude regular or irregular waves, the exact wetting of the body geometry below and above the still waterline and its impact on ship's restoring, semi-empirical nonlinear viscous damping as well as sloshing effects due to moving fluids internally to the vessel or trapped on the deck, *Spanos* (2002). The employed random waves are considered to follow a Gaussian process and are generated by a *Longuet-Higgins* model for both long and short crested waves. The flow through the openings is approached in a stationary way, a hydraulic model that is based on a modified Bernoulli equation, assuming that the flow rate is governed by the difference of the water head in neighbouring spaces interconnected with an opening(s).

The simulation method has been extensively tested and validated with comparisons to experimental measurements for a variety of cases and conditions, *Spanos et. al* (2002), *Spanos* (2002), *ITTC* (2002), (2005), thus it can be considered rather reliable and robust.

However, the high accuracy achieved by use of this method is computationally demanding. The computational performance could be improved when interested in specific probability levels, instead of analyzing the full behavior of the damaged ship as herein questioned. This might be achieved by application of probabilistic methods (like first or second order reliability methods FORM/SORM) as appropriate for the estimation of the time to capsize T_{CAP} to exceed threshold times.

The RoRo/Passenger Ferry

The RoRo/Passenger ferry employed in the present investigation, has been previously investigated by *ITTC* (2002) and (2005). The main dimensions are given in Table 1 below, both in full and model scale, as the calculations have been executed in the model one.

Table 1: Main dimension of the investigated RoRo/Passenger ship, source: ITTC (2002)

	Full Scale	Model Scale	Units
Scale	1:1	1:40	

L_{BP}	170.00	4.25	m
B	27.80	0.695	m
T	6.25	0.156	m
Displ.	17300	0.270	tn
D_{CAR}	9.00	0.225	m
KG	12.50	0.313	m

The basic damage case has been defined assuming a damage opening of 8.10 m longitudinal length (acc. to SOLAS Part B, Ch.II-1, Reg. 8.4), an unlimited vertical extension and triangular penetration of B/5. This damage case corresponds to the worst-case according to SOLAS'90 regulations. The opening is located about amidships resulting to a flooding of two adjacent compartments. For this damage case the equilibrium angle in calm water equals 3.2 degrees to port due to an asymmetry of the damaged compartments, as shown in Figure 2.

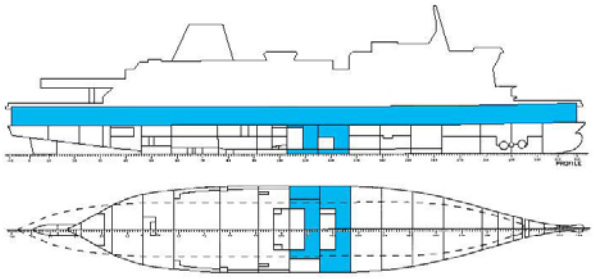

Figure 2 Two compartments damage case, source: ITTC (2002)

TIME TO CAPSIZE FOR THE DAMAGED FERRY

The numerical simulations account for initial conditions regarding the damage in calm water, zero speed and the damaged compartments below waterline being fully flooded. In that way any transient flooding effects were bounded and flooding in waves was dominant. The simulated beam waves were long-crested and deduced from a JONSWAP spectrum with the peak period randomly ranging between 3.5 and 6.0 times of square root of Hs and the peak enhancement parameter γ randomized between 1.0 and 4.0.

The typical behavior of the roll motion, for the non-survival tests, namely those leading to capsize of the vessel by the time of three (3) hours, is that shown in Figure 3. The vessel gradually heels under the effect of the accumulated floodwater on the car deck until the critical conditions were developed and then the vessel capsizes in a few wave periods.

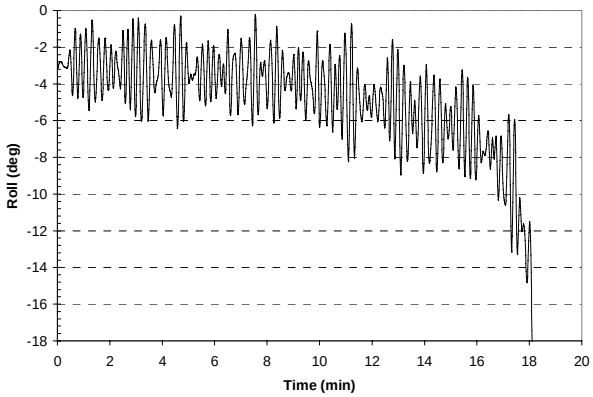

Figure 3 Sample roll time series of capsize test

The Survive Limit

The dependence of the time to capsize on the wave height is plotted in Figure 4. There, the time to capsize T_{CAP} is systematically recorded for selected values of the significant wave height Hs. For example, for Hs = 2.50 m the time to capsize ranges from 30 min (0.5 hr) up to 140 min (2 hrs and 20 min), with a mean value around 60 min (1 hr). When Hs equals 2.00 m none capsize occurred within 180 min (3 hr) simulation. The symbol shown at 180 min is to remind the execution of those tests.

The results of Figure 4 clearly demonstrate the presence of a limit wave height at 2.00 m where below that the T_{CAP} is infinite and above it the T_{CAP} converges asymptotically to the limit. This is actually a critical wave height corresponding to the studied damage case. We call this critical wave height the survive limit and distinguish it from the survive boundary, which is the lower boundary of the transition area between fully safe and unsafe conditions as pointed in Figure 4. Apparently, both survive (lower) and capsize (upper) boundaries

in the transition area asymptotically converge to the survive limit. The existence of the survive limit is explained from the fact that a least and finite wave height is necessary for the flooding of the car deck, which stands above the water line at the height of the damage freeboard.

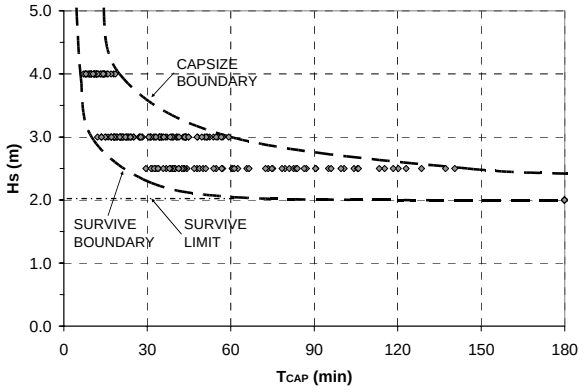

Figure 4 Time to capsize vs wave height

The boundaries recorded in Figure 4 for the RoRo/Passenger ferry are similar to boundaries for the Large Passenger ship as reported by Van't Veer (2004), where differently, the progressive flooding through a complicated internal arrangement was the prevailing flooding process. The fundamental difference of the boundaries between these two types of ship (RoRo/Passenger and cruiser) is the area between the survive boundary and the survive limit, which results rather small for the RoRo/Passenger ship compared to the Large Passenger. This rather small area evidences the substantial limited margins for the control of the time to capsize for the RoRo/Passenger ships.

When the waves are slightly higher than 2.0 m, namely between 2.0 and 2.50 m, a wide dispersion for the time to capsize occurs, revealing the rather random character of the flooding process as well as the reduced predictability at these conditions. When the waves are even higher then an abrupt reduction of the T_{CAP} is observed, with the time range becoming narrower and the mean value restricted to about 15 min (for Hs = 4.0 m).

Figure 5 samples the evolution of the mean value and the standard deviation over the sequence of the numerical simulation tests for the two cases those of Hs = 4.00 m and Hs = 2.50 m. The statistical convergence for the higher wave height of 4.00 m is apparent, whereas a slower (or even lack of) convergence is observed for the lower wave height of 2.50 m.

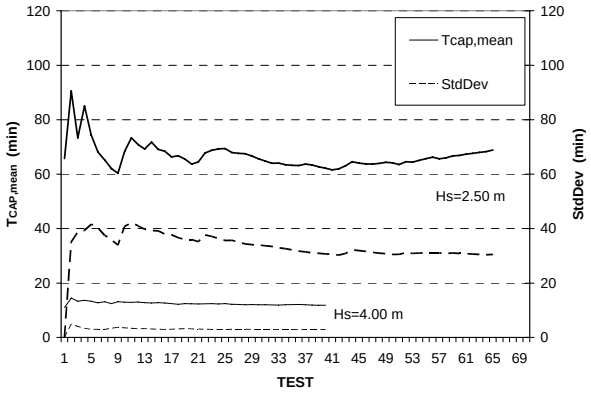

Figure 5 Mean value and standard deviation of T_{CAP}

In view of the damage stability of the RoRo/Passenger, the above findings are well correlated to the results of an investigation by *Vassalos* and *Papanikolaou* (2002) on the survive capacity of SOLAS'90 ships, which has been estimated on the basis of numerical and physical tests for a large sample of about thirty RoRo/Passenger ships, and was found about Hs=2.5 m. That estimation was actually based on the 30 min *survive boundary* (following Stockholm Agreement test procedures), as can be observed in Figure 4. Evidently, the ultimate survive capacity of the ship, namely regardless timeframes, is lower than 2.5 m, namely equal to 2.00 m, determined by the *survive limit*.

Parametric Investigation

To better observe the effect of the parameters that participate in the definition of the damage case on the time to capsize a parametric study has been conducted where the basic parameters have been changed to define four additional tests series, the Series 2 up to 5. For Series 2, the length of the damage opening has been reduced to the half-length of that of the basic Series 1. The vertical center of gravity has been increased by 30 cm for Series 3, with a

proportional reduction of GM. The pitch has been fixed for Series 4 in order to cancel any possible *dead water* on deck, which may result in presence of trim and which drastically affect the stability of the vessel, *Pawlowski* (2006). In the last Series 5 the height of the car deck, the freeboard accordingly, has been reduced by 0.50 m.

For each of the above test series a similar procedure to Series 1, the basic case, has been applied for the generation of numerical statistics, which are shown in Figure 6.

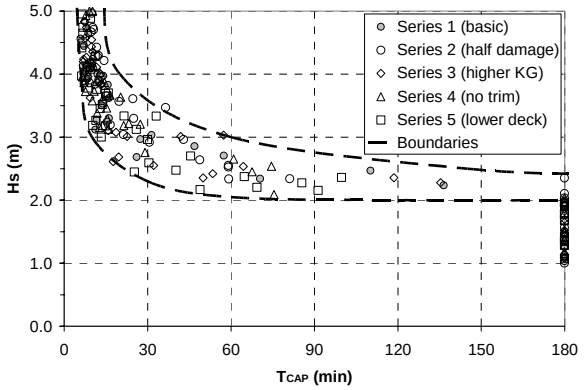

Figure 6 Numerical statistics for time to capsize

The above mess of results reveals an important fact, namely that none of the studied changes alters substantially the survive boundary results as determined from the basic damage case. The survive limit of 2.00 m is still recognizable, with the time to capsize converging asymptotically to this limit and all the tests below that wave height are survivals within three (3) hours.

PROBABILITY OF TIME TO CAPSIZE

Probability derivation

In order to derive a robust probabilistic formulation of the time to capsize for the damaged RoRo/Passenger ship in waves the numerical statistics of all the test series, as defined above, have been taken into account.

The derived statistical probability density of the time to capsize together with a corresponding regression analysis approach, are presented in Figure 7.

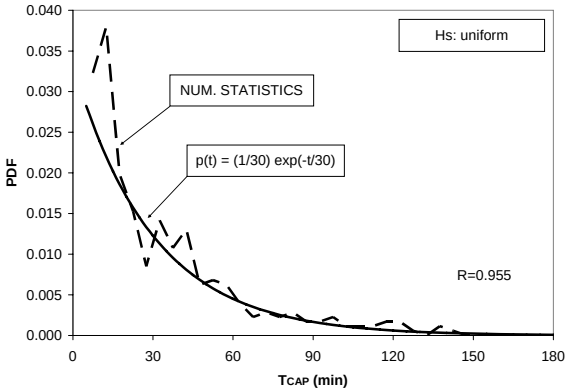

Figure 7 Probability of Time to Capsize of the RoRo/Passenger in waves, with Hs uniformly above survive limit

It is remarkable that the regression curve corresponds to an exponential probability distribution over the time to capsize T_{CAP} in min. The parameter defining the distribution equals (1/30), relating the time to capsize to a characteristic time of 30 min, which independently happens to be equal to the regulatory time for the safe evacuation of SOLAS'90 ships. In probabilistic terms this parameter determines the average capsize rate in the set conditions. Hence, the expected time to capsize for the RoRo/Passenger ship flooded in waves, is predicted to be one capsize every 30 min.

The above derived probability distribution has been based on a *uniform distribution* of the significant wave height Hs over the range considered, namely between the survive limit and 5.00 m. If another perspective of the time to capsize is considered, for example that corresponding to some particular wave statistics, then this probability needs to be modified accordingly.

Specifically, if the conditional probability of T_{CAP} for a certain wave height value Hs is considered, then this probability can be easily derived from the data of Figure 4. Such distribution varies around a mean value with definite width and has zero density for low capsize times. Apparently, it substantially deviates from the exponential probability distribution of Figure 7, and the exponential distribution proposed earlier by *Jasionowski*

(2006) for the conditional probability of T_{CAP} for certain Hs.

Another perspective of more general interest is to apply the wave height distribution recorded in collision events, as it has been introduced by the E.U. research project HARDER (2000). According to this distribution the probability of wave height gradually decreases in the higher wave height values, see *Tagg* (2002). When applying such distribution, the numerical statistics inherently change and the probability of the time to capsize results to that presented in Figure 8.

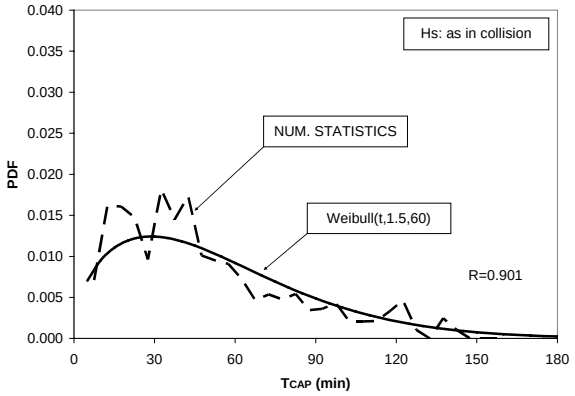

Figure 8 Probability of Time to Capsize of the RoRo/Passenger in waves, with Hs as in collision events

This probability distribution can be approached by a Weibull distribution with the two parameters a=1.5 and b=60. In comparison to the uniform distribution of the wave height applied in Figure 7, it shows that the lower waves, which are closer to the survive limit and are correlated with the wide range distributions of T_{CAP}, contribute more than the higher waves that correspond to shorter times T_{CAP}. As a result, the probability for a zero time to capsize vanishes with a relevant shift of the probability mass towards longer times.

Survive for long time

The above probability distributions for the time to capsize T_{CAP} have been derived through a pure numerical statistics approach and express the perspective of T_{CAP} for a damaged RoRo/Passenger ship in waves, in the first case assuming a uniform distribution of the wave height and in the second, assuming the waves to be distributed more realistically according to historical data of the waves during the collision events. According to these results the probability of a ship to remain upright for a certain time after the damage and waves be higher than 2.00 m (the survive limit) can be estimated as figured in Table 2.

Table 2: Probability to capsize in late times

	T_{CAP} later than	30 min	1 hr	2 hr	3 hr
Waves	Uniform	36.8 %	13.5 %	1.80 %	0.20 %
	collision statistics	70.2 %	36.8 %	5.90 %	0.55 %

According to these numbers the differences between the two cases assumed, are practically limited within the first hour period after damage incidence. After the first hour, the two distributions converge to zero and practically to each other. The probability to survive for long times after damage, namely after three (3) hours, and in presence of waves higher than the survive limit, is quite small practically negligible.

Considering that Table 2 provides the conditional probability of capsize in waves higher that 2.00 m and that the probability of waves higher than 2.00 equals 10% according HARDER project, the expectations after the damage are: in 90% of the damage cases the ship will survive (because Hs < 2.00 m), and in 10% she will not survive (Hs > 2.00 m). Where that 10% is further analyzed into 6.3% capsize within the first hour, 3.1% within the second hour, and just 0.6% to capsize later than 2 hours. It is reminded that the derived results have been based on the criterion of actual capsize instead of other conventional capsize criterion (e.g. loss of stability or exceeding a certain roll angle), hence, the estimated probabilities form an upper boundary for the expected times to capsize.

CONCLUSIONS

The present investigation has shown the critical character of the *survive limit* on the survivability of a damaged RoRo/Passenger ship. The ship will survive any case in which

incident waves are below the survive limit, and will eventually soon or late capsize any case over this limit.

The time the ship takes to capsize in non-survival cases, is reduced rapidly with the increase of the wave height above the survive limit. This rapid reduction has been found to be quite independent of the basic assumptions on the ship loading condition, the damage opening and the depth of car deck. These findings suggest that the RoRo/Passenger ferry disposes apparently no practical time margins for safe evacuation and abandonment.

ACKNOWLEDGMENTS

The presented work has been conducted under the research project SAFEDOR (Design, Operation and Regulation for Safety), SP 2.1, which is funded by the European Commission under the FP6 Sustainable Surface Transport Programme, Contract No. FP6-IP-516278. The European Commission and the authors shall not in any way be liable or responsible for the use of any knowledge, information or data presented, or of the consequences thereof.

REFERENCES

HARDER, E.C. research project, Harmonization of Rules and Design Rational, DG XII-BRITE, 2000 - 2003.

IMO – Maritime Safety Committee, 78th session, MSC 78/WP.14, May 20, 2004

IMO – Maritime Safety Committee, 80th session, MSC 80/WP.11/Add/1/Rev.1, May 19, 2005

IMO – Maritime Safety Committee, 82nd session, MSC 82/WP.13, December 4, 2006

ITTC - The Specialist Committee on Prediction of Extreme Ship Motions and Capsizing, Final Report and Recommendations to the 23rd ITTC, Proc. of the 23rd ITTC, Vol. II, 2005, pp. 633-649.

ITTC - The Specialist Committee on Stability in Waves, Final Report and Recommendations to the 24th ITTC, Proc. of the 24th ITTC, Vol. II, 2005, pp. 383-390.

Jasionowski, A., Fast and accurate flooding prediction – analytical model. E.U. research project SAFEDOR, SP.2.1, Doc. Id. SAFEDOR-D-WP2.1.3-2006-11-30-SSRC-rev.0, 2006

Papanikolaou, A., Spanos, D., Boulougouris, E., Eliopoulou, E. and Alissafaki, A., Investigation into the Sinking of the RoRo Passenger Ferry Express Samina, Proc. Of the 8th Inter. Conf. on the Stability of Ships and Ocean Vehicles, Madrid, Sep. 15-19, 2003.

Pawlowski, M., Effect of Decks on Survivability of Ro-Ro vessels. Proceedings of the 9th Inter. Conf. On Stability of Ships and Ocean Vehicles, Rio de Janeiro, Brazil, Sep. 25-29, 2006.

SAFEDOR, E.U. research project, SP2.1, Fast and accurate flooding prediction – analytical model. Project No. IP-516278, 2005 - 2007.

Spanos, D., Papanikolaou, A., On the Stability of Fishing Vessels with Trapped Water on Deck. Journal Ship Technology Research-Schiffstechnik, Vol. 48, Sep. 2001.

Spanos, D., Maron, A., Papanikolaou A., On the Motions of a Flooded Ro-Ro Ferry in Beam Seas. Proc. of 10th Inter. Congress of International Maritime Association of Mediterranean, Crete, Greece, May 14-18, 2002.

Spanos, D., Time Domain Simulation of Motion and Flooding of Damaged Ships in Waves. Doctoral Thesis, Ship Design Lab., National Technical University of Athens, 2002.

Tagg, R., Tuzcu, C., A performance-based assessment of he survival of damaged ships – Final outcome of the EU research project HARDER, Proc. of the 6th Inter. Ship Stability Workshop, Webb Institute, 2002.

Van't Veer, R., De Kat, J. , Cojean, P., Large Passenger Ship Safety: Time-to-Flood Simulations, Marine Technology, Vol. 41, No. 2, 2004, Apr., pp. 82-88.

Vassalos, D., Oestvik, I. and Konovessis, D., Design for Safety: Development and Application of a Formalised Methodology, Proc. of the 7th Inter. Marine Design Conference, May 21-24, 2000, Kyongju, Korea, pp. 151-165.

Vassalos, D., Papanikolaou, A., Stockholm Agreement – Past, Present, Future (Part 1 & 2). Marine Technology, Vol. 39, Part 1: No. 3, July 2002, pp. 137-158, Part 2: No. 4, October 2002, pp. 199-210.

Extensions to a Pressure-Correction Method for Simulation of Progressive Flooding

Pekka Ruponen

Napa Ltd & Helsinki University of Technology, Finland

ABSTRACT

The latest improvements and advances of the simulation method for progressive flooding of damaged passenger ships, developed at Helsinki University of Technology in close co-operation with Napa Ltd are presented. This includes the derivation of the pressure-correction equation for openings with high vertical extent and a simple sensitivity analysis of the developed method for the opening parameters, such as critical pressure heads.

KEYWORDS

Flooding simulation, progressive flooding, pressure-correction method, sensitivity analysis

INTRODUCTION

Napa Ltd and Helsinki University of Technology have in co-operation developed a novel time-domain simulation method for progressive flooding. The principle idea of applying pressure-correction technique for flooding simulation was presented in Ruponen (2006), based on the assumption that all openings are relatively small. Some examples of the validation of this method were presented in Ruponen et al. (2006). In this paper, an extension of this simulation method is presented, along with a brief revisit to the theoretical background. Furthermore, a preliminary study on the sensitivity of the simulation results on the applied parameters for the modelled openings is presented.

The pressure-correction technique is very suitable for the flooding cases, where also air compression and the resulting airflows are significant. However, for the cause of simplicity, in this paper it is assumed that the air pressure is constant throughout the flooding process.

PRESSURE-CORRECTION METHOD FOR FLOODING SIMULATION

Background

Usually flooding simulation methods are based on the volumes of floodwater that are integrated explicitly from the flow velocities that are calculated from Bernoulli's equation. The water height differences are then calculated from the volumes of water with the heel and trim angles taken into account. However, the applied simulation method is based on a completely different approach, where the volumes are calculated on the basis of water heights and the heel and trim angles. This is reasonable as the water height is physically more meaningful than the volume of water since it represents the hydrostatic pressure. Consequently, the progress of the floodwater can be solved implicitly on the basis of the pressures in the rooms and the velocities in the openings.

The ship model for flooding simulation can be considered as an unstructured and staggered grid (Fig. 1). Each modelled room is used as a

single computational cell. However, the flux through a cell face is possible only if there is an opening that connects the rooms (cells).

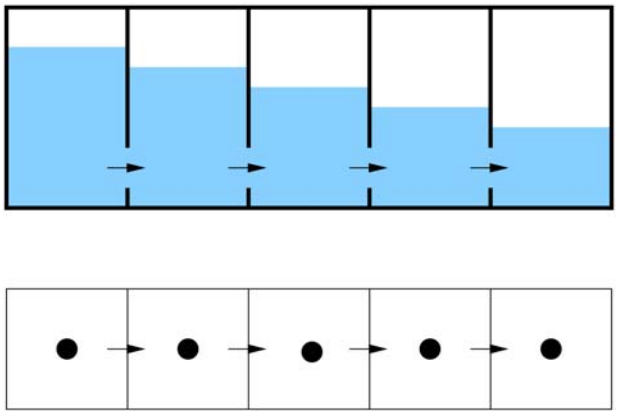

Fig. 1: Staggered grid in flooding simulation

Governing Equations

At each time step the conservation of mass must be satisfied in each flooded room. The equation of continuity for water is:

$$\int_{\Omega} \frac{\partial \rho}{\partial t} d\Omega = -\int_{S} \rho_w \mathbf{v} \cdot d\mathbf{S} \qquad (1)$$

where ρ_w is density, **v** is the velocity vector and **S** is the surface that bounds the control volume Ω. The normal vector of the surface points outwards from the control volume, hence the minus sign on the right hand side of the equation.

The mass balance for water, i.e. the residual of the equation of continuity, in the room *i* can be expressed as:

$$\Delta \dot{m}_{w,i} = \rho_w S_{fs,i} \frac{dH_{w,i}}{dt} + \rho_w \sum_k Q_{w,k} \qquad (2)$$

where S_{fs} is the area of free surface in the compartment (assumed to be constant during the time step), H_w is the water height and Q_w is the volumetric water flow through an opening in the compartment. The index *k* refers to an opening in the room *i*.

The velocities in the openings are calculated by applying Bernoulli's equation for a streamline from point A that is in the middle of a flooded room to point B in the opening:

$$\int_A^B \frac{dp}{\rho} + \frac{1}{2}\left(u_B^2 - u_A^2\right) + g\left(h_B - h_A\right) = 0 \qquad (3)$$

where *p* is air pressure, *u* is flow velocity and *h* is height from the reference level. It is assumed that the flow velocity is negligible in the center of the room ($u_A = 0$).

The equation (3) applies for inviscid and irrotational flow. The pressure losses in the openings and pipes are taken into account by applying semi-experimental discharge coefficients. Consequently, the mass flow through an opening *k* is:

$$\dot{m}_{w,k} = \rho_w Q_{w,k} = \rho_w C_{d,k} A_k u_k \qquad (4)$$

where $Q_{w,k}$ is the volumetric flow through the opening, $C_{d,k}$ is the discharge coefficient, A_k is the area of the opening and u_k is velocity. Basically equation (4) applies only to very small openings. In the next chapter, the handling of tall openings is considered in detail.

Bernoulli's equation for water flow through the opening *k* that connects the compartments *i* and *j* (positive flow from *i* to *j*) can be written in a form of a pressure loss:

$$\frac{1}{2} K_k' \dot{m}_{w,k} \left| \dot{m}_{w,k} \right| = \left(P_i - P_j\right)_k \qquad (5)$$

where the absolute value is used to define the direction of the flow. The dimensional pressure loss coefficient is defined as:

$$K_k' = \frac{1}{\rho_w C_{d,k}{}^2 A_k^2} \qquad (6)$$

The total pressure difference for an opening *k* that connects the compartments *i* and *j* is:

$$\left(P_i - P_j\right)_k = \rho_w g \cdot \left[f(i,k) - f(j,k) \right] \qquad (7)$$

where the following auxiliary function is used:

$$f(i,k) = \max\left(H_{w,i} - H_{o,k}, 0\right) \tag{8}$$

where H_w is the height of the water level and H_o is the height of the opening, measured from the same horizontal reference level. It is also possible to deal with openings that can be formed when structures (e.g. closed doors or down-flooding hatches) collapse under the pressure of the floodwater.

Pressure-Correction Equation

The linearization of equation (5) results in:

$$K'_{w,k}\left|\dot{m}^*_{w,k}\right|\dot{m}'_{w,k} = P'_i - P'_j \tag{9}$$

Consequently, by using equations (2) and (9), the following pressure-correction equation can be derived (see Ruponen, 2006):

$$\sum_k \frac{F(i,k)\cdot H'_{w,i} - F(j,k)\cdot H'_{w,j}}{K'_{w,k}\rho_w\left|Q^*_{w,k}\right|} + \frac{3}{2}\frac{\rho_w S_{fs,i}}{\Delta t} H'_{w,i} = -\Delta\dot{m}^*_{w,i} \tag{10}$$

where the following auxiliary function is used:

$$F(i,k) = \max\left[\text{sign}\left(H_{w,i} - H_{o,k}\right), 0\right] \tag{11}$$

Equation of Motion

The previous study (Ruponen et al., 2006) was based on the assumption of quasi-stationary motions of the flooded ship. In order to get more realistic results, the roll motion $\phi(t)$ is solved from the following equation:

$$A_{xx,tot}\cdot\ddot{\phi} + B_{xx,tot}\cdot\dot{\phi} + M_{st}(\phi) = M_{ext}(V_{w,i}) \tag{12}$$

where $A_{xx,tot}$ is the sum of inertia and added mass and $B_{xx,tot}$ represents linear damping. M_{st} is the righting moment and M_{ext} is the heeling moment due to floodwater. The natural roll period and critical damping ratio for the intact ship can be obtained from the roll decaying test or seakeeping calculations. The trim and draft are still considered to be quasi-stationary.

EXTENDED HANDLING OF TALL OPENINGS

Calculation of Volumetric Flow

In the previous chapter, a pressure-correction equation was derived by assuming that the openings are so small that they can be considered as points. In practice, this simplification is not always valid. Therefore, it is essential that the simulation method is extended to deal with tall openings as well.

A more realistic, yet simple, representation for an opening with significant vertical height, such as an open door, is a straight line with a given area. A similar approach was used in Dillingham (1981) for calculation of two-dimensional flow over a bulwark and in Pawlowski (2003) for an opening with a constant width. However, in practice this method requires an additional assumption that the flow velocity is always perpendicular to the opening. The opening line can be considered as three separate openings since the sections $\overline{AB}$, $\overline{BC}$ and $\overline{CD}$ are treated individually, see Fig 2.

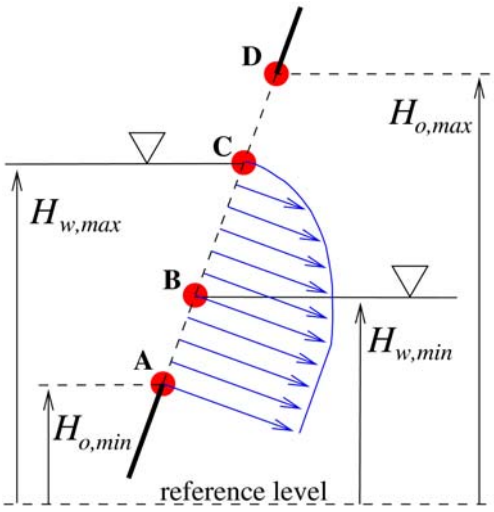

Fig. 2: Opening line

The section $\overline{AB}$ corresponds to an opening point with the same area since the flow through

this section depends on both water heights but not on the vertical location of the opening. Consequently, no separate handling is needed.

The section $\overline{CD}$ corresponds to an opening point for airflow. Consequently, the shape of the opening has no effect on the computation of airflow. In this paper, it is assumed that all rooms are fully vented, and consequently air pressure is constant.

The section $\overline{BC}$ needs to be treated with a different way since the volumetric flow through this section must be integrated. This affects also the pressure-correction equation for water heights. A detailed description of the applied methods is given in the following.

The volumetric water flow through the section $\overline{BC}$ is obtained by integration of the flow velocity u over the corresponding part of the opening line (see Fig. 3):

$$Q_{w.BC} = b \cdot \int_0^{\overline{BC}} u \cdot dl \qquad (13)$$

where b is the width of the opening.

Similarly to the case of a one-dimensional opening point, let us consider a streamline from point E that is in the middle of the flooded room, to point F that is in the opening between the points B and C. The following heights for the points along the streamline are used:

$$\begin{aligned} h_E &= H_C \\ h_F &= H_B + l \cdot \sin\beta \end{aligned} \qquad (14)$$

where l is the distance from the point B along the opening line and β is the angle between the reference level and the opening line, see Fig. 3.

The flow velocity is obtained from equation (3) and the pressure losses are taken into account in the form of a discharge coefficient. Consequently, the following equation for the volumetric water flow through the section $\overline{BC}$ can be obtained:

$$Q_{w.BC} = C_d b \int_0^{\overline{BC}} \sqrt{2g\left[H_{w,max} - \left(H_B + l \cdot \sin\beta\right)\right]}\, dl \qquad (15)$$

where C_d is the discharge coefficient for the opening when the jet discharges into air.

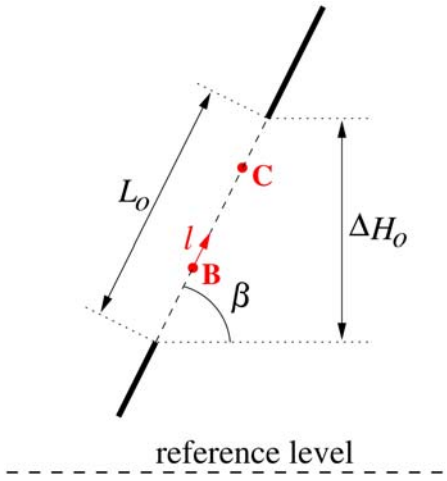

Fig. 3: The angle between the opening line and the horizontal reference level

It is practical to assume that the changes of the water height are rather small, so that $H_{w,max} \approx H_C$ and $H_{w,min} \approx H_B$. Consequently, equation (15) can be written as:

$$Q_{w.BC} = C_d b \cdot \int_0^{\overline{BC}} \sqrt{2g\left[H_C - \left(H_B + l \cdot \sin\beta\right)\right]}\, dl \qquad (16)$$

This can be evaluated analytically:

$$Q_{w.BC} = C_d \cdot b \cdot \frac{2 \cdot \sqrt{2g}}{3 \cdot \sin\beta} \cdot \left[\left(H_C - H_B\right)^{\frac{3}{2}} - \left(H_C - H_B - \overline{BC}\sin\beta\right)^{\frac{3}{2}}\right] \qquad (17)$$

The inclination angle of the opening line, i.e. the angle between the water levels and the opening (Fig. 3), can be evaluated on the basis of the vertical distance between the end points of the opening line (ΔH_o). Consequently:

$$\sin\beta = \Delta H_o / L_o \qquad (18)$$

Equation (17) can be presented in a simpler form since the vertical distance between the points B and C is:

$$H_C - H_B = \overline{\mathrm{BC}} \cdot \sin\beta \tag{19}$$

Hence, the volumetric flow, equation (17), can be approximated with the following equation:

$$Q_{w.BC} = C_d \cdot b \cdot \frac{2 \cdot \sqrt{2g}}{3 \cdot \sin\beta} \left(H_C - H_B\right)^{\frac{3}{2}} \tag{20}$$

The area of the opening between the points B and C is:

$$A_{BC} = b \cdot \overline{\mathrm{BC}} = b \cdot \frac{\left(H_C - H_B\right)}{\sin\beta} \tag{21}$$

Therefore, equation (20) can be simplified to:

$$\begin{aligned} Q_{w.BC} &= C_d b \frac{2\sqrt{2g}}{3\sin\beta} \left(H_C - H_B\right) \sqrt{H_C - H_B} \\ &= C_d A_{BC} \frac{2}{3} \sqrt{2g\left(H_C - H_B\right)} \end{aligned} \tag{22}$$

The basic form of the rearranged equation for the volumetric flow (22) is the same as in the equation for the flow through a one-dimensional opening, multiplied by the coefficient 2/3. This relation is used in the following when the pressure-correction equation is derived.

Pressure-Correction Equation

The equation (22) can be presented in the form of a pressure loss, similarly to equation (5). The mass flow of water through the section $\overline{\mathrm{BC}}$ is:

$$\dot{m}_{w,BC} = \rho_w \cdot C_d \cdot A_{BC} \cdot \frac{2}{3} \sqrt{2g\left(H_C - H_B\right)} \tag{23}$$

and the square of the mass flow, divided by two is:

$$\begin{aligned} &\frac{1}{2} \dot{m}_{w,BC} \left|\dot{m}_{w,BC}\right| \\ &= \rho_w^2 \cdot C_d^2 \cdot A_{BC}^2 \cdot \frac{4}{9} \cdot g\left(H_C - H_B\right) \end{aligned} \tag{24}$$

This can be rearranged to:

$$\begin{aligned} &\frac{1}{2} \cdot \left(\frac{1}{\frac{4}{9} \cdot \rho_w \cdot C_d^2 \cdot A_{BC}^2} \right) \cdot \dot{m}_{w,BC} \left|\dot{m}_{w,BC}\right| \\ &= \rho_w g\left(H_C - H_B\right) \end{aligned} \tag{25}$$

Moreover, this can be simplified by applying the dimensional pressure loss coefficient, defined in (6). Therefore, equation (25) can be written as:

$$\frac{1}{2} \cdot \frac{9}{4} \cdot K'_w \dot{m}_{w,BC} \left|\dot{m}_{w,BC}\right| = \rho_w g\left(H_C - H_B\right) \tag{26}$$

The basic form of this equation is similar to the pressure loss equation for one-dimensional opening (5), but the dimensional pressure loss coefficient is multiplied by a constant factor of 9/4. Therefore, the same form of the pressure-correction equation can be used when this additional coefficient is taken into account.

The total volumetric water flow through the opening *k* consists of two parts:

$$Q^*_{w,k} = Q^*_{w,AB,k} + Q^*_{w,BC,k} \tag{27}$$

Consequently, the pressure-correction equation (10) for water heights in the case of two-dimensional openings can be rewritten as:

$$\begin{aligned} &\sum_k \left[\frac{H'_{w,i} - H'_{w,j}}{K'_{w,AB,k} \rho_w \left|Q^*_{w,AB,k}\right|} \right. \\ &\left. + \frac{4}{9} \cdot \frac{G(i,,j) \cdot H'_{w,i} - G(j,i) \cdot H'_{w,j}}{K'_{w,BC,k} \rho_w \left|Q^*_{w,BC,k}\right|} \right] \\ &+ \frac{3}{2} \frac{\rho_w S_{fs,i}}{\Delta t} H'_{w,i} = -\Delta \dot{m}^*_{w,i} \end{aligned} \tag{28}$$

where the following auxiliary function is used:

$$G(i,j) = \max\left[\mathrm{sign}\left(H_{w,i} - H_{w,j}\right), 0\right] \tag{29}$$

The first term on the left hand applies for the water flow discharging into water since the mass flow depends on both water heights. The

second term on the left hand side is for the water flow discharging into air since this part of the mass flow only depends on the water height on the maximum pressure side. The underlined term is taken into account only if the room is not filled with water. In principle, the basic form of the pressure-correction equation is exactly the same as in the case of one-dimensional opening points, equation (10).

Discontinuities should be avoided during the iteration process in order to ensure convergence,. Therefore, the points B and C are kept constant during the time step. This simplification should not cause significant error if the applied time step is sufficiently short.

The applicability of this implementation has been tested by performing comparative simulations, where the tall openings were modelled with several individual points. An example of the comparisons is presented in Fig. 4.

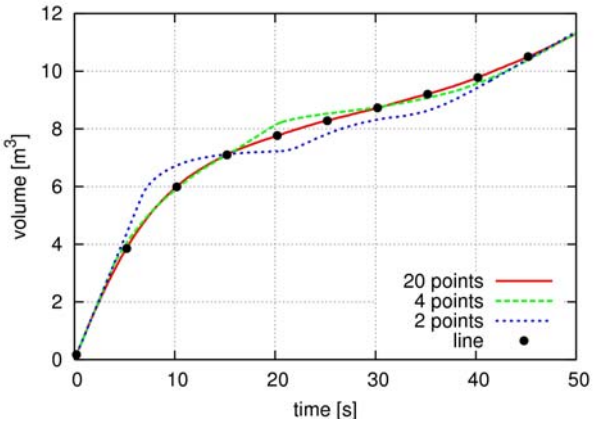

Fig. 4: Comparison of different modelling techniques for a tall opening

In this case, 20 evenly distributed opening points give practically the same result as one vertical opening line. The difference is increased as the number of opening points is decreased. When the whole opening is submerged (volume of floodwater is larger than 10 m^3) the modelling of the opening does not affect anymore.

SENSITIVITY ANALYSIS

Background

The current knowledge on leaking and collapsing of non-watertight structures is rather limited. The presented case study provides some initial framework for the future experimental studies with various structures.

Damage Case

The studied case is a two-compartment damage in a medium sized passenger ship of 40 000 GT. The flooded compartments contain crew cabins and store areas. All doors are considered to be initially closed. The modelled rooms and openings (i.e. the computational grid) are shown in Fig. 5.

Simulations were performed with a constant time step of 1.0 s. The applied convergence criterion corresponds to a water height difference of 0.05 mm. It was checked that a shorter time step or a stricter criterion did not affect the results.

The values for leaking and collapsing pressure heads and leaking ratios, presented in IMO SLF47/INF.6 (2004) were used as a basic case. However, the presented A_{ratio} values, are quite high. Vartiainen (2006) has concluded that much smaller values might be more realistic. Therefore, these values were reduced by 50 % for the other simulations. The applied values are listed in Table 1. In all cases, H_{leak} = 0.0 m and C_d = 0.6 were used for all openings.

The equilibrium floating position is shown in Fig. 6 and the calculated time histories for heeling and total volume of floodwater are presented in Fig. 7 and Fig. 8, respectively. In the studied case the heeling is very minimal due to the large initial stability and symmetry in the flooding process. The applied A_{ratio} values seem to have a remarkable effect on the time-to-flood. On the other hand, a 20 % increase in the critical pressure head for collapsing has much smaller effects on the flooding process.

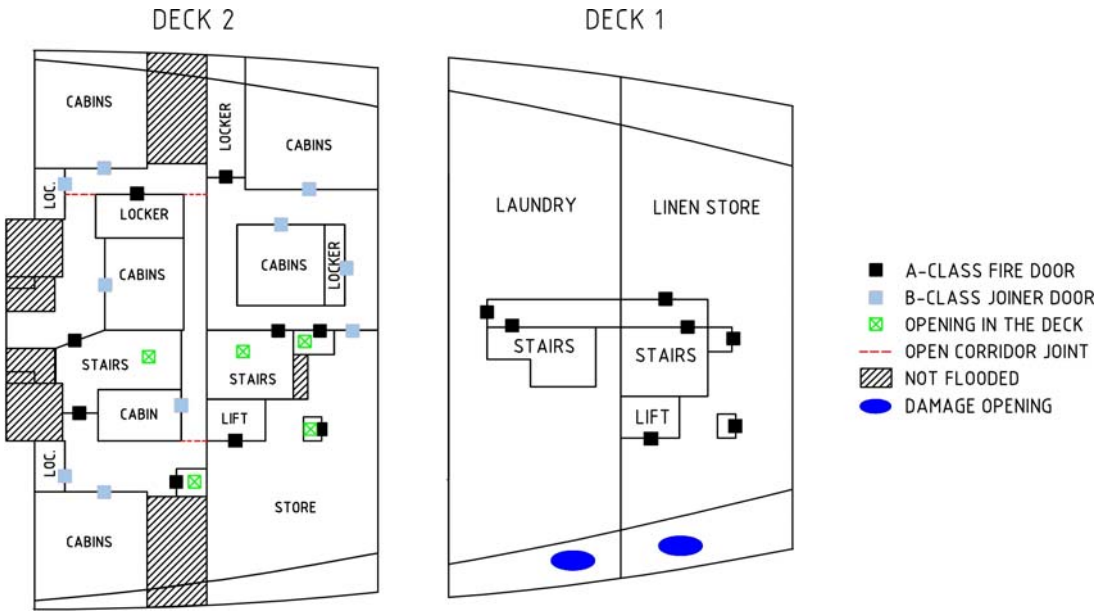

Fig. 5: Modelled rooms and openings, deck 2 (left) and deck 1 (right)

Table 1: Applied parameters for leaking and collapsing of non-watertight doors

Case	*A-class*		*B-class*	
	H_{coll}	A_{ratio}	H_{coll}	A_{ratio}
SLF47/INF.6	2.0 m	0.10	1.5 m	0.20
A_{ratio} –50%	2.0 m	0.05	1.5 m	0.10
A_{ratio} –50% H_{coll} +20%	2.4 m	0.05	1.8 m	0.10

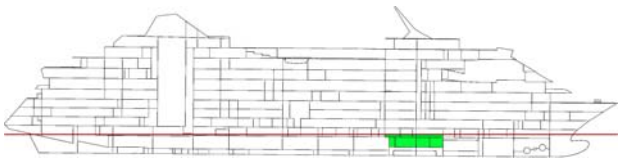

Fig. 6: Studied damage case, final equilibrium floating position

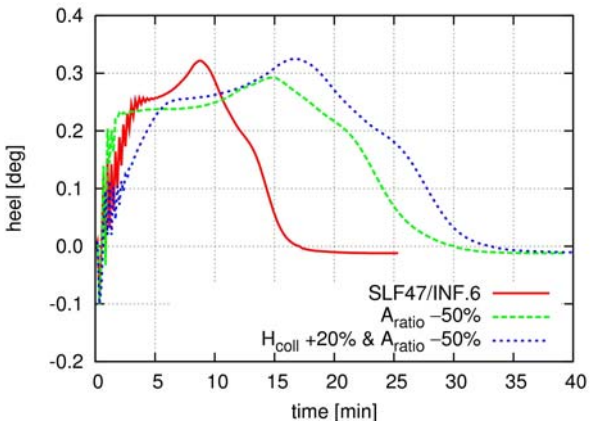

Fig. 7: Calculated heeling angle with various parameters for closed doors

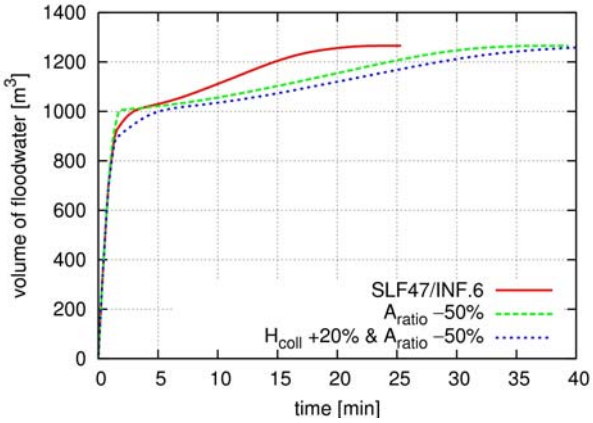

Fig. 8: Calculated total volume of floodwater with various parameters for closed doors

CONCLUSIONS

An enhanced version of the simulation method for progressive flooding with the use of pressure-correction technique has been presented. The calculated case study could be solved easily and the iterations converged properly.

Some notable conclusions can be drawn from the results of the sensitivity analysis. In particular, high A_{ratio} values can lead to a situation, where the door will not collapse at all, since the leaking through the door is so significant that the pressure difference remains small. In the studied case, collapsing of doors took place only on deck 1, during the first two minutes of the flooding. Consequently, it is of uttermost importance that the failure process of different door types is systematically studied with full scale experiments. On the other hand, the results are also promising since a small difference in the critical pressure head for collapsing does not cause significant changes in the time-to-flood and the overall flooding process.

Even the best simulation methods cannot provide realistic results if the input parameters for potential openings, such as closed doors, are not known, accurately enough. Therefore, systematic studies are necessary in order to increase the reliability of flooding simulations.

ACKNOWLEDMENTS

Anna-Lea Routi and Aker Yards are thanked for providing the ship design for the sensitivity analysis.

REFERENCES

Dillingham, J. 1981. Motion Studies of a Vessel with Water on Deck, Marine Technology, Vol. 18, No. 1, pp. 38-50.

IMO SLF47/INF.6 2004. Large Passenger Ship Safety: Survivability Investigation of Large Passenger Ships, submitted by Finland, 11. June 2004.

Pawlowski, M. 2003. Accumulation of Water on the Vehicle Deck, Proc. Instn Mech. Engrs. Vol. 217 Part M: J. Engineering for the Maritime Environment, pp. 201-211.

Ruponen, P. 2006. Pressure-Correction Method for Simulation of Progressive Flooding and Internal Air Flows, Schiffstechnik – Ship Technology Research, Vol. 53, No. 2, pp. 63-73.

Ruponen, P., Sundell, T., Larmela, M. 2006. Validation of a Simulation Method for Progressive Flooding, Proceedings of the 9th International Conference on Stability of Ships and Ocean Vehicles, Rio de Janeiro, Brazil, 25-29.9.2006, Vol. 2, pp. 607-616.

Vartiainen, M. 2006. Evaluation of Flooding Simulation as a Ship Design Tool, Master's Thesis, Helsinki University of Technology, 100 p.

Time Domain Simulation of Cross-Flooding for Air Pipe Dimensioning

Pekka Ruponen

Napa Ltd & Helsinki University of Technology, Finland

Anna-Lea Routi

Aker Yards, Finland

ABSTRACT

An efficient method for the dimensioning of air pipes from the voids by using a novel time-domain flooding simulation tool is presented. The principles of the applied simulation method are briefly described and a thorough case study for the cross-flooding time in a U-shaped void of a modern large passenger ship design is reported. The presented method can be used for assessing sufficient dimensions for the air pipes. Furthermore, the required detail level for modelling of the cross-duct and the applied parameters for the pressure losses are discussed.

KEYWORDS

cross-flooding, simulation, air pipe, IMO Resolution A.266

INTRODUCTION

The IMO Resolution A.266 (VIII) for assessment of the cross-flooding times is currently being revised with special attention to the effect of counter air pressure in rooms, where the ventilation level is restricted. In IMO SLF50/WP.1 Annex 2 (2007), it is stated that full ventilation can be assumed if the area of the air pipes is at least 10 % of the area of the cross-flooding openings. Thus, for example the effect of the air pipe length is not considered at all for large pipes.

An efficient and practical method for assessing the cross-flooding time with all kinds of arrangements is dedicated time-domain flooding simulation, where the compression of air and the resulting airflows are properly taken into account. This kind of simulation is accepted as an alternative method for the assessment of cross-flooding time in the revised Resolution A.266.

Peters et al. (2003) have applied a time-domain flooding simulation and seakeeping tool for studying the effectiveness of various cross-flooding arrangements in naval ships. Vredeveldt and Journée (1991) and Xia et al. (1999) have considered cross-flooding and the counter air pressures with a simplified model. In this paper, a combination of these two approaches is presented, with relation to the revised Resolution A.266.

U-shaped voids are used in passenger ship designs since there are several benefits. Firstly, the voids give good protection against minor side damages, for example when steering the vessel into quay. Furthermore, they prevent unallowed oil leakage into sea as the voids form a kind of double hull. Due to these benefits, also the A-index is slightly increased. If the breadth of the side spaces is reasonably small, the U-shaped void does not significantly reduce the volume of the machinery space, and consequently, the design is feasible.

SIMULATION METHOD

Background

The presented cross-flooding calculations were performed with the NAPA Flooding Simulation tool, developed in close co-operation between Helsinki University of Technology (TKK) and Napa Ltd. The principles of the method are briefly described in the next section and in detail in Ruponen (2006). This implicit and iterative method allows time-accurate and efficient solutions for flooding problems that include airflows. The simulation method has been validated with dedicated model tests and some results have been presented in Ruponen et al. (2006).

Governing Equations

At each time step the conservation of mass must be satisfied in each flooded room, both for water and air. In general, the equation of continuity is:

$$\int_{\Omega} \frac{\partial \rho}{\partial t} d\Omega = -\int_{S} \rho \mathbf{v} \cdot d\mathbf{S} \qquad (1)$$

where ρ is the density of the fluid, **v** is the velocity vector and **S** is the surface that bounds the control volume Ω. The normal vector of the surface points outwards from the control volume, hence the minus sign on the right hand side of the equation.

The velocities in the openings are calculated by applying Bernoulli's equation for a streamline from point A that is in the middle of a flooded room to point B in the opening. Consequently:

$$\int_{A}^{B} \frac{dp}{\rho} + \frac{1}{2}\left(u_B^2 - u_A^2\right) + g\left(h_B - h_A\right) = 0 \qquad (2)$$

where p is air pressure, u is flow velocity and h is the height from the reference level. It is also assumed that the flow velocity is negligible in the center of the room ($u_A = 0$).

The equation (2) applies for inviscid and irrotational flow. The pressure losses in the openings and pipes are taken into account by applying semi-experimental discharge coefficients. Consequently, the mass flow through an opening is:

$$\dot{m} = \rho Q = \rho C_d A u \qquad (3)$$

where Q is the volumetric flow through the opening, C_d is the discharge coefficient and A is the area of the opening. For pipes and ducts, the discharge coefficient is usually calculated from the sum of the pressure loss coefficients k_i, so that:

$$C_d = \frac{1}{\sqrt{1 + \sum_i k_i}} \qquad (4)$$

The flooding process is assumed to be isothermal. Therefore, Boyle's law can be applied and the density of air is assumed to be linearly dependent on the pressure:

$$\rho_a = \frac{\rho_0}{p_0} p \qquad (5)$$

where ρ_0 is the density of air at the atmospheric pressure p_0.

Pressure-Correction Technique

The ship model for flooding simulation can be considered as an unstructured and staggered grid (Fig. 1). Each modelled room is used as a single computational cell. However, the flux through a cell face is possible only if there is an opening that connects the rooms (cells). In this study, all openings were modelled as one-dimensional points with the given area and discharge coefficient. However, the same technique can easily be applied also for openings with more complex shape.

Water level in each room is considered to be flat and horizontal plane. Thus the sloshing effects are not taken into account.

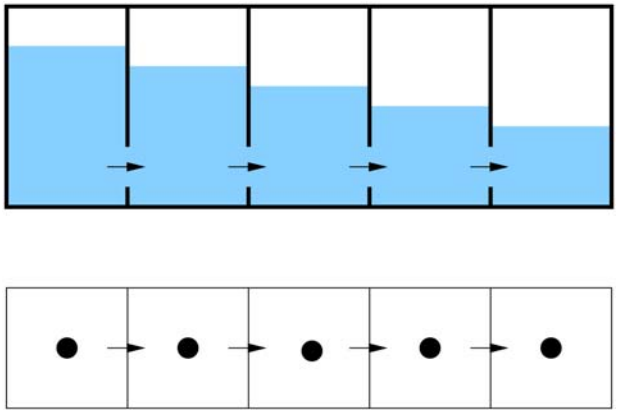

Fig. 1: Staggered grid in flooding simulation

Usually flooding simulation methods are based on the volumes of floodwater that are integrated explicitly from the flow velocities that are calculated from Bernoulli's equation. The water height differences are then calculated from the volumes of water with the heel and trim angles taken into account. However, the applied simulation method is based on a completely different approach, where the volumes are calculated on the basis of water heights and the heel and trim angles. This is reasonable as the water height is physically more meaningful than the volume of water since it represents the hydrostatic pressure. Consequently, the progress of the floodwater can be solved implicitly on the basis of the pressures in the rooms and the velocities in the openings.

The basic idea of a pressure-correction method is that the equation of continuity and the linearization of the momentum equation (Bernoulli) are used for the correction of the pressures until the iteration is converged and both the continuity and the conservation of momentum are satisfied at the same time.

Equation of Motion

This study concentrates on a statutory approach, where the damaged compartments are considered to be flooded immediately and only the cross-flooding to the equalizing side is calculated in time domain. Basically, this is just an improved and more accurate version of the formula in the Resolution A.266. The background for this simplified approach is presented in Solda (1961). Consequently, the motions of the ship are considered to be quasi-stationary and the sea is assumed to be calm.

CROSS-FLOODING EXAMPLE

Damage Case

The studied case is a U-shaped void, surrounding machinery spaces in a modern large passenger ship design. The tested damage case includes several compartments that are flooded immediately, and thus considered to be open to sea. Consequently, the initial heeling angle after the damage is large (10 degrees).

Cross-Duct

The sides of the U-shaped void are connected by a cross-duct that consists of four parts due to the longitudinal girders. In order to study the effect of the detail level in the modelling, three different models of the cross-duct were tested (Fig. 2):

- Level A: each girder defines a room partition
- Level B: cross-duct is considered as a single room
- Level C: cross-duct is considered as a single opening in the centerline

Fig. 2: Schematic representation of the different detail levels for modelling of the cross-duct

It is somewhat questionable what values should be used for the discharge coefficients of the openings. In general, $C_d \approx 0.6$ has usually been used in flooding simulations. However, this can be far too conservative when flooding through a cross-duct with several girders is considered. Most of the pressure losses are likely to take place in the inlet, where the discharging jet is initially formed. The subsequent openings will then have a smaller effect on the jet, and therefore, also the pressure losses are likely smaller.

In Level A, $C_d = 0.65$ is used for all openings in the duct. In Levels B and C, the applied discharge coefficients were obtained by using the formula in the proposed revision of the Resolution A.266 (IMO SLF50/WP.1 Annex 2, 2007). This is based on the RANSE computations, presented in Pittaluga and

Giannini (2006). In Level B, C_d = 0.65 was used for the opening on the damaged side and 0.45 for the other one and in Level C, C_d = 0.40 was used to represent the whole duct.

Air compression inside the cross-duct was ignored (Levels A and B) since the volume of the duct is minimal when compared to the volume of the whole U-void.

Air Pipes

Each side of the void is equipped with two separate air pipes. The pressure losses in these pipes were estimated by applying the formulae, presented in the Resolution A.266 (Table 1). Thus the effects of air compressibility were ignored. However, the effects of pipe diameter D and length L were taken into account. The unity for the outlet was excluded since it was already included in the calculation of the discharge coefficient, see equation (4). This procedure is in agreement with the proposed revision of the Resolution A.266 (IMO SLF50/WP.1 Annex 2, 2007).

Table 1: Applied pressure losses in the air pipes (according to Resolution A.266)

Component	Value
Friction	$k = 0.02\,L/D$
Inlet	$k = 0.51$
90 deg double mitre bend (2 pcs)	$k = 2 \cdot 0.43 = 0.86$

A constant time step of 0.2 s was used. The applied convergence criterion corresponds to a water height difference of 0.05 mm. It was checked that a shorter time step or a stricter convergence criterion did not have any notable effect on the results.

SIMULATIONS

Quasi-Stationary vs. Dynamic Heeling

In order to study the effects of the simplified approach with quasi-stationary motions, one case was simulated also with dynamic roll motion, using estimations for the added mass and linear damping. The comparison with quasi-stationary simulation is presented in Fig. 3.

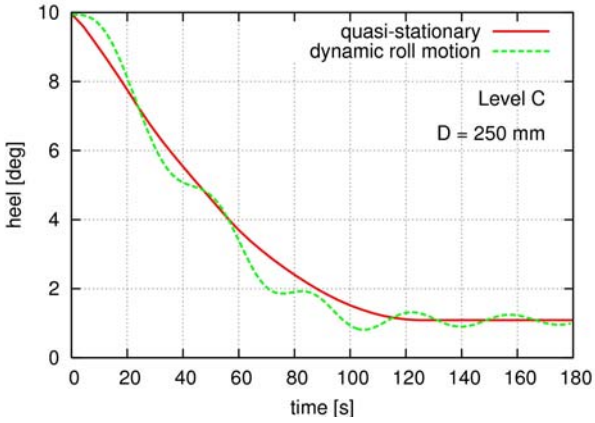

Fig. 3: Comparison of the heel angles with quasi-stationary method and dynamic roll motion

It seems that the quasi-stationary method results in slightly longer equalization times, and hence it is considered to be suitable for statutory calculations. In general, the results are very similar with both approaches.

Effect of the Cross-Duct Modelling

Comparisons of the heeling angle and over pressure in the equalizing side of the void are presented in Fig. 4 and Fig. 5, respectively. The equalization process is estimated very similarly with all tested modelling levels of the cross-duct. However, Level C gives much larger maximum over pressure in the void during the flooding. This may result from the assumption of full ventilation in the duct.

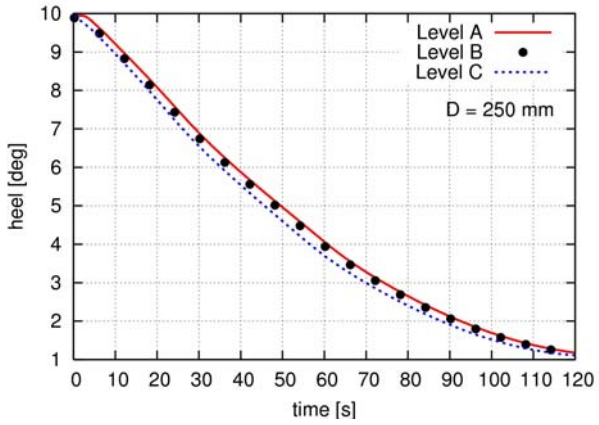

Fig. 4: Comparison of the time histories for the heeling angle with different modelling levels of the cross-duct

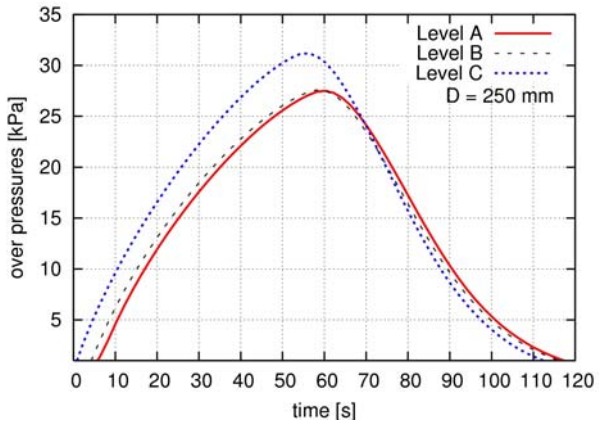

Fig. 5: Comparison of the time histories for over pressure in the equalizing side with different modelling levels of the cross-duct

Air Pipe Dimensioning

The simulations for the dimensioning of the air pipes were performed with the cross-duct modelling Level C. The pipe diameter was increased until there was no difference, when compared to the results from the simulation with full ventilation in the void. The results for the heeling angle, over pressure and volume of floodwater in the equalizing side are presented in Fig. 6, Fig. 7 and Fig. 8, respectively.

The area of the largest pipe (D = 400 mm) is 9.9 % of the area of the cross-flooding openings. The results for the heeling angle and volume of water are very close to the results from the simulation with fully vented void.

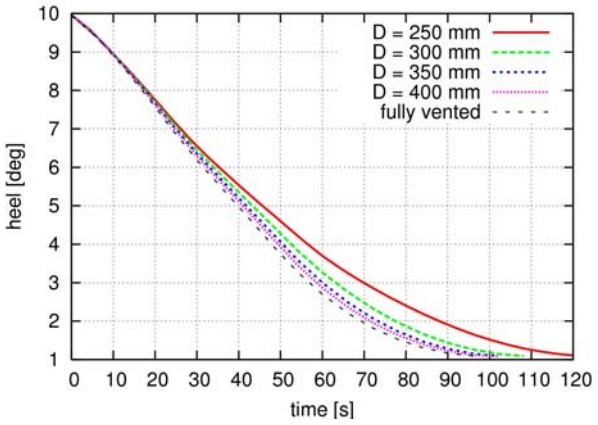

Fig. 6: Comparison of heeling angle with different sizes of air pipes

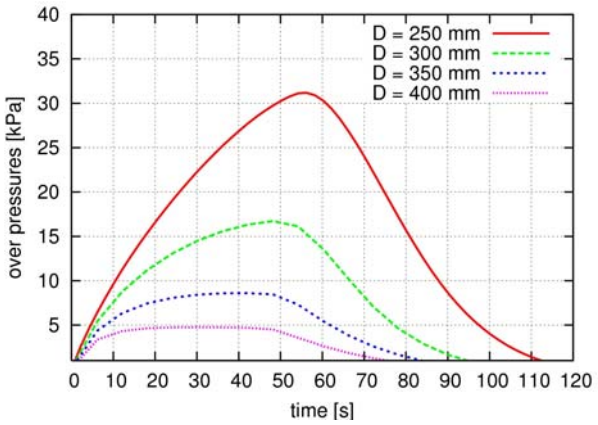

Fig. 7: Comparison of over pressure in the equalizing side with different sizes of air pipes

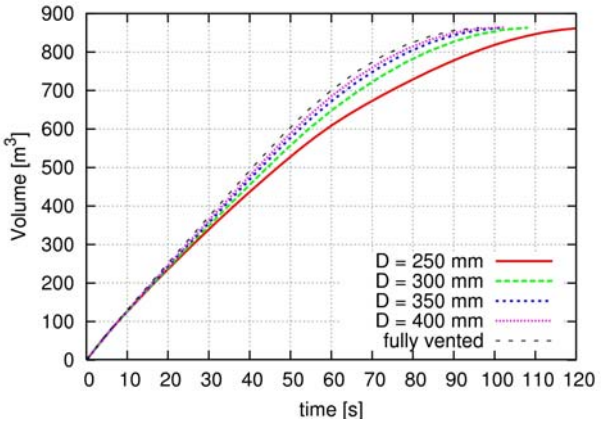

Fig. 8: Comparison of floodwater volume in the equalizing side with different sizes of air pipes

The effect of air pipe diameter is not notable in the beginning of the equalization process.

Thereafter, near the equilibrium condition, the effect is more significant.

On the basis of these results, it seems that in this particular case, the criterion of 10 % area for the air pipes in the revised Resolution A.266 seems to be reasonable. However, no general conclusions can be made without systematic simulations with many different ship designs.

Realistic Damage Case

The presented simulations were based on the statutory approach, where the damaged rooms are considered to be immediately flooded. For comparison, a separate case, where only the U-void is damaged, was calculated both with the statutory approach and with a modelled damage opening of 5.0 m^2. Simulations were performed with two different air pipe diameters.

The results for the time histories of heeling are presented in Fig. 9. The formula of the Resolution A.266 gives an equalization time of 131 s, which is slightly conservative, when compared to the simulations.

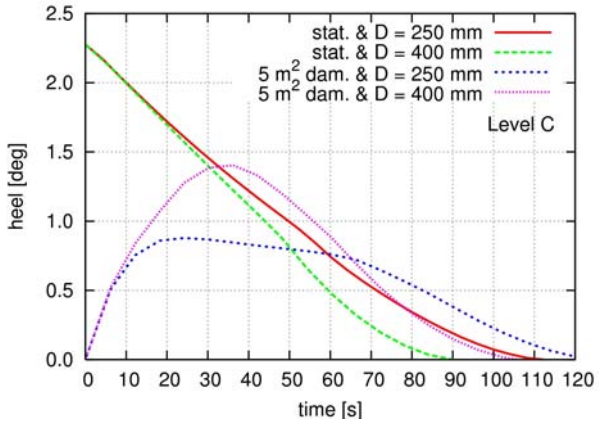

Fig. 9: Comparison of heeling angle with the statutory case and with 5.0 m^2 damage opening, simulated with two different air pipe diameters

When also the damage opening is modelled, the compression of air in the damage side of the void slows down the flooding from the sea. Consequently, the maximum heeling angle is decreased with smaller air pipes, even though the equalization time is longer. It might be reasonable to take this phenomenon into account with damages to rooms that are located far below the water line.

CONCLUSIONS

Time-domain flooding simulation, with the compression of air taken into account, seems to be a very efficient and practical tool for assessing the cross-flooding times more realistically than the simplified formula in the Resolution A.266.

However, it is obvious that more dedicated CFD computations and large scale model tests are needed in order to develop and verify the simple formulae for pressure losses in various cross-flooding arrangements. Furthermore, experimental and computational data on the pressure losses for airflow in the ventilation pipes are needed. In the presented simulations it was assumed that the formulae for water flow in pipes could also be used for assessing pressure losses in the case of airflow. However, dedicated studies are needed in order to justify this procedure.

Fully quasi-stationary calculation of the ship motions seems to be justified in the statutory approach since there is no transient heeling in the start of the flooding, unless the cross-duct is very large and the cross-flooding time is minimal. On the other hand, in such a situation, accurate assessment of the cross-flooding time is not needed.

In realistic flooding simulation, the heeling angle approaches the equilibrium condition almost asymptotically. The last seconds of the equalization are definitely insignificant, and therefore, some generally accepted criterion for the practical limits of the equilibrium should be established.

REFERENCES

IMO SLF50/WP.1 Annex 2 2007. Recommendation on a Standard Method for Evaluating Cross-Flooding Arrangements.

Peters, A. J., Galloway, M., Minnick, P. V. 2003. Cross-Flooding Design Using Simulations, Proceedings of the 8th International Conference on Stability of Ships and Ocean Vehicles, Madrid, Spain, 2003, pp. 743-755.

Pittaluga, C., Giannini, M. 2006. Pressure Losses Estimation for Structural Double Bottom by CFD Technique, CETENA Technical Report, published in internet (cited 14.5.2007), http://www.sname.org/committees/tech_ops/O44/sdsiscg/49/A266-1.pdf and http://www.sname.org/committees/tech_ops/O44/sdsiscg/49/A266-2.pdf

Ruponen, P. 2006. Pressure-Correction Method for Simulation of Progressive Flooding and Internal Air Flows, Schiffstechnik – Ship Technology Research, Vol. 53, No. 2, pp. 63-73.

Ruponen, P., Sundell, T., Larmela, M. 2006. Validation of a Simulation Method for Progressive Flooding, Proceedings of the 9th International Conference on Stability of Ships and Ocean Vehicles, Rio de Janeiro, Brazil, 25-29.9.2006, Vol. 2, pp. 607-616.

Solda, G. S. 1961. Equalisation of Unsymmetrical Flooding, Transactions of Royal Institute of Naval Architects, RINA, Vol. 103, pp. 219-225.

Vredeveldt, A. W., Journée, J. M. J. 1991. Roll Motion of Ships due to Sudden Water Ingress, Calculations and Experiments, RINA'91, International Conference on Ro-Ro Safety and Vulnerability the Way Ahead, London, United Kingdom, 17-19. April 1991, Vol. I.

Xia, J., Jensen, J. J., Pedersen, P. T. 1999. A Dynamic Model for Roll Motion of Ships Due to Flooding, Schiffstechnik – Ship Technology Research, Vol. 46, pp. 208-216.

Session 3: Investigation on Severe Stability Incidents

Session Chairman: A. Jost A. Papanikolaou

1) P. Valanto:

   “New Research into the MV Estonia Disaster”

2) R.Imstøl:

   “MV Estonia, a Plausible Sinking Scenario”

New Research into the MV Estonia Disaster

Petri Valanto

Hamburg Ship Model Basin HSVA

ABSTRACT

Since March 2006 the HSVA-Consortium, that is, the HSVA and the Technical University of Hamburg-Harburg (TUHH) together with the company TraffGo HT, which is specialized in evacuation simulation software, is investigating the MV Estonia accident for the Swedish Governmental Agency for Innovation Systems (VINNOVA). Some first preliminary results of the on-going investigation are presented. These results are mainly based on the motion simulation of the damaged ship in seaway carried out in the HSVA with the program ROLLS, including the simulation of the water sloshing on the vehicle deck. The results give an improved picture of the early phases of the accident.

KEYWORDS

MV Estonia, Ship Motion Simulation; Water on Deck; Shallow-Water-Equations; Capsizing; Evacuation Simulation.

INTRODUCTION

The MV Estonia sank on September 28, 1994 in the Baltic Sea on its way from Tallinn to Stockholm. According to official documents at least 852 human lives were lost in this accident, which makes it one of the worst in the European maritime history. The Joint Accident Investigation Commission (JAIC) published its report few years after the accident in 1997. This report gives a picture of the accident, which understandably is not complete and appears also partly controversial. The discussion on the MV Estonia has not calmed down after all these years and perhaps as a consequence the Swedish Government authorized a new study in 2005. Since March 2006 two consortia, the SSPA-Consortium and the HSVA-Consortium with their partners are separately investigating the sinking sequence of the MV Estonia. This paper gives information on the methods used in the on-going HSVA investigation and on some first preliminary results.

It is believed that in the framework of the relatively limited research budget the best contribution to the already existing studies could be delivered using as advanced simulation techniques as possible, both for the capsizing and sinking of the vessel and for the evacuation of the passengers and crew.

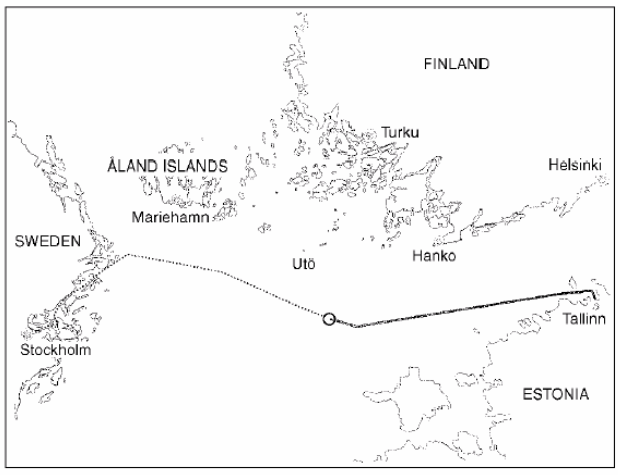

Fig. 1: The route and accident site of the MV Estonia (JAIC, 1997).

Since the beginning of the investigation by JAIC various organizations have carried out hydrostatic analyses of the capsizing and the consequent sinking of the vessel. The later

hydrostatic analyses did not provide results essentially deviating from the earlier ones. Therefore in the HSVA investigation simulation of the ship motions together with the flooding of the vehicle deck will be carried out. Here the inflow to and outflow from the vehicle deck are crucial. The models used in the past for describing this detail have not always been very advanced. In this study new ways to model the inflow-outflow will be applied.

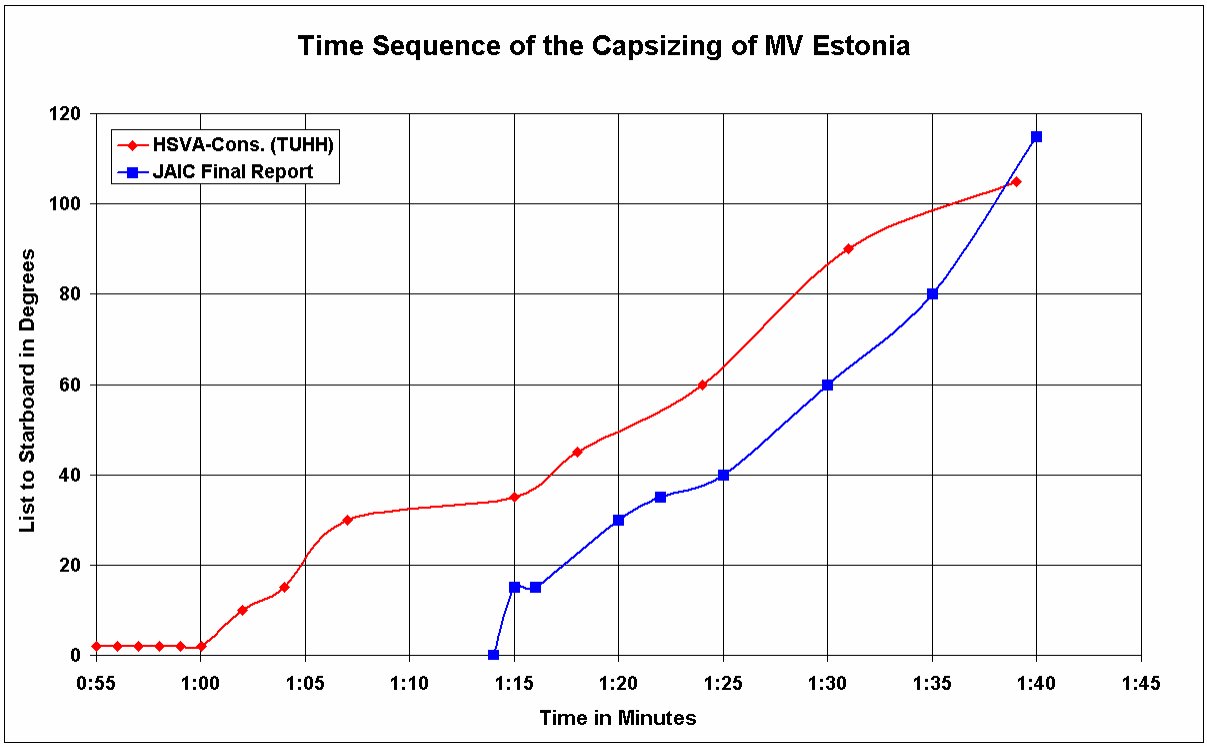

Fig. 2: Development of list to starboard during the MV Estonia accident.

On the other hand an evacuation analysis will help to establish as complete picture of the MV Estonia accident as possible. In our analysis with evacuation software AENEAS, which has the capability to account for the ship motions, the actual crew and passenger population of the MV Estonia at the time of the accident is modeled. First evacuation analyses with the real MV Estonia population and the newly estimated ship's list as a function of time were carried out. For purpose of comparison also evacuation analyses according to the IMO guidelines will be carried out. It is expected that the differences between the Estonia evacuation and the IMO advanced evacuation analysis will turn out to be considerable. This may help to develop the guidelines further. The evacuation analysis is still far from complete and is not reported further here.

The HSVA-consortium research is strongly based on survivors' testimonies (SPF, FAIB), physical facts, and numerical analysis. The very early survivors' statements have been given somewhat more emphasis than the later ones. However, some later interviews carried out by the interest groups working on MV Estonia have given some additional information often supporting our conclusions based on the early testimonies. A new time sequence of the course of the accident in form of ship's list as a function of time was established purely on the basis of the survivors' testimonies by the TUHH, the second partner in the HSVA–Consortium. This sequence of the ship's list is one of the crucial facts to be reproduced with the motion simulation of the damaged ship. Figure 2 shows the new time sequence of the capsizing of the MV Estonia together with the list development reported by the JAIC. There is a clear difference between these two time-histories. The HSVA

consortium believes that the actual accident started earlier, around 01:00, and not at 01:14 as stated by JAIC. The values of list in the TUHH-curve are based on subjective observations made by the survivors. It is possible that the actual values of list were at certain points somewhat lower than those felt and reported by the survivors.

THE ACCIDENT

Track of the Vessel

Figure 3 reproduced from the JAIC Final Report (1997) shows the MV Estonia's track during the last hour. The red circles and the ellipse mark areas where the visor, an unknown object and various loose items lay on the seabed, based on sonar measurements carried out in October 1994 (Nuorteva, 1995). These are hard facts in the Estonia investigation: The vessel must have passed very near these points.

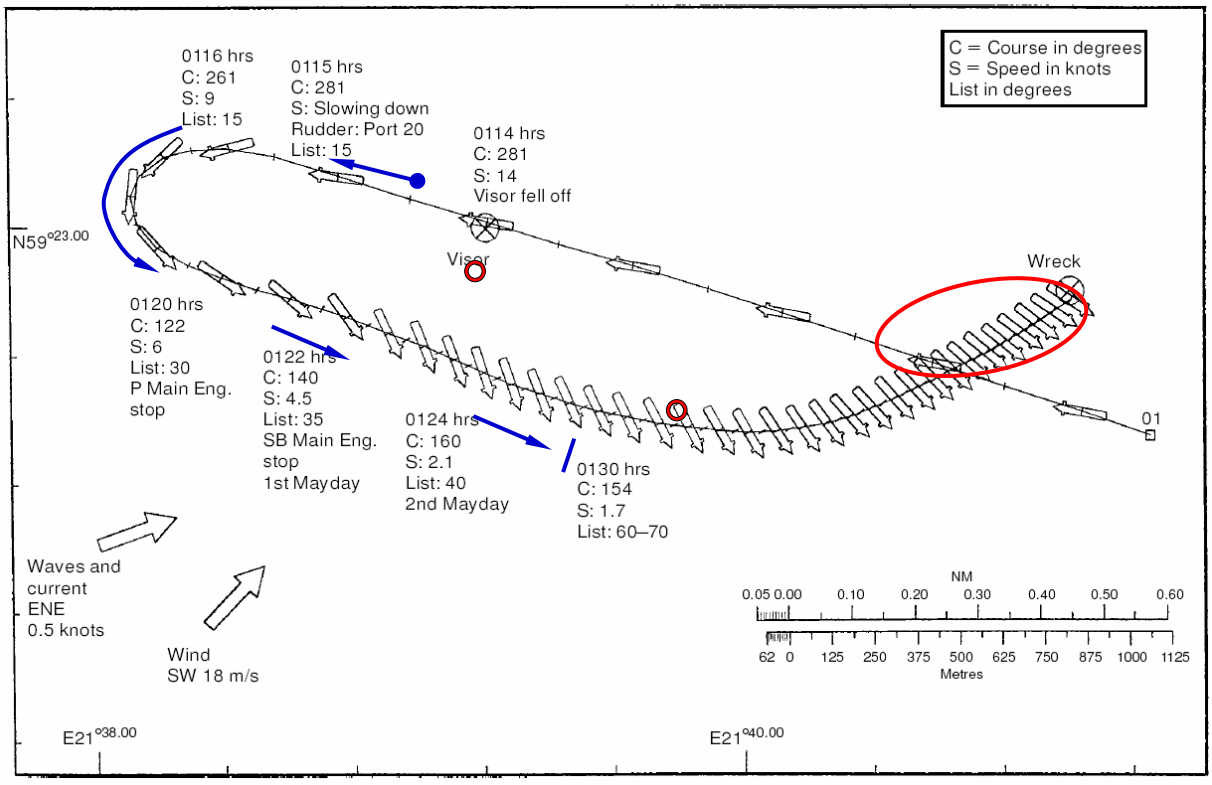

Fig. 3: MV Estonia's track during the last hour, as composed by the Navigation Simulator at the Maritime Academy in Kalmar, Sweden (JAIC, 1997).

The blue arrows in the figure show the part of the track, which is subject to be defined with the help of the survivors' testimonies and physical facts related to the behavior of the damaged vessel in the seaway of the night to September 28, 1994.

Start of the Accident

The accident can be considered to have started around 01:00, when many survivors heard and felt two to three heavy blows from the bow, after which a scraping sound apparently coming from under the vessel was heard by several survivors. After this the vessel experienced 2-3 deep sudden heels to starboard. The vessel straightened a little, but a considerable list remained.

Disconnection of the Bow Visor

It is known that the visor must have dropped in quite an early phase of the accident and according to JAIC pulled the ramp completely open. These conclusion have, however, been put into question by various interest groups working on MV Estonia. The bridge of the MV Estonia was constructed so that it was not possible to see the bow visor. Even if the

officers on the bridge could not see the visor itself, as shown in Figure 4, they may have seen that the spray flying upwards, when the bow hit a new wave was very different, because the visor had dropped. Also the feel of the ship at each wave impact must have changed, because the vessel without the visor had now a very blunt bow shape above the waterline. It is, however, very likely that the officers on the bridge at that moment did not realize that the visor, due to built-in interlocking, may have also pulled the ramp open.

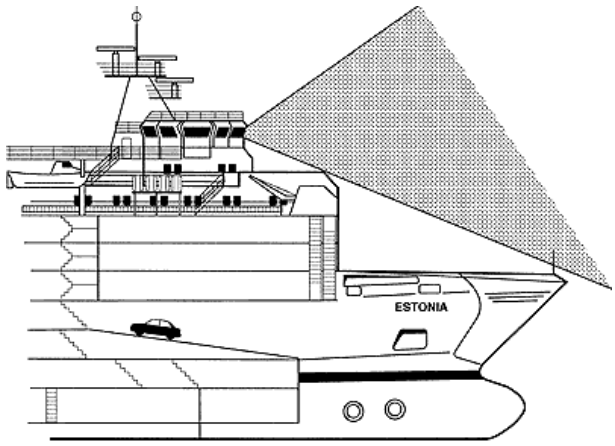

Fig. 4: Approximate field of vision from the bridge (JAIC, 1997).

It is likely that the visor dropped quite soon after the first sudden heel, if not already earlier: The crew member C42[1] (interview 29.09.94 in Tallinn) was in his cabin around 01:00 reading a book. Suddenly the vessel listed to the starboard side so heavily that objects fell down from the cabin table. C42 dressed rapidly and went out of the cabin. In the corridor he met the first and second engineers (C46 and C38). One of them said “the visor went off” or “the visor was pushed up, it would be good if we would get the vessel to shore”. He got the impression that the locks holding the ramp had loosened and through there water came in. So already few minutes after 01:00 some members of the crew knew that the visor had dropped or opened, and that the ramp was leaking.

[1] The code refers to the confidential list Witness Key.xls shared by the two consortia.

If the visor disconnected from the vessel advancing 15 kn, it of course had in the beginning approximately the same horizontal velocity as the ship. When the visor hit the water surface its velocity slowed down drastically. In this situation it is very likely that the advancing ship hit the visor.

Thus it is only natural that the visor has a deep dent obviously caused by the bulb of the advancing ship. As a results of such collision the visor would be pushed away by the relatively narrow bulb, in this case to the port side, where the MV Estonia underwater hull shows some minor damages. A visor pushed beside by the narrow bulb is still ahead of the ship hull advancing 14-15 kn. Further contacts between the visor and the advancing ship hull are very likely to have taken place. Thus the scraping noise, heard by some survivors as noise coming from underneath their cabins on Deck 1, was probably caused by the ship running over the visor, which could not sink fast enough to avoid contact with the advancing ship.

In order to throw some light on these early phases of the accident the following cases were investigated with the program HSVA Rolls. A description of the program can be found in (Valanto, 2006).

NUMERICAL SIMULATION

Scenario 0a: Visor and Ramp both 1 m open

The MV Estonia runs on the course 287° in a sea state having a significant wave height of 4.2 m and modal period of 8.0 s. The waves come at 45° from the port bow quarter. The visor is loose in its position: There is a 1 m high horizontal gap between the visor and the ship shell just below the visor. The ramp has been pulled 1 m open at its upper end. This scenario is plausible as an initial scenario.

The triangular shaped openings between the ramp and its frame on both sides of the ramp were modeled in the motion computations of the damaged ship with the program Rolls. The effect of the somewhat opened visor on the inflow rate was estimated, in absence of other sources, with the experimental results by SSPA

(2007). These suggest that the inflow rate would be reduced by 70 percent in comparison with the situation without the visor.

Simulation result: In this scenario the inflow rate of about 10-20 m³/min is relatively small from the point of view of the ship stability. However, also this amount certainly appears considerable for an observer on the vehicle deck or somebody observing this via a TV-monitor, like the crew in the Engine Control Room (ECR) did.

The water accumulates slowly on the vehicle deck; in ca. 26 min the list of the ship reaches 10°. The list increases gradually as the water volume on the vehicle deck increases. If no corrective action were taken, the ship would be in danger to capsize after more than 3 hours.

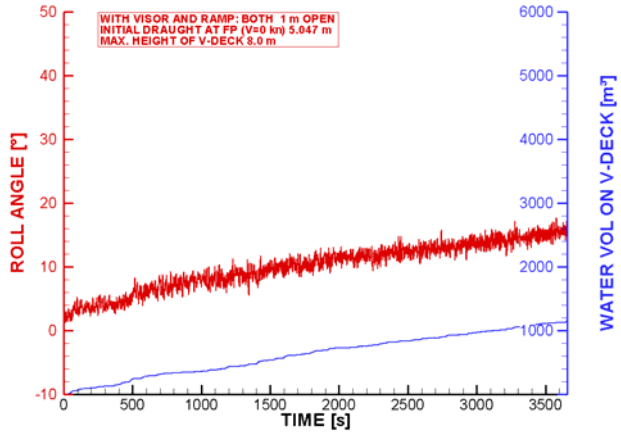

Fig. 5: Roll angle and water volume on the vehicle deck when both the visor and ramp are about 1 m open.

This scenario may have taken place before the ramp opened, but not for very long, as the gradually increasing list, e.g. 7° after 10 min, would have been noticed sooner or later by the crew. The simulation does not indicate any sudden heeling or other sudden ship motions.

- ⇨ The flooding rate in this scenario is too slow for it to be the final scenario for the flooding of the vehicle deck.
- ⇨ The scenario can be true for the very initial phase of the accident, but not for very long, as the slowly increasing list would have been observed by the crew.

Scenario 0b: Without Visor, Ramp 1 m open

The MV Estonia runs on the course 287° in a sea state having a significant wave height of 4.2 m and modal period of 8.0 s. The visor has dropped away. The ramp has been pulled open 1 m at its upper end. This scenario is not plausible according to JAIC, as there is nothing which can hold the ramp in this partially open position. It is, however, favored by some interest groups working on the Estonia case, perhaps because the ramp at the wreck resting on the seabed is approximately in this position.

Simulation result: In this scenario the inflow rate of about 70-80 m³/min is considerable from the point of view of the ship stability and certainly appears massive for an observer on the vehicle deck or on a TV-monitor. In addition in this case the airflow at the open gaps beside the ramp consisting of the ship speed and a component of the wind outside may have speeded the finer water spray coming in up to about 20 m/s or more.

The water accumulates on the vehicle deck; in ca. 7 min the list of the ship reaches 10°. The list increases monotonously as the water volume on the vehicle deck increases. If no action were taken, the ship would be in danger to capsize in about 40 minutes. Due to the gradually increasing list the situation would have been noticed by the crew relatively soon. Even after a considerable list there would have been enough time to take action against the water inflow on to the vehicle deck. The simulation does not indicate any sudden heeling or other sudden ship motions.

This scenario is difficult from the point of view of the ramp position. The wave forces the ramp would encounter in this inclined position would be considerable, thus no weak support can hold the ramp in this partially open position. The ramp weights about 12.5 tons. It is, however, light enough to be moved by the waves the ship encountered in the night of the accident.

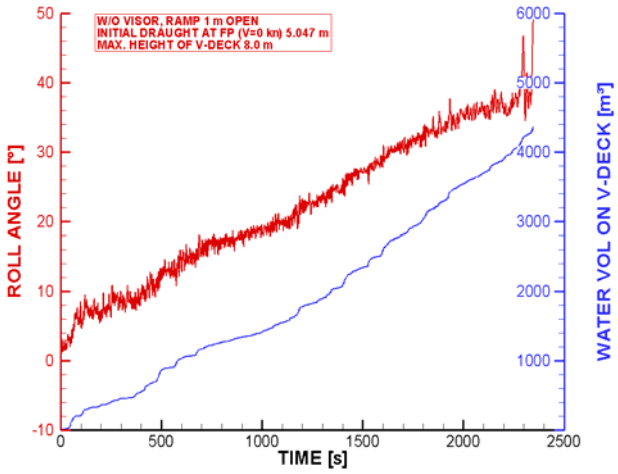

Fig. 6: Roll angle and water volume on the vehicle deck without visor when the ramp is about 1 m open.

- ⇨ The flooding rate is perhaps somewhat too slow for this scenario to be the final scenario for the flooding of the vehicle deck.
- ⇨ The inflow to the vehicle deck could hardly remain unnoticed by the crew. In this scenario the ship gets a list of 14-15° in 10 min. After this observation the crew would still have had sufficient time to take action against the inflow.
- ⇨ This scenario does not fit to the known technical facts reported by the JAIC.

Scenario 1: Without Visor, Ramp fully Open

The MV Estonia runs on the course 287° in a sea state having a significant wave height of 4.2 m and modal period of 8.0 s. The visor has dropped away. The ramp has been pulled fully open. This scenario is the accident scenario according to JAIC.

Simulation result: In this scenario the computed inflow rates vary between 300-700 m³/min, which are of course relatively high also from the point of view of the ship stability. This scenario is very likely to have taken place, but not for very long, as the increasing list, over 10° in three to four minutes would certainly have been noticed by the crew. If no corrective were be taken, the ship would be in severe danger to capsize in little more than 10-20 minutes, which did not happen. The likely further progressive flooding of the vessel leading to sinking is at the moment not considered.

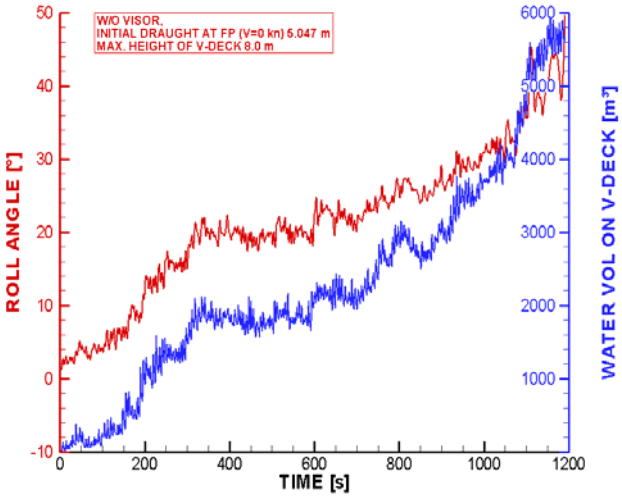

Fig. 7: Roll angle and water volume on the vehicle deck without visor when the ramp is fully open.

Notice that the curve in Figure 7 describing the water volume on the vehicle deck has a somewhat rougher look than the earlier curves shown in Figures 5-6: This is due to the open bow ramp, which allows more water sloshing in and out of the vehicle deck than in the earlier cases with the bow ramp only about 1 m open.

- ⇨ The flooding rate is suitable for this scenario to be the final scenario for the flooding of the vehicle deck.
- ⇨ The inflow to the vehicle would certainly be noticed by the crew. In this scenario the ship gets a list of over 10° in 3-4 minutes. If the crew in this scenario would not rapidly slow down or turn the ship, it would capsize. This scenario can be considered in general to fit with most testimonies by survivors and to known technical facts.

Discussion

The JAIC Final Report assumes that the waves hit the visor and made it to break loose. The visor was banging against the ship structures, and after a while it fell off pulling the ramp completely open. Through the open ramp enormous amount of water flowed on to the vehicle deck and the ship heeled. This scenario is plausible also in view of the preliminary

simulation results above provided that the following two questions can be answered:

(1) What caused the sudden heel described by many survivors? The survivors` testimonies appear to indicate that one first heard strange “metallic” noises from the bow (two to three heavy blows), second some scraping noises appearing to come from underneath the ship hull, and third one experienced sudden, violent heeling to starboard. Some survivors explain that they expected the ship to straighten and to roll back towards the other side, but this never happened. After the sudden heel to starboard the ship straightened somewhat, but a significant list remained.

(2) How can the JAIC scenario be combined with the statements of the three crew members, who reported they saw water spraying on both sides the closed bow ramp after the ship already had a significant list?

THE SUDDEN HEEL

Introduction

A negative intact stability, e.g. due to water on the vehicle deck, would cause the ship to have two positions of stable equilibrium, that is, the ship would be stable, when inclined with the angle of loll to either side. The rolling motion between these two positions of equilibrium, with the associated overshooting of the roll angle can of course cause a sudden heeling experienced by the passengers and crew onboard. In case of MV Estonia, which had a small initial list to starboard and then heeled further to starboard, this possibility does not appear to be the explanation for the sudden heeling.

If the sudden heel had been caused by a wave an intact ship would have straightened afterwards. Thus the assumption of a large wave alone causing the big heel does not appear to be very likely.

If the heeling had been related to water accumulating on the vehicle deck, a more gradual increase in the list would have been likely. A somewhat distant possibility is that the ship encountered, just after the ramp was pulled open, some very large waves, which very rapidly brought considerable amount of water on to the vehicle deck. Even then the sudden list would most likely not have been as impressive as reported. This is a possible, but perhaps an unlikely scenario.

Finally there is the possibility that the sudden heel was not a consequence of wave forces or of massive ingress of water, but a consequence of the ship starting to turn to port initiated by the officers on the bridge. To the present author this appears to be a plausible hypothesis for the sudden heeling motion and will be investigated below.

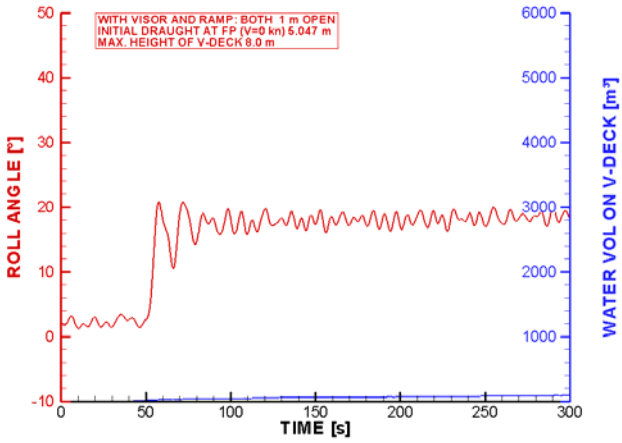

Fig. 8: Case (a): Roll angle and water volume on the vehicle deck, when both the visor and ramp are about 1 m open, start of turn at t=50 s.

In their testimonies the survivors P28 and P30 describe a turn to port. The P28 also describes how the ship heeled so heavily to starboard that furniture inside started to move. The person P28 also fell on the deck due to a sudden heeling motion (Schager, 2006). A HSVA technician on the full-scale trials of the MV Viking Sally, that is, later MV Estonia, experienced something quite similar. He was on the upper deck, when the ship started a Zigzag-maneuver: He remembers he had difficulties to stay on his feet and he heard how objects were falling down from tables and shelves, because of the sudden heeling due to the start of the turn.

Turn to Port

The location of the visor, the debris dropped from the ship listing heavily and the position and orientation of the wreck quite strongly hint that the ship made a turn to port, before it capsized and sank. See Figure 3 for illustration of the vessel's track. In addition the second officer E1 on watch onboard the MV Mariella tracking MV Estonia that night saw in the corner of his eye on the radar screen the track of a hasty, sharp turn to port made by MV Estonia (FAIB, 1994).

It is also very plausible to assume that the officers on the bridge of the MV Estonia decided to make a turn to port. They may not have been fully aware of what was wrong with the ship, but they certainly knew that something had changed. Strange noises from the bow had been reported to the bridge. They may have known that they had water on the vehicle deck. If they were in contact with crew members in the engine control room, at worst these could have told that plenty of water sprayed onto the vehicle deck on both sides of the closed ramp. Even if the officers on the bridge had assumed that the visor had broken or dropped away, they could at this situation not have the knowledge that the falling visor could pull the ramp fully open. A turn to port would bring the wind and the waves to the

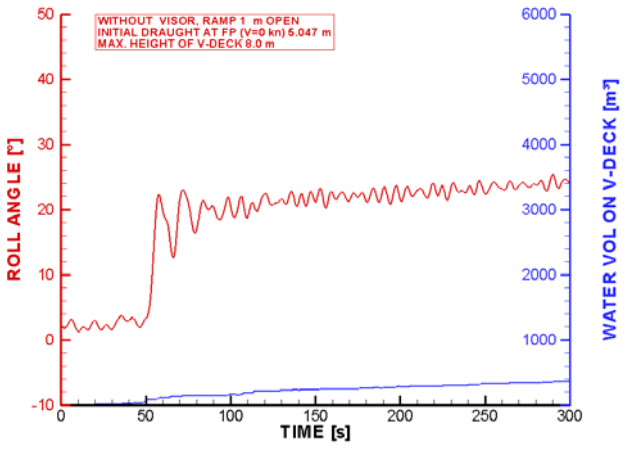

Fig. 9: Case (b): Roll angle and water volume on the vehicle deck, without visor, with the ramp about 1 m open, start of turn at t=50 s.

starboard side. This would have a straightening effect on the ship's list. In this light the turn to port appears a plausible measure to try to improve the situation of the ship.

It is well known that when a ship starts a sudden turn to port, an overshooting of the heeling angle to starboard takes place. This overshooting can in certain conditions be quite significant, e.g. objects can slide on tables and drop down. There is, however, very little information available of how large this overshooting angle can be, on a ship in seaway, when there is water on the vehicle deck.

The water on the deck accumulates to the starboard side due to the sudden heeling and also due to the centrifugal acceleration caused by the turning of the ship. Thus the officers on the bridge may have themselves been surprised of the magnitude of the heeling that now followed.

It is perhaps not absolutely sure whether the ship ramp opened before or after the ship started its turning maneuver. Therefore the sudden heeling motion due to the sharp turn to port was simulated in three basic situations:

a) The ship with both the loose visor and the bow ramp 1 m open.

b) The ship without visor and the bow ramp 1 m open.

c) The ship without visor and the bow ramp completely open.

In all cases the ship speed amounts to 15 kn, the steady turning diameter of the ship's turn is 2.9 ship lengths (L_{pp}) (JAIC Supp. 523, 1996; SSPA, 2007). The full centrifugal acceleration due to the turn is reached in 14 seconds from the start of the turn. In the beginning a large oscillation (overshoot) to the outer side of the turn takes place. After a while the static heel balances the centrifugal acceleration acting on the ship. This situation lasts as long as the ship turns. Thus the heeling angle is not returning to zero. This was also noticed by some of the survivors in their testimonies, even if they did not know the reason for the sudden heeling.

In the case (a) the simulations provide a step of 18-19° in the heeling angle curve, the heel angle reaches 20° and remains high, as shown

in Figure 8. The transient roll oscillations after the step dampen rapidly. The water inflow on to the vehicle deck is not strongly influenced by the increased heel of the vessel, and the ship list remains practically constant. The water volume on the vehicle deck is in this particular case small. The situation has an almost quasistatic character and does not appear to correspond as well with the survivors' testimonies as the case (c) below.

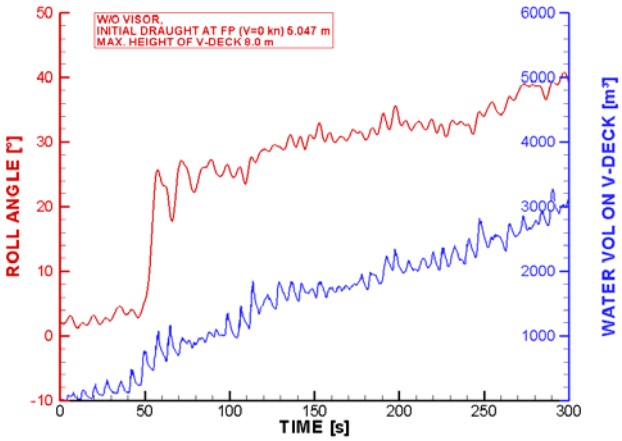

Fig. 11: Case (c): Roll angle and water volume on the vehicle deck, without visor, ramp fully open, start of turn at t=50 s. Second realization of random waves.

Case (b): If the simulation for the case (a) is carried out without the visor, the curves look in the beginning very similar, with the exception that the additional heeling increases the inflow onto the vehicle deck and the ship would be in danger to capsize in less than 20 minutes. For this reason, even if problematic from the point of view of the ramp position, this scenario cannot be left out of further consideration as the main scenario.

In the case (c) the step is a little higher (19°-22°) leading to a momentary heeling angle of up to 26°. The water sloshing on the vehicle deck is likely to contribute to the magnitude of the sudden heeling motion. In this case the inflow through the completely open bow increases due to the sudden heel. Figures 10 and 11 illustrate the case with two different random wave realizations used in the simulations.

The actual magnitude of the sudden heeling motion depends on the ship's actual position in the waves, ship speed, rate of turning, height of the center of gravity and also how rapidly the ship starts to turn. Further the amount of water on the vehicle deck and its motion can influence the situation. For these reasons the three cases in Figures 8 to 11 should be taken only as examples.

It should be taken into account that the survivors' estimates of the felt heeling angle getting up to 45-50° may be too high. Person P28 explained further that after the initial overshooting he could see a metal plate stick out of the hull (the stabilizer fin) on the port side. This implies a heeling angle of at least ca. 15°-18°, which is not far from the few examples shown above in Figures 8-11. The following conclusions can be drawn based on the simulations carried out.

- ⇨ A sharp turn to port gives a plausible explanation to the sudden heeling motion of the ship reported by the survivors.
- ⇨ The amount of water on the vehicle deck, as shown in Figures 8-11, appears to contribute to the magnitude of the sudden heeling motion.

Water on the Vehicle Deck - Water onto Deck 1

Many survivors coming up from their cabins on Deck 1 reported water either on the Deck 1, or on the way up in the staircases, when they were passing Deck 2, that is, the vehicle deck. One of the important questions in the case of the MV Estonia is, how did the water come on to Deck 1, the next deck below the vehicle deck? This question is crucial from the point of view of the damage scenario. Either the water came from the vehicle deck as JAIC has suggested, or it came from somewhere deeper down, as suggested e.g. by Holtappels and Hummel (GGE, 1999). The survivors from the Deck 1 reported encounters with relative small amounts of water on their way out of their cabins just after the sudden heel, that is, when the ship still had a relatively moderate list.

Hydrostatic considerations indicate that a relatively high list is needed before the water reaches the openings in the central casing and can flow down on to Deck 1. This would take

place quite late in the course of the accident, thus the persons from Deck 1 would hardly have had time to escape. The numerical simulation of the motion of the ship and of the water on the vehicle deck gives a more refined picture than the hydrostatic analysis.

The numerical computations show how the water flows in from the open ramp to both sides of the central casing on the vehicle deck. The simulations show wilder sloshing motion in the longitudinal direction, when the ramp is fully open compared with those cases, when it is only about 1 m open.

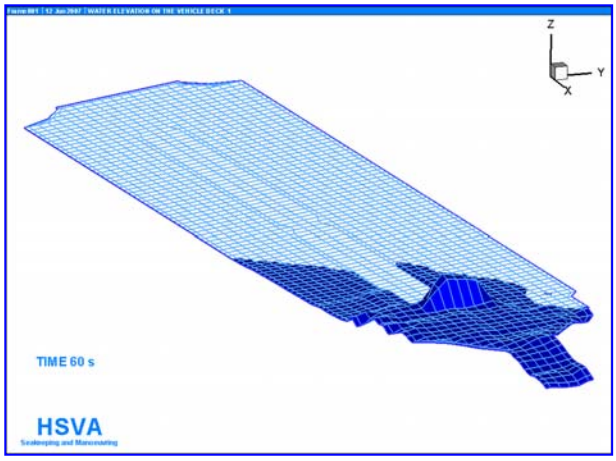

Fig. 12: Waves on the vehicle deck coming through the fully open ramp slosh against front face of the central casing and splash water high up.

See the incoming wave hitting the front face of the central casing in Figure 12. The numerical grid on the vehicle deck is coarse, and the shallow-water-equations used in the computations are an idealization of the reality. Thus this small detail cannot be described very accurately by the numerical model, but in reality the wave at the front face of the central casing would have splashed water high up making the video camera fixed on this front face wet, as described by three crew members in the Engine Control Room (ECR). It is likely that this can take place only when the ramp is open.

As the vessel is rolling and pitching in the waves, the water sloshes around on the vehicle deck. Some water may splash into the staircases of the central casing and flow down onto Deck 1 below. The flooding of the vehicle deck starts from the bow, as also shown in Figures 12-14. Thus it is more likely that in the early phases of the accident water would flow into the front compartments on the Deck 1 than those further aft. This is also supported by the testimonies of those who survived from the Deck 1, as shown in Figures 15-16. Depending on the case as early as 3-4 minutes after the start of the accident some water can flow down to Deck 1 through the front staircases in the central casing.

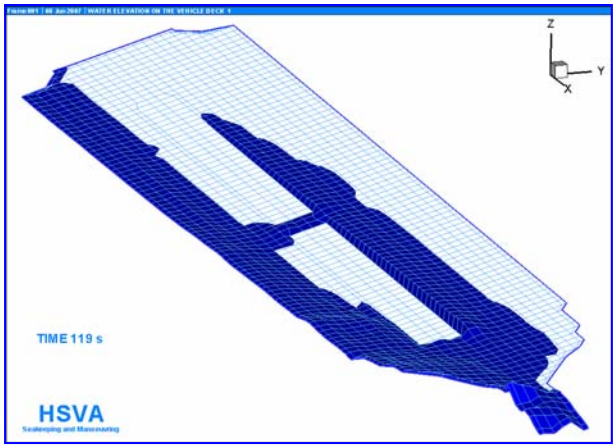

Fig. 13: Waves slosh water onto the vehicle deck through the fully open ramp. The flooding starts from the bow. Before the turn starts the heeling angle is relatively small.

In the ECR motorman C7 was looking into a monitor showing the camera view towards the pilot door located in front at the starboard side of the ship. He reported water sloshing in this area between the cars and reaching up to the level of the cars, that is, 40-50 cm high (Kurm, 2007). In the simulations the water sloshing on the vehicle deck almost always floods this area. Thus the simulated results are in full harmony with the statement by C7.

The GGE Enclosure 12.4.4.161 (Holtappels and Hummel, 1999) contains an interview with retired pilot Bo Söderman concerning his observations of water on deck of the MV Estonia on 26 December 1993, that is, on another earlier trip. Pilot Söderman says “In my opinion there was 5-10 cm water over the whole area of the vessel’s car deck. The water was splashing about 1 m high against the bulkhead with the stairways (centre casing).”

This statement directly supports the computed results of the water sloshing on the vehicle deck and splashing high against the central casing walls.

A further interesting point is added when one looks what happens on the vehicle deck, if the vessel makes a turn. When the vessel starts the turn to port, it heels suddenly to starboard, and the water on the port side of the vehicle deck flows towards the central casing, where the water level rises and in addition the water sloshes high against the port side central casing

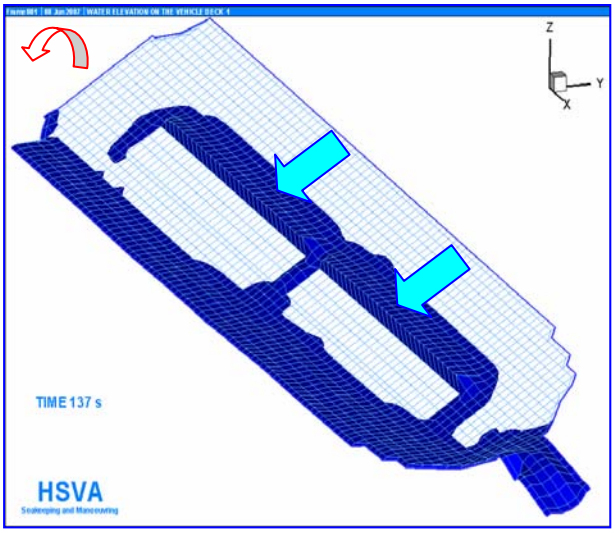

Fig. 14: When the turn has started at 120 s. the ship heels suddenly, the water on the vehicle deck rushes to starboard and the water level rises momentarily high on the port side wall of the central casing as it flows towards the lower starboard side.

wall and can easily flow into the staircases and from there down on to Deck 1 below. Figure 14 illustrates this moment. Many of the cabins of those survivors, who reported water on Deck 1 are located directly starboard of the staircases, that is, “downhill”, exactly where water would flow in a ship having a significant starboard list. See Figure 16.

- ⇨ Water flows in from the opening at the bow to ***both sides*** of the central casing on the vehicle deck. Thus in this case this dynamic distribution of water is more even than a hydro-static distribution would be. Therefore values of list estimated hydrostatically for a given amount of water on the vehicle deck are in this case likely to be somewhat too high.
- ⇨ If the ramp was open, it is likely that incoming waves hit the front face of the central casing splashing water high towards the camera fixed on this face possibly making the camera wet, as described by the crew members in ECR.
- ⇨ The flooding of the vehicle deck started from the bow. As the ship was rolling and pitching in the waves, it is likely that some water splashed or flooded into the staircases in the central casing and flowed further down in to the front compartments on Deck 1.

The sudden heeling motion caused a momentary high water level on the port side of the central casing. This most likely contributed to water being able to flow down to the front compartments on Deck 1. This matches well

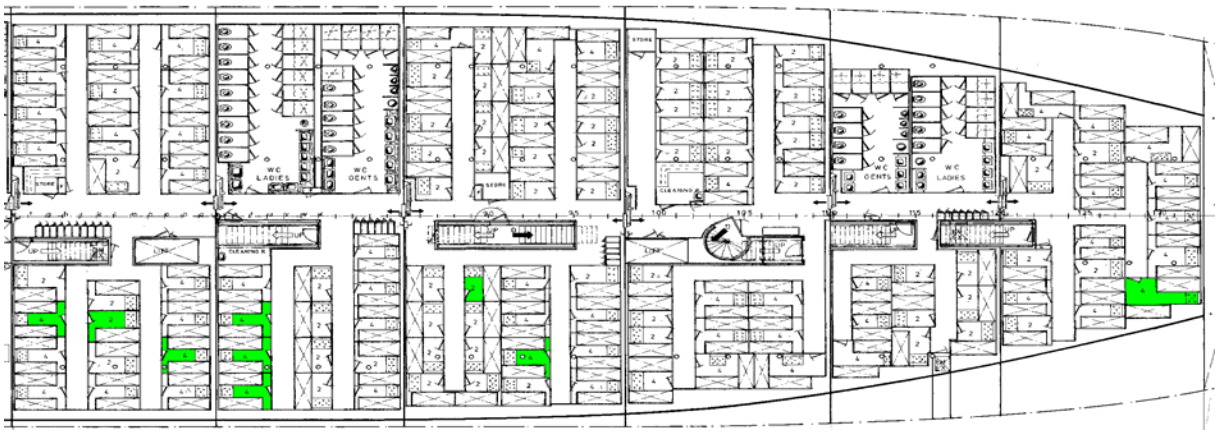

Fig. 15: Location of survivors, who reported water on Deck 2 (Vehicle deck) above, but not on Deck 1

with the testimonies of the survivors, who came up from Deck 1 just after the sudden heel and encountered water on the way up.

TESTIMONIES FROM CREW MEMBERS

It would be important to know exactly what the crew members saw and what they reported about the situation on the vehicle deck. Unfortunately the statements are to certain extent controversial with each other, and sometimes also controversial with physical facts. Therefore any selection of the statements will unavoidably be somewhat subjective. Thus also other interpretations than the one below are possible.

According to the interview on 03.10.94 at the security police in Tallinn, at 00:45 AB Seaman on watch (C16) was on the vehicle deck just in front of ramp and heard a crash from behind the ramp. C16 stated further that everything was fine on the vehicle deck at that time.

After the accident in the hospital the crew member C15 overheard a discussion according to which AB Seaman on watch C16 had been on the vehicle deck and said into walkie-talkie that there was lots of water on vehicle deck and that they should abandon the ship. This interview took place on 30.09.94 in Bromma.

Another crew member C6 has confirmed the information from C15.

The AB Seaman on watch (C16) obviously never returned to the vehicle deck later on, thus it can be assumed that he made this call with the walkie-talkie around 00:45.

The three crew members in the ECR (motorman C7, system engineer C33, and 3rd engineer C36) reported seeing water coming in on the monitor showing the ramp. In the first interview the motorman C7 said:

At 00:46 there was a narrow stream of water or a jet at the right hand side of the bow ramp. Little after the moment when the sudden heeling took place C7 came into ECR and the 3rd engineer said to him: “The situation is serious (or bad), while the ramp has become broken.” According to the Swedish translation of this first interview on 29.09.1994 in Turku the motorman C7 saw large waves on the vehicle deck. After a new interview with C7 this statement has been corrected by Kurm (2007) as follows:

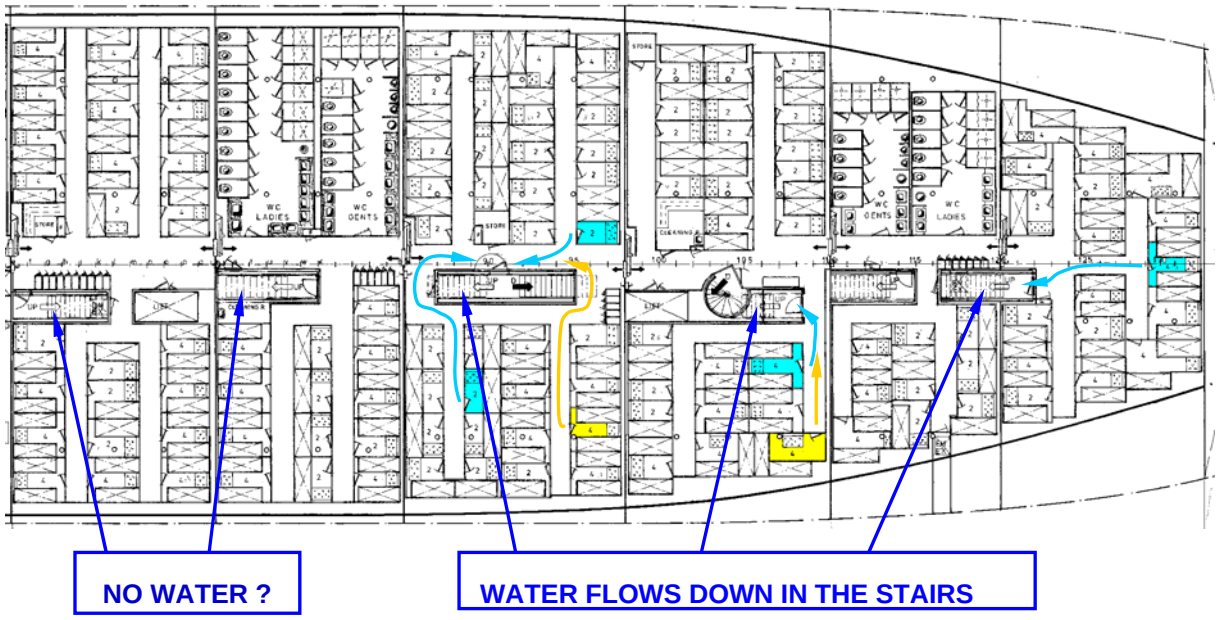

Fig. 16: Location of survivors, who reported water on Deck 1, and their likely escape routes,

First, C7 did not see water in the camera viewing the ramp, but in the camera, which was looking over to starboard from the centre of the ship. It was a camera below the ceiling directed towards the pilot door; and the floor

could only be seen in the narrow passage that had been left between the cars so that the pilot could pass through. It was not possible to see the floor in the camera looking at the ramp, which the 3rd engineer and the system engineer were looking at. All three men confirmed this (Kurm, 2007).

Second, C7 has never talked about the waves of water reaching up to the cars. He saw that "water had gathered at the side of the deck, reaching up to the lights of cars in the outermost row … and as the ship was rolling, it was flowing from one end to another." Thus, there was about 40 to 50 cm of water on the starboard side, and the ship already had list, how else water could have gathered on the starboard side of the ship (Kurm, 2007).

The 3rd engineer testified on 3.10.94 in Tallinn: I saw on the monitor after the impacts that large quantities of water were being pressed in through the sides of the ramp and under the ramp. There were no seals at the ramp itself, or at its sides.

The 3rd engineer C36 said on 31.03.95 at Landvetter Airport: After the blows I saw in the monitor showing the ramp that water was penetrating between ramp and hull at such a high pressure that the camera was hit. I realized that the vessel rolled 3° to starboard and 1.5° to port and the next time much more to starboard and upright and then a very heavy heel to starboard. Then I heard the voice of AB Seaman on watch (C16) on the walkie-talkie that water was coming in.

The mentioned video camera was probably situated below the level of the fourth deck, that is, about 4.0 - 4.5 m above the vehicle deck, on the front face of the center casing, about 25 meters from the ramp. C36 testified further about the amount of water that came in on both sides of the ramp: As if one would throw water in with buckets. So it was not some individual drops.

In general the three crew members were speaking of lots of water coming in at the sides of the ramp. Let us interpret the statement of C36 literally: A bucket has a capacity of around 10 liters. Let us assume that as much as 5 buckets of water came in per second. This makes 3 m^3 in one minute. This amount is so small that the ship is really not in danger. However, according to the motorman, the 3rd engineer had said that the situation was bad, as the ramp was broken.

The AB Seaman on watch (C16) had understood this obviously already earlier around 00:45 when he said into the walkie-talkie that there was lots of water on vehicle deck and that they should abandon the ship. After this C16 went on to the bridge, where the captain was concerned that the ship would be late. Later C16 was ordered to go down to the vehicle deck to check the situation again. He was at the information desk on Deck 5, when the sudden heel occurred. He claims he tried to reach the vehicle deck. He reached the Deck 4, but he could not get further down because passengers fleeing from below clogged the narrower stairs leading down from Deck 4. Thus he did not go down on to the vehicle deck anymore and he is still alive today. It can be only added that after the accident divers found over 35 victims in the lobby on Deck 4 (JAIC, 1997), which is located just one floor below the information desk, at which C16 had been standing. Also all three crew members in ECR managed to escape. All four were safe in life rafts already at 01:24-01:30, that is, very much at the same time as the officers on the bridge sent their MAYDAY, about 40-45 minutes after the call of the AB Seaman on watch (C16) on the walkie-talkie.

According to the their testimonies the three crew members saw water only on the monitor screens in the ECR. They have not reported being on the vehicle deck themselves. The AB Seaman on watch C16 himself has never reported seeing water on the vehicle deck. Yet they all understood to abandon the ship sufficiently early. Their testimonies may not give a complete picture of what the crew members knew, what they did and when this took place.

Discussion

If we believe in the JAIC scenario, we still have the problem with the open ramp assumed in the JAIC scenario and the closed, but broken ramp observed by the three members of the crew. Here are some alternatives to explain the dilemma.

(1) The crew members saw the ramp just before it was pulled open by the visor. They may also have left the engine control room somewhat earlier than they have reported.

(2) How could the video camera on the center casing observing the ramp be sprayed with water? One answer to this question could be that the speed of the finer spray coming from the opening at the bow could perhaps just reach the camera and make it wet. Second answer is perhaps better: If the ramp was open, waves coming in at almost full ship speed could have sloshed against the front face of the central casing splashing some water high up to the video camera located at height 4.0 - 4.5 m above the vehicle deck. It was not possible to see the floor in the camera looking at the ramp (Kurm, 2007). Thus the crew members in the ECR were not able to see whether any water was sloshing on the deck between the ramp and the front face of the center casing, but they could certainly see if the camera was splashed with water.

If the camera was sprayed with water, how could the crew in ECR see clearly the ramp and the spray on both sides of it on the monitor connected to this camera? There were lights on the vehicle deck. The ramp had a dark color. Outside it was dark. Could it be possible that the ramp was open, and that the crew members saw just a dark opening, where always earlier the ramp had been?

(3) They all observed correctly and told the truth, and the ship sank with the ramp only slightly open, that is, in the position of only about 1-1.4 m open, which at the moment does not appear to be mechanically possible. This would imply changes in the JAIC scenario.

CONCLUSIONS

Based on the survivors' testimonies the following conclusion can be drawn:

⇨ The accident can be considered to have started, as reported by the TUHH, already around 01:00 and not at 01:14 as stated by the JAIC.

The investigation with the motion simulation of the damaged ship including the sloshing of water on the vehicle deck gives plausible explanations in following issues:

⇨ When water was sloshing on the vehicle deck, limited amounts of water could flow down on to Deck 1 trough the front staircases in the central casing already at early phases of the accident.

⇨ In view of the water being able to flow from the vehicle deck down to the Deck 1 at the early phases of the accident, the assumption of damage deeper down on the hull as a cause for the water on Deck 1 appears superfluous.

⇨ The sudden heel was probably caused by the start of the turn of the vessel initiated by the officers on the bridge.

⇨ The main flooding of the vehicle deck probably took place, after the visor had dropped, either trough the completely open bow ramp or through the bow ramp at least about 1 m open, when the ship was turning.

⇨ The scenario of the visor and ramp being loose, let's say both about 1 m open, is not likely to be the main flooding scenario for the vehicle deck. The inflow rate appears to be too small for this. This implies that the visor dropped off relatively early and did not hang on the vessel until the ship heeled to near or over 90°.

The HSVA investigation is going on, thus all results presented are preliminary.

ACKNOWLEDMENTS

The financial support of the Swedish Governmental Agency for Innovation Systems (VINNOVA) is gratefully acknowledged. All work presented was conducted with a grant from VINNOVA, under the file reference number 2005-02901.

REFERENCES

FAIB, The Accident Investigation Board of Finland. (Onnetto-muustutkintakeskus). Transcripts of the Testimonies of the Survivors and other Persons related to the MV Estonia accident, 1994.

Holtappels, P., Hummel, W., ("The German Group of Experts", GGE), Investigation Report on the capsizing on 28 September in the Baltic Sea of the Ro-Ro Passenger Vessel MV Estonia, 1999.

JAIC, Final Report on the Capsizing on 28 September 1994 in the Baltic Sea of the Ro-Ro Passenger Vessel MV ESTONIA. The Joint Accident Investigation Commission of Estonia, Finland, and Sweden, 1997.

JAIC Supp. 523, (JAIC Supplement 523) Rintala, S. and Karppinen, T., MV Estonia Accident Investigation - Numerical predictions of the water inflow to the car deck, Technical Report VALC174, VTT Manufacturing Technology, Espoo 1996.

Kurm, M. Presentation on behalf of the Committee of Experts formed for the investigation of circumstances related to the transport of equipment for military use on the passenger ferry Estonia in September 1994. The Estonia Debate Continues, International Workshop 11 May 2007 Glasgow, Scotland.

Nuorteva, J., Sea Floor Deposits, A Map to JAIC Supplement 501, 1995.

Schager, B., Personal Communication, 2006.

SPF, National Board of Psychological Defence of Sweden (Styrelsen för psykologiskt försvar, SPF), Estoniasamlingen. Transcripts of the Testimonies of the Survivors and other Related Persons.

SSPA, Allenström, B., Thorsson, S.: MV Estonia – Manoeuvring tests and Bow Ramp Flooding tests. SSPA Report 4006 4100-1, 2007.

Valanto, P., Time-Dependent Survival Probability of a Damaged Passenger Ship II – Evacuation in Seaway and Capsizing. HSVA Report No 1661, Hamburgische Schiffbau-Versuchsanstalt GmbH, 2006. Available on www.hsva.de.

MV Estonia, a Plausible Sinking Scenario

Rolf Imstøl
Bergen University College

ABSTRACT

This paper shows how the assertion, set forth by the German group of experts, that MV Estonia was leak may make perfect sense. A possible similarity between the MV Estonia the MV Al Salam Boccaccio 98 cases is established and the paper may give essential erudition to two major disasters costing the life of nearly 2000 seafarers. Though not a point by itself the paper hints how an imprudent investigation may lead naval architectural analyses astray.

KEYWORDS

MV Estonia, MV Al Salam Boccaccio 98, Ro-Ro Pax, Pilot doors, disaster, capsizing, foundering.

INTRODUCTION

The official approach to the Estonia sinking has been that water flowed into the garage by an open bow-ramp. However, a German group of experts early pointed that the ship was leak. This assertion, which was regarded as physical impossible by the investigating specialists at the MV Estonia workshop in May 2007, is analyzed in this paper.

A central point is why Estonia sunk by stern when the German group of experts maintains water was up-flooding fairly far ahead. Use of ballast as well as drainage of bilge is suggested to explain how trim caused by the forward inflow might have been controlled by pumps prior to the ship suffering energy black-out.

In the aftermath of The Herald of Free Enterprise disaster even the most fearless masters must be expected to be very anxious about water accumulating at car-deck. Consequently one may not rule out that masters, at time of emergency, attempt to improve the insufficient drainage of these ships. Furthermore, since the scenario of water penetrating Estonia by the bow-ramp only, has

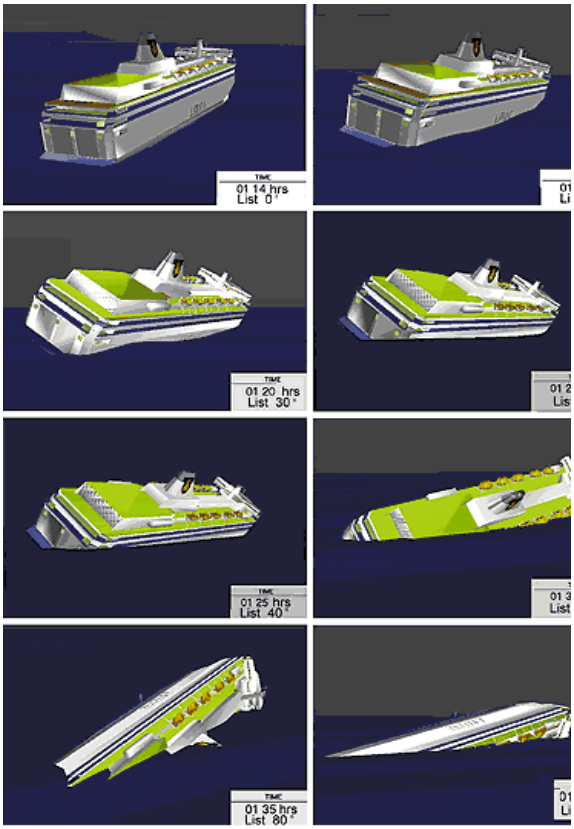

Figure 1: Computer generated scenario by JAIC. The author presumes these pictures are based on testemony by survivors rather than by simulation of any scenario [1, Fig. 13.3].

never been properly established, I early got the sensation that water might have penetrated the hull by some of the starboard side doors. Unfortunately, my hunch, that ship commands could consider such means, at time of emergency, was later highlighted in the Al Salam Boccaccio 98 disaster, in 2006, where 1069 seafarer lost their life.

For Estonia as well as Al Salam Boccaccio 98 one has to explain how the buoyancy represented by the freeboard as well as the car-deck was lost. While a leak bow-ramp might have been contributing in the MV Estonia case a similar scenario is not plausible for Al Salam Boccaccio 98. She had a fixed bow and her collision bulkhead was extended up to the forecastle deck in front of the garage. Furthermore, her initial water flooding was due to the fire fighting rather than water penetration of the hull.

A missing video from the official Estonia investigation, which might have thrown some light about an alleged artificial sand-heap covering one of the pilot doors as well as the leakage, has been central for this article. Though I have used much effort on this topic no information has been gained. I have, however, learned that the technical information regarding the Swedish attempt to protect the wreck from divers is missing as well.

THE DISASTER AND THE INVESTIGATION

MV Estonia foundered in bad, but not extreme, weather September 28th 1994 and 852 seafarers lost their lives while 137 were rescued. Shortly after the disaster governors of Sweden, Finland and Estonia decided, based on purely ethical reasons that one should not search for and bring up the 757 bodies still missing. The approx 130 bodies already sighted were left inside the wreck. Though the biggest underwater entrepreneur, experienced from the Alexander Kielland disaster, recommended rapid search and rescue for bodies surrounding the wreck such search was never carried out [1].

When the governors defined the site of the wreck as a sea tomb, relevant laws were issued in all the tree countries to prevent divers from entering it. The Swedish government took upon them to cover the wreck by concrete sheets but they were forced to abandon the project due to public resistance.

The official investigation was performed by a Joint Accident Investigation Committee (JAIC) consisting of Sweden, Finland and Estonia [2]. A German group of experts made their own investigation on behalf of the shipyard and these experts were so alarmed by the proceedings of JAIC that they published their 1st report prior to the JAIC report and another one some years later [3& 4].

In 2005 Swedish authorities initialized a project headed by Swedish Ship Research Centre (SSPA) to analyze the disaster. The project should start from the recent JAIC studies and it should analyze all known evidence to obtain a better understanding of the sinking. The project seems impeded by the tomb protection laws as new surveys have been shut out by authorities [5]. This seems strange since the tomb covering was aborted to uphold the needs of future investigations. [6]

In 2006 Swedish authorities started a criminal technological investigation of some of the videos taken from the seabed. The mandate was extended a year later to include the first video surveys as well. The criminal technological investigation did, however, not include investigation of an alleged artificial sand heap [7].

In May 2007 a Swedish financed workshop regarding the Estonia disaster took place in Glasgow. The technical presentations indicate that variations of the JAIC scenario were still being focused on though this time improved

simulation models were used. The original JAIC scenario may shortly be summarized:

> **MV Estonia lost her visor and her bow-ramp was forced open after which she maintained full speed heading up against the foul weather thus flooding her car-deck. During the foundering process, when Estonia sank, stern first, upside down, the ramp is expected to have closed itself.**

The scenario of the German Group of Experts, which so far has been rejected by specialists as physically impossible, may be summarized:

> **MV Estonia forced her way against hard weather with a weakened bow visor and ramp. The ship suffered a minor leakage which flooded the pool compartment. Simultaneously water cascaded into the garage by leakages at the side of the bow ramp.**

OBSERVATIONS AND OTHER FACTS

The survivors' observations:

Water cascading in beside the bow-ramp had been observed at the engine control monitor for considerable time prior to disaster [5]. A similar monitor was located in the chart-room adjacent to the coning-position.

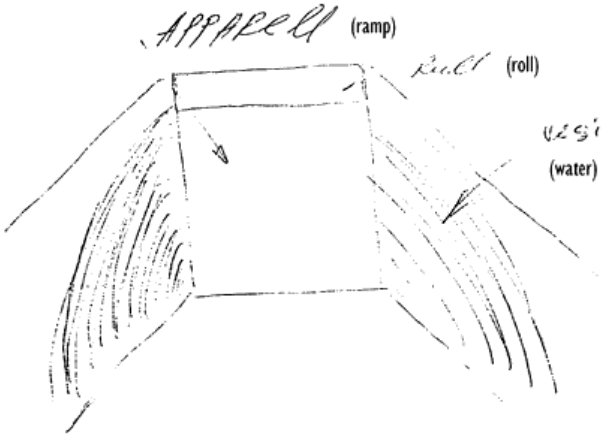

Figure 2: The water inflow observed at the engine control monitor [2, Fig. 6.1].

- The bow visor was observed flexing prior to disaster and water was observed cascading up between the hinges of the visor [8, p65]. Though one could not see the visor from the coning-position a lookout would have been able to study it from the forward staircases [2, $3.2.7].

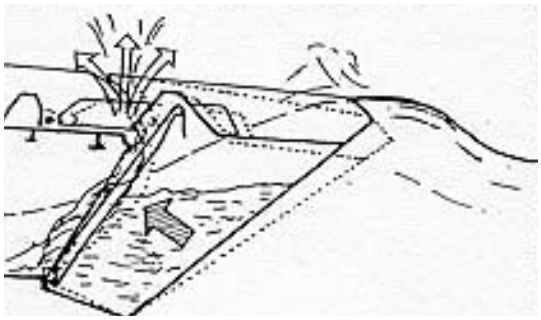

Figure 3: Observed water cascading up behind the visor [4, $31].

- The disaster was pre-warned by passengers who noticed water up-flooding from the pool compartment. This fact was disputed at the workshop, but my impression is that many sided with the German group of experts in this matter [3, p35]. NOTE: I have no personal opinion whether there was up-flooding or not, I merely analyze the situation if it was.
- The bilge pump was started prior to disaster [8, p71].
- A tentative MayDay was noticed by another ship at this time, but it was weak and as it was not repeated; nobody took any notice [4, $22.1].
- The disaster was initiated by huge roll and pitch [3, p36].
- A strong bang which experts at the workshop considered to be made by slamming, rather than explosion, was heard.
- MV Estonia was observed to have turned shortly after the huge roll & pitch [8, p225].
- The bow-visor was observed to be attached to the wreck when Estonia foundered by 6 survivors [8, p118].
- The bow-ramp had been observed to be closed shortly prior to foundering by survivors walking on it [5].

- The ship is reported to have done a banana-turn. That is; the ship command reduced speed and initiated a turn to starboard then huge heel forced an uncontrolled turn to port [8, p. 225].

Other facts

- The time domain scenario by JAIC (Fig 1) seems to be more or less agreed on.
- Concerning a harbor control exercise performed shortly prior to departure the JAIC report states: *The Swedish inspectors leading the exercise have been interrogated by the Commission and have stated that the vessel was in good condition and very well maintained*. This has been highly disputed and 2 Swedish journalists have written an interesting, though alarming, book on the subject [9]. They assert the Swedish inspector in charge wanted to prevent the ship from sailing and that he called his superiors in this respect. The journalists further pointed that a Swedish commission member withdrew from the commission when he was deprived of his right to write a divergent opinion regarding the seaworthiness. The commission member, a psychologist, interpreted the statement by the Swedish chief inspector to be about the finery of the ship, rather than the seaworthiness.
- The rear-ramp was observed to be slightly open. The German group of experts has suggested it might have been opened deliberately to drain water from the car-deck [4, $31].

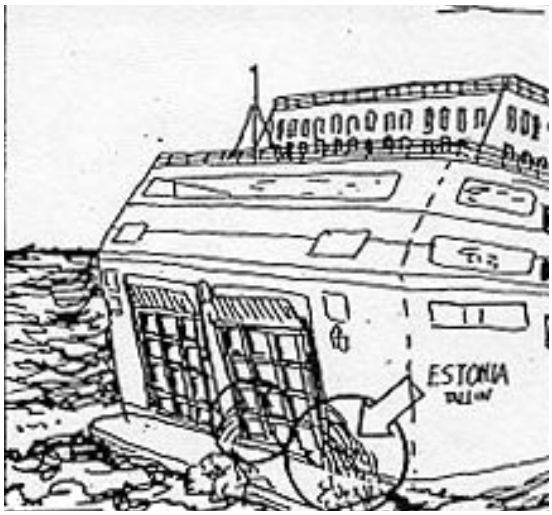

Figure 4: The German group of experts has suggested the rear ramp was opened to drain out the water that flowed in by the bow ramp [4, $31].

- Radio-logs by the Swedish high command may have been lost [8, p169].
- The bow-ramp was found slightly open and marks on the underside prove it must have been knocked against the fore peak at least once. While JAIC as well as present investigation groups seem to believe the bow-ramp stayed open for considerable time and closed itself when the ship foundered, others have suggested it might have been forced open after the foundering. The damage might as well be of earlier date.
- The bow-visor was found far west of the wreck, in a position that Dr Valanto at the workshop considered natural if the ship turned shortly after loosing her visor.
  - Since the German group of experts thinks the location of the visor contradicts observations by survivors the group has suggested the bow visor was dislocated shortly after the foundering.
  - The finish radar-plot is missing. The master of Silja Europe pointed at the interrogation that the plot by JAIC was obviously wrong [8, p213]. Dr. Valanto of HSVA seems to agree on this because the elapsed route does not

comply with the drift he estimates the ship might have had. The opinion of the master should of course carry much weight, when the surveillance plots were not to find; the master was designated On the Scene Commander (OSC) [2, $7.1].

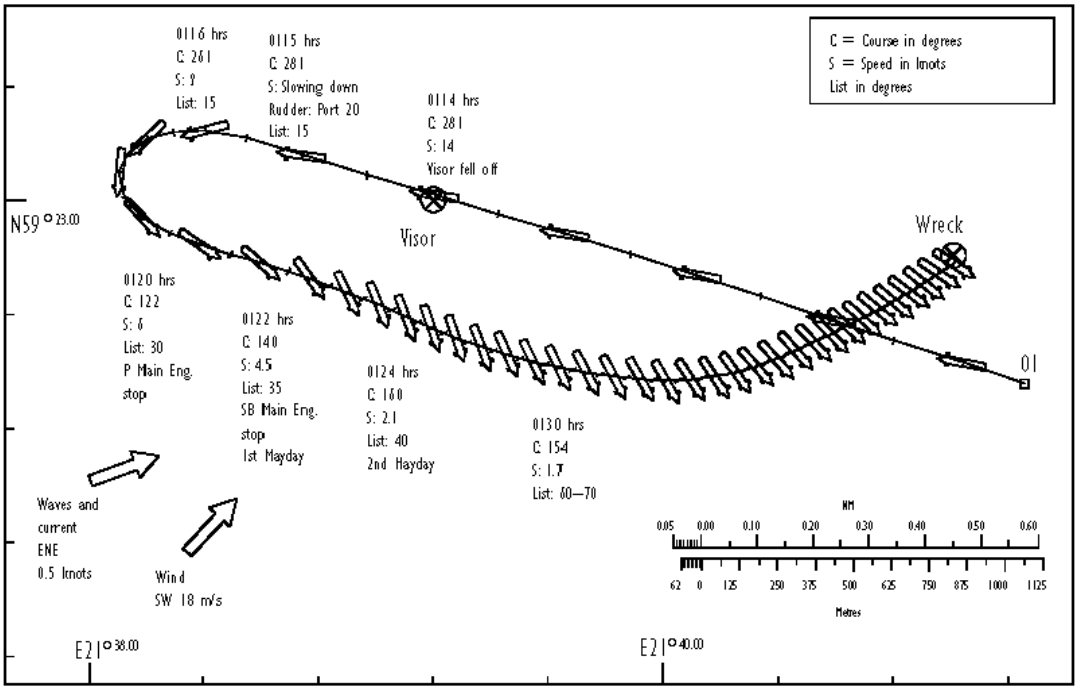

Figure 5: The JAIC plot shows how they expect the ship headed up against foul weather after the visor has been lost [2, Fig 13.2].

- Though present stability analyzes make use of better simulation software than the previous, no scenarios so far analyzed, seem to have been found physically possible by simulations.
- The doors separating the car-deck from the stairways were fire-resistant but not watertight. The aft most of these doors was, according to the German group of experts, very wide and had no threshold in order to facilitate easy transport of storage.
- The port heel tank is expected to have been full and the starboard empty at departure [2, $5.3]. The workshop was told that the cross-over valve separating these tanks would open automatically if the watertight doors should be closed. Consequently, such ballasting could heel the ship in all damage situations, port side damages exempted.
- The fore peak is expected to have been full. [2, $5.3]
- Model tests presented by SSPA at the workshop indicate the bow ramp would have bounced wildly up and down if the ship encountered the waves with full speed. Unfortunately SSPA refuses to hand out a copy of this very interesting video.

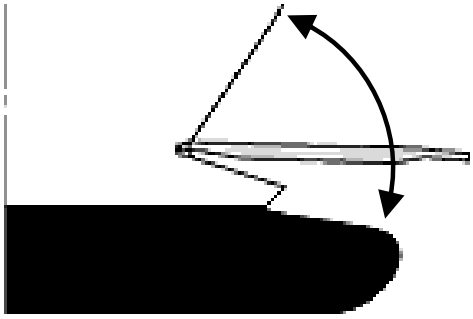

Figure 6: Model tests shows the bow-ramp would bounce wildly and close itself for the oncoming waves [2, Fig 10.2].

- SSPA informed at the workshop that the rip off forces acting on the hinges have never been analyzed. Though the question was repeatedly raised, none of the experts

suggested that strength analyzes of the hinges might prove the open ramp scenario to be physically possible. Later Swedish authorities strangely argued that it has not been within the mandate of SSPA to take the strength of the hinges into account. Though the call for bid actually points that the JAIC description of the sinking process should be used as starting point it was hopefully not the authorities' intention to duplicate the JAIC work. NOTE: Neither the call for bid, nor the bid itself, indicate model test and simulations, were not to take prudent consideration to the natural laws of science.

- Anders Björkman states: *The forward starboard pilot door is situated in that area (at frame 122) and should thus have been visible on the mudline video. However, the video films of both 1 October (seabed survey) and 2 December (mud line survey) have been edited in just that area, i.e. the films have been cut and the superstructure side and the pilot door cannot be seen!* [10, $1.16].

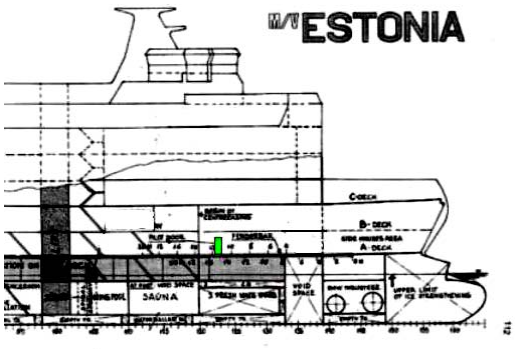

Figure 7: The figure shows how the mud level was expected to be at the site of the forward starboard pilot door [10, Fig 1.16.4].

- Anders Björkman further states: *The Gregg Bemis dive expedition 2.24 inspected the area (Section D) in 2000 and found that the superstructure side was covered by sand (!) up to the level of the fender between hull and superstructure that didn't match the seabed mud, i.e. sand had been deposited against the wreck to change/raise the mud line and to cover the superstructure side and the pilot door. The whole area below the wreck - where you could have seen the superstructure side in 1994 - was filled with sand in 2000! It can hardly have been swept in by, say currents.* [10, $1.16]
  - The assistant director of prosecutions of Estonia could not give any information at the workshop regarding the alleged artificial sand-heap.
  - Later Swedish authorities have informed that their archive does not hold any technical information regarding the aborted protection of the wreck. The only documentation received is the governmental decree which orders the work immediately stopped with one exemption; the pressure banks could be completed. I have learned from NCC that these pressure banks should support the concrete sheets rather than the ship. Furthermore they should not be located close to the wreck. When NCC and the salvage company Smidt were released from the contract no sand-filling had been done close to the wreck and they do not know anything about the alleged sand-heap. The only remaining contractor, the gravel-covering specialist Van Oord, has not responded to questions in this regard.

About the observations highlighted in this paper

The observations selected for this paper are those which I have found explanatory to the leak scenario I am presenting. To my knowledge the scenario is not contradicted by other observations.

The Swedish historian Knut Carlquist who, by profession, should be expected to be able to analyze statements, seems to back the observations collected by the German group of experts.

NUMERIC SIMULATIONS

At the workshop two different approaches to the simulations were presented.

- HSVA (Hamburg Ship Model Basin) uses a fluid-mechanical model.
- SSRC (Ship Stability Research Centre) seems to use a more traditional hydrostatic model.

If my understanding of these models is correct, than the first of them may have the highest theoretic potential while the last requires less calculation. At the workshop Dr. Valanto of HSVA informed that their model, in contrast to the more traditional ones, indicate that water will stay quite flush with the deck when ships are moving in waves. Consequently more water would accumulate in rough weather by this model, prior to the low frequency instability of the trapped water becomes overwhelming. At that moment one may assume that the initial roll may be quite huge as the trapped water moves from the unstable 0 heel to one of the two relatively large low frequency lurching angles. This partly explains the big roll & pitch. Furthermore, and generally speaking, one may assume water to accumulate at passenger ships' freeboard decks for many damage scenarios where one at present, assumes water will drain off!

While the behavior of ships and inflow of water through openings in the hull is well known, the Estonia simulations are sensitive to down-flooding trough various openings from the car-deck. Since these are not statically submerged one has to simulate the flow under, beside, in front of, and abaft the trucks due to roll and pitch of the ship itself. This is hardly an easy task and it is far from obvious that the simulations will produce unambiguous results. This was emphasized at the workshop when professor Vassalos, responding to question, pointed that they considered their SSRC-simulator to handle this problem conservatively. However, engineering history proves calculus considered to be conservative, frequently have been far too optimistic. Another question is what is to be considered conservative in a situation like this. Conservative while ruling out a scenario is quite another thing than being conservative proving a scenario to be possible. Consequently various down-flooding models may be needed.

To put above reasoning in other words: When the simulation-model is uncertain one may crudely categorized the results:

1) Despite uncertainties the simulations proves that the ship would sink by the scenario
2) Despite uncertainties the simulations indicates that the ship might sink by the scenario
3) The Simulations of the scenario give no indication
4) Despite uncertainties the simulations indicates that the ship might not sink by the scenario
5) Despite uncertainties the simulations proves that the ship would not sink by the scenario

Scenarios fitting well with observations should fall into category 5 to be ruled out while scenarios fitting badly with observations should be categorized as 1, maybe 2, to be taken into consideration. In my view, based hydrostatic logics as well as rude estimates by an offshore simulator, I will categorize the scenario here presented as category 2.

THE PROPOSED PLAUSIBLE SCENARIO:

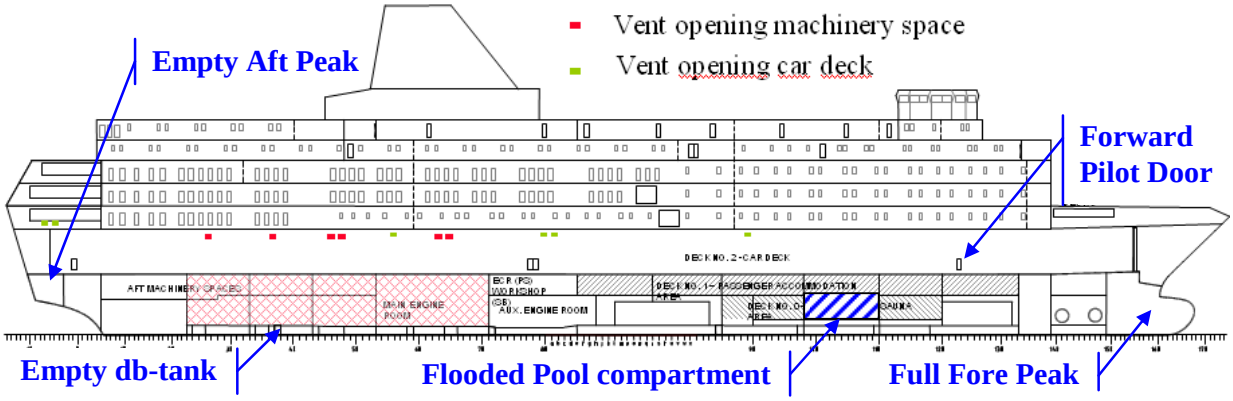

Figure 8: Inflow points according to Chalmers University at the workshop and ballast distribution according to JAIC

The only scenario I find to comply with above observations is as follows: Sometimes during the evening of disaster, the pool-compartment, situated forward at the lover deck, started to leak. Additionally, the leakage beside the bow-ramp seems to have been more predominant on her last voyage (Fig. 2). The sketch by the engineer on duty indicates that the water-level in front of the ramp may have been approx 6m above CWL and the flow seems to have been rather constant [5]. Such flow fits with the observation that the visor was flexing as one may expect the visor was forced open by the wave impact; otherwise closing.

Flooding of the pool compartment would of course make the bow work harder and the pressure on the ramp would be higher than normal. As long as the trim was by stern, the ship could drain water from the car-deck by opening the rear ramp as suggested by the German group of experts. However, sooner or later the ship would be likely to trim by head. Due to starboard heel and the gradient of the car-deck the starboard pilot door would become the lowest point of the car-deck and it would be the best option for additional drainage.

Flooding of the pool-compartment would cause the ship to trim forward entailing the bow to work harder and the inflow beside the bow-ramp to increase. Under such circumstances it seems quite likely that the ship command would discharge ballast from the full fore peak to reduce the pressure on the bow. Though one should have checked the keel for leakage if the water on the car-deck stowed ahead, one may hardly blame the command if they, unknowing of the leakage, attempted to raise the bow by emptying the fore peak and filling the db-tank to reduce strain on the bow. If they really felt they were in hurry they might have ballasted the aft peak as well though this would cause rather great free surface moment.

As previously mentioned the German group of experts has suggested that the forward starboard pilot door was opened to discharge suspect cargo. I find it more likely the door might have been opened to drain water and save the ship. We know, from the Al Salam Boccaccio 98 disaster that such use was at least mentioned [11 & 12].

When the ship command of Estonia learned that water flowed up from the pool-compartment, they must be expected to have started the bilge pump. Though bilge pumps

are rather small it is far from obvious it might not have checked such a small leakage as advocated by the German group of experts.

If the leakage was small and ballast as well as bilge pumps were running the ship could have been altering trim by stern thus bringing the water at the car-deck to be distributed over a greater area. Consequently the longitudinal as well as the transversal stability would deteriorate. Simultaneously the bow was weighted down by water inside the visor and, to some extent, water on the forecastle deck. If this water was released during a short period of time, the longitudinal equilibrium could falter and provoke an internal monster wave which would dislocate cargo longitudinally as well as transversally. The centre-casing would combine roll and pitch movements caused by internal water flow on the car-deck because the water had to circumvent the centre-casing.

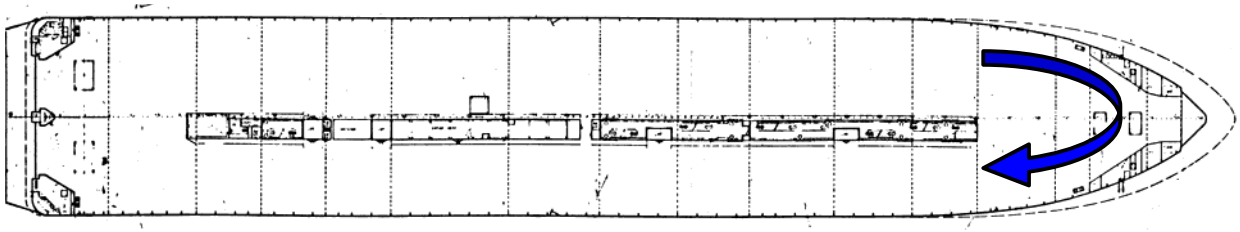

Figure 9: Car-deck & centre-casing. The centre-casing may very well create circular water-flow thus combining the roll & pitch.

A turn, to port, might have been initiated by a wheel order causing the big roll and pitch and subsequent starboard list. However, it might have been the other way around as well. The underlying instability finally initiated the big roll and pitch where after the starboard list initiated the turn to port. The reduced speed and the banana turn indicate that something of the sort happened [8, p. 225]. Reduced speed might have reduced the anti-heel effect and induced roll! It might have brought about pitch as well [3, p36]. How the rudder actually was used is difficult to say as only observations of the wake will indicate the rudder angle. A starboard turn might have been initiated and then, if the ship preferred to go starboard due to heel, the rudder may have been turned by the ship command.

Down-flooding of water from the garage to the lower decks would be by the stairways through the fire-doors which one may presume had been knocked of during the huge roll and pitch. The aft most of these doors had been made flush with the car-deck and very wide in order to facilitate carts to enter the elevator. Consequently down-flooding by this door must be expected to be much higher than by the other doors.

If any pilot doors were open, one may expect that inflow by them and down-flooding from car deck eventually could heel the ship some 40º. Then the ventilators penetrating the hull at the top of the garage would be submerged and inflow would increase (Fig 8). The down flooding of engine-compartments could very well be faster than down-flooding as well as inflow through the hole forward. This could submerge the aft part of the centre-casing with its ventilator shaft and staircases. Consequently the down-flooding rate of engine rooms would increase considerably.

Though some air would be trapped in the engine-rooms this would not necessarily be sufficient to prevent the ship from foundering when the forward part was flooded from the garage and air escaped by the hole in the pool-compartment.

If one is to believe the observations of 6 survivors that the visor was attached when Estonia foundered; somebody dislocated the

visor afterwards. The direction and distance of the dislocation seem reasonable if the intention was to make it look like MV Estonia foundered when she tried to escape the weather with open bow. If the bow visor was deliberately dislocated it seems reasonable to believe attempts were done to rip off the bow-ramp and dislocate that as well. This might explain the damage to the bow-ramp. If the pilot doors were open at time of disaster salvage of the ship would surely uncover this.

Very accurate numeric simultaneous or model test might prove the scenario here suggested to bee physically impossible. However, there is hardly any reason to state, by a mere glance at the problem that Estonia could not sink the way she did, due to a rather small forward hole.

Some second thoughts about the proposed scenario.

The scenario above suggested is the one best complying with the information from the German group of experts. However, the suggested sinking scenario is independent of the whereabouts of bow visor and the ramp. Consequently a modification could be suggested:

> **MV Estonia headed up against rough weather at full speed with her bow visor flexing and her ramp leaking severely. Some of her pilot doors at leeward were kept open to drain water from her car-deck and ballast as well as bilge pump was used to trim her by stern. The bow-ramp was never lowered and the damage below the ramp was due to cargo operations prior to the voyage. The visor might have been knocked off causing the ship command to turn the ship or it might have been the other way around. The ship command, knowing about the leakage, was forced to turn and the turn itself started the huge heel and the visor was knocked partly off by wave forces combined with huge roll & pitch.**

The lack of a reasonable sinking scenario combined with the general distrust of the investigation seems to have nurtured many speculations regarding manipulation of the wreck. Most of these are unimportant to the international ship stability expertise and should not be included in this paper. However, if sand was filled below the forward part of the ship to hide evidence and prevent erudition this should concern us.

THE HUMAN FACTOR

JAIC assumed that Estonia maintained course and speed up against the weather when ship command should be able to observe at the monitor that the bow-ramp was totally open. I am not convinced this is the only plausible hypothesis regarding the course of action. I find it more likely that ballast might have been used and that a pilot door might have been opened. Another fair presumption, if the situation developed slowly, is that ship command telephoned superiors for advice.[1] If this was the case we should expect it happened no later then the bilge pumps were started and a weak, tentative MayDay was heard. Radio-logs of coastal and satellite radios should be able to indicate the answer to this question. Unfortunately, radio-logs by the Swedish high command may have been lost [8, p169].

Human factors might as well have influenced the examination of the scene of disaster itself since it could not follow any national structure of investigation. The Swedish historian Knut Carlquist describes the Estonia investigation as rather strongly influenced by political control [8, $5].

[1] As far back as 1978 the captain of Amoco Cadiz realized the utility of modern communication when he requested the company whether or not he could engage tugs.

- At the evening of disaster the Swedish government decided that the word salvage should not be used as it could be interpreted as salvaging the ship [8, p166]. Furthermore the prime minister indicated bow failure might have been the cause. The Swedish director of maritime safety pointed that Sweden was not ruled by ministers and he called attention to the importance of the independence of the authorities [9, p. 63]. He further argued that the ship had to be salvaged; *700 persons are still there and it would be remarkable if they are to find their final rest in the ocean* [8, p 174]. According to Knut Carlquist the prime minister let a former public prosecutor hang the director and the director was transformed to a non-person over night.
- Since the prime minister to become promised to salvage the ship above decision should not have been of any importance (the sitting government lost the election shortly prior to the disaster) [5]. However, when taking office the new prime minister appointed an Ethical Board as an alibi in the salvage conflict [8, p. 183].
- Shortly afterwards the director of maritime safety was squeezed to resign his commission.

Apart from the influence of political command the naval architects investigating the disaster might as well have been somewhat predetermined as they surely should have foreseen another Herald of Free Enterprise disaster. That is; the Swedish / Finish deviation from international rules invited for such a disaster and it had been forewarned by the DIANA-II incident [2 $11.3]. Though the investigators might not have known about the DIANA-II incident prior to the Estonia disaster they definitely did so during the investigation. Self-acting remorse by the Swedish Finish naval architectural community is surely understandable, but the investigation might have been severely hampered if design rather than observations were put at focus. The lack of correlation between proposed naval architectural scenarios and observations has later been noted of by the Estonian Assistant Director of Prosecutions [5]. Similar problems seem to have burdened the MV Rocknes investigation as well [13].

CONCLUSION

1) The scenario here presented seems to be in harmony with most witness observations and it should be considered plausible until it has been proven impossible by detailed simulations.
2) Important evidence could have been secured if the ship had been salvaged.
3) Seafaring authorities are advised to act precautionary and to do their outmost to inform mariners of the potential hazards of drainage by pilot doors [14].
4) The recommendation of the Egyptian Technical Committee that drainage systems of car-decks should not be based on gravity only seems well motivated [15].
5) Relevant authorities are advised to investigate if huge amounts of sand have been filled under the wreck.

AUTHORS' BIOGRAPHIES

Rolf C. Imstøl, a former merchant officer, holds the current position of head of the marine technical department at Bergen University College. Furthermore, he acts as marine technical & nautical consultant for solicitors working on behalf of many bereaved as well as some survivors in the Al Salam Boccaccio 98 and Rocknes cases. He has previously published a set of articles regarding the Rocknes capsize as well as a harbinger to this article; Accidents Involving Passenger Ship Stability [13 & 16].

REFERENCES

Communication between Swedish Authorities and Stolt Comex Seaway (Norwegian /Swedish), The Swedish Public

Record Office.

Joint Accident Investigation Committee, Final Report, Estonia 1997.

The German group of experts, Investigation Report #1 (Swedish), Ahlers & Vogel, Hamburg 1997.

The German group of experts, Investigation Report #2, http://www.estonia.xprimo.de/estonia/index.html

Lars Borgnäs, The truth at 80m depth (Swedish), Swedish National Broadcasting, Stockholm 2007

Swedish Governmental Decree, June 19th 1996.

Håkan Bergstedt, Swedish Criminal Technological Laboratory, March 22 2007.

Knut Carlquist, the Silent Game (Swedish), Stockholm 2001.

Mats Holm & Susanna Popova, the Protocol (Swedish), Finland 2003.

Ander Björkman, Disaster Investigation, July 2007: http://heiwaco.tripod.com/ekatastrofkurs.htm

Voices from beyond the grave echo doomed Red Sea ferry's final hours, Lloyds List 24th of July 2006

Black box transcript reveals four hours of confusion and fear as ferry sank, Lloyds List 24th of July 2006

Rolf Imstøl, The capsize of MV Rocknes, Norwegian Technical Review, Oslo 2005

UNESCO, The Precautionary Principle, March 2005

The International Technical Committee formed to Investigate and Analyze the causes for the sinking of the Ferry ASSALAM BOCCACCIO 98 in the Red Sea in February 2006, Technical Report, Egypt 2006.

Rolf Imstøl, Accidents Involving Passenger Ship Stability, The Design and Operation of Passenger Ships conference, London 2007

Link to the authors Estonia home-site

http://home.hib.no/ansatte/rci/Estonia

Session 4: Simulation of Parametric Rolling

Session Chairman: Prof. N. Umeda Dr. V. Belenky

1) J.Juncher Jensen, J. Vidic-Perunovic, P.T.Pedersen:

   "Influence of Surge Motion on the Probability of Parametric Roll in a Stationary Sea State"

2) Y. Ogawa:

   "An examination for the numerical simulation of parametric roll in head and bow seas"

3) T. Fujiwara, Y. Ikeda:

   "Effects of Roll Damping and Heave Motion on Heavy Parametric Rolling of a Large Passenger Ship in Beam Waves"

4) C. A. Rodriguez, C. Holden, T. Perez, I. Drummen, M. A. S. Neves, T.I. Fossen:

   "Validation of a Container Ship Model for Parametric Rolling"

5) H. Hashimoto, N. Umeda, G. Sakamoto:

   "Head-Sea Parametric Rolling of a Car Carrier"

Influence of Surge Motion on the Probability of Parametric Roll in a Stationary Sea State

J. Juncher Jensen, Jelena Vidic-Perunovic and P. Terndrup Pedersen

Department of Mechanical Engineering, Technical University of Denmark, Kgs. Lyngby, Denmark

ABSTRACT

A typical parametric roll scenario for a ship in head waves implies that the roll motion is coupled with vertical motion of the vessel. The added resistance of the ship is increased when the bow pitches down in a wave crest. As a consequence, the ship speed is slowed down and, hence, the roll resonance condition might be changed. In an attempt to study the influence of this speed variation in waves on parametric roll, the procedure for estimation of probability of parametric roll by Jensen and Pedersen (2006) has been extended to account for the surge motion of the vessel.

KEYWORDS

Parametric roll, FORM, mean out-crossing rate

INTRODUCTION

The roll motion of ships can lead to various types of failures ranging from seasickness over cargo shift and loss of containers to capsize of the vessel. Hence, it is important to minimise the roll motion during a voyage. A special problem is parametric roll as it constitutes a bifurcation problem making it difficult for the ship master to predict the onset of parametric roll as well as to devise procedures to eliminate it if it happens. Large roll angles typically built up over 10 to 20 wave periods. Examples from model test are shown in France et al. (2003).

Linear models based on the Mathieu equation clearly show that parametric roll is a bifurcation problem govern by a sinusoidal variation in the restoring moment during a regular wave passage and that the roll period should be about twice the encounter period to initiate parametric roll.

In real sea states the problem is less obvious. The wave profile along the length of the vessel is now described by random waves, reflecting the wave spectrum of sea. Thereby, also the restoring moment changes randomly. Furthermore, the resonance condition between the roll and encounter periods cannot be satisfied at any point in time.

In the present study the focus is on the resonance condition and, as the encounter period depends on the forward speed, the instantaneous surge velocity is estimated and used in the determination of the encounter period. Thus the previously applied time domain sea keeping model in Jensen and Pedersen (2006) is extended to include the surge mode. Calculations are then carried out for same container vessel in order to investigate the role of this surge motion for the probability of experiencing parametric roll.

The First-Order Reliability Method (FORM) is used to get the probability distributions as it has been shown, Jensen and Pedersen (2006) and Jensen (2007), to be an accurate and efficient procedure for estimation of the extreme value statistics of even very non-linear responses like parametric rolling.

FIRST-ORDER RELIABILITY METHOD APPLIED TO WAVE LOADS

Design point and reliability index

In the First-Order Reliability Method (FORM), the excitation or input process is a stationary stochastic process. Considering in general wave loads on marine structures, the input process is the wave elevation and the associated wave kinematics. For moderate sea states the wave elevation can be considered as Gaussian distributed, whereas for severer wave conditions corrections for non-linearities must be incorporated. Such corrections are discussed and accounted for by using a second-order wave theory in a FORM analysis of a jack-up platform (Jensen and Capul, 2006). In the present paper dealing with the roll motion of a ship, linear, long-crested waves are assumed and hence the normal distributed wave elevation $H(X,t)$ as a function of space X and time t can be written

$$H(X,t) = \sum_{i=1}^{n} \left(u_i c_i(X,t) + \overline{u}_i \overline{c}_i(X,t) \right) \qquad (1.1)$$

where the variables $u_i, \overline{u}_i$ are uncorrelated, standard normal distributed variables to be determined by the stochastic procedure and with the deterministic coefficients given by

$$\begin{aligned} c_i(x,t) &= \sigma_i \cos(\omega_i t - k_i X) \\ \overline{c}_i(x,t) &= -\sigma_i \sin(\omega_i t - k_i X) \\ \sigma_i^2 &= S(\omega_i) d\omega_i \end{aligned} \qquad (1.2)$$

where ω_i, $k_i = \omega_i^2 / g$ are the n discrete frequencies and wave numbers applied. Furthermore, $S(\omega)$ is the wave spectrum and $d\omega_i$ the increment between the discrete frequencies. It is easily seen that the expected value $E[H^2] = \int S(\omega) d\omega$, thus the wave energy in the stationary sea is preserved. Short-crested waves could be incorporated, if needed, but require more unknown variables $u_i, \overline{u}_i$.

From the wave elevation, Eqs. (1.1) - (1.2), and the associated wave kinematics, any non-linear wave-induced response $\phi(t)$ of a marine structure can in principle be determined by a time domain analysis using a proper hydrodynamic model:

$$\phi = \phi(t \,|\, u_1, \overline{u}_1, u_2, \overline{u}_2, ..., u_n, \overline{u}_n, \text{ initial conditions}) \qquad (1.3)$$

Each of these realisations represents the response for a possible wave scenario. The realisation which exceeds a given threshold ϕ_0 at time $t=t_0$ with the highest probability is sought. This problem can be formulated as a limit state problem, well-known within time-invariant reliability theory (Der Kiureghian, 2000):

$$\begin{aligned} &g(u_1, \overline{u}_1, u_2, \overline{u}_2, ..., u_n, \overline{u}_n) \equiv \\ &\phi_0 - \phi(t_0 \,|\, u_1, \overline{u}_1, u_2, \overline{u}_2, ..., u_n, \overline{u}_n) = 0 \end{aligned} \qquad (1.4)$$

The integration in Eq. (1.4) must cover a sufficient time period $\{0, t_0\}$ to avoid any influence on $\phi(t_0)$ of the initial conditions at $t=0$, i.e. to be longer than the memory in the system. Proper values of t_0 would usually be 1-3 minutes, depending on the damping in the system. Hence, to avoid repetition in the wave system and for accurate representation of typical wave spectra n = 15-50 would be needed.

An approximate solution can be obtained by use of the First-Order Reliability Method (FORM). The limit state surface g is given in terms of the uncorrelated standard normal distributed variables $\{u_i, \overline{u}_i\}$, and hence determination of the design point $\{u_i^*, \overline{u}_i^*\}$, defined as the point on the failure surface $g=0$ with the shortest distance to the origin, is rather straightforward, see e.g. Jensen (2007). A linearization around this point replaces Eq. (1.4) with a hyperplane in 2n space. The distance β_{FORM}

$$\beta_{FORM} = \min \sqrt{\sum_{i=1}^{n} \left(u_i^2 + \overline{u}_i^2 \right)} \qquad (1.5)$$

from the hyperplane to the origin is denoted the (FORM) reliability index. The calculation of the design point $\{u_i^*, \overline{u}_i^*\}$ and the associated value of β_{FORM} can be performed by standard reliability codes (e.g. Det Norske Veritas, 2003). Alternatively, standard optimisation

codes using Eq. (1.5) as the objective function and Eq. (1.4) as the constraint can be applied.

The deterministic wave profile

$$H^*(X,t) = \sum_{i=1}^{n} \left(u_i^* c_i(X,t) + \overline{u}_i^* \overline{c}_i(X,t) \right) \qquad (1.6)$$

can be considered as a design wave or a critical wave episode. It is the wave scenario with the highest probability of occurrence that leads to the exceedance of the specified response level ϕ_0.

Mean out-crossing rates and exceedance probabilities

The time-invariant peak distribution follows from the mean out-crossing rates. Within a FORM approximation the mean out-crossing rate can be written as follows, Jensen and Capul (2006):

$$\nu(\phi_0) = \frac{1}{2\pi\beta_{FORM}} e^{-\frac{1}{2}\beta_{FORM}^2} \sqrt{\sum_{i=1}^{n} \left(u_i^{*2} + \overline{u}_i^{*2} \right) \omega_i^2} \qquad (1.7)$$

Thus, the mean out-crossing rate is expressed analytically in terms of the design point and the reliability index. For linear processes it reduces to the standard Rayleigh distribution. Finally, on the assumption of statistically independent peaks and, hence, a Poisson distributed process, the probability of exceedance of the level ϕ_0 in a given time T can be calculated from the mean out-crossing rate $\nu(\phi_0)$:

$$P\left[\max_T \phi > \phi_0 \right] = 1 - e^{-\nu(\phi_0)T} \qquad (1.8)$$

The FORM is significantly faster than direct Monte Carlo simulations, but most often very accurate. In Jensen and Pedersen, (2006) also dealing with parametric rolling of ships in head sea the FORM approach was found to be two orders of magnitude faster than direct simulation for realistic exceedance levels and with results deviating less than 0.1 in the reliability index.

PARAMETRIC ROLL IN HEAD SEA

A very comprehensive discussion of intact stability can be found in a recent ITTC report on ship stability in waves, ITTC (2005). The report discusses various modes of failure, i.e. capsize and the prediction procedures available. Some codes, e.g. LAMP, France et al. (2003) and Shin et al. (2005), seem to be very general and can tackle all problems with reasonable accuracy, but are very time-consuming to run, restricting the application to regular waves or very short stochastic realisations.

Other procedures have more limiting capabilities. An example is the ROLLS procedure, Kroeger (1986). In this procedure, the instantaneous value of the righting arm *GZ* is in irregular waves calculated approximately using the so-called Grim's effective wave. The heave w, pitch θ and yaw ψ motions are determined by standard strip theory formulations, whereas the surge motion is calculated from the incident wave pressure distribution. The advantage of this formulation compared to full non-linear calculations is the much faster computational speed, still retaining a coupling between all six- degrees-of-freedom, Krüger et al. (2004).

In the present procedure a simplified version of the ROLLS procedure is applied. The heave motion w is taken to be a linear function of the wave elevation and the closed-form expressions given by Jensen et al. (2004) are used. Pitch is only included through the static balancing of the vessel in waves in the calculation of the *GZ* curve. Furthermore, the sway and yaw motions are ignored as the vertical motions have the largest influence on the instantaneous *GZ* curve. The damping is modelled by a standard combination of a linear, a quadratic and a cubic variation in the roll velocity. Furthermore, the analysis is restricted to head wave. With these simplifications the equilibrium equation for roll ϕ reads, with a dot signifying time derivative,

$$\ddot{\phi} = -2\beta_1\omega_\phi\dot{\phi} - \beta_2\dot{\phi}\left|\dot{\phi}\right| - \frac{\beta_3\dot{\phi}^3}{\omega_\phi} - \frac{\left(g - \ddot{w}\right) GZ(\phi)}{r_x^2} \qquad (2.1)$$

where r_x is the roll radius of gyration and g the acceleration of gravity. The roll frequency ω_ϕ is given by the metacentric height GM_{sw} in still water:

$$\omega_\phi = \frac{\sqrt{gGM_{sw}}}{r_x} \tag{2.2}$$

The surge motion u is determined from the equilibrium equation:

$$\ddot{u} = \frac{1}{1.05\Delta}\int_{-D}^{h_{cog}+w} p(z,t)B(z)dz + 10g\left(\frac{\dot{u}}{V}\right)^3 \tag{2.3}$$

The added mass of water in surge is thus taken to be 5 per cent of the displacement Δ and the pressure p is the incident linear wave pressure. Hence, radiation and diffraction effects are ignored. The integral is calculated for the ship cross section at the centre of gravity. The integration is from the draft D of the vessel to the instantaneous position $h_{cog} + w$ of the free surface. Here h_{cog} is the wave elevation at the centre of gravity and $B(z)$ the breadth variation over this section. The second term on the right hand side is an attempt to model the action of the captain to maintain the constant speed V in waves.

It is clear that the model, Eqs. (2.1)-(2.3) is very simplistic, but it is well-suited to illustrate the proposed stochastic procedure as it can model parametric rolling.

The instantaneous GZ curve in irregular waves is estimated from numerical results for a regular wave with a wave length equal to the length L of the vessel and a wave height equal to $0.05L$. These numerical results are fitted with analytical approximations, see Jensen and Pedersen (2006).

In a stochastic seaway the following approximation of the instantaneous value of the righting arm $GZ(t)$ is then applied:

$$GZ(\phi,t) = GZ_{sw}(\phi) + \frac{h(t)}{0.05L}\left(GZ\left(\phi, x_c(t)\right) - GZ_{sw}(\phi)\right) \tag{2.4}$$

This linear relation between GZ and h is clearly an assumption which needs validation. It is used here for the sake of simplicity, but also because the model, Eq.(2.1), by itself only gives an approximate description of reality.

The instantaneous wave height $h(t)$ and the position of the crest x_c are determined by an equivalent wave procedure somewhat similar to the one used by Kroeger (1986):

$$a(t) = \frac{2}{L_e}\int_0^{L_e} H\left(X(x,t),t\right)\cos\left(\frac{2\pi x}{L_e}\right)dx$$

$$b(t) = \frac{2}{L_e}\int_0^{L_e} H\left(X(x,t),t\right)\sin\left(\frac{2\pi x}{L_e}\right)dx$$

$$X(x,t) = \left(x + \left(V + \dot{u}\right)t\right)\cos\psi$$

$$h(t) = 2\sqrt{a^2(t) + b^2(t)}$$

$$x_c(t) = \begin{cases} \frac{L_e}{2\pi}\arccos\left(\frac{2a(t)}{h(t)}\right) & \text{if } b(t) > 0 \\ L_e - \frac{L_e}{2\pi}\arccos\left(\frac{2a(t)}{h(t)}\right) & \text{if } b(t) < 0 \end{cases}$$

(2.5)

It is seen that the coupling between roll and surge is solely through the term $X(x,t)$ in Eq.(2.5).

Stationary sea conditions are assumed and specified by a JONSWAP wave spectrum with significant wave height H_s and zero-crossing period T_z. The frequency range is taken to be $\pi \le \omega T_z \le 3\pi$ covering the main part of the JONSWAP spectrum.

Solutions are obtained by embedding the time domain simulation routine, Eqs. (2.1)-(2.3) in a standard FORM code. In the present case, the software PROBAN (Det Norske Veritas, 2003) is used.

NUMERICAL EXAMPLE

A container ship with same main particulars given in Jensen and Pedersen (2006) as Ship #1 is considered. The speed is chosen such that the mean encounter frequency is close to twice the roll natural frequency.

The GZ curves are shown in Figure 1 and 2 and it is clear that a significant reduction in righting lever occurs when the wave crest moves from

AP to 0.25L forward of AP. The lowest value of *GZ* occurs when the wave crest is at amidships. This is quite typical for ships with fine hull forms like container ships.

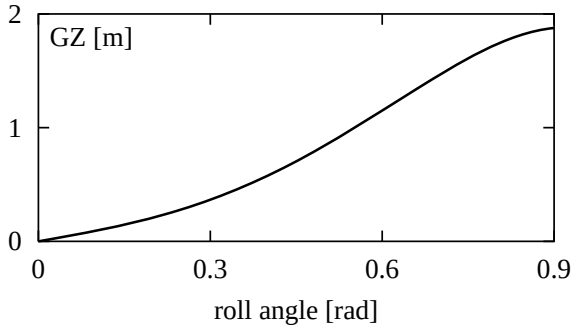

Figure 1: GZ curve in still water.

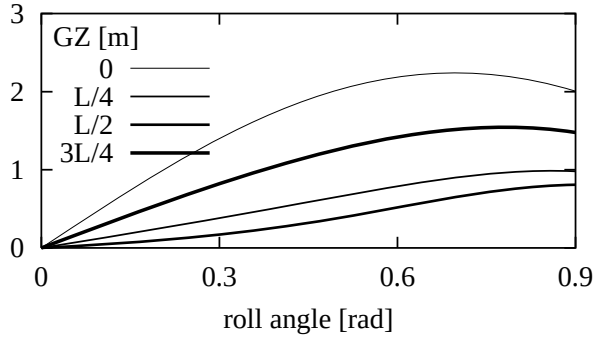

Figure 2: GZ curves in regular waves with wave length equal to the ship length L and a wave height equal to 0.05L. Wave crest positions at x_c= 0, 0.25L, 0.5L, 0.75L and L.

In order to show that Eq. (2.1) can model parametric roll, calculations have been performed with a regular wave with an encounter frequency close to twice the roll frequency, Jensen and Pedersen (2006). Two wave heights are used: one (3.65 m) where parametric roll is not triggered and one slightly higher (3.7 m) where parametric roll develops. The roll motions for the two wave heights are shown in Fig. 3. The onset of parametric roll and its saturation level are clearly noticed.

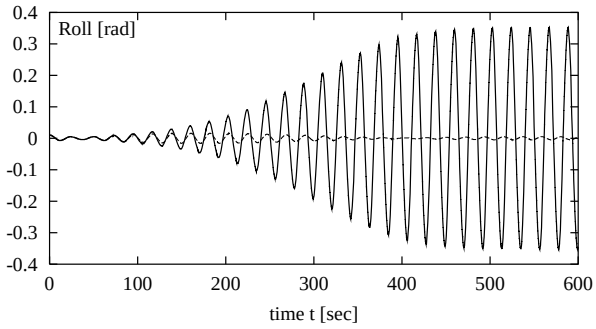

Figure 3: Parametric roll in a regular wave (solid line) and the roll response for a slightly smaller regular wave (dashed line), Jensen and Pedersen (2006).

In the following, results are shown for a sea state with significant wave height H_s = 12 m and zero-crossing wave period T_z = 11.7 s. The zero-crossing period is chosen such that parametric roll can be expected due to occurrence of encounter frequencies in the range of twice the roll frequency. Note, however, that neither the encounter frequency nor the roll frequency is constant in irregular waves. It is also noted that the reliability index β_{FORM} is inversely proportional to the significant wave height H_s, Jensen (2007).

The time domain simulations are carried out from $t = 0$ to $t = t_0$ = 180 s. The effect of the initial condition ($\phi(t = 0) = 0.01$ radians, $\dot{\phi}(t = 0) = 0$) is negligible after about 20 s, but in order to build up parametric roll a longer duration is needed. With n = 25 equidistant frequencies, the wave repetition period relative to the ship is about 200 s depending on the forward speed. In principle the duration to built parametric role could be almost infinity, but the use of longer simulation times than 180 s only changes the mean out-crossing rates, and hence the probability of occurrence, marginally, Jensen (2007).

In the following, results for the design point, i.e. the most probable scenario, corresponding to a roll response of 0.5 rad are shown. The surge acceleration is sown in Fig. 4. The ship velocity is influenced by surge velocity as shown in Fig. 5. The vessel is on average slowed down slightly even with an additional thrust applied.

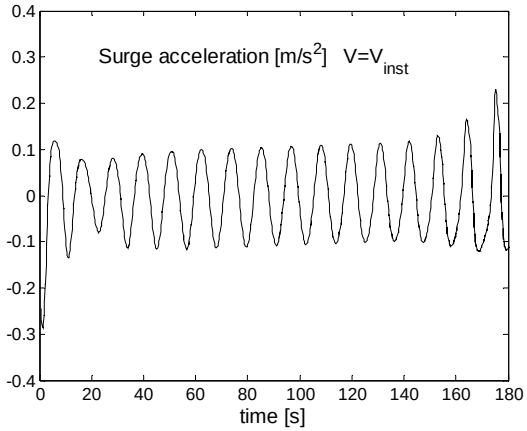

Figure 4: Surge acceleration.

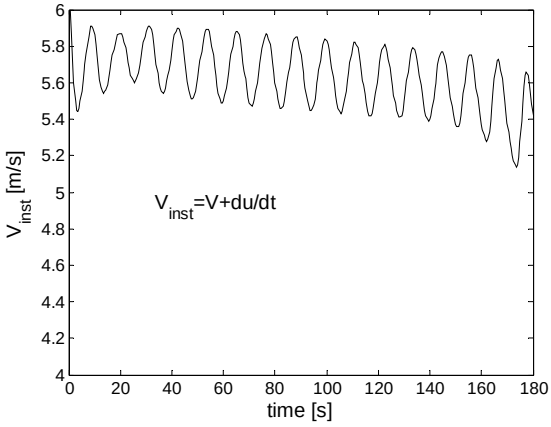

Figure 5: Effect of surge velocity effect on ship velocity.

The critical wave episode, Eq.(1.6), at amidships as function of time for the case with constant ship speed V = 6 m/s is given in Fig. 6. The wave does not change very much from about 20 s to140 s where after the wave elevation changes into a transient wave. An interesting observation is that the critical wave episode then basically turns out to be a sum of two contributions: firstly, a 'regular' wave with encounter frequency close to twice the roll frequency and a wave height just triggering parametric roll and, secondly, a 'transient' wave with magnitude depending on the prescribed roll response. The reason for the first regular frequency term is the need for a fairly small, but regular wave of sufficient duration and amplitude to trigger the possibility for bifurcation into parametric roll. The second more transient part of the critical wave episode then amplifies this initial parametric roll response to the value prescribed. This behaviour was also found in Jensen and Pedersen (2006).

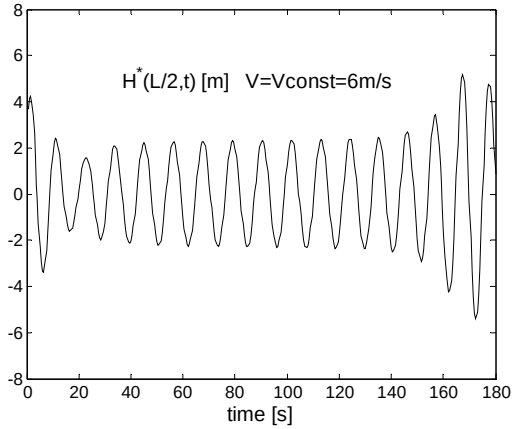

Figure 6 Critical wave episode at amidships, considering the ship speed as constant.

Due to the velocity variations induced by the surge velocity, the critical wave episode changes slightly as shown in Fig.7. The wave shape now has longer crests and sharper troughs due to the slow down when the wave crest is at the fore ship and opposite when amidships.

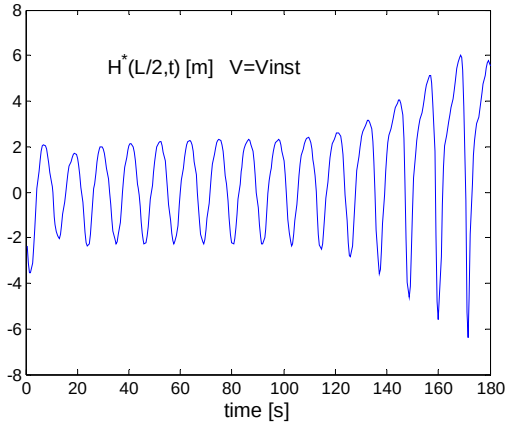

Figure 7: Critical wave episode at amidships, considering the ship speed as varying with the surge velocity.

The associated most probable roll response is given in Fig.8 for the case with varying ship speed. It does not differ very much from the case with constant speed, Jensen and Pedersen (2006)

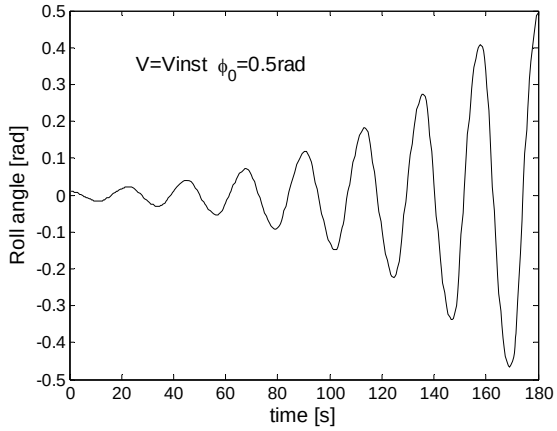

Figure 8: Most probable roll response leading to a roll angle equal to 0.5 rad at t=180 s.

The reliability index β_{FORM} as a function of the limiting roll angle ϕ_0 is presented in Fig. 9. The reliability index is seen to increase when surge effect is accounted for. The corresponding mean out-crossing rate, Eq. (1.7), is shown in Fig. 10 and decreases accordingly. This reduced probability of occurrence is explained by the fact that the surge velocity affects the encounter frequency and, hence, tends to violate the parametric roll resonant condition.

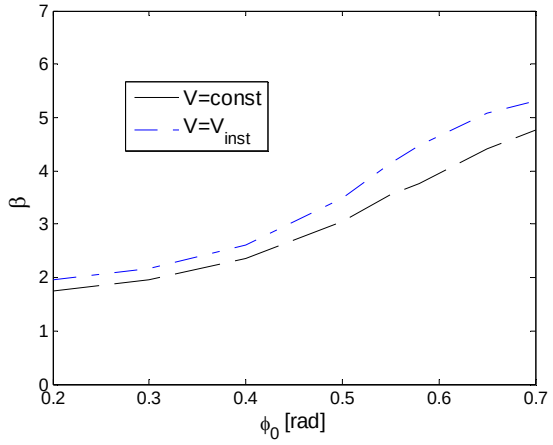

Figure 9: Reliability index as a function of limiting roll angle.

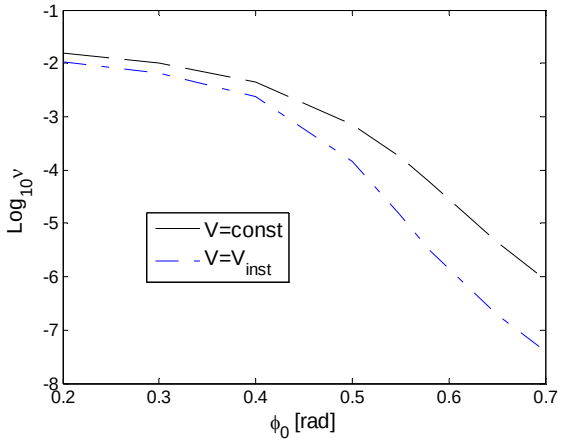

Figure 10: Mean out-crossing rate as a function of limiting roll angle.

CONCLUSIONS

An efficient procedure is presented for calculation of non-linear extreme responses of marine structures subjected to stationary stochastic wave loads. The first step in the procedure requires a formulation of a time domain description of the response as a function of the wave elevation and wave kinematics. This formulation is then implemented in a standard first-order time-invariant reliability (FORM) code, which for given values of the response will solve for the associated design points and reliability indices. An analytical expression, Eq. (1.7), for the mean out-crossing rate in terms of these results is given and the extreme value distribution of the response is then readily obtained by Eq. (1.8). Due to the efficient optimisation procedures implemented in standard FORM codes the calculation is very fast. The ability of the FORM procedure to deal with very low probabilities of occurrence should also be noted. This is a clear advantage over direct simulation methods.

The procedure is illustrated by application to the roll motion of a ship. Surge has been modelled in addition to the roll motion and the effect of surge velocity is accounted for in the calculation of the encounter frequency. For the numerical case considered, the mean out-crossing rate of the limiting roll angle diminishes if surge motion is included. This

means that the probability of exceeding a given maximum roll angle decreases.

It should be stressed again that the present hydrodynamic model, Eq.(2.1)-(2.3), is a simplified model. It is chosen for the present study because it can represent parametric roll with physically plausible results. The present formulation, Eqs.(2.1)-(2.5), requires around 10 minutes of CPU time per sea state, heading and speed.

ACKNOWLEDGEMENT

The present study was partly supported by the European Commission under the FP6 Sustainable Surface Transport Programme, namely the Integrated project SAFEDOR (Design, Operation and Regulation for Safety, task 2.3) Contract No. FP6-IP-516278.

The second author (JVP) greatly acknowledges the financial support from the Danish Center for Maritime Technology and the European Commission through the Network of Excellence on Marine Structures project MARSTRUCT, Contract No. FP6-PLT-506141

REFERENCES

Der Kiureghian, A. The geometry of Random Vibrations and Solutions by FORM and SORM. *Probabilistic Engineering Mechanics*, 2000, Vol. 15, pp 81-90.

Det Norske Veritas. Proban, General Purpose Probabilistic Analysis Program, Version 4.4, 2003.

France, W.N., Levadou, M., Treakle, T.W., Paulling, J.R., Michel, R.K. and Moore, C. An Investigation of Head-Sea Parametric Rolling and Its Influence on Container Lashing Systems. *Marine Technology*, 2003, Vol. 40, No. 1, pp 1-19.

ITTC Specialist Committee on Stability in Waves (chaired by J. O. de Kat), Final Report and Recommendation, In Proceedings of the 24th International Towing Tank Conference (eds D. Clarke and A.P. Mesbahi), Univ of Newcastle upon Tyne, September, 2005, pp. 369-408.

Jensen, J.J., Mansour, A.E. and Olsen, A.S. Estimation of Ship Motions using Closed-Form Expressions. *Ocean Engineering,* 2004, Vol. 31, pp 61-85.

Jensen J.J. and Capul, J. Extreme Response Predictions for Jack-up Units in Second Order Stochastic Waves by FORM. *Probabilistic Engineering Mechanics*, 2006, Vol. 21, No. 4, pp 330-337.

Jensen, J.J. and Pedersen, P.T. Critical Wave Episodes for Assessment of Parametric Roll. *Proc. IMDC'06*, 2006, Ann Arbor, May, pp 399-411.

Jensen, J.J. "Efficient Estimation of Extreme Non-linear Roll Motions using the First-order Reliability Method (FORM)", Accepted for publication in J. Marine Science and Technology, 2006

Krüger, S., Hinrichs, R. and Cramer, H. Performance Based Approaches for the Evaluation of Intact Stability Problems. *Proc. PRADS'2004,* 2004, Travemünde, September, Germany.

Kroeger, H.-P. Rollsimulation von Schiffen im Seegang. *Schiffstechnik,* 1986, Vol. 33, pp 187-216.

Shin, Y.S., Belenky, V.L., Paulling, J.R.,Weems, K.M. and Lin, W.M. Criteria for Parametric Roll of Large Containerships in Head Seas. *Transactions of SNAME*, 2004, Vol.112, pp 14-47.

An examination for the numerical simulation of parametric roll in head and bow seas

Yoshitaka Ogawa

Ship Structural Standards Research Group, National Maritime Research Institute, Japan
Mitaka, Tokyo, Japan

ABSTRACT

Numerical study was carried out using a nonlinear time domain simulation method in accordance with the nonlinear strip method approach. Effects of wave period, wave height and ship speed on the parametric roll were examined through the comparison with the amplitude of roll, which was measured by the free running model experiments in regular and irregular waves.

It is found that the computed 1/10 highest mean of roll by means of the present method with the adequate number of times of simulation gives good agreement with the measured amplitude although the computed maximum amplitude of parametric roll explains experiments merely qualitatively. It was clarified that the roll damping on the parametric roll is significant through the computation of parametric roll using various roll damping.

KEYWORDS

Parametric roll; head and bow seas; nonlinear strip method; maximum and 1/10 highest mean; roll damping; 4 degrees of freedom.

INTRODUCTION

It is well known that the parametric roll is expected to occur when the wave encounter frequency is close to the double of the natural roll frequency of the vessel. Therefore, several approaches, which are mainly focused on the periodic change of the restoring force as the ship advances through the waves, have been investigated to analyze the phenomenon in the last decade years (e.g., Belenky, 2006; Neves, 2006,). As a result, a substantial progress has been achieved to evaluate the parametric roll in regular waves. However, there are some rooms for the improvement of the evaluation of the parametric roll in irregular waves although several studies have been carried out intensively (e.g. Hashimoto, 2006). In addition, several studies (e.g., Taguchi, 2006) investigated the occurrence of the parametric roll not only in the head seas but also in other wave encounter angle. In particular, it is important practically to examine the parametric roll in head and bow seas in terms of cargo damage, which occurs due to the combination of large vertical and horizontal acceleration. Therefore, it is important to examine the parametric roll using the practical model without cumbersome computations not only in the head seas but also in other wave encounter angle.

Based on these backgrounds, numerical study has been carried out using a nonlinear time domain numerical simulation method in accordance with the nonlinear strip method approach.

Firstly, the effects of the number of times and the duration time on the result of numerical simulation were examined by the comprehensive simulation with varying the combination of phase angle of each wave component in each simulation.

Secondly, using the present numerical model, which was narrowed the degrees of freedom down to four, the effect of waves on parametric roll were examined through the comparison with the roll motion, which was measured by the free running model experiments in regular and irregular waves.

Thirdly, the effect of the roll damping on the parametric roll was examined through the comparison of experiments with the numerical results using various roll damping.

COMPUTATIONS

Numerical Model

Ship motions were estimated by the time domain simulation program, developed by the National Maritime Research Institute of Japan (Ogawa, 2005) in accordance with a nonlinear strip method approach (Fujino et al., 1983).

The program, NMRIW, was developed by means of the latest results of a seakeeping and maneuvering study. The NMRIW's numerical model is based on a nonlinear strip theory approach in which forces due to the linear and nonlinear potential flow are combined with maneu-vering forces and viscous drag forces. Generally, it is difficult to compute nonlinear wave loads in bow and quartering seas by means of the conservative time do-main estimation method. Using the present method, wave loads in bow and quartering seas can be estimated rationally.

To describe these hydrodynamic forces rationally, the equation of motion is described in the horizontal body axes coordinate system (Hamamoto et al., 1993). Using the horizontal body axes coordinate system, large rotational angles in severe wave and wind conditions are retained in the equation of motion.

Ship motion components are determined from a set of 6 differential equations of motion with its origin at the center of gravity G. With respect to rotations, a right-handed convention is always used. Equations of motion are solved in the time domain by means of a 4th-order Runge-Kutta scheme.

The Froude-Krylov force, which has considerable effect on the nonlinearity of ship motions, is estimated by the integration of the hydrostatic and hydrodynamic wave pressure along the instantaneous wetted surface of the hull at each time step.

With respect to the sectional wave radiation force and potential value at each time step, the integral equation method is used. Source and doublet are distributed at the origin of each section to avoid the irregular frequency, in accordance with Ohmatsu's method (Ohmatsu, 1975).

In terms of the sectional diffraction force in the present method, it was computed by solving the Helmholtz equation at each time step. The viscous effect of roll damping due to ship hull and bilge keels can be estimated with various empirical formulae.

The propeller thrust is described by means of the propeller characteristic. The hull resistance is a function of an instantaneous speed and draft. The rudder is controlled by the PID control.

The sea surface and wave kinematics are described based on the linear wave theory. The sea surface of irregular waves is described by the linear superposition of regular waves with random phase.

Ship motions estimated by means of this method were verified through the comparison with the many kinds of model tests. Fig. 1 and Fig.2 shows examples of the vertical acceleration of a post-panamax container carrier, which was used in the present study (Ogawa, 2007). The fundamental frequency component, a, is divided by L/g (L : ship length, g : the acceleration of gravity). It is found that wave height has a significant effect on the amplitude of the vertical acceleration. It is also found that the computed amplitude of the vertical acceleration gives good agreement with experiments not only in head seas but also in bow seas.

Fig. 3 shows examples of the roll motion of the post-panamax container carrier, which was used in the present study. The fundamental frequency component, Φ, are divided by wave slope $k\zeta$ (k: wave number, ζ : wave slope). It

is also found that the computed amplitude of the roll motion gives good agreement with experiments. It is confirmed that the present method taking account of hydrodynamic forces in each time step can estimate ship motions well when parametric roll does not occur.

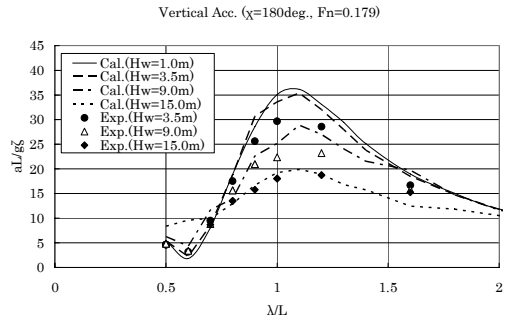

Fig. 1: The response amplitude operator of vertical acceleration at F.P. of a post-panamax container carrier (χ=180deg., Fn=0.179) (Ogawa, 2007)

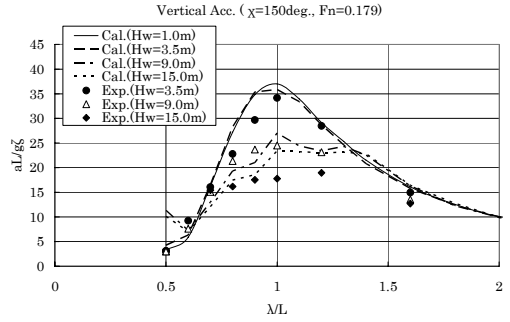

Fig. 2: The response amplitude operator of vertical acceleration at F.P. of a post-panamax container carrier (χ=150deg., Fn=0.179) (Ogawa, 2007)

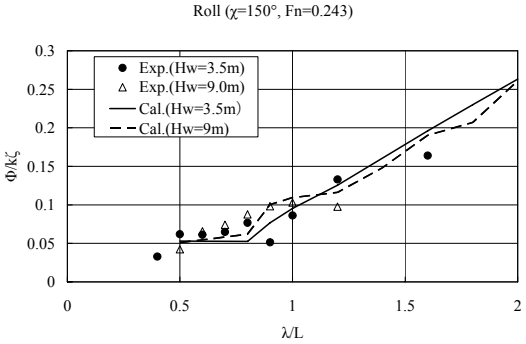

Fig. 3: The response amplitude operator of rolling of a post-panamax container carrier (χ=150deg., Fn=0.243)

Mathematical Model of Roll Motion

In the present study, the degrees of freedom of numerical model was narrowed down to four (sway, heave, roll, pitch) because the main purpose is to examine the parametric roll using the practical model without cumbersome computations not only in the head seas but also in other wave encounter angle. Using this model, the numerical procedure of surge and yaw in larger sea state with slower ship speed were neglected.

On the basis of the assumption, the equation of roll motion can be described as follows:

$$\left(I_{xx}+J_{xx}\right)\ddot{\phi}+a\dot{\phi}+b\dot{\phi}\left|\dot{\phi}\right|+W\left\{GZ_0\left(\phi\right)+GZ_w\left(\phi;t\right)\right\} = M\left(t\right) \quad (1)$$

Here I_{xx} denotes an inertia moment in roll and J_{xx} denotes an added inertia moment in roll. a and b denote the linear and quadratic damping coefficient. W denotes the displacement. GZ_0 and GZ_w denote the restoring arm and restoring arm variation due to wave. M denotes the heel-induced hydrodynamic roll moment. Roll moment owing to sway, heave and pitch is considered in this term.

In terms of the numerical simulation of the parametric roll in irregular waves, incident wave was realized by the sum of 200 components of waves in accordance with the 1964 ISSC spectrum. To take account of the non-ergodic nature of parametric roll, 20 times simulations with the duration of 2500 seconds of ship scale were carried out in each condition. The combination of phase angle of each wave component was varied in each simulation.

Fig. 4 shows the example of the probability density function of pitch and roll amplitude. The horizontal axis denotes the pitch and roll angle. Dotted lines show the approximation of Gaussian distribution of those computed probability density function. It is found that the probability density function of the computed pitch amplitude of 20 times simulations with the duration of 2500 seconds can be approximated by the Gaussian distribution. However, it is also found that the probability density function of the computed roll amplitude is much different with the Gaussian distribution due to non-ergodic nature of parametric roll although a certain distribution can be approximated.

EXPERIMENTS

Model and Measuring Instruments

A detailed explanation of experiments has been published previously (Taguchi et al., 2006 and 2007). However, the part relevant to this study is repeated here. A series of a free runnning test in waves by means of the model of a post-panamax container carrier was carried out to measure parametric roll.

The tests were conducted at the Square Basin (80 m×80 m×4.5m) of the National Maritime Research Institute of Japan. Table 1 presents the ship's main particulars. Before the test, the model was ballasted to the correct draft, trim and the GM.

Six degree of ship motions were measured by means of optical fiber gyro and gyro accelerometer. Relative water heights at stem, S.S.5 and A.E.. Lateral acceleration beneath the upper deck at S.S. 8 was measured by means of accelerometers.

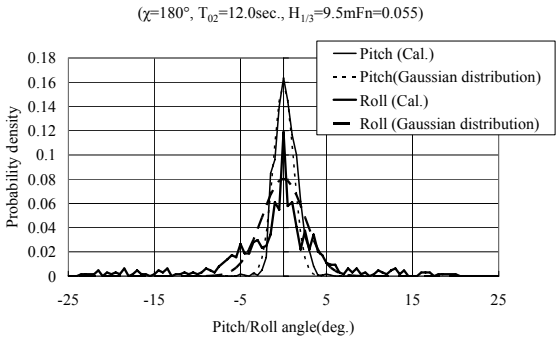

Fig. 4 The probability density function of pitch and roll amplitude (χ=180deg., Fn=0.055, T_{02}=12.0 sec., $H_{1/3}$=9.5m)

Table 1: Main particulars of the container carrier

	Ship	model
Length (L_{pp}) (m)	283.8	3.7
Breadt(B) (m)	42.8	0.558
Draft(d) (m)	14.0	0.183
GM (m)	1.08	0.014
Displacement (m^3)	106970	0.237
Block coefficient (C_b)	0.63	0.63
Natural roll period T_Φ(sec.)	30.3	3.5

Conditions

A series of tests in regular and irregular waves was carried out to allow a comparison with an analytical study. An experiment in regular waves was carried out in head (180 deg.) and bow (165deg., 150deg. and 135deg.) seas. The mean ship speed in waves was varied within a service speed of this post-panamax container carrier (Froude number = 0.239). Experiments were carried out in various wave heights (3.8m to 15.3m). Wave length was also varied in the experi-ments (wave length ratio λ/Lpp = 0.9 to 2.4; λ:wave length).

Tests in irregular waves were also carried out in head (180 deg.) and bow (165deg., 150deg. and 135deg.) seas with various significant wave heights (3.8m to 15.3m). The ISSC spectrum was used for a wave spectrum of irregular waves. The mean wave period, T_{02}, was also varied (9.5sec. to 15.5sec.). The propeller revolution was varied in accordance with the ship speed in the still water (Froude number in the still water, F_{ns} = 0.07 to 0.15) to examine the effect of ship speed on parametric rolling.

NUMERICAL RESULTS

Roll Motion in Regular Waves

Fig. 5 and Fig. 6 give examples of the time history of the parametric roll in head and bow seas, respectively. It is found that the parametric roll occurs with double of the wave encounter period.

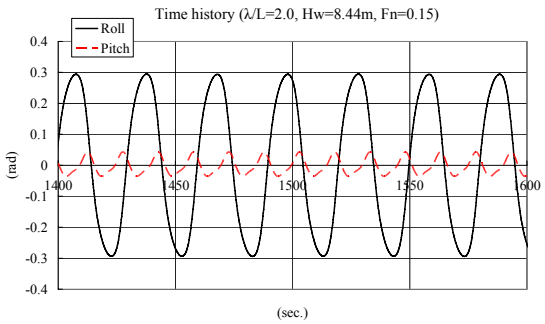

Fig. 5: The time history of roll and pitch in regular waves (χ=180deg, λ/L=2.0, Hw=8.4m, Fn=0.15)

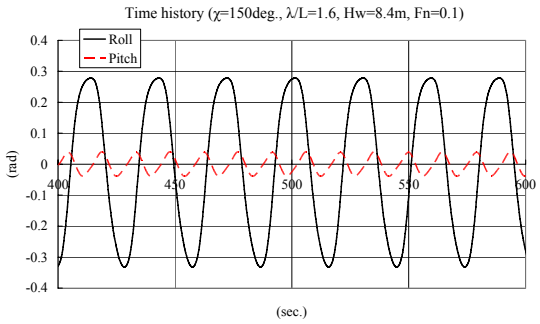

Fig. 6: The time history of roll and pitch in regular waves (χ=150deg, λ/L=1.6, H_w=8.4m, Fn=0.1)

Fig. 7 and Fig. 8 show the amplitude of parametric roll as a function of wave encounter period. The horizontal axis is the ratio of the wave encounter period, T_e, to the natural roll period, T_Φ. It is found that computed range, in which parametric rolling resonance occurs, gives good agreement with measured range. It is verified that the computed amplitude of parametric roll by means of the present method gives good agreement with experiments although there are some discrepancies in the small sea states of bow seas.

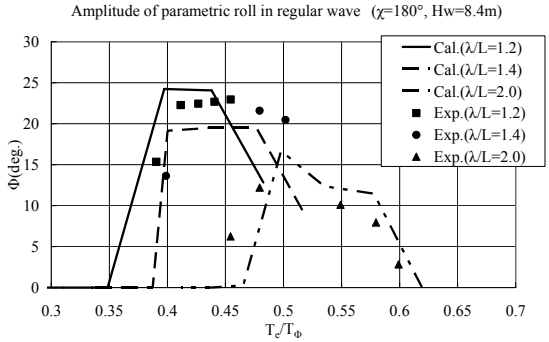

Fig.7: The relation of a wave encounter period with the amplitude of parametric roll (χ=180deg., H_w=8.4m)

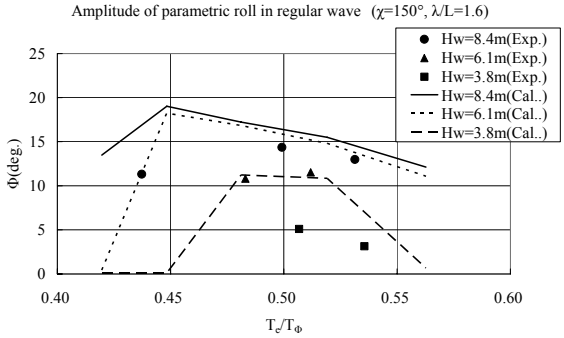

Fig. 8: The relation of a wave encounter period with the amplitude of parametric roll (χ=150deg., λ/L=1.6)

Effect of Wave Period on Roll Motion in Irregular Waves

Fig. 9 gives examples of the time history of the parametric roll in bow irregular waves. It is found that the parametric roll occurs with double of the period of pitch.

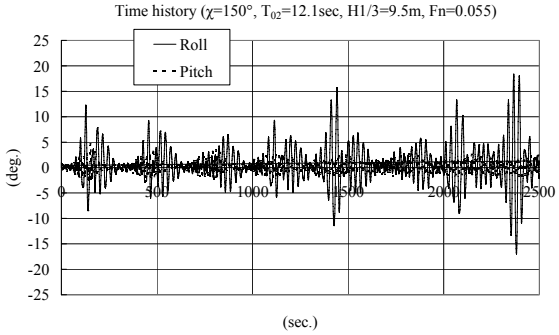

Fig. 9: The time history of roll and pitch in irregular waves (χ=150deg, T_{02}=12.0sec, $H_{1/3}$=9.5m, Fn=0.055)

Fig. 10 and Fig. 11 show the maximum and 1/10 highest mean of amplitude of roll as a function of mean wave period, T_{02}, in head and bow seas. In experiments, the parametric roll occurred except waves of the mean wave period of 9.5sec. It is verified that the computed parametric roll occurred in the same condition as experiments. It is found that computed 1/10 highest mean of roll gives good agreement with experiments. It is also found that the computed maximum amplitude qualitatively agrees with experiments in terms of mean wave period although there is certain discrep-

ancy between the computed maximum amplitude and experiments.

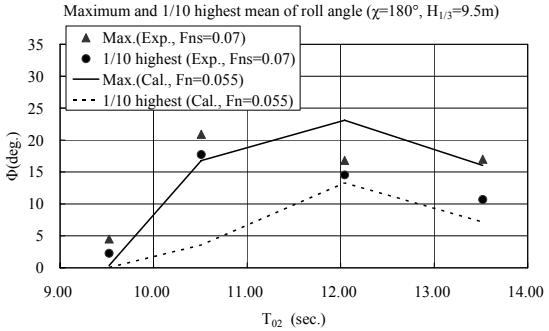

Fig. 10: The effect of mean wave period on roll in irregular waves (χ=180deg., $H_{1/3}$=9.5m)

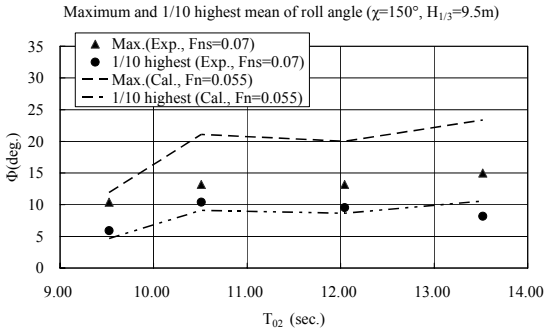

Fig. 11: The effect of mean wave period on roll in irregular waves (χ=150deg., $H_{1/3}$=9.5m)

Effect of Wave Height on Roll Motion in Irregular Waves

Fig. 12 and Fig. 13 show the maximum and 1/10 highest mean of amplitude of roll as a function of significant wave height, $H_{1/3}$, in head and bow seas. In experiments, the parametric roll occurred except waves of the significant wave height of 3.8m. It is verified that the computed parametric roll occurred with the same significant wave height as experiments. It is found that computed 1/10 highest mean of roll gives good agreement with experiments. It is also found that the computed maximum amplitude qualitatively agrees with experiments in terms of wave height although there is certain discrepancy between the computed maximum amplitude and experiments.

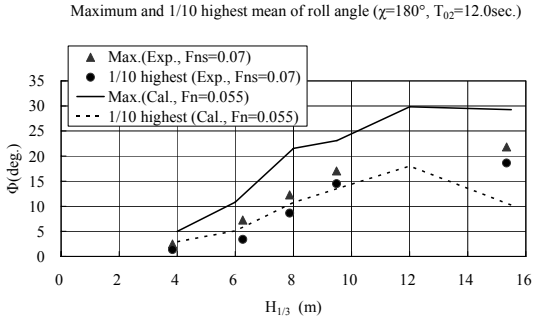

Fig. 12: The effect of significant wave height on rolling in irregular waves (χ=180deg., T_{02}=12.0sec.)

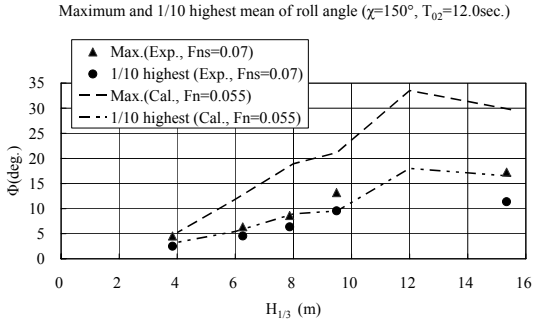

Fig. 13: The effect of significant wave height on rolling in irregular waves (χ=150deg., T_{02}=12.0sec.)

Effect of Wave Direction on Roll Motion in Irregular Waves

Fig. 14 and Fig. 15 show the maximum and 1/10 highest mean of amplitude of roll as a function of wave direction, χ. In experiments, the parametric roll occurred except waves of χ=135deg. However, it is found that the computed parametric roll occurred except waves in bow seas (χ=135deg.) with Fn=0.1. It is found that computed 1/10 highest mean of roll gives good agreement with experiments. It is also found that the computed maximum amplitude qualitatively agrees with experiments in terms of wave direction although there is certain discrepancy between the computed maximum amplitude and experiments.

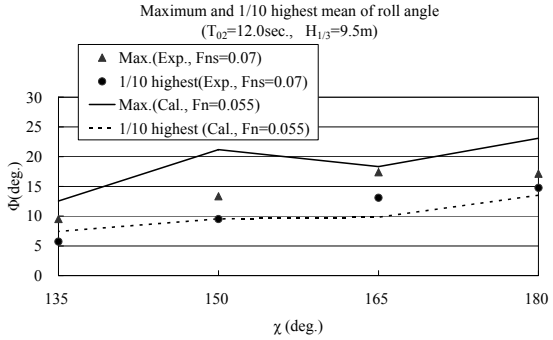

Fig. 14: The effect of wave direction on rolling in irregular waves (Fn=0.055, T_{02}=12.0sec., $H_{1/3}$=9.5m)

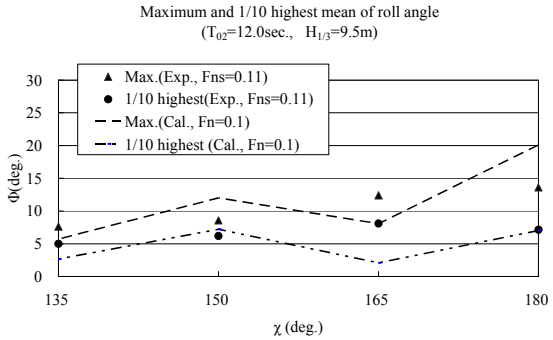

Fig. 15: The effect of wave direction on rolling in irregular waves (Fn=0.1, T_{02}=12.0sec. $H_{1/3}$=9.5m)

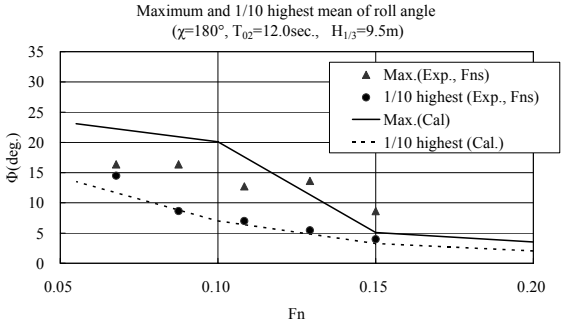

Fig. 16: The effect of ship speed on rolling in irregular waves (χ=180deg., T_{02}=12.0sec., $H_{1/3}$=9.5m)

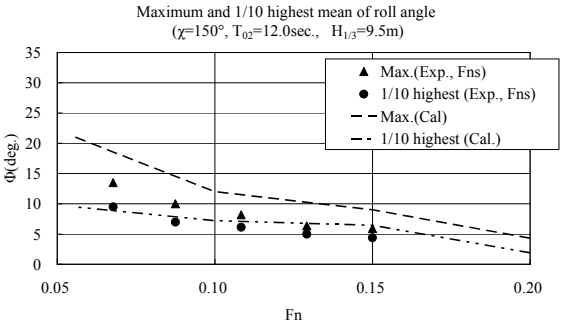

Fig. 17: The effect of ship speed on rolling in irregular waves (χ=150deg., T_{02}=12.0sec., $H_{1/3}$=9.5m)

Effect of Ship Speed on Roll Motion in Irregular Waves

Fig. 16 and Fig. 17 show the maximum and 1/10 highest mean of amplitude of roll as a function of Froude number in head and bow seas. In experiments, parametric roll occurred in all conditions shown in Fig.16 and Fig.17. It is verified that the computed parametric roll also occurred in the same conditions as experiments. It is found that computed 1/10 highest mean of roll gives good agreement with experiments. It is also found that the computed maximum amplitude qualitatively agrees with experiments in terms of ship speed although there is certain discrepancy between the computed maximum amplitude and experiments.

Effect of Ship Speed on Roll Damping in Irregular Waves

To examine the effect of roll damping on the parametric roll, the computation by means of the roll damping increased by 10% was carried out. In this computation, both the linear and the quadratic damping coefficients were increased by 10%. Fig. 18 shows the maximum and 1/10 highest mean of amplitude of roll as a function of significant wave height, $H_{1/3}$, in head seas. This figure corresponds to the Fig.12. It is found that the roll damping has much effect on the roll amplitude. It is also found that the computed parametric roll by means of the increased roll damping gives agreement with the measured maximum amplitude.

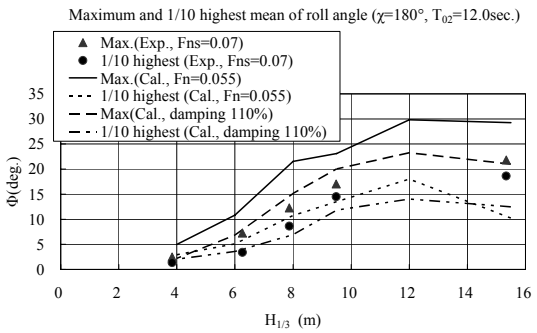

Fig. 18: The effect of roll damping on parametric roll in irregular waves (χ=180deg., T_{02}=12.0sec.)

CONCLUSIONS

Numerical study was carried out using a nonlinear time domain simulation method of 4 degrees of freedom. Effects of wave period, wave height and ship speed on the amplitude of parametric roll were examined. The effect of roll damping was also examined. Conclusions are as follows:

1) Computed amplitude of parametric roll by means of the present method gives good agreement with the measured amplitude in regular waves.

2) The present method explains the parametric roll in terms of wave period, wave height and ship speed.

3) The computed 1/10 highest mean of roll gives good agreement with experiments. However, there is certain discrepancy between the computed maximum amplitude and the experiment although the present computation explains experiments qualitatively.

4) The probability density function of the computed roll amplitude is much different with the Gaussian distribution due to non-ergodic nature of parametric roll although the probability density function of the computed pitch amplitude can be approximated by the Gaussian distribution.

5) The roll damping has much effect on the roll amplitude. The computed parametric roll by means of the increased roll damping gives agreement with experiments.

ACKNOWLEDGEMENT

A part of the present study was carried out cooperating with the Japan Ship Technology Research Association through the part of the Japanese project for the stability safety that is supported by the Nippon Foundation.

REFERENCES

Belenky, V. et.al. (2006). "Numerical Procedures and Practical Experience of Assessment of Parametric Roll of a Container Carrier", Proc. of 9th International Conference on Stability of Ships and Ocean Vehicles, pp 119–130.

Fujino, M, and Chiu, F (1983). "Vertical Motions of High-speed Boats in Head Sea and Wave Load," J Soc Naval Arch Japan, Vol 154, pp 151–163.

Hamamoto, M, and Kim, YS (1993). "A New Coordinate System and the Equations Describing Manoeuvring Motion of Ship in Waves," J Soc Naval Arch of Japan, Vol 173, pp 209–220.

Hashimoto, H. et.al. (2006). "Experimental and Numerical Studies on Parametric Roll of a Post-Panamax Container Ship in Irregular Waves", Proc. of 9th International Conference on Stability of Ships and Ocean Vehicles, pp 181–190.

Neves, M. et.al. (2006). "An investigation on Ro;; Parametric Resonance in Regular Waves", Proc. of 9th International Conference on Stability of Ships and Ocean Vehicles, pp 199–108.

Ogawa, Y. et. al. (2005). "The effect of a bow flare shape on the water impact pressure", International Journal of Offshore and Polar Engineering (IJOPE), Vol.16, No.2, 2005.

Ogawa, Y. (2007). "A Study on Nonlinear Wave Loads of a Large Container Carrier in Rough Seas", The 10th International Symposium on Practical Design of Ships and other Floating Structures (PRADS2007), 2007.

Ohmatsu, S (1975). "On the Irregular Frequencies in the Theory of Oscillating Bodies in a Free Surface," Papers of Ship Res Inst, Tokyo, Vol 48, pp 1–13.

Taguchi, H (2006). "Parametric Rolling of a Ship in Head and Bow Seas (PART2 Effect of Steady Heel) ", Conference Proceedings of the Japan Scoety of Naval Architects and Ocean Engineers, Vol.3, pp 197-200.

Taguchi, H (2007). "Parametric Rolling of a Ship in Head and Bow Seas (PART3 A Model Experiment in Irregular Waves) ", Conference Proceedings of the Japan Scoety of Naval Architects and Ocean Engineers, Vol.4, pp 185-188.

Effects of Roll Damping and Heave Motion on Heavy Parametric Rolling of a Large Passenger Ship in Beam Waves

Tomo Fujiwara and Yoshiho Ikeda

Department of Marine System Engineering, Graduate School of Engineering,

Osaka Prefecture University

ABSTRACT

In this paper, effects of the roll damping and heave motion on the heavy parametric rolling in beam waves are experimentally investigated. Model experiments of a model of a large passenger ship with attached various bilge keels in beam waves demonstrate that roll damping affects occurrence and amplitude of the parametric rolling. To investigate the effect of heave motion, model experiments of the same model ship without bilge keel are carried out. The results demonstrate that the parametric rolling in beam waves may be caused by relative heave motion to wave surface due to heave resonance.

KEYWORDS

Parametric rolling; Beam sea; Large passenger ship; Dead ship; Damping; Bilge keel; Stability.

NOMENCLATURE

ϕ : roll angle

ϕ_0 : roll amplitude

$\phi_{\max}$: maximum roll amplitude at the peak of parametric rolling

H_w : wave height

$H_{w\,mim}$: minimum wave height for occurring parametric rolling

ζ_0 : wave amplitude ($=H_w/2$)

Z_0 : heave amplitude

T_{nr} : roll natural period

T_{nh} : heave natural period

T_r : roll period

T_h : heave period

T_e : encounter wave period ($=T_h$)

T_w : incident wave period

T_{rp} : encounter wave period at the peak of parametric rolling

INTRODUCTION

In the previous papers by the present authors (2005), it was experimentally found that heavy roll motion with much larger amplitude than that of the 1st harmonic resonance appears for a large passenger ship with twice wave period of encounter in heavy beam seas. Since the roll motion has twice period of encounter and almost similar period to half of the roll natural period of the ship, the authors pointed out that the roll motion must be a parametric rolling. Following the paper, Munif et. al. (2006) confirmed that when the ship has no bilge keels, parametric rolling occurs in wide range of heading angles including head and following seas as well as beam seas as shown in Fig. 1. It

was also pointed out by them that the encounter periods at which the rolling phenomena have peaks are different in head and beam waves as shown in Fig. 2. They pointed out that large variation of *GZ* value in beam waves due to the flat and shallow stern-bottom and large flare of bow can induce the parametric rolling.

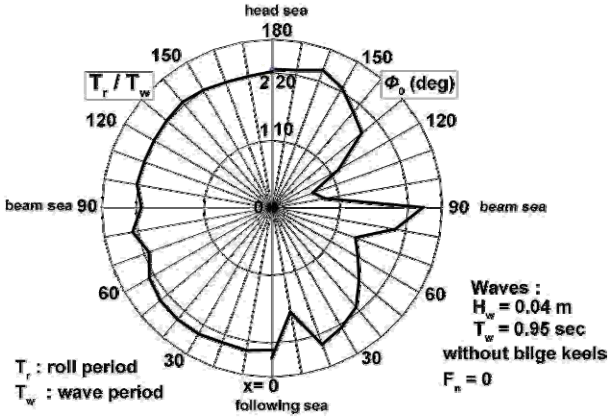

Fig. 1 Amplitude and period of parametric rolling in all heading angles of regular waves.

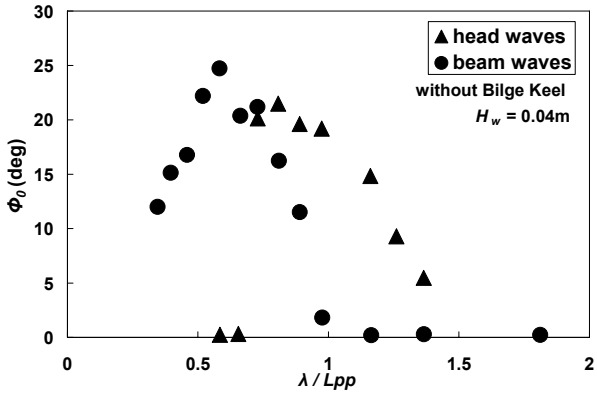

Fig. 2 Difference of wave periods at which parametric rolling appears in beam and head waves.

In the present paper, effects of the roll damping and heave motion on the heavy roll motion with a period of twice of the encounter wave period are experimentally investigated. First, by changing the roll damping systematically, the effect of the roll damping on the rolling is investigated. The results demonstrate that the roll damping significantly affect the region of the occurrence and the amplitude of the roll motion. Secondly, experiments for the same model ship are carried out to investigate the reason why such heavy rolling occurs in beam waves. The results suggest that the heavy rolling in beam waves may occur due to parametric resonance due to the variation of *GM* in time produced by time varying draft due to relative heave motions of a ship with respect to wave surface.

EXPERIMENTAL PROCEDURE

The ship used in the present study is a 110,000GT passenger ship designed by Fincantieri for an international cooperated research on damage stability of large passenger ships in IMO. The body plan and the principal particulars are shown in Fig. 3 and Table 1, respectively.

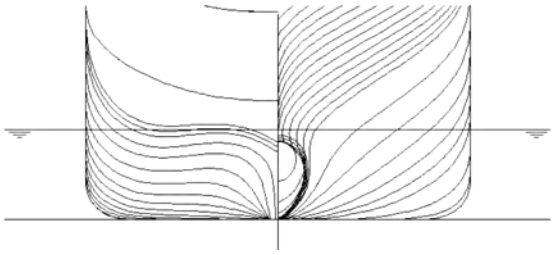

Fig. 3 Body plan of the ship.

Table 1 Principle particulars.

	Full Scale	Model
Scale	1/1	1/125.32
L_{OA}	290 m	2.200 m
L_{PP}	242.24 m	1.933 m
Breadth	36 m	0.287 m
Draft	8.4 m	0.067 m
Displacement	53,010 ton	26.98 kg
GM	1.579 m	0.0126 m
T_{nr}	23 sec	2.05 sec
BK width	1.1 m	0.0088 m
BK location	BK1: s.s.3.0 - 5.0 BK2: s.s.5.25 - 6.0	

In the experiments, the model ship was located in transverse direction in the towing tank of Osaka Prefecture University, and ship motions (roll, heave, pitch, sway and drift) are measured in regular beam waves with 0.04m height in model scale. Yaw and surge motions are fixed.

Size and location of Bilge Keel

The bilge keels designed for the ship are divided into two parts, a short forward (BK1) and a long aft ones (BK2). It was confirmed by Munif et. al.(2006) that the designed bilge keel (BK1+BK2) can completely suppress parametric rolling in any heading angles except for head and following waves. However, parametric rolling occurred in the case of the short bilge keel (BK1) in beam waves. Therefore, in the present experiments, areas of bilge keels are systematically changed from BK1 to the designed full one (BK1+BK2). The bilge keel length and attached position are shown in Table 2.

Table 2 Size and location of bilge keel in the experiments.

	BK location s.s. no.	BK Length	Area of Bilge Keel / Area of Designed Bilge Keel
BK1	5.25 - 6.00	150 mm	0.273
Mid 1	5.00 - 6.00	200 mm	0.364
Mid 2	4.75 - 6.00	250 mm	0.455
Mid 3	4.70 - 6.00	260 mm	0.473
Mid 4	4.60 - 6.00	280 mm	0.509
Mid 5	4.50 - 6.00	300 mm	0.545
Mid 6	4.25 - 6.00	350 mm	0.636
BK2	3.00 - 5.00	400 mm	0.727
BK1 + BK2	5.25 - 6.00 + 3.00 - 5.00	150 mm + 400 mm	1.000

Free Roll Test

Free decay tests of the model ship with attached various bilge keels are carried out, and the roll damping in terms of the extinction coefficient *N* at roll amplitude of 20° and the roll natural period are obtained.

In Fig. 4, the obtained results of the extinction coefficient *N* are shown. Since the ship has relatively small bilge radius, the extinction coefficient *N* is relatively large such as 0.018 even for naked hull. The *N* increases with increasing area of bilge keels, and reaches 0.03 for the designed full bilge keel.

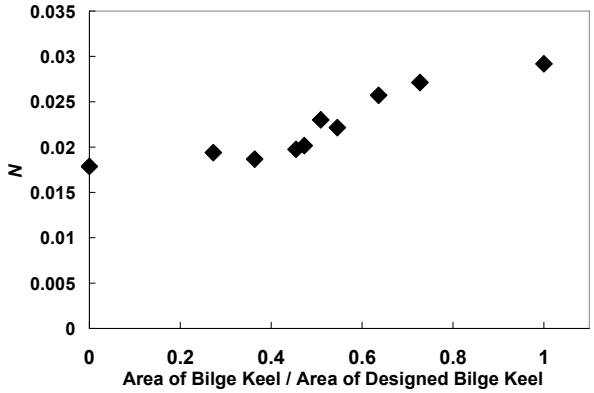

Fig. 4 Measured N coefficients at roll amplitude of 20 degrees for various bilge keel sizes.

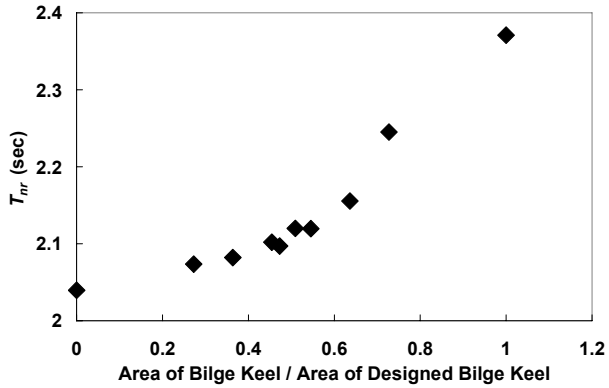

Fig. 5 Variation of roll natural period, T_{nr}, for various size of bilge keels.

In Fig. 5, roll natural periods are shown. The roll natural period increases with increasing area of bilge keels, and reaches a period 16% longer than that for naked hull.

Measurement of Parametric Rolling in Beam Sea

In Fig. 6, the maximum roll amplitudes of parametric rolling for each bilge keel in regular beam waves of 0.04m height are shown. The results demonstrate that the peaks of parametric rolling rapidly decrease with increasing area of bilge keels, or roll damping, and disappears at half area of the designed bilge keel. The roll periods shown in Fig. 7 clearly demonstrate that the period of roll motion changes from twice of encounter periods to the encounter ones at the point when the parametric rolling disappears in Fig. 6.

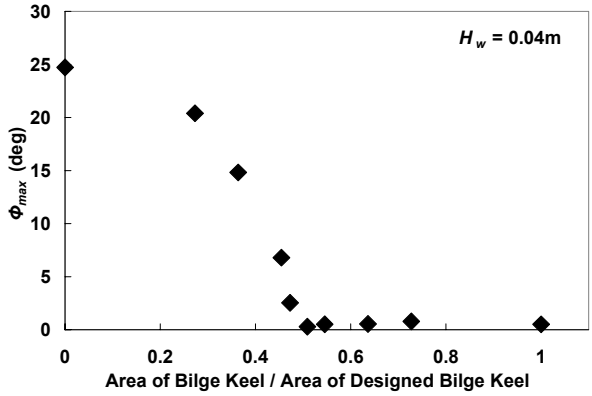

Fig. 6 Effect of area of bilge keels on maximum amplitude of parametric rolling in regular beam seas.

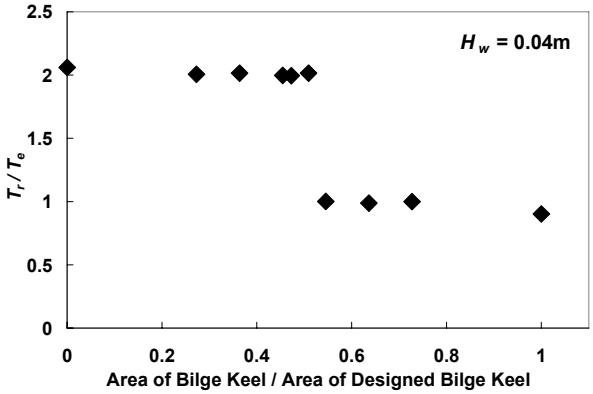

Fig. 7 Effect of the area of bilge keels on the ratio of the roll period to encounter wave period in regular beam seas.

The time histories of motions for the case where the model rolls with the period twice the encounter wave period are shown in Figs. 8 and 9. The time history of rolling motion shown in Fig. 8, which is a case when parametric roll amplitude is large, is substantially sinusoidal. On the contrary, the time history of the roll motion shown in Fig. 9, when parametric rolling amplitude is very small, is non-sinusoidal, and includes not only the component of twice period of the encounter wave period but also the component of the encounter wave period.

In order to clarify the effect of roll damping on parametric rolling in beam seas, measurements of ship motions of the model in the cases with BK1, Mid2-BK, Mid3-BK and without bilge keel are carried out in regular beam waves with various wave heights. The results of the experiments are shown in Fig. 10. These results demonstrate that the minimum wave height at which parametric rolling appears increases with increasing roll damping, and that the roll amplitudes saturate with increasing wave height, and the saturated roll amplitudes also depend on the roll damping.

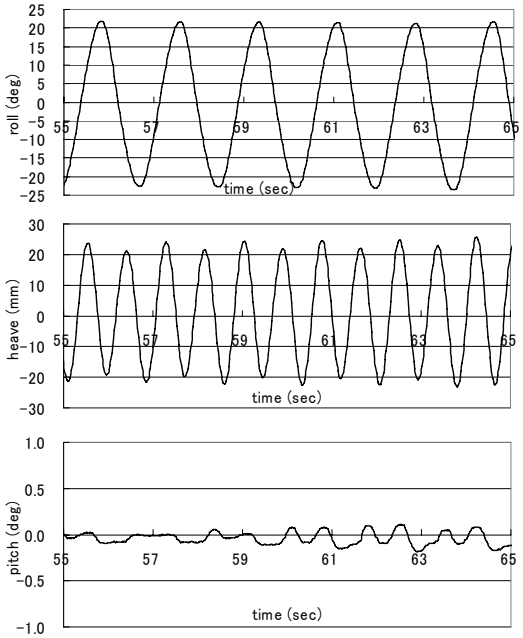

Fig.8 Time histories of ship motions without bilge keel.

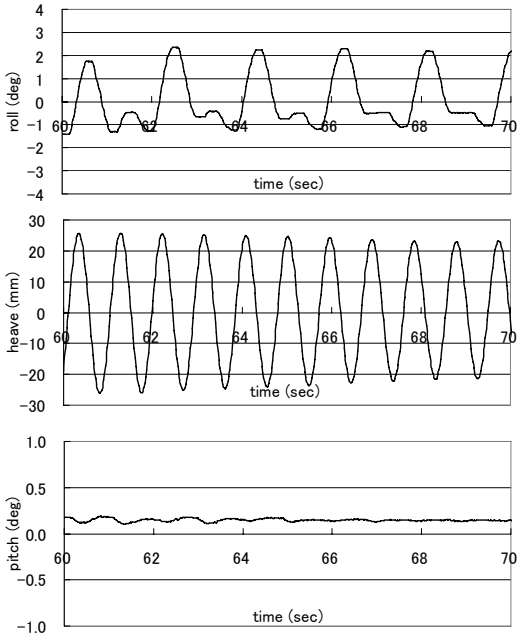

Fig.9 Time histories of ship motions with Mid3 bilge keel.

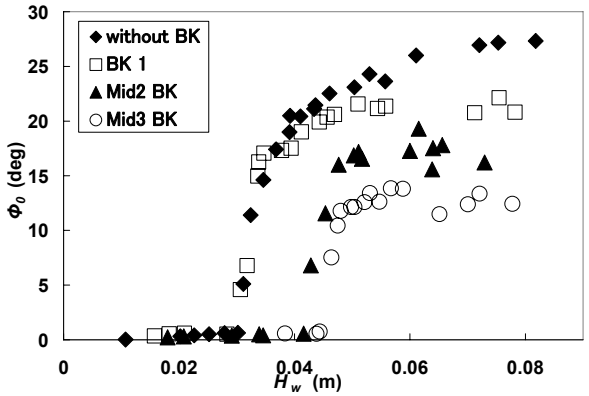

Fig. 10 Roll amplitude as a function of the wave height for the cases with parametric rolling of the ship in regular beam seas.

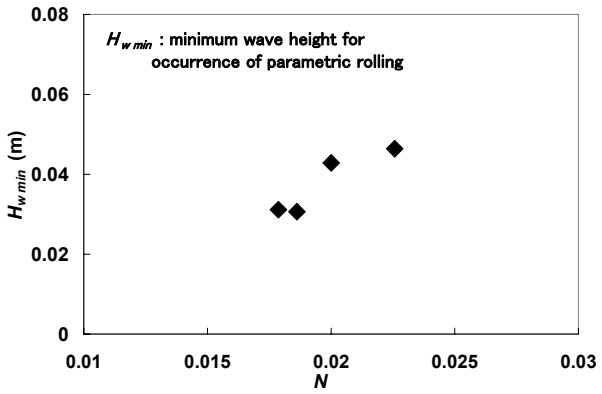

Fig.11 Effect of roll damping on critical wave height for occurrence of parametric rolling of the large passenger ship in beam seas.

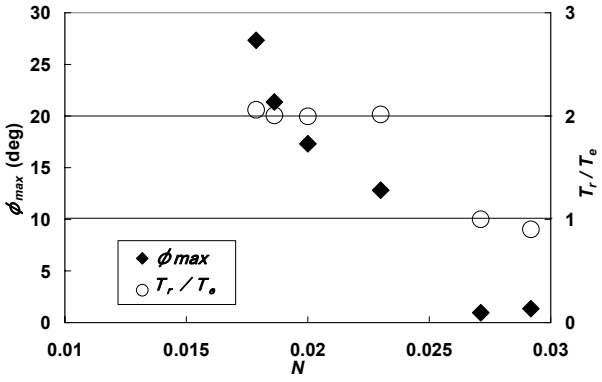

Fig.12 Effect of roll damping on maximum parametric roll angle $\phi_{\max}$ and ratio of roll period to wave period in 0.04m wave height.

The relation between the roll damping and the critical wave height for the occurrence of parametric rolling, which is deduced from the experimental results shown in Fig. 10, is shown in Fig. 11. Using the figure, we can determine the roll damping required to eliminate parametric rolling in beam seas for the large passenger ship. The relation between the roll damping and the maximum parametric rolling amplitude at 0.04m waves is shown in Fig. 12. Using the figure, we can determine the required roll damping limiting parametric rolling to a prescribed amplitude in beam seas. For example, N should be larger than 0.024 to maintain the roll amplitude to less than 10 degrees in 0.04m beam waves.

CAUSE OF PARAMETRIC ROLLING IN BEAM WAVES

The cause of the parametric rolling in beam waves has not been clarified yet. In this section, the authors will investigate the cause of the large rolling.

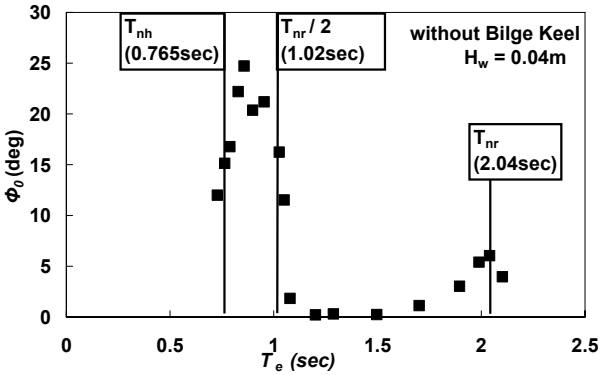

Fig. 13 Measured roll amplitude without bilge keel in regular beam waves

In Fig. 13, the measured roll motion amplitudes in beam waves are shown with indicated roll natural period T_{nr}, its half T_{nr} / 2 and the heave natural period T_{nh}. It can be seen that large parametric rolling appears at the period between half of roll natural period and heave natural period. The results may suggest that heave resonance causes parametric rolling in beam waves. In order to investigate this hypothesis, measurements of roll motions of the model ship are carried out for various roll natural periods. Roll natural periods of the ship are systematically changed by changing moment of inertia, as shown in Table 2. This means that the centre of gravity of the ship keeps at original location.

Table 2 Conditions of model experiments

T_{nr} (sec)	T_{nh} Exp. (sec)	T_{nh} Cal. (sec)	T_w (sec)	H_w (m)
1.18	0.750	0.740	0.40 ~ 1.18	0.04
1.40	0.760		0.45 ~ 1.40	
1.66	0.727		0.50 ~ 1.65	
2.04	0.765		0.60 ~ 2.30	
2.39	0.733		0.70 ~ 2.40	
2.92	0.760		1.00 ~ 2.92	
3.33	0.740		1.40 ~ 1.70	

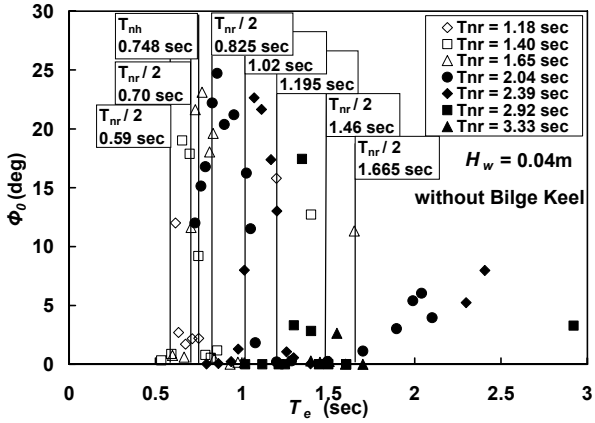

Fig. 14 Parametric rolling in beam waves for various roll natural periods.

The experimental results shown in Fig. 14 demonstrate that with changing roll natural period roll amplitude in parametric rolling also changes. From the experimental results shown in Fig.14, the dependency of roll natural period on encounter wave period at the peaks of parametric rolling in beam waves is obtained as shown in Fig. 15. The horizontal bar at each mark shows the region where the parametric rolling occurs. The results demonstrate that the peak period of the parametric rolling approximately coincides with half of roll natural period. However, when roll natural period T_{nr} is smaller than 1.65sec, the peak periods are close to half of T_{nr}, while for larger T_{nr}, the peak periods are smaller than half of T_{nr}.

Effects of the ratio of roll natural period to heave natural period, T_{nr} / T_{nh} on the peak of roll amplitude of the parametric rolling are shown in Fig. 16. Intuitively, maximum parametric rolling should appear when T_{nr} / T_{nh} is equal to 2, if heave resonance causes parametric rolling in beam waves. The results shown in Fig. 16, however, demonstrate that maximum parametric rolling occurs at T_{nr} / T_{nh} of 2.67.

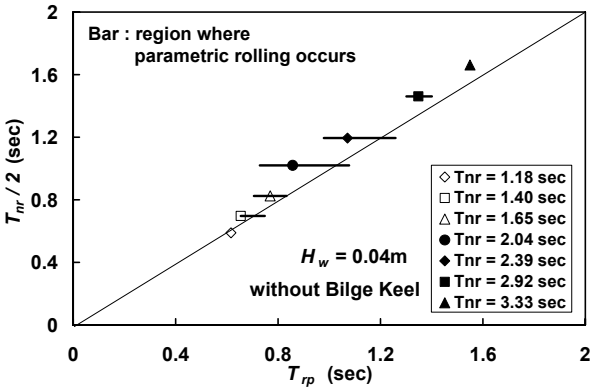

Fig. 15 Relationship between half of roll natural period and peak period of parametric rolling in beam waves.

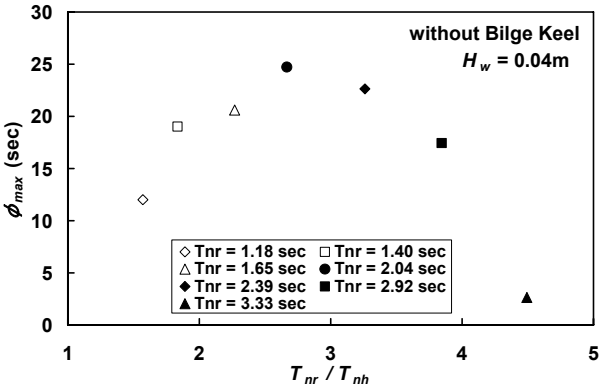

Fig. 16 Effect of ratio of roll natural period to heave natural period on maximum roll amplitudes at peaks of parametric rolling in beam waves.

Fig. 17 shows roll amplitude at each peak of the parametric rolling for various roll natural period in beam waves. We can see large skew in the figure. The skew may be caused by the nonlinearity of *GZ* at large roll amplitude as can be seen in Fig. 18. The *GZ*-curve shows that *GZ* at 25 degrees of roll angle is larger by 16.2% than the linear value, $GM\phi$.

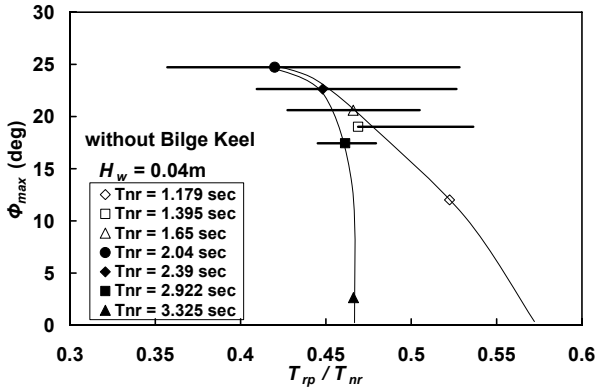

Fig. 17 Maximum roll amplitude at peaks of parametric rolling in beam waves for various roll natural period.

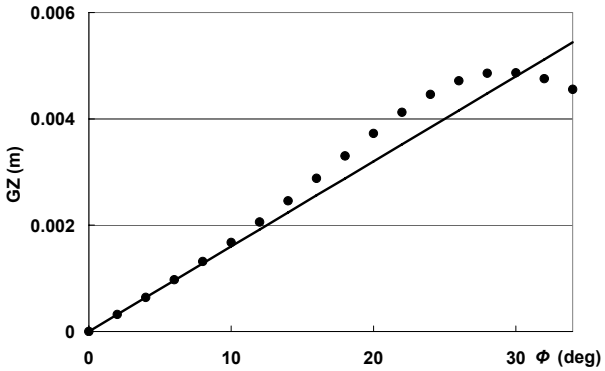

Fig.18 Non-linearity of *GZ*-curve of the model in calm water.

Response of heave motion

Measured amplitudes and phase angles from incident waves of heave motions are shown with calculated results by a strip method (OSM) in Figs. 19, 20 and 21. In Fig. 19 the heave amplitudes for the cases where parametric rolling occurs are plotted, and in Fig. 20 those when no parametric rolling occurs are plotted. We can see that both response functions are similar, and cannot find any significant differences. In Fig. 21, the measured phase angles of heave motion with respect to encounter waves are shown. The results show the phase angle rapidly changes near the heave natural period as well known. It should be noted that the phase angles in heave resonant condition may change the relative heave motion with respect to the water surface, and that it may cause time variation of the *GZ* value in beam waves.

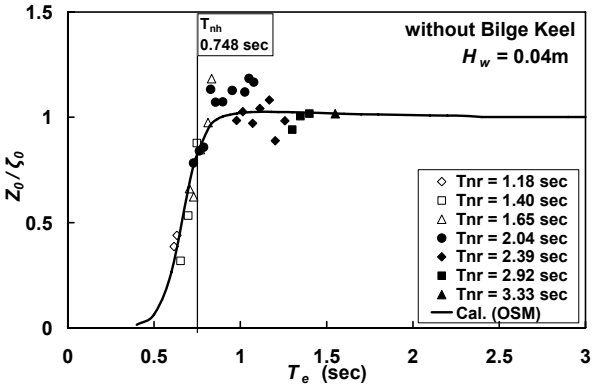

Fig. 19 Heave response curve when parametric rolling occurs.

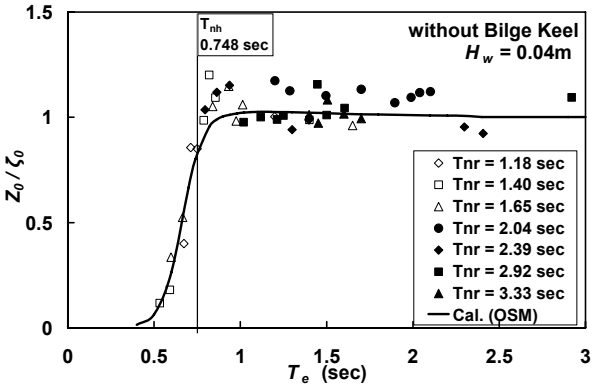

Fig. 20 Heave response curve when parametric rolling does not occur.

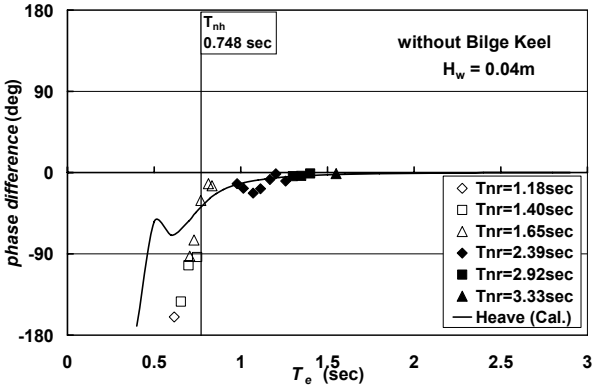

Fig. 21 Phase angle of heave motion vs. incident wave encounter period for the cases where parametric rolling occurs.

Calculation of relative heave motion

Using measured data of heave motions and encounter waves, relative heave motions with respect to wave surface can be calculated. The calculated results are shown in Figs. 22-27. The results demonstrate that relative heave motions are large in the region where large

parametric rolling occurs. In these figures the heave natural period and the half of roll natural period are also shown. We can see the peaks of the parametric rolling are located between these two periods in almost all cases. The parametric rolling becomes large when the two periods are close to each other. As shown in Fig. 25, however, large parametric rolling and large relative heave motion can be seen even if the two periods are different from each other by about 50%. It should be noted that the peak periods of the parametric rolling are near half of roll natural period when the heave natural period and the half of roll natural period are relatively separate.

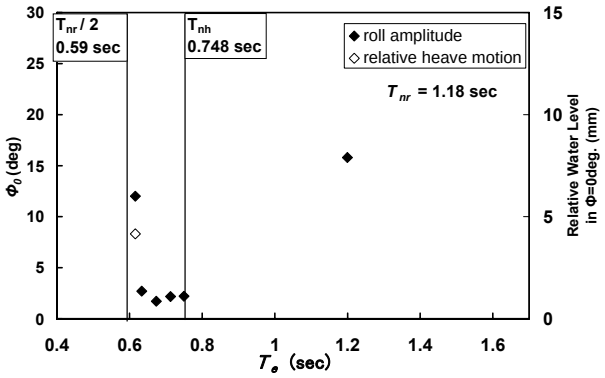

Fig. 22 Parametric rolling in beam waves and relative heave motion. Calculated at T_{nr} =1.18sec.

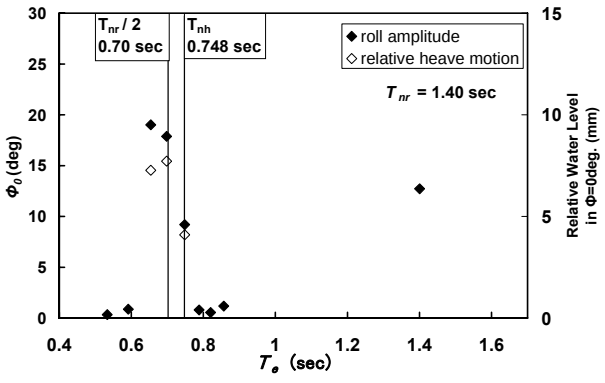

Fig. 23 Parametric rolling in beam waves and relative heave motion. Calculated at T_{nr} =1.40sec.

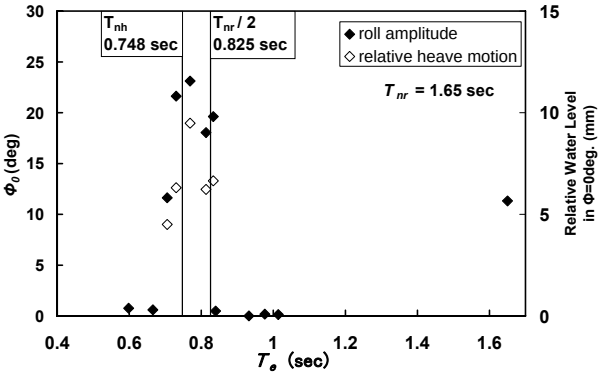

Fig. 24 Parametric rolling in beam waves and relative heave motion. Calculated at T_{nr} =1.65sec.

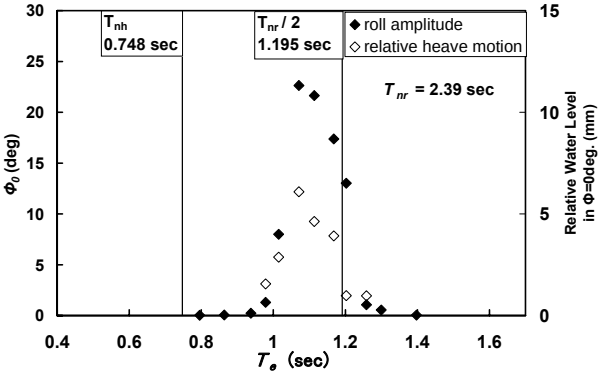

Fig. 25 Parametric rolling in beam waves and relative heave motion. Calculated at T_{nr} =2.39sec.

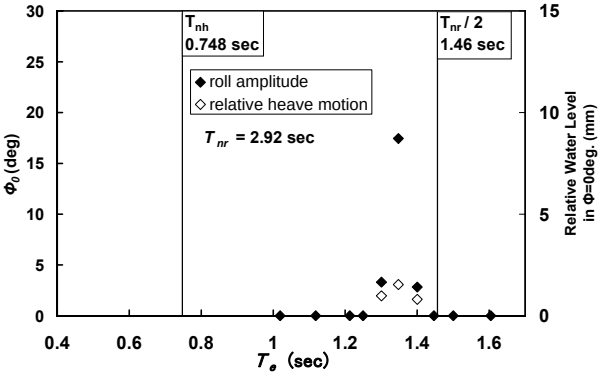

Fig. 26 Parametric rolling in beam waves and relative heave motion. Calculated at T_{nr} =2.92sec.

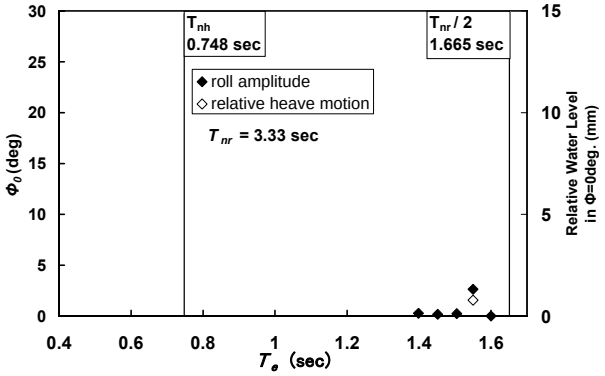

Fig. 27 Parametric rolling in beam waves and relative heave motion. Calculated at T_{nr} =3.33sec.

The relative heave motions can generate time variation of the draft of the ship, and the *GZ* curves for different drafts can be calculated by a hydrostatic calculation. An example of the calculated *GZ* is shown in Fig. 28. From this result, large variation of *GZ* values of the ship in beam waves can be confirmed. Kuroda et. al. (2002) also pointed out that variation of relative water level could change GZ value drastically in the 1st harmonic resonance of heave motion.

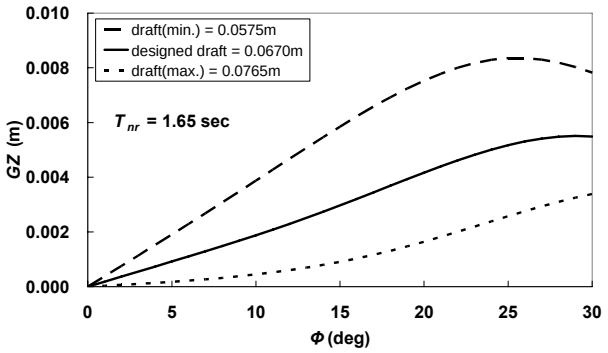

Fig. 28 Calculated *GZ* curve when draft is assumed to be changed due to relative heave motion in beam waves.

CONCLUSIONS

In the present study, effects of roll damping and heave motion on parametric rolling of a large passenger ship in beam waves are experimentally investigated and the following conclusions are obtained:

1) When the ship has the designed bilge keel, parametric rolling does not occur in beam waves. However, parametric rolling occurs when size of the bilge keel is smaller than half of the area of the designed bilge keels.

2) Roll damping significantly affects the critical wave height for occurring of parametric rolling in beam waves. The critical wave height increases with increasing roll damping. The amplitude of the parametric rolling rapidly increases with wave height above the critical one, and saturates to a maximum one which also depends on the roll damping.

3) Parametric rolling of a ship in beam waves may be caused by relative heave motion due to heave resonance. The vicinity of heave natural period and half of roll natural period may be the key factor for the occurrence of the phenomenon.

ACKNOWLEDMENTS

The authors acknowledge Associate professor Toru Katayama of Osaka Prefecture University for many valuable suggestions for this study.

REFERENCES

Ikeda Y, Munif A, Katayama T, Fujiwara T, 2005, “Large Parametric Rolling of a Large Passenger Ship in Beam Seas and Role of Bilge Keel in Its Restraint”, Proc. of 8th International Ship Stability Workshop.

Ikeda Y, Katayama T, Munif A, Fujiwara T, 2005, “Experimental Identification of Large Parametric Rolling of a Large Passenger Ship”, Conference Proc. of the Japan Society of Naval Architects and Ocean Engineers, No.1, pp.91-pp94.

Munif A, Ikeda Y, Fujiwara T, Katayama T, 2006, “Parametric Roll Resonance of a Large Passenger Ship in Dead Ship Condition in All Heading Angles”, Proc. of 9th International Ship Stability Workshop.

Kuroda T, Ikebuchi T, Ikeda Y, 2002, “Non-Linear Features in Large Amplitude Ship Motions (2nd Report) ”, Proc. of The Society of Naval Architects of Japan, No.192, pp.237-pp246.

Validation of a Container Ship Model for Parametric Rolling

Claudio A. Rodríguez

Department of Naval Architecture and Ocean Engineering, LabOceano/COPPE, Federal University of Rio de Janeiro

Christian Holden[1]

Department of Engineering Cybernetics, Norwegian University of Science and Technology

Tristan Perez

Centre for Ships and Ocean Structures (CESOS), Norwegian University of Science and Technology

Ingo Drummen

Centre for Ships and Ocean Structures (CESOS), Norwegian University of Science and Technology

Marcelo A. S. Neves

Department of Naval Architecture and Ocean Engineering, LabOceano/COPPE, Federal University of Rio de Janeiro

Thor I. Fossen

Department of Engineering Cybernetics, Norwegian University of Science and Technology

ABSTRACT

The objective of this work is to formulate a nonlinear, coupled model of a container ship during parametric roll resonance, and to validate the model using experimental data.

KEYWORDS

Ship stability; parametric resonance; non-linear equations; ship motions; roll motion

INTRODUCTION

Parametric resonance is a phenomenon where changes in the model parameters induce a resonance. This is known to occur for the rolling of ships with significant changes of restoring characteristics due to wave passage along the hull and wave excited vertical motions — typical ships affected by this are fishing vessels and container ships. The phenomenon is characteristic when sailing in head or stern seas with wave lengths similar to the ship length, encounter frequency of about twice the roll natural frequency, and wave heights above a ship-dependant threshold value.

Neves and Rodríguez (2005a, b, 2006a) developed a third-order model describing strongly coupled heave, roll and pitch restoring terms via a multivariable Taylor expansion up to the third order. This model has been validated against experimental results for fishing vessels (Neves and Rodríguez, 2005a, b, 2006a).

[1] Corresponding author. E-mail: c.holden@ieee.org

In this work, the proposed model is used to describe the motion of a container ship. The parameters are determined numerically from the vessel loading condition and line drawings An alternative (more accurate) methodology based on the instantaneous determination of the calm water and wave pressure fields, is introduced. This is achieved employing a dedicated panel method code. The fidelity of the container ship model is then assessed using experimental data of a 1:45 scale model of a container vessel with an overall length of 294 m. This vessel has a large, flat, overhanging stern and pronounced bow flare — characteristics representative for modern container vessels, and known to be prone to parametric roll resonance.

The experiments were conducted in a towing tank in head seas regular and irregular waves for different forward speeds and wave heights and frequency. Parametric roll resonance was observed in some runs, but not in others, giving us a wide range of conditions with which to verify the model. Free roll decay tests were also performed in calm water.

MODEL

A linear or non-linear 1DOF model can, in certain cases, capture the rolling of ships. In the case where parametric resonance may occur, however, the nonlinear coupling between pitch, roll and heave are important to understand the phenomenon. This gives rise to the 3DOF model presented in Neves and Rodríguez (2006a):

Let

$$\mathbf{s} = \begin{bmatrix} z(t) & \phi(t) & \theta(t) \end{bmatrix}^T \tag{1}$$

where z is the heave displacement, ϕ is the roll and θ is the pitch angle of the vessel.

This gives a model

$$(\mathbf{M}+\mathbf{A})\ddot{\mathbf{s}} + \mathbf{B}(\dot{\phi})\dot{\mathbf{s}} + \mathbf{c}_r(\mathbf{s},\zeta) = \mathbf{c}_{ext}(\zeta,\dot{\zeta},\ddot{\zeta}) \tag{2}$$

where $\mathbf{M} \in \mathbf{R}^{3\times3}$ is the diagonal rigid body inertia of the vessel. $\mathbf{A} \in \mathbf{R}^{3\times3}$ is the hydrodynamic generalized added mass. $\mathbf{B} \in \mathbf{R}^{3\times3}$ is the hydrodynamic damping, which is non-linear in roll. $\mathbf{c}_\mathbf{r} \in \mathbf{R}^3$ is the non-linear vector of restoring forces and moments, which depends on the relative motions between ship hull and wave elevation $\zeta(t)$. The vector $\mathbf{c}_{ext} \in \mathbf{R}^3$ represents the external wave excitation forces and moments, which change with wave heading, encounter frequency, wave amplitude and time, and it is assumed—for simplicity—to be independent of the state variables $\mathbf{s}$.

Added Mass and Damping

The hydrodynamic mass and damping matrices can be expressed as

$$\mathbf{A} = \begin{bmatrix} Z_{\ddot{z}} & 0 & Z_{\ddot{\theta}} \\ 0 & K_{\ddot{\phi}} & 0 \\ M_{\ddot{z}} & 0 & M_{\ddot{\theta}} \end{bmatrix} \tag{3}$$

$$\mathbf{B} = \begin{bmatrix} Z_{\dot{z}} & 0 & Z_{\dot{\theta}} \\ 0 & K_{\dot{\phi}}(\dot{\phi}) & 0 \\ M_{\dot{z}} & 0 & M_{\dot{\theta}} \end{bmatrix} \tag{4}$$

where all terms except for $K_{\dot{\phi}}$ can be evaluated by means of potential theory. Mathematically, $K_{\dot{\phi}}$ can be approximated as

$$K_{\dot{\phi}}(\dot{\phi})\dot{\phi} = K_{\dot{\phi}}\dot{\phi} + K_{\dot{\phi}|\dot{\phi}|}\dot{\phi}\left|\dot{\phi}\right| \tag{5}$$

This consists of a linear part (potential and linear skin friction) and a nonlinear term (viscous effects). Linear and non-linear coefficients in (5) may be computed using the formulae given in Himeno (1981). Alternatively, the damping can be estimated from data of roll decaying tests at the appropriate forward speed of the vessel.

Non-Linear Restoring Forces and Moments

The vector $\mathbf{c}_r$ of non-linear restoring forces and moments can be approximated as

$$\mathbf{c}_r = \mathbf{c}_r^{(1)} + \mathbf{c}_{r(m)}^{(2)} + \mathbf{c}_{r(w)}^{(2)} + \mathbf{c}_{r(m)}^{(3)} + \mathbf{c}_{r(3)}^{(3)}$$
$$= \begin{bmatrix} Z_r^{(1)} \\ K_r^{(1)} \\ M_r^{(1)} \end{bmatrix} + \begin{bmatrix} Z_{r(m)}^{(2)} + M_{r(w)}^{(2)} \\ K_{r(m)}^{(2)} + M_{r(w)}^{(2)} \\ M_{r(m)}^{(2)} + M_{r(w)}^{(2)} \end{bmatrix} \qquad (6)$$
$$+ \begin{bmatrix} Z_{r(m)}^{(3)} + M_{r(w)}^{(3)} \\ K_{r(m)}^{(3)} + M_{r(w)}^{(3)} \\ M_{r(m)}^{(3)} + M_{r(w)}^{(3)} \end{bmatrix}$$

where indices (1), (2) and (3) respectively refer to first, second and third order terms.

The first order terms correspond to the calm water hydrostatics:

$$Z_r^{(1)} = Z_z z + Z_\theta \theta = \rho g A_0 z - \rho g A_0 x_{f_0} \theta$$
$$K_r^{(1)} = K_\phi \phi = \Delta \overline{\mathrm{GM}} \phi$$
$$M_r^{(1)} = M_z z + M_\theta \theta = -\rho g A_0 x_{f_0} z + \Delta \overline{\mathrm{GM}}_L \theta$$

where ρ is water density, g is the acceleration of gravity, A_0 is the waterplane area, x_{f_0} the longitudinal coordinate of the centroid of the waterplane area, $\overline{\mathrm{GM}}$ is the transverse metacentric height, and $\overline{\mathrm{GM}}_\mathrm{L}$ the longitudinal metacentric height.

Two different effects cause second- and third-order terms: subscripts (m) refer to body motions and (w) to wave effects. Derivations of these actions, based on multivariable Taylor series expansions have been presented in Neves and Rodríguez (2005a, 2006a):

$$Z_{r(m)}^{(2)} = \frac{1}{2}\left(Z_{zz} z^2 + 2 Z_{z\theta} z\theta + Z_{\phi\phi} \phi^2 + Z_{\theta\theta} \theta^2 \right)$$
$$K_{r(m)}^{(2)} = K_{z\phi} z\phi + K_{\phi\theta} \phi\theta$$
$$M_{r(m)}^{(2)} = \frac{1}{2}\left(M_{zz} z^2 + 2 M_{z\theta} z\theta + M_{\phi\phi} \phi^2 + M_{\theta\theta} \theta^2 \right)$$

The second-order restoring forces caused by waves can be written as

$$Z_{r(w)}^{(2)} = Z_{\zeta z}(t) z + Z_{\zeta\theta}(t) \theta$$
$$K_{r(w)}^{(2)} = K_{\zeta\phi}(t) \phi$$
$$M_{r(w)}^{(2)} = M_{\zeta z}(t) z + M_{\zeta\theta}(t) \theta$$

Third order restoring forces due to body motions can be written as

$$Z_{r(m)}^{(3)} = \frac{1}{6}\left(Z_{zzz} z^3 + 3 Z_{zz\theta} z^2 \theta + 3 Z_{z\theta\theta} z\theta^2 + Z_{\theta\theta\theta} \theta^3 + 3 Z_{\phi\phi z} z\phi^2 + 3 Z_{\phi\phi\theta} \phi^2 \theta \right)$$
$$K_{r(m)}^{(3)} = \frac{1}{6}\left(K_{\phi\phi\phi} \phi^3 + 3 K_{zz\phi} z^2 \phi + 3 K_{\theta\theta\phi} \theta^2 \phi + 6 K_{z\phi\theta} z\phi\theta \right)$$
$$M_{r(m)}^{(3)} = \frac{1}{6}\left(M_{zzz} z^3 + 3 M_{zz\theta} z^2 \theta + 3 M_{z\theta\theta} z\theta^2 + M_{\theta\theta\theta} \theta^3 + 3 M_{\phi\phi z} z\phi^2 + 3 M_{\phi\phi\theta} \phi^2 \theta \right)$$

Finally, third order restoring forces due to waves can be written as

$$Z_{r(w)}^{(3)} = Z_{\zeta\zeta z}(t) z + Z_{\zeta zz}(t) z^2 + Z_{\zeta\zeta\theta}(t) \theta + Z_{\zeta z\theta}(t) z\theta + Z_{\zeta\phi\phi}(t) \phi^2 + Z_{\zeta\theta\theta}(t) \theta^2$$
$$K_{r(w)}^{(3)} = K_{\zeta\zeta\phi}(t) \phi + K_{\zeta z\phi}(t) z\phi + K_{\zeta z\theta}(t) \theta$$
$$M_{r(w)}^{(3)} = M_{\zeta\zeta z}(t) z + M_{\zeta zz}(t) z^2 + M_{\zeta\zeta\theta}(t) \theta + M_{\zeta z\theta}(t) z\theta + M_{\zeta\phi\phi}(t) \phi^2 + M_{\zeta\theta\theta}(t) \theta^2$$

Note the strong coupling between all three degrees of freedom. Also note that the time-dependant terms are explicit functions of the wave elevation $\zeta(t)$, and therefore implicit functions of time. Further details and analytical expressions relating the coefficients to the characteristics of the vessel can be found in Neves and Rodríguez (2005a, 2006a). In this paper a more general procedure is introduced for the computation of the *derivatives* of the Taylor series expansions.

Calm Water Derivatives

In equation (6) the terms $c_{r(m)}^{(2)}$ and $c_{r(m)}^{(3)}$ describe the changes in the restoring characteristics of the vessel due to the changes in pressure associated with the bodily motions of the vessel.

It is possible to show that nonlinear hydrostatic actions may be expressed as:

$$Z(z, \phi, \theta) = \rho g (\nabla_1 - \nabla_0)$$

$$K(z,\phi,\theta) = \rho g\left[\nabla_0 z_G \sin\phi + \nabla_1\left(y_{B1}\cos\phi - z_{B1}\sin\phi\right)\right]$$

$$M(z,\phi,\theta) = \rho g\left[\nabla_0 z_G \cos\phi\sin\theta - \nabla_1\left(x_{B1}\cos\theta + y_{B1}\sin\phi\sin\theta + z_{B1}\cos\phi\sin\theta\right)\right]$$

where ∇_0 is the average submerged volume, $\nabla_1(z,\phi,\theta)$ is the instantaneous submerged volume, z_G is the vertical coordinate of centre of gravity and $x_{B1}(z,\phi,\theta)$, $y_{B1}(z,\phi,\theta)$ and $z_{B1}(z,\phi,\theta)$ are the coordinates of instantaneous centroid of ∇_1. These expressions allow the numerical determination of all the calm water derivatives appearing in equation (6). This is achieved by means of suitably discrediting the instantaneous displaced hull for generic displacements $[z,\phi,\theta]$. Tables A1 and A2 in the Appendix show the second and third order coefficients.

Wave Effect Derivatives

The terms $\mathbf{c}^{(2)}_{r(w)}$ and $\mathbf{c}^{(3)}_{r(w)}$ in Equation (6) describe the changes in the restoring characteristics of the vessel due to the cyclic changes in pressure associated with the wave profile moving along the hull.

In regular seas, incident wave elevation can be written as

$$\zeta(x,y,t;\chi) = A_w\cos(kx\cos\chi + ky\sin\chi - \omega_e t) \quad (7)$$

where A_w is wave amplitude, k wave number, χ wave heading and ω_e encounter frequency, and the special coordinates are described relative to an inertial coordinate system traveling with the vessel.

The velocity potential for the undisturbed incident wave is given by

$$\phi_I(x,y,z,t) = \frac{A_w g}{\omega_w}e^{kz}\sin[k(x\cos\chi + y\,\mathrm{sen}\,\chi) - \omega_e t]$$

The first and second order generalized Froude-Krilov forces are:

$$F_j^{FK(1)}(t) = \rho\iint\frac{\partial\phi_I}{\partial t}n_j\,\mathrm{d}S$$

$$F_j^{FK(2)}(t) = \frac{1}{2}\rho\iint(\nabla\phi_I.\nabla\phi_I)n_j\,\mathrm{d}S \quad (8)$$

where n_j is the normal to the hull surface, j = *3*, *4* and *5* for heave, roll and pitch, respectively. After computing the forces for a ship at arbitrary positions, the wave passage derivatives may be obtained according to the expressions given in Tables A3 and A4 in the Appendix.

Since the waves are regular, the coefficients can be described as a sum of a sine and a cosine term. For instance, the second-order term $K_{\zeta\phi}(t)$, which is proportional to wave amplitude, can be written as

$$K_{\zeta\phi}(t) = A_w\left[K_{\zeta\phi c}\cos(\omega_e t) + K_{\zeta\phi s}\sin(\omega_e t)\right] \quad (9)$$

where $K_{\zeta\phi c}$ and $K_{\zeta\phi s}$ are constants.

Similarly, the third-order terms $K_{\zeta z\phi}(t)$ and $K_{\zeta\phi\theta}(t)$ (also proportional to wave amplitude) can be expressed as

$$K_{\zeta z\phi}(t) = A_w\left[K_{\zeta z\phi c}\cos(\omega_e t) + K_{\zeta z\phi s}\sin(\omega_e t)\right]$$

$$K_{\zeta\phi\theta}(t) = A_w\left[K_{\zeta\phi\theta c}\cos(\omega_e t) + K_{\zeta\phi\theta s}\sin(\omega_e t)\right] \quad (10)$$

Note that these two functions represent periodic excitation of roll, and are multiplied with, respectively, $z(t)\phi(t)$ and $\theta(t)\phi(t)$. z and θ are both periodic functions dependent on wave amplitude.

The third-order term $K_{\zeta\zeta\phi}(t)$, proportional to the square of the wave amplitude, can be written as

$$K_{\zeta\zeta\phi}(t) = A_w^2\left[K_{\zeta\zeta\phi 0} + K_{\zeta\zeta\phi c}\cos(2\omega_e t) + K_{\zeta\zeta\phi s}\sin(2\omega_e t)\right] \quad (11)$$

which comprises a constant term plus a super-harmonic of double the encounter frequency.

CHARACTERISTICS OF THE VESSEL

To test the fidelity of the model, numerical simulations were compared to experimental results. The experiments were conducted on a 1:45 scale model of a 294m long container

ship. The main characteristics of the vessel can be found in Table 1.

Table 1: Vessel main characteristics (full scale)

Displacement	76,468,800 kg
Hull length	280.982 m
Hull breadth amidships	32.26 m
Hull draught amidships	11.75 m
Roll radius of gyration	12.234 m
Transverse metacentric height	1.843 m

The ship's stability curve can be seen in Figure 1.

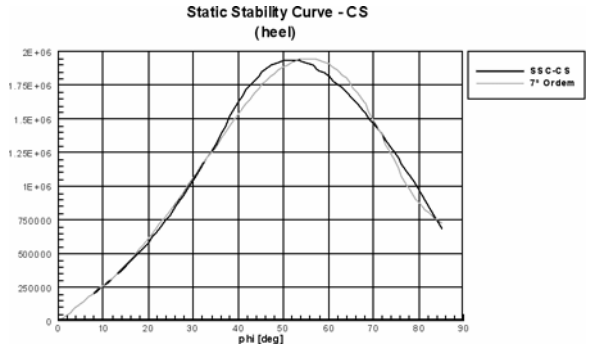

Fig. 1: Static stability curve and the odd seventh-order fit.

TESTED CONDITIONS

In this paper, we consider only the regular wave conditions. A total of 22 tests were performed in regular seas. The test conditions can be seen in Table 2.

The first column is the Froude number. The second column is the encounter frequency. The third column is the ratio of the encounter frequency to the vessel's natural roll frequency. Parametric resonance is known to occur when this is approximately 2. The fourth column is the wave height, and the last column is the test number. The tests were performed in order of increasing test number.

Table 2: Tested conditions

F_n	ω_e	Tuning	H (m)	Test #
0.1035	0.5519	1.85	5	1173
	0.5519	1.85	7	1181
0.1035	0.5677	1.91	5	1175
	0.5677	1.91	7	1183
0.1035	0.5756	1.93	3	1179
0.0879	0.5662	1.90	5	1192
0.0931	0.5723	1.92	5	1193
0.0983	0.5783	1.94	5	1191
			3	1177
0.1035	0.5844	1.96	5	1172
			7	1180
0.1087	0.5904	1.98	5	1184
0.1137	0.5963	2.00	5	1185
0.1189	0.6023	2.02	5	1186
0.1241	0.6084	2.04	5	1187
0.1345	0.6204	2.08	5	1188
0.1397	0.6265	2.10	5	1190
0.1448	0.6324	2.12	5	1189
0.1035	0.5933	1.99	3	1178
0.1035	0.6031	2.03	5	1174
0.1035	0.6231	2.09	5	1176
			7	1182

RESULTS

Some of the results from the experiments, plotted together with the simulation results, can be seen in Figures 2–19. The figures match the order in Table 2, which corresponds to decreasing values of λ / L.

It can be observed that the model provides a good description of the phenomenon for all length ratios; both in terms of roll amplitude and rate of amplification. Conditions with/ without parametric resonance are well modeled, as shown in Figure 20, except for the test cases corresponding to tunings in both extremes of the range of instability for the $\lambda / L = 1.00$ wave condition, at which the bifurcation points are quite sensitive to variation of parameters. It should be noted that the sensitivity of the limits of stability to changes in the system parameters has already been pointed out in Neves and Rodríguez (2006b) in particular with regard to changes in initial conditions.

The differences near the regions of bifurcations defined by limits of stability may be observed in Figure 20, which shows a comparison in the frequency domain of different maximum roll amplitudes for waves of length equal to the ship length and $A_w = 2.5\text{m}$. A condition for $A_w = 3.5\text{m}$ is also included. In Figure 21 we can see the complete numerical mapping of roll amplitudes (indicated by the scaled color variation) for different tunings (or, equivalently, forward speeds) and wave amplitudes for the same $\lambda / L = 1.00$ wave condition.

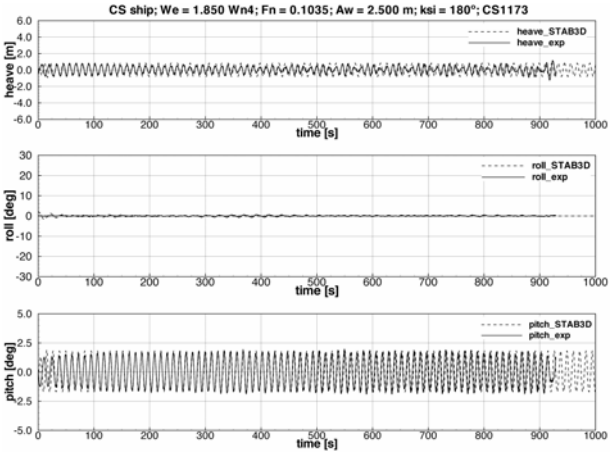

Fig. 2: Exp. 1173 ($\lambda / L = 1.10$). No parametric resonance.

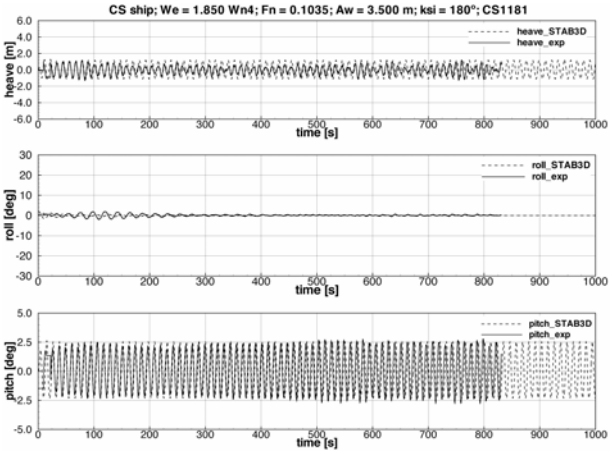

Fig 3: Exp. 1181 ($\lambda / L = 1.10$). No parametric resonance.

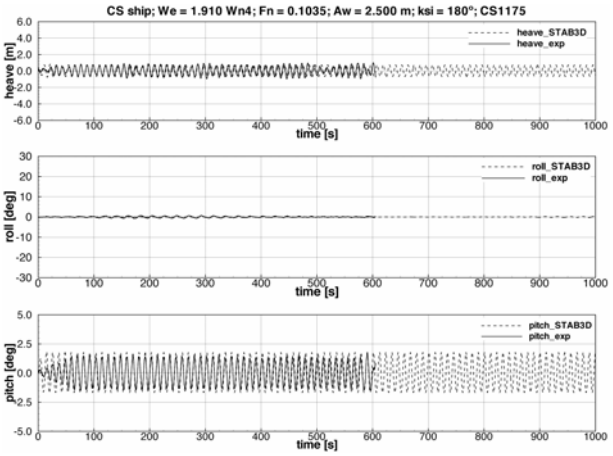

Fig. 4: Exp. 1175 ($\lambda / L = 1.05$). No parametric resonance.

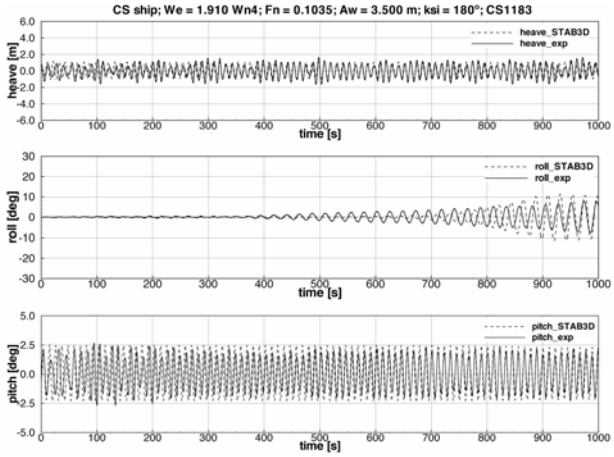

Fig. 5: Exp. 1183 ($\lambda / L = 1.05$). Weak amplification.

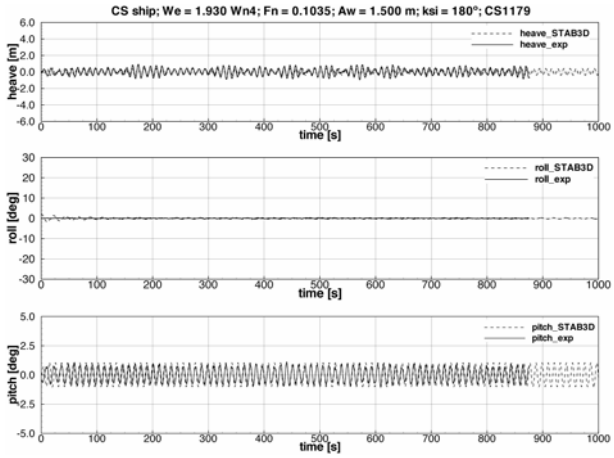

Fig. 6: Exp. 1179 ($\lambda / L = 1.02$). No parametric resonance.

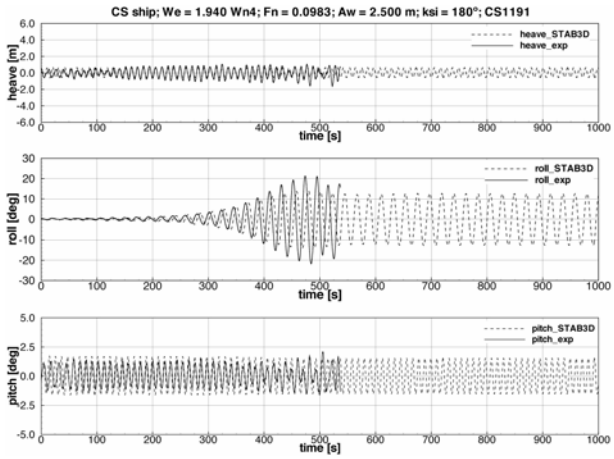

Fig. 7: Exp. 1191 ($\lambda / L = 1.00$). Parametric resonance occurs.

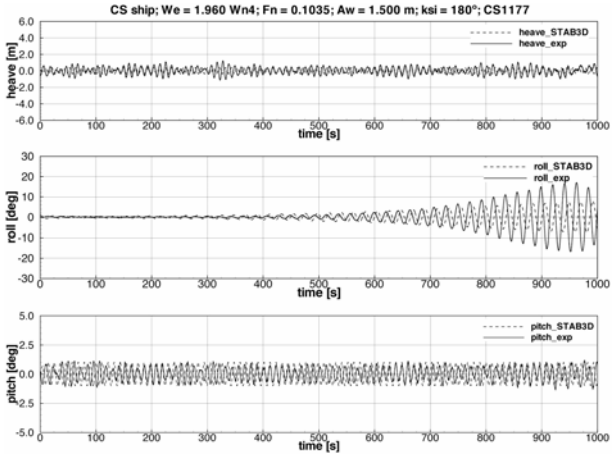

Fig. 8: Exp. 1177 ($\lambda / L = 1.00$). Weak amplification.

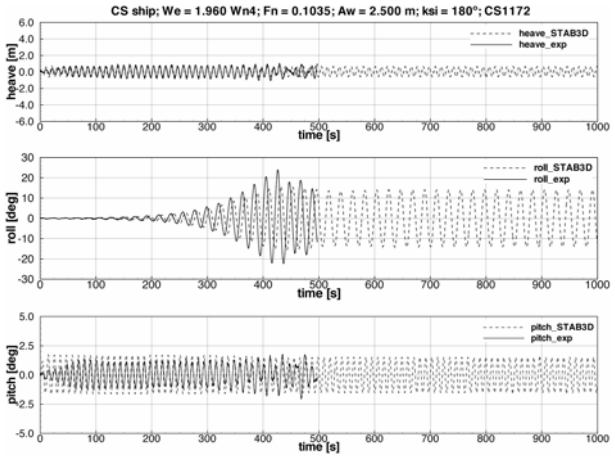

Fig. 9: Exp. 1172 ($\lambda / L = 1.00$). Parametric resonance occurs.

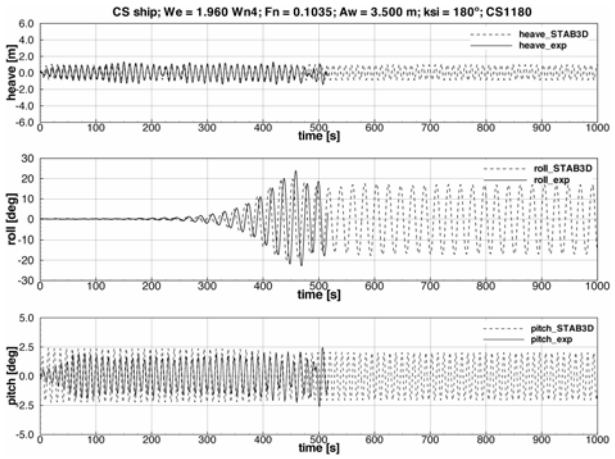

Fig. 10: Exp. 1180 ($\lambda / L = 1.00$). Parametric resonance occurs.

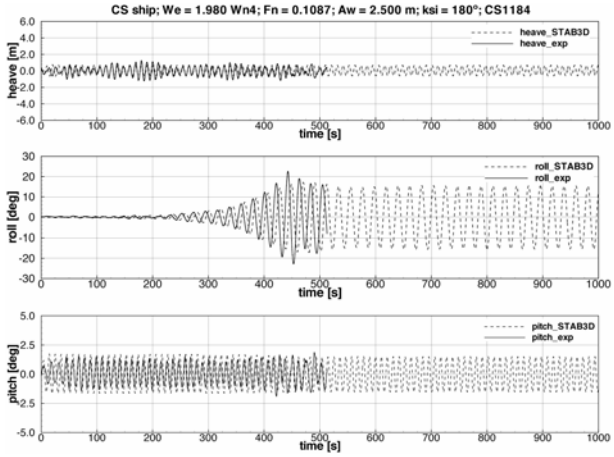

Fig. 11: Exp. 1184 ($\lambda / L = 1.00$). Parametric resonance occurs.

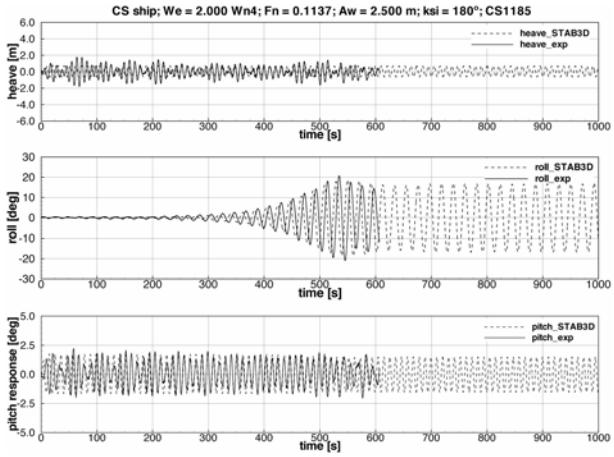

Fig. 12: Exp. 1185 ($\lambda / L = 1.00$). Parametric resonance occurs.

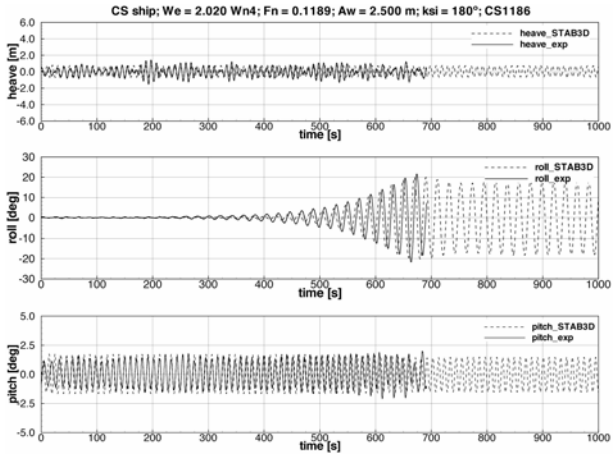

Fig. 13: Exp. 1186 ($\lambda / L = 1.00$). Parametric resonance occurs.

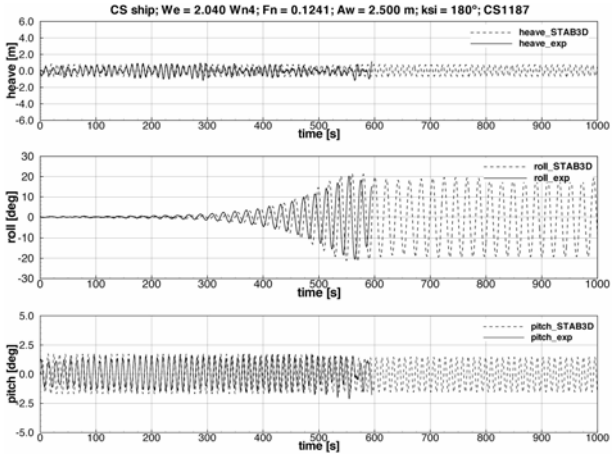

Fig. 14: Exp. 1187 ($\lambda / L = 1.00$). Parametric resonance occurs.

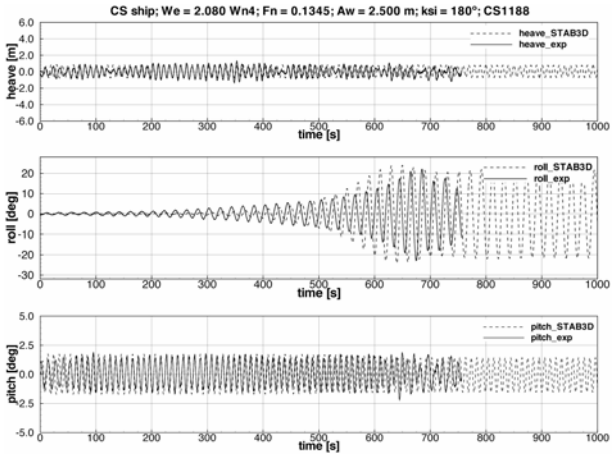

Fig. 15: Exp. 1188 ($\lambda / L = 1.00$). Parametric resonance occurs.

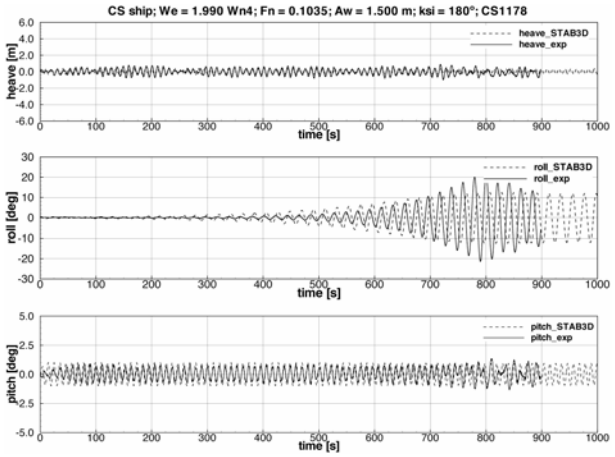

Fig. 16: Exp. 1178 ($\lambda / L = 0.97$). Parametric resonance occurs.

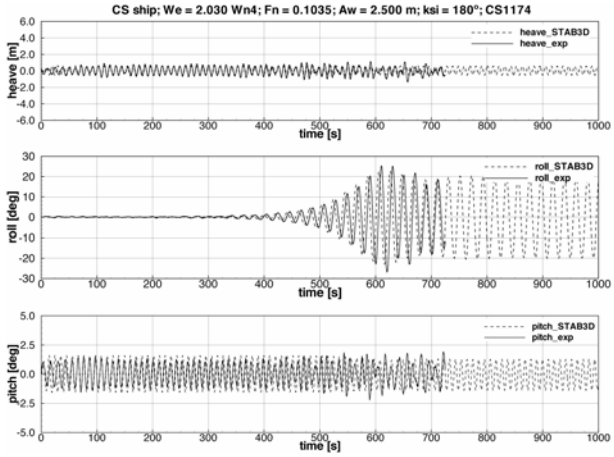

Fig. 17: Exp. 1174 ($\lambda / L = 0.95$). Parametric resonance occurs.

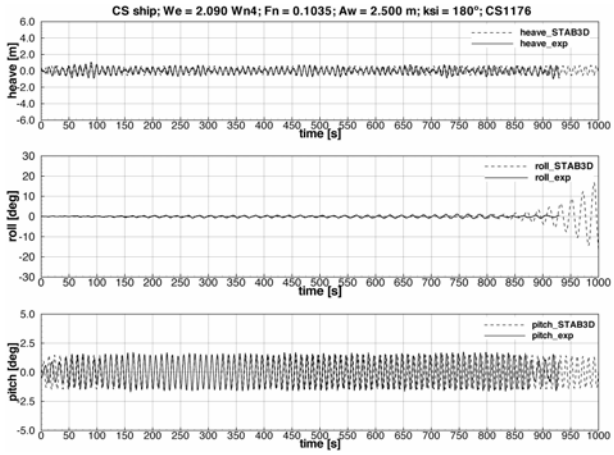

Fig. 18: Exp. 1176 ($\lambda / L = 0.90$). No parametric resonance.

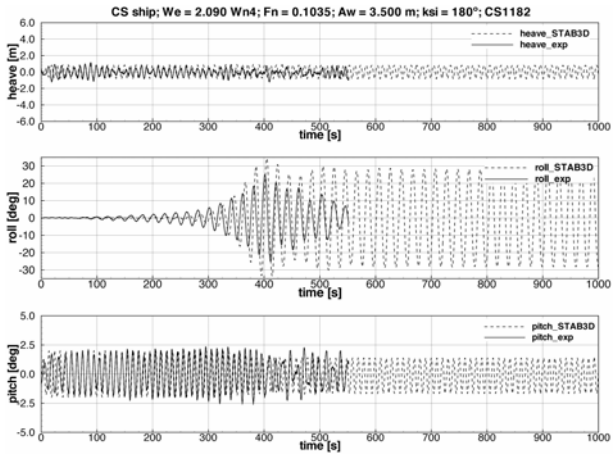

Fig. 19: Exp. 1182 ($\lambda / L = 0.90$). Parametric resonance occurs.

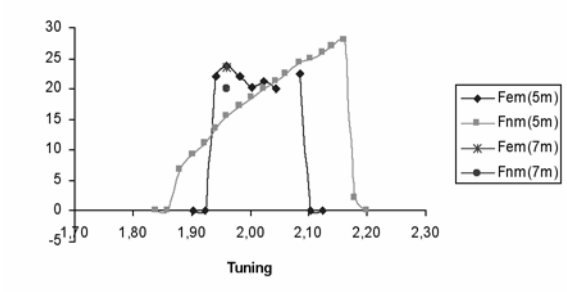

Fig. 20: Maximum roll amplitudes for $\lambda / L = 1$. Subscript e is experimental results, subscript n numerical. Number in parenthesis is wave height.

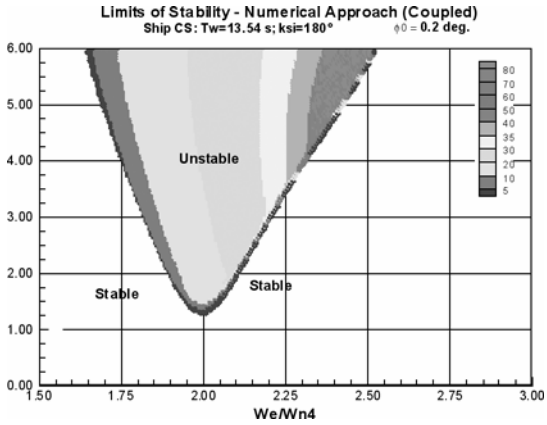

Fig. 21: Limits of stability for $\lambda / L = 1$.

CONCLUSIONS

A third order model for parametric resonance with coupling in roll-pitch-heave previously developed and validated with fishing vessels has been applied to a large container ship and validated showing good agreement with experimental and numerical results.

The accuracy of the model was best for heave and roll, while there was some discrepancy between experimental and numerical results for pitch for some conditions.

The model shows good agreement with the experimental results for roll in both experiments where parametric roll excitation occurred, and where it didn't occur. The range of encounter frequencies in which parametric excitation did occur is relatively wide. For these conditions the effects of tuning, speed and wave amplitude are clarified, as shown in Figures 20–21.

ACKNOWLEDGEMENTS

The present cooperative investigation is partially supported in Brazil by CNPq within the STAB project (Nonlinear Stability of Ships). The Brazilian authors also acknowledge financial support from LabOceano-COPPE/UFRJ and CAPES.

Thanks are due to UFRJ undergraduate student Vinicius L. Vileti, who ran a lot of simulations; to Luiz Cristóvão G. Coelho and Guilherme T. M. Alves from Intergraph-PUC, for the development of relevant parts of the computational code.

REFERENCES

Himeno, Prediction of ship roll damping — state of the art. Report No 239, Department of Naval Architecture and Marine Engineering, The University of Michigan 1981.

Neves, Rodríguez, A non-linear mathematical model of higher order for strong parametric resonance of the roll motion of ships in waves. Marine Systems & Ocean Technology, Sociedade Brasileira de Engenharia Naval 2005a

Neves, Rodríguez, A coupled third order model of roll parametric resonance. *Maritime Transportation and Exploration of Ocean and Coastal Resources*, p. 243-253 2005b.

Neves, Rodríguez, On unstable ship motions resulting from strong non-linear coupling. *Ocean Engineering*, 33:1853-1883 2006a.

Neves, Rodríguez, An Investigation on Roll Parametric Resonance in Regular Waves, Proceedings, 9th International Conference on Stability of Ships and Ocean Vehicles (STAB 2006), p 99-108 (Vol. 1), Rio de Janeiro, 2006b.

APPENDIX

Table A1 – Hydrostatic restoring coefficients (calm water): second order

Heave	Roll	Pitch
$Z_{zz} = -\frac{\partial^2 Z}{\partial z^2}$	$K_{zz} = 0$	$M_{zz} = -\frac{\partial^2 M}{\partial z^2}$
$Z_{z\phi} = 0$	$K_{z\phi} = -\frac{\partial^2 K}{\partial z \partial \phi}$	$M_{z\phi} = 0$
$Z_{z\theta} = -\frac{\partial^2 Z}{\partial z \partial \theta}$	$K_{z\theta} = 0$	$M_{z\theta} = -\frac{\partial^2 M}{\partial z \partial \theta}$
$Z_{\phi\phi} = -\frac{\partial^2 Z}{\partial \phi^2}$	$K_{\phi\phi} = 0$	$M_{\phi\phi} = -\frac{\partial^2 M}{\partial \phi^2}$
$Z_{\phi\theta} = 0$	$K_{\phi\theta} = -\frac{\partial^2 K}{\partial \phi \partial \theta}$	$M_{\phi\theta} = 0$
$Z_{\theta\theta} = -\frac{\partial^2 Z}{\partial \theta^2}$	$K_{\theta\theta} = 0$	$M_{\theta\theta} = -\frac{\partial^2 M}{\partial \theta^2}$

Table A2 – Hydrostatic restoring coefficients (calm water): third order

Heave		
$Z_{zzz} = -\frac{\partial^3 Z}{\partial z^3}$	$Z_{zz\phi} = 0$	$Z_{zz\theta} = -\frac{\partial^3 Z}{\partial z^2 \partial \theta}$
$Z_{z\phi\phi} = -\frac{\partial^3 Z}{\partial z \partial \phi^2}$	$Z_{\phi\phi\phi} = 0$	$Z_{\phi\phi\theta} = -\frac{\partial^3 Z}{\partial \phi^2 \partial \theta}$
$Z_{z\theta\theta} = -\frac{\partial^3 Z}{\partial z \partial \theta^2}$	$Z_{\phi\theta\theta} = 0$	$Z_{\theta\theta\theta} = -\frac{\partial^3 Z}{\partial \theta^3}$

Roll		
$K_{zzz}=0$	$K_{zz\phi}=-\frac{\partial^3 K}{\partial z^2\partial\phi}$	$K_{zz\theta}=0$
$K_{z\phi\phi}=0$	$K_{\phi\phi\phi}=-\frac{\partial^3 K}{\partial\phi^3}$	$K_{\phi\phi\theta}=0$
$K_{z\theta\theta}=0$	$K_{\phi\theta\theta}=-\frac{\partial^3 K}{\partial\theta^2\partial\phi}$	$K_{\theta\theta\theta}=0$

Pitch		
$M_{zzz}=-\frac{\partial^3 M}{\partial z^3}$	$M_{zz\phi}=0$	$M_{zz\theta}=-\frac{\partial^3 M}{\partial z^2\partial\theta}$
$M_{z\phi\phi}=-\frac{\partial^3 M}{\partial z\partial\phi^2}$	$M_{\phi\phi\phi}=0$	$M_{\phi\phi\theta}=-\frac{\partial^3 M}{\partial\phi^2\partial\theta}$
$M_{z\theta\theta}=-\frac{\partial^3 M}{\partial z\partial\theta^2}$	$M_{\phi\theta\theta}=0$	$M_{\theta\theta\theta}=-\frac{\partial^3 M}{\partial\theta^3}$

Heave-roll-pitch coupling		
$Z_{z\phi\theta}=0$	$K_{z\phi\theta}=-\frac{\partial^3 K}{\partial z\partial\phi\partial\theta}$	$M_{z\phi\theta}=0$

Table A3 – Derivatives due to wave passage: second order

$Z_{\zeta z}(t)=-\frac{\partial F_3^{FK(1)}}{\partial z}$	$K_{\zeta z}(t)=0$	$M_{\zeta z}(t)=-\frac{\partial F_5^{FK(1)}}{\partial z}$
$Z_{\zeta\phi}(t)=0$	$K_{\zeta\phi}(t)=-\frac{\partial F_4^{FK(1)}}{\partial\phi}$	$M_{\zeta\phi}(t)=0$
$Z_{\zeta\theta}(t)=-\frac{\partial F_3^{FK(1)}}{\partial\theta}$	$K_{\zeta\theta}(t)=0$	$M_{\zeta\theta}(t)=-\frac{\partial F_5^{FK(1)}}{\partial\theta}$

Table A4 – Derivatives due to wave passage: third order

Heave		
$Z_{\zeta\zeta z}(t)=-\frac{\partial F_3^{FK(2)}}{\partial z}$	$Z_{\zeta\zeta\phi}(t)=0$	$Z_{\zeta\zeta\theta}(t)=-\frac{\partial F_3^{FK(2)}}{\partial\theta}$
$Z_{\zeta zz}(t)=-\frac{\partial^2 F_3^{FK(1)}}{\partial z^2}$	$Z_{\zeta z\phi}(t)=0$	$Z_{\zeta z\theta}(t)=-\frac{\partial^2 F_3^{FK(1)}}{\partial z\partial\theta}$
$Z_{\zeta\phi\phi}(t)=-\frac{\partial^2 F_3^{FK(1)}}{\partial\phi^2}$	$Z_{\zeta\phi\theta}(t)=-\frac{\partial^2 F_3^{FK(1)}}{\partial\theta^2}$	$Z_{\zeta\phi\phi}(t)=0$

Roll		
$K_{\zeta\zeta z}(t)=0$	$K_{\zeta\zeta\phi}(t)=-\frac{\partial F_4^{FK(2)}}{\partial\phi}$	$K_{\zeta\zeta\theta}(t)=0$
$K_{\zeta zz}(t)=0$	$K_{\zeta z\phi}(t)=-\frac{\partial^2 F_4^{FK(1)}}{\partial z\partial\phi}$	$K_{\zeta z\theta}(t)=0$
$K_{\zeta\phi\phi}(t)=0$	$K_{\zeta\phi\theta}(t)=0$	$K_{\zeta\phi\theta}(t)=-\frac{\partial^2 F_4^{FK(1)}}{\partial\phi\partial\theta}$

Pitch		
$M_{\zeta\zeta z}(t)=\frac{\partial F_5^{FK(2)}}{\partial z}$	$M_{\zeta\zeta\phi}(t)=0$	$M_{\zeta\zeta\theta}(t)=\frac{\partial F_5^{FK(2)}}{\partial\theta}$
$M_{\zeta zz}(t)=\frac{\partial^2 F_5^{FK(1)}}{\partial z^2}$	$M_{\zeta z\phi}(t)=0$	$M_{\zeta z\theta}(t)=-\frac{\partial^2 F_5^{FK(1)}}{\partial z\partial\theta}$
$M_{\zeta\phi\phi}(t)=-\frac{\partial^2 F_5^{FK(1)}}{\partial\phi^2}$	$M_{\zeta\phi\theta}(t)=-\frac{\partial^2 F_5^{FK(1)}}{\partial\theta^2}$	$M_{\zeta\phi\theta}(t)=0$

Head-Sea Parametric Rolling of a Car Carrier

Hirotada Hashimoto, Naoya Umeda and Genta Sakamoto

Osaka University, JAPAN

ABSTRACT

Recently, a report of head-sea parametric rolling of 50 degrees for a car carrier in the Northern Atlantic was published. To investigate parametric rolling of a car carrier, the authors carried out experimental and numerical study for a latest car carrier in regular and irregular head seas. In the experiment at a towing tank, significant head-sea parametric rolling was observed both in regular and long-crested irregular waves. Numerical simulation using restoring variation with Froude-Krylov, radiation and diffraction components qualitatively explained these experimental outcomes, and its accuracy depends on the precision of restoring variation estimation. In irregular seas, significant non-ergodicity was confirmed both in model experiment and numerical simulation.

KEYWORDS

Parametric Rolling; Car Carrier, Head Seas, Irregular Seas, Restoring Variation, Non-Ergodicity

INTRODUCTION

It has been agreed to set standards for a restoring variation problem including parametric rolling at the International Maritime Organization (IMO) in 2005. In the background of this agreement, there are reports of serious accidents of parametric rolling of a post-Panamax containership and a pure car and truck carrier (PCTC). In particular, there is a definite example of the PCTC: the PCTC Aida suffered head-sea parametric rolling with about 50 degrees of maximum roll angle in the Azores Islands waters in 2003, and she experienced head-sea parametric rolling again in 2004, which was successfully recorded by a sensor (Sweden, 2004).

To investigate these accidents, Hua (2006) conducted the numerical simulation for the Aida based on the Froude-Krylov assumption, and reported that parametric rolling occurs in regular head seas and does not occur in irregular head seas. Finally he concluded that the reason why the Aida suffered parametric rolling is that she had accidentally met with an almost regular wave group. However, this conclusion could invite further discussion.

Therefore, the authors conducted the free running model experiment for a latest PCTC having a similar hull form like the Aida. As a result, significant parametric rolling has been measured both in regular and irregular head seas with the designed GM value. Comparison between an experimental result and a numerical simulation was also conducted, and prediction accuracy of the present mathematical model for parametric rolling prediction is examined. Furthermore, roll restoring variation in head seas, which is an important factor for quantitative prediction of parametric rolling, was measured and compared with the theoretical estimation with dynamic effect on restoring variation taken into account.

SUBJECT SHIP AND MATHEMATICAL MODEL

The principal particulars of the PCTC used for this research is shown in Table 1.

Table 1: Principal particulars

item	value
length: L_{PP}	192.0 m
breadth: B	32.26 m
depth: D	37.0 m
mean draught: T	8.18 m
block coefficient: C_b	0.54
longitudinal position of centre of gravity from a midship: x_{CG}	4.67 m aft
metacentric height: GM	1.25 m
natural roll period: T_ϕ	22.0 s

The mathematical model for parametric rolling prediction in regular head seas is expressed as eq.(1). Although this model is a 1DOF of roll model, heave and pitch motions are taken into account to estimate restoring variation. Restoring moment in waves is calculated as a sum of two components. One is the nonlinear Froude-Krylov component, which is calculated by integrating wave pressure up to wave surface. The other is the dynamic effect, which consists of radiation and diffraction components acting on a heeled asymmetric hull.

As the prediction accuracy of restoring moment could be improved if the dynamic component is included, which was examined in the past research for a post-Panamax containership by the authors (Umeda et al., 2005), we also took into account radiation and diffraction components for the subject car carrier. The dynamic effect is calculated by applying a strip theory to a heeled hull as a linear component with respect to wave height. This effect is considered as an additional effect on GZ by dividing calculated dynamic roll moment with a ship displacement.

$$(I_{xx} + J_{xx})\ddot{\phi} + A\dot{\phi} + B|\dot{\phi}|\dot{\phi} + WGZ(t,\zeta,\theta,\phi,\eta_W) = 0 \quad (1)$$

I_{xx}: inertia of roll moment, J_{xx}: added inertia of roll moment, ϕ: roll angle, A: linear coefficient of roll damping, B: quadratic coefficient of roll damping, W: ship displacement, GZ: righting arm, t: time, ζ: displacement in heave, θ: pitch angle, η_W: wave elevation

The mathematical model for long-crested irregular seas is extended from that for regular seas. In calculation, the instantaneous nonlinear Froude-Krylov component is calculated by taking relative irregular wave elevation in each 2-dimensional section of the hull with transfer functions of heave and pitch motions obtained by a strip method for an upright hull. Dynamic effect component is also calculated as a linear superposition with transfer functions of GZ calculated as radiation and diffraction components. Here dynamic effect is calculated under the assumption that it has the linear relationship with the roll angle. In this research, dynamic effect is obtained for 10 degrees of heel condition. Linear and quadratic damping coefficients are obtained from roll decay test with several different speeds.

HEAD-SEA PARAMETRIC ROLLING IN REGULAR SEAS

Amplitude of Parametric Rolling

The partially restrained free running experiment with a 1/64 scaled model of the car carrier was conducted at the towing tank of Osaka University. A ship model is towed by an elastic rope connected to the bow in regular head seas. Measured steady roll amplitude of parametric rolling for several Froude numbers and wave lengths is shown in Fig.1. Here the wave height is 3.2 m in full scale.

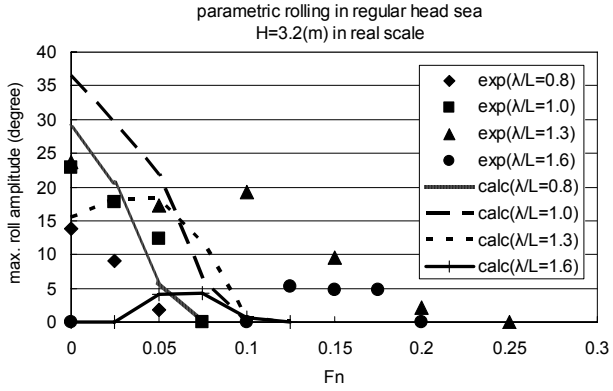

Fig. 1: Maximum roll amplitude of parametric rolling with constant wave height

The parametric rolling amplitude decreases as the wave length increases. This is because the

roll restoring variation becomes most significant where the wave length is almost equal to ship length. Moreover, since the wave slope decreases as the wave length increases, restoring variation decreases for a constant wave height.

The Froude number, which satisfies the parametric rolling condition where encounter period is a half of natural roll period under the assumption of linear restoring at the upright condition is shown in Table 2. This Froude number is used in the guidance for the master of the IMO, and it almost corresponds to the experimentally obtained Froude number where parametric rolling amplitude becomes the most significant.

Table 2: Froude number where the encounter period becomes a half of the natural roll period

λ/L	Fn	heading
0.8	0.035	following sea
1.0	0.003	head sea
1.3	0.068	head sea
1.6	0.139	head sea

In the experimental result of λ/L=1.3, two peaks of the maximum roll amplitude of parametric rolling can be found at Fn=0.0 and Fn=0.1. It was confirmed that two coexisting steady states, e.g. the upright condition and parametric rolling, could be confirmed at Fn=0.0 with different initial disturbances. The time series of roll motion is shown in Fig.2. This is supposed to be a sub-critical bifurcation. Since parametric rolling is a nonlinear phenomenon, its initial value dependency was pointed out and confirmed by analytical solutions and numerical simulation. (Hashimoto and Umeda, 2004) It is interesting that the existence of sub-critical bifurcation has been confirmed by model experiment.

Numerical result can explain the qualitative natures of the experimental result. The roll amplitude decreases as the wave length increases, and the occurrence region shifts to higher speed. However the numerical prediction overestimates the maximum roll amplitude of parametric rolling for each wave lenght. The sub-critical bifurcation observed in the model experiment could not be confirmed through the numerical simulations with various initial roll angles in the same conditions as the experiment.

Fig.3 and Fig.4 show the comparison of the maximum roll amplitude between the experiment and the calculation with constant Froude number of 0.0 and various wave heights for two different wave length to ship length ratios. In the case of λ/L=1.0, the calculation can simulate qualitative natures of parametric rolling but overestimate the maximum roll amplitude. In the case of λ/L=1.3, the calculated amplitude is almost 2 times as large as the measured one at H/λ=0.017. One possible reason of this significant difference is the existence of sub-critical bifurcation.

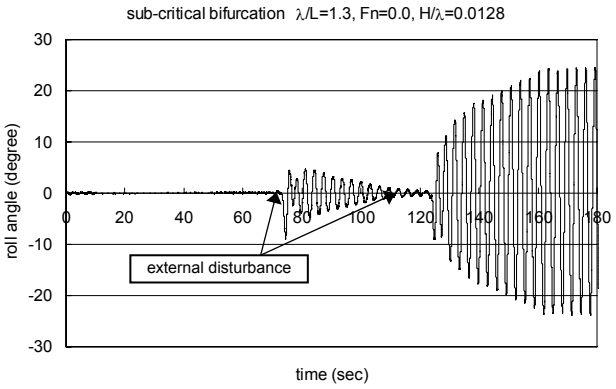

Fig. 2: Experimentally observed sub-critical bifurcation

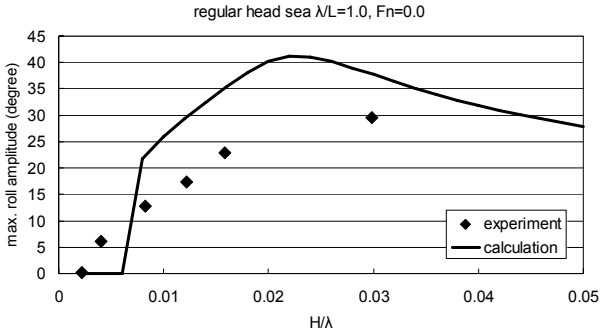

Fig. 3: Roll amplitude of parametric rolling with λ/L=1.0

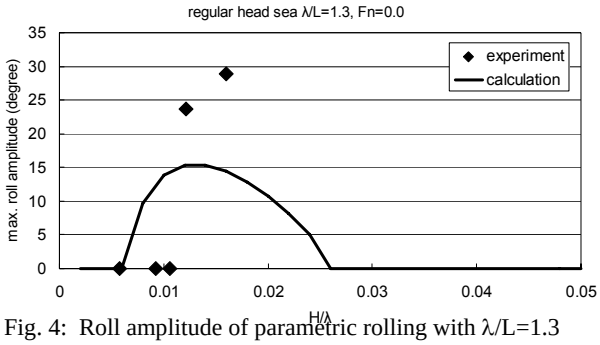

Fig. 4: Roll amplitude of parametric rolling with λ/L=1.3

These comparisons indicate that the present mathematical model can predict head-sea parametric rolling of the car carrier only qualitatively.

Characteristics of restoring variation

Restoring variation in regular head waves, which is important for parametric rolling prediction, was measured by a captive model experiment. In the experiment, ship model is fixed with 10 degrees of heel angle and towed by a towing carriage in regular head waves. Here the model is fixed in surge, sway, yaw and roll and is free in heave and pitch. From the measured roll moment, the restoring variation around the centre of ship gravity is obtained.

Fig.5 shows the comparison of GZ variation in regular head waves with λ/L=1.0, and Fig.6 does with λ/L=1.3. The experimental result indicates that the amplitude of restoring variation decreases as wave length increases for a constant wave height. The numerical estimations are based on following two methods; one takes both Froude-Krylov and dynamic effect components into account and the other does Froude-Krylov moment on its own. Both results qualitatively agree with experimental result, however both estimations overestimate the amplitude of GZ variation to some extent. The tendency of restoring variation that its amplitude decreases as the wave lenght increases is reproduced by the numerical estimation. Although the difference in the amplitude of variation between experiment and calculation with λ/L=1.3 is small compared with λ/L=1.0, its prediction accuracy still remains not in quantitative but in qualitative.

Since agreement of maximum roll amplitude of parametric rolling with λ/L=1.3 in Fig.1 is much better than that with λ/L=1.0 as well as the estimation of roll restoring variation, it might be concluded that the disagreement of restoring variation is one of the reasons why numerical prediction overestimates the parametric rolling danger in regular head seas.

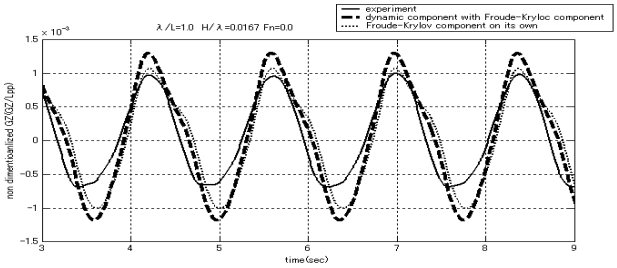

Fig. 5: Restoring variation in regular head seas with λ/L=1.0 and Fn=0.0

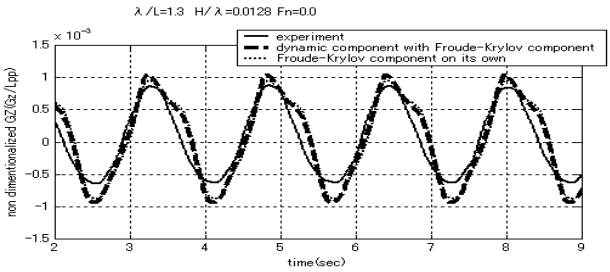

Fig. 6: Restoring variation in regular head seas with λ/L=1.3 and Fn=0.0

HEAD-SEA PARAMETRIC ROLLING IN IRREGULAR SEAS

Maximum Roll Angle of Parametric Rolling

A free running model experiment towed by an elastic rope was carried out in long-crested irregular seas. Following the assumed condition where the PCTC Aida encountered, 5.31m of significant wave height, 9.76 seconds of wave mean period where the peak period corresponds to the wave period of the regular wave whose length is 1.3 times as long as the ship length were used, and ship model was towed with several Froude numbers. Model runs in irregular waves were repeated four to six times with different phase sets of the ingredient waves for each Froude number, and

numerical simulation is done for the same time duration as the model runs, about 17 minutes in full scale for one run.

The mathematical models for parametric rolling prediction in irregular seas used here are two methods: one takes the restoring variation calculated with Froude-Krylov component on its own into account, and the other does Froude-Krylov component, radiation and diffraction components. Heave and pitch motions are calculated with transfer functions obtained by a strip method for a non-heeled hull, and they are used in the calculation of Froude-Krylov and dynamic effect components.

Fig.7 shows the measured and calculated maximum roll angles of parametric rolling for each Froude number. In the experiment, significant parametric rolling was observed in irregular waves like the PCTC Aida, and its maximum roll angle exceeds 30 degrees at Fn=0.0. The maximum roll angle of parametric rolling decreases as Froude number increases, and parametric rolling disappears at Fn=0.15. Since the peak period corresponds to the wave period of a regular wave which length is 1.3 times as long as the ship length, Fn=0.07 is obtained as the most relevant speed for parametric rolling occurrence under the linear roll restoring. However most significant parametric rolling was observed at Fn=0.0.

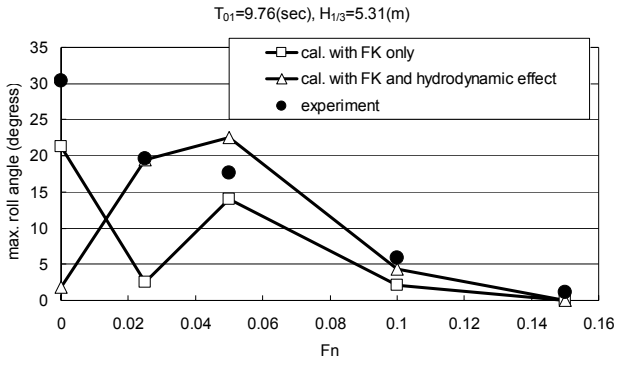

Fig. 7: Maximum roll angle in long-crested irregular head seas

In higher speed region, the numerical simulation can predict the maximum roll angle of parametric rolling with practical accuracy. In lower speed region, however, the calculated results do not agree with the experimental result in maximum roll angle. Moreover, the significant difference among two calculation results is found. Since two numerical calculations have used the same wave data, initial values and coefficients in the mathematical model, we can conclude that this large difference among two calculations is from small difference of estimation of restoring variation.

Characteristics of restoring variation

Restoring variation in long-crested irregular head seas was measured as well as the regular wave case. Here, comparison of time series of heave, pitch and restoring variation, and probability density function of GZ between model experiment and numerical estimation are shown in Figs.8-11. Here Froude number is 0.0. Fig.8 and Fig.9 indicate that heave and pitch motions can be estimated with sufficient accuracy by a strip method without taking heeled condition into account. As shown in Fig.10, the dynamic effect on restoring variation in irregular waves is not as significant as the post post-Panamax containership (Hashimoto et al., 2006). Moreover, it is confirmed that there is almost no difference in restoring variation for the subject PCTC between the experiment and the two calculations.

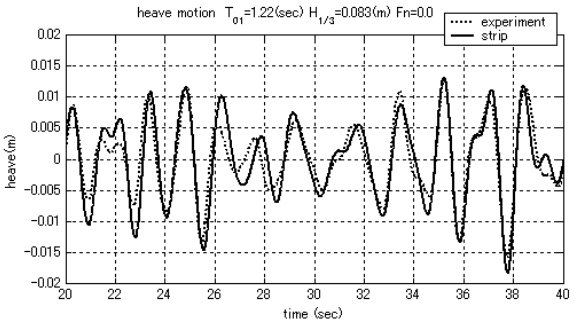

Fig. 8: Comparison of heave motion in irregular seas

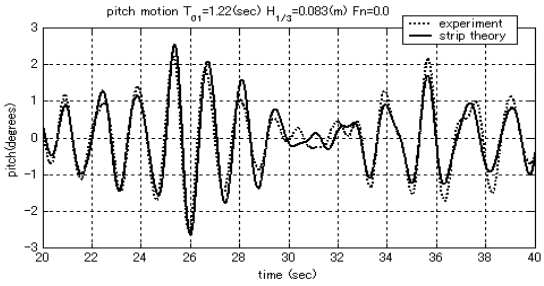

Fig. 9: Comparison of pitch motion in irregular seas

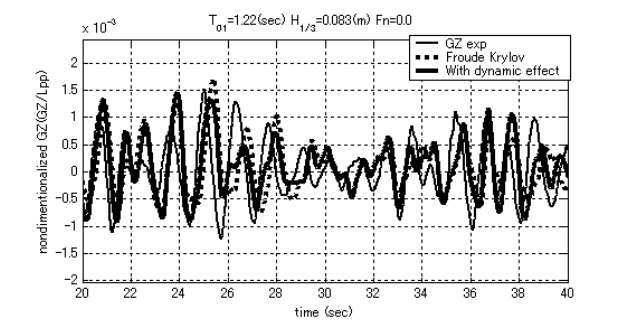

Fig. 10: Comparison of GZ variation in irregular seas

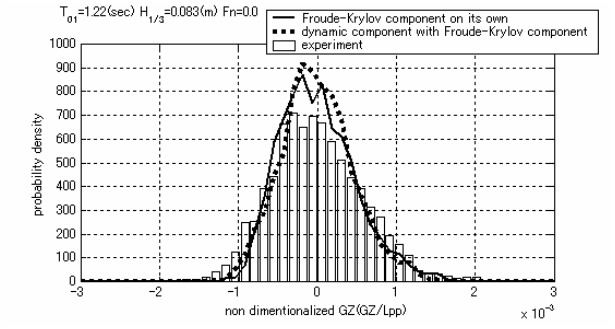

Fig. 11: Comparison of Probability density function of GZ in irregular seas

Since it was confirmed that the estimation of restoring variation used for the numerical simulation of parametric rolling has practical accuracy, it indicates that small difference in restoring variation produces the significant difference of maximum roll angle as shown in Fig.7.

Non-Ergodicity

Fig.12 and Fig.13 show the measured and calculated maximum roll angles of parametric rolling for four different realizations. If the phenomenon of parametric rolling has ergodicity, the maximum values for different realizations tend to a certain value. However there is scatter of maximum roll angles of parametric rolling both in the model experiment and the numerical simulation.

Although Hua (2006) had reported that parametric rolling does not occur in his numerical simulation for the PCTC Aida in irregular waves, non-ergodicity could be one of the reasons why no parametric rolling occurs because he just tested one realization. Considering these facts, it is essential that numerical simulation should be repeated using different random phase sets because of the significant non-ergodicity of parametric rolling.

How to deal with non-ergodicity of parametric rolling in irregular seas is important issue, so that further discussion is needed for appropriately planning experiments and simulations.

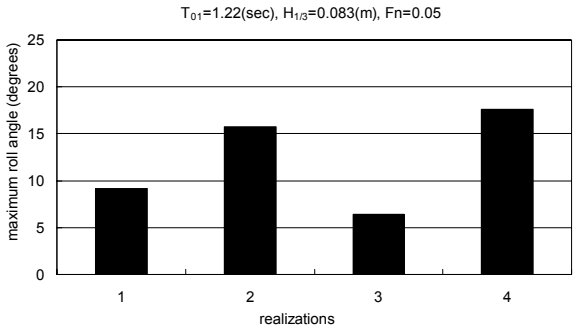

Fig.12: Maximum roll angle for 4 different realizations (experiment)

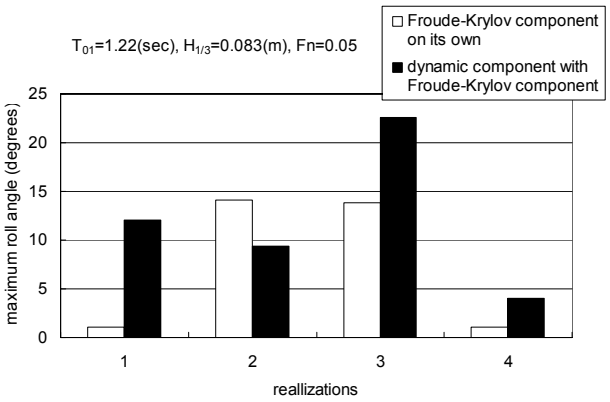

Fig.13: Maximum roll angle for 4 different realizations (calculations)

CONCLUSIONS

1) Free running model experiment of a car carrier was conducted and significant parametric rolling exceeding 20 degrees in regular head seas and 30 degrees in irregular head seas was observed.
2) Sub-critical bifurcation, which is the feature of a nonlinear phenomenon, was observed in the experiment.
3) Numerical simulation could estimate the occurrence region of parametric rolling and its amplitude qualitatively. For more accurate prediction, the improvement of the estimation precision of roll restoring variation is needed.

4) Significant non-ergodicity of parametric rolling in irregular seas has been confirmed both in the experiment and the numerical simulation. It would be important to discuss how to deal with the non-ergodicity from a practical point of view.

ACKNOWLEDMENTS

This research was supported by a Grant-in Aid for Scientific Research of the Japan Society for promotion of Science (No. 18360415). A part of this research was done as the stability project (SPL) of Japan Ship Technology Research Association in 2006 fiscal year supported by Nippon Foundation, and a fundamental research developing association for shipbuilding and offshore of the Shipbuilders' Japan. The authors express their sincere gratitude to the above organizations.

REFERENCES

Sweden: Recordings of Head sea Parametric Rolling on a PCTC, SLF47/INF.5, IMO, 2004

Hua, J., Palmquist and G. Lindgren: An Analysis of the Parametric Roll Events Measured Onboard the PCTC AIDA, Proceedings of the 9th International conference on stability of ships and ocean vehicles (STAB), Vol. 1, pp. 109-118, 2006

Umeda, N., Hashimoto, H., Sakamoto, G. and Urano, S.: Research on estimation of roll restoring variation in waves, Conference proceedings of the Kansai society of naval architects, Vol.24, pp. 17-19, 2005 (in Japanese)

Hashimoto, H. and Umeda, N.: Nonlinear Analysis of Parametric Rolling in Longitudinal and Quartering Seas with Realistic Modeling of Roll-Restoring Moment, Journal of Marine Science and Technology, Vol. 9(3), 2004

Hashimoto, H., Umeda, N., Sakamoto, G. and Bulian, G.: Estimation of Roll Restoring Moment in Long-Crested Irregular Waves, Conference proceedings of the Japan society of naval architects and ocean engineers, Vol.3, pp. 201-204, 2006

Session 5: Surf-riding, broaching and capsizing in following/quartering seas

Session Chairman: Prof. St. Grochowalski Prof. K.J. Spyrou

1) N. Umeda, M. Shuto, A. Maki:

   "Theoretical Prediction of Broaching Probability for a Ship in Irregular Astern Seas"

2) A.Matsuda, H. Hashimoto, T. Momoki:

   "Non-linear Hydrodynamic Force Measurement System in Heavy Seas for Broaching Prediction"

3) F.Kluwe, St.Krüger:

   "Using Full-Scale Capsizing Accidents for the Validation of Numerical Sea-keeping Simulations"

Theoretical Prediction of Broaching Probability for a Ship in Irregular Astern Seas

Naoya Umeda, Masakazu Shuto and Atsuo Maki,

Osaka University, JAPAN

ABSTRACT

For developing the performance-based intact stability criterion focusing on broaching, the authors firstly extended their numerical simulation model on broaching in regular waves to irregular waves, and validated it with the existing full scale data in irregular waves. Secondly, we numerically evaluated the probability of broaching by using the extended model together with a judging criterion of broaching. Thirdly, an analytical method for calculating broaching probability was formulated with given deterministic thresholds of broaching in regular waves. Finally we confirmed that the theoretically predicted values of broaching probability well agree with those from the numerical simulation. Therefore, the authors believe the newly proposed theoretical procedure can be used for the performance-based intact stability criteria at the IMO.

KEYWORDS

Broaching, Surf-riding, Astern Seas, Narrow-Band Spectrum, Probability, Performance-Based Intact Stability Criteria

INTRODUCTION

At the International Maritime Organization (IMO) revision of the Intact Stability Code started in 2002 and, other than its prescriptive rules, performance-based criteria are requested to be developed by 2010. This new criteria should cover three major capsizing scenarios: restoring variation problems such as parametric rolling, stability under dead ship condition and manoeuvring-related problems such as broaching. It was expected to be a probabilistic stability assessment based on physics by utilising first principle tools. Regarding broaching among the three scenarios, quantitative prediction of broaching in regular waves was realised with a numerical simulation model in time domain if data from limited numbers of captive model tests are available. (Umeda and Hashimoto, 2006) Moreover, a deterministic threshold of its occurrence can be directly estimated by applying a heteroclinic bifurcation analysis so that tedious repeat of numerical simulation can be avoided. (Umeda, Hori et al., 2006) However, for realising probabilistic stability assessment required at the IMO, numerical modelling of broaching in irregular waves and estimation of broaching probability in irregular waves are indispensable.

Unfortunately, no remarkable progress on the probabilistic approach on broaching has been reported so far. Although broaching in regular waves was discussed as a kind of transition from periodic states to non-periodic states, ship motion in irregular waves is almost always not periodic. It is difficult even to define the wave phase velocity in irregular waves while surf-riding, which is a prerequisite for broaching, is defined as a phenomenon that a ship runs with the wave phase velocity. On the other hand, ocean waves are not completely random. Since it has a narrow-banded spectrum, a phenomenon similar to that in regular waves can be realised even in ocean waves. This can be justified that several reports of broaching exists from mariners without a record of time series (Du Cane and Goodrich, 1962) but few

model experiment on broaching in irregular waves with statistical accuracy seems to be available in existing literatures (e.g. Rutgersson and Ottosson, 1987). This might be because existing seakeeping and manoeuvring basins are too small to obtain broaching records for a ship model running with high speed in irregular waves. A possible exception can be found in a full-scale measurement with a pleasure fishing craft at Japanese coastal area by Motora et al. (1982).

Based on the above situation, the authors attempted to extend their numerical model for regular waves, which had been validated with the free-running model experiments in regular waves, to that for irregular waves and to validate it with Motora's full scale data at sea. Then we identified samples of broaching records from the time series obtained by numerical simulation in time domain. Finally, based on a theoretical work on surf-riding in irregular waves by Umeda (1990), we developed a theory for calculating broaching probability in irregular waves with the deterministic threshold of broaching in regular waves and then compared the theoretical result with numerical experiments.

NUMERICAL MODELLING OF BROACHING IN IRREGULAR WAVES

As an extension of the model for regular waves proposed by the authors (Umeda and Hashimoto, 2002), a surge-sway-yaw-roll mathematical model in irregular stern quartering waves is proposed here, based on the coordinate system shown in Fig. 1. A long-crested irregular wave train is assumed to propagate in the direction of ξ of the space-fixed coordinate system O-ξ, η, ζ and a ship is assumed to be situated with the heading angle, χ, from the wave direction. The ship fixed horizontal coordinate system G-x, y, z with the origin at the centre of ship gravity, G, has the x-axis pointing towards the bow, the y axis to starboard and the z-axis downwards. In calm water, the positive rudder angle normally induces the positive yaw rate. When the surge and sway velocities described with u and v, the position of the ship centre of gravity, (ξ_G, η_G), are calculated as follows:

$$\xi_G = \int_0^t (u\cos\chi - v\sin\chi)d\tau \tag{1}$$

$$\eta_G = \int_0^t (u\sin\chi + v\cos\chi)d\tau \tag{2}$$

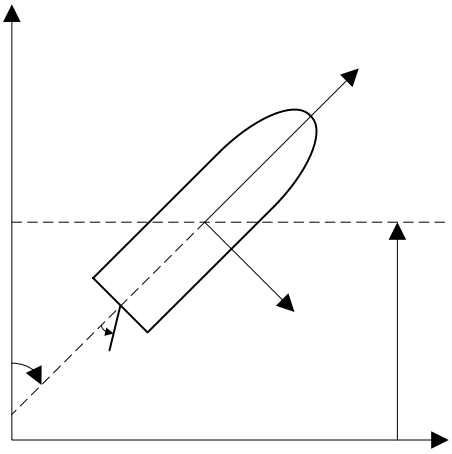

Fig. 1: co-ordinate systems

If we assume that ocean waves can be modelled with the ITTC spectrum, S(ω, α), the ocean wave elevation, ζ_w, can be calculated as follows:

$$\zeta_w(\xi_G,\eta_G,t) = \int_0^\infty \int_{-\pi/2}^{\pi/2} \sqrt{2S(\omega,\alpha)d\omega d\alpha}\cdot\cos(\omega t - k\xi_G\cos\alpha - k\eta_G\sin\alpha + \delta_b) \tag{3}$$

Here δ_b is a random number ranging from 0 to 2π.

Assuming that the wave elevation and ship motion due to waves are small and ignoring their higher order terms, the following mathematical model in irregular waves can be obtained:

$$(m+m_x)\dot{u} = \{T_P(u;n) - R(u) + X_W(\xi_G,\eta_G,t,\chi)\}$$

$$(m+m_y)\dot{v} = \{-(m+m_x)ur + Y_v(u;n)v + Y_r(u;n)r + Y_\phi(u)\phi$$

$$+Y_\delta(u;n)\delta+\underline{Y_w(\xi_G,\eta_G,t,u,\chi;n)}\ \}$$

$$(I_{ZZ}+J_{ZZ})\dot{r}=\{N_v(u;n)v+N_r(u;n)r+N_\phi(u)\phi+N_\delta(u;n)\delta$$

$$+\underline{N_w(\xi_G,\eta_G,t,u,\chi;n)}\ \}$$

$$(I_{xx}+J_{xx})\dot{p}=\{m_x z_H ur+K_v(u;n)v+K_r(u;n)r+K_P(u)p+K_\phi(u)\phi$$

$$+K_\delta(u;n)\delta+\underline{K_w(\xi_G,\eta_G,t,u,\chi;n)}-mgGZ(\phi)\ \} \quad (4)$$

The symbols used here are defined in the nomenclature.

SUBJECT SHIP AND CONDITIONS

In this paper, the pleasure fishing craft used by Motora et al. (1982) was selected for enabling us to utilise their data. Its length between perpendiculars is 7.14 m, its breadth is 1.87m, its depth is 0.63 m, its draught is 0.3835m and its GM is 0.715 m. The resistance, propulsion and manoeuvring coefficients in calm water were based on captive model tests by Motora et al. (1982) and Fuwa et al. (1983) Wave-induced forces were estimated with a linear slender body theory (Umeda and Renilson, 1992a). The numerical model for regular waves had been compared with the free-running model tests with the subject ship by Fuwa et al. (1983) and good agreements in the occurrence of broaching in regular waves between the simulation and experiment had been reported. (Umeda and Renilson, 1992b)

In the full scale tests by Motora et al. (1982) the ship ran with about 8.5 knot in following wind waves or stern quartering wind waves whose heading angle is about 30 degrees from the wave direction. The wave height visually estimated ranged from 1.0 m to 1.5 m and the wave length did from 10m to 15m. For comparison sake, numerical calculations in this paper were carried out under the following condition. The ship runs with the constant propeller revolution that is capable to propel the ship with 8.5 knot in calm water and with the auto pilot courses of 5 degrees and 30 degrees from the direction of long-crested irregular waves. The significant wave height, $H_{1/3}$, is 1.25 m, the mean wave period, T_{01}, is 2.392 seconds. Here the auto pilot has a proportional control law with 1.0 of the rudder gain. The initial condition is that the ship speed is 8.5 knot in the direction of the auto pilot course. The rudder angle limit is 30 degrees both in the full scale test and the numerical calculation.

COMPARISON WITH FULL SCALE TEST

The numerical calculation was conducted under the condition of Motora's full scale tests with the auto pilot course of 5 degrees with many different realisations and the authors attempted to find calculated results similar to the published time series of the full scale tests shown in Figs. 2-3. In this case, while the rudder angle saturates in the negative direction, the yaw angular velocity has a peak of 0.2 radians per second in the positive direction. Then, after one cycle of yaw angular velocity, the rudder angle gradually increases from its minimum limit. The calculated result having the similar qualitative nature was successfully selected as shown in Figs. 4-5. This means that a typical broaching in irregular waves recorded in the full scale test can be reproduced by the numerical calculation for the same ship, operational and wave conditions. It should be noted here that time series of incident waves, other than the representative wave properties, are different between the two and manual steering was used in the full scale tests while the auto pilot was used in the calculation. Nevertheless, the success of qualitative reproduction of broaching time series suggests that the proposed numerical model can be useful for investigating broaching behaviours in irregular waves.

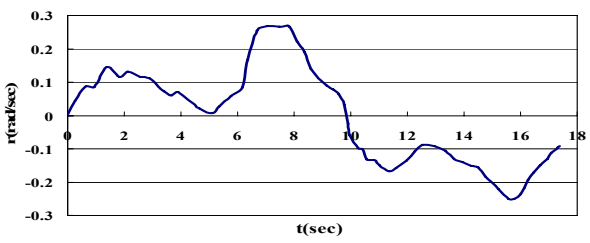

Fig. 2: yaw angular velocity measured in the physical experiment (Motora et al., 1982)

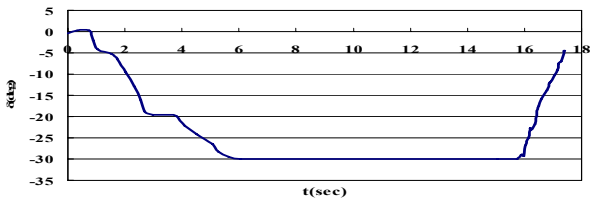

Fig. 3: rudder angle measured in the physical experiment (Motora et al., 1982)

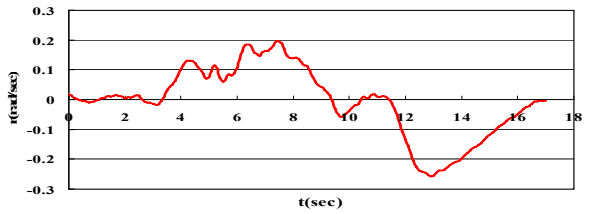

Fig. 4: yaw angular velocity calculated in the numerical experiment

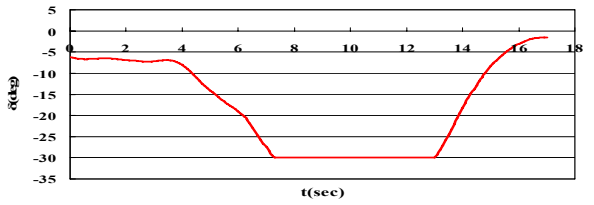

Fig. 5: rudder angle calculated in the numerical experiment

ROUGH ESTIMATE OF BROACHING PROBABILITY BY NUMERICAL EXPERIMENT

As a next step, the authors conducted numerical experiments by utilising the validated numerical model under the same condition but with the auto pilot course of 30 degrees for the duration of 2000 seconds per realisation. Here five different realisations for irregular waves were used. An example is shown in Figs. 6-8. Although the auto pilot course is set to be 30 degrees from the wave direction, the calculated course scatters between 5 degrees and 90 degrees and the rudder angle often reaches its limit in the negative direction. This means that the ship faces a significant difficulty to keep her straight course.

Then the following judging criterion for broaching (Umeda et al., 1999) was applied to the calculated time series and the occurrence of broaching was identified.

$$\delta = \delta_{MAX}, r < 0, \dot{r} < 0 \quad \text{or} \quad \delta = -\delta_{MAX}, r > 0, \dot{r} > 0 \tag{5}$$

The broaching probability can be roughly estimated as the ratio of the number of the events satisfying the above judging criterion to the number of zero-crossing wave cycle at the centre of gravity. If zero crossing wave cycle involves two events or more, it was regarded as one event per wave cycle. The calculated results are shown in Fig. 9. Since broaching is a nonlinear phenomenon, the broaching probabilities estimated from different realisations scatter to some extent. The ensemble average of them is about 0.28. This means that broaching can occur once every three wave encounters. The confidence interval of this estimate can be evaluated with the formula of binomial distribution (Paroka and Umeda, 2006) and its evaluation will be our future task. The confidence interval, however, is obviously small because the number of the wave cycle is very large and the estimated probability is sufficiently high.

THEORY FOR ESTIMATING BROACHING PROBABILITY

It is desirable to estimate the broaching probability in irregular waves with a given deterministic threshold of broaching in regular waves, which can be calculated by numerical simulations in time domain or a global bifurcation theory. This, considering that broaching occurs within one or two waves, the authors attempted to develop a theory for estimating broaching probability. First, the deterministic threshold of broaching in regular waves, *S*, are estimated as a function of wave height, *H*, and the wave period, *T*. Then, based on Longuet-Higgins's theory (Longuest-Higgins, 1983) under the assumption of narrow-banded wave, a joint probability of local wave height and local wave period can be calculated as follows:

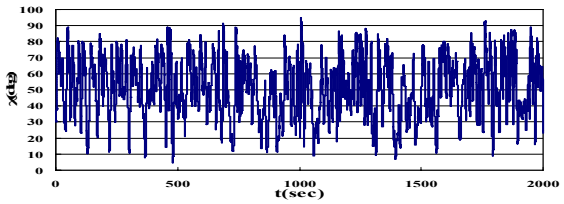

Fig. 6: heading angle from wave direction in a numerical experiment

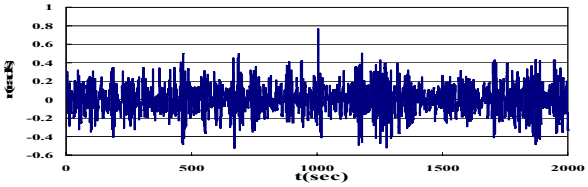

Fig. 7: yaw angular velocity in a numerical experiment

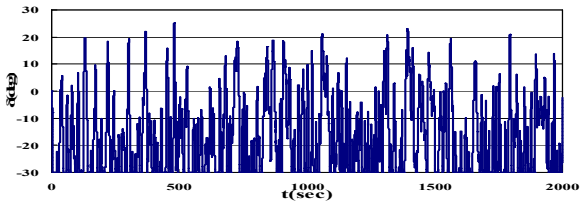

Fig: 8 rudder angle in a numerical experiment

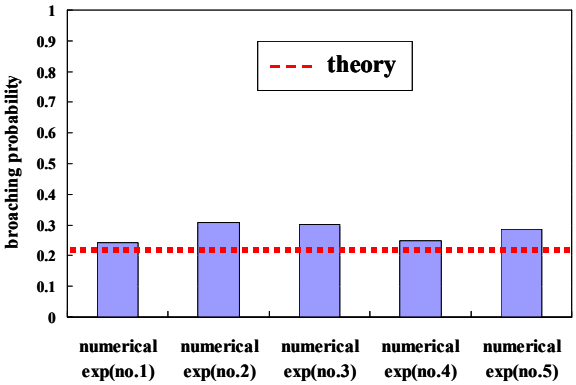

Fig.: 9 comparison in broaching probability between numerical experiments and theory with $H_{1/3}$=1.25 m and T_{01}=2.392s

$$p(H,T)=\frac{2\times(1.414)^3(H/H_{1/3})^2}{\sqrt{\pi}\nu}\exp\left\{-1.414^2\left(\frac{H}{H_{1/3}}\right)^2\left[1+\frac{(T/T_{01}-1)^2}{\nu^2}\right]\right\} \quad (6)$$

Here ν is a parameter for band width and ν is 0.4256 for the Pierson-Moskowitz type wave spectrum such as the ITTC one. Finally, if we assume that the occurrence of broaching does not depend on an initial condition, the broaching probability per wave encounter, P, can be calculated as follows:

$$P=\iint_{S(H,T)} p(H,T)\frac{1}{H_{1/3}T_{01}}dHdT \quad (7)$$

If we take the effect of initial condition on the occurrence of broaching, we may follow the methodology used by Umeda (1990) for surf-riding.

The numerical results using Eq. (7) were 0.211 under the condition used for the numerical experiment. This theoretical value is slightly below the values from the numerical experiments, as shown in Fig. 8. Since this theory efficiently estimates broaching probability, it is useful for discussing the relationship among broaching, wave condition, rudder area and so on. This theory is also promising as a tool for providing design and operational criteria as a part of new performance-based criteria for broaching.

CONCLUSIONS

The following conclusions were drawn based on this work.

1) The authors firstly extended their numerical simulation model for regular waves to irregular waves, and validated it with the existing full scale data in irregular waves.
2) We numerically evaluated the probability of broaching by using the extended model together with a judging criterion of broaching.
3) A theory for calculating broaching probability was developed with given deterministic thresholds of broaching in regular waves. And it was confirmed that the theoretically predicted values of broaching probability well agree with those from the numerical simulation.

4) The methodology proposed here is expected to be utilised for the performance-based intact stability criteria discussed at the IMO.

ACKNOWLEDMENTS

This research was supported by a Grant-in Aid for Scientific Research of the Japan Society for promotion of Science (No. 18360415). It was partly carried out as a research activity of SPL project of Japan Ship Technology Research Association in the fiscal year of 2006, funded by the Nippon Foundation. The authors express their sincere gratitude to the above organizations.

REFERENCES

Du Cane, P. and G.J. Goodrich, The following Sea, Broaching and Surging, Transaction of the Royal Institution of Naval Architects, vol. 104, pp. 109-140, 1962.

Fuwa, T., Sugai K., Yoshino, T. Yamamoto, T.: An Experimental Study on Broaching of a Small High Speed Craft, Papers of Ship Research Institute, No. 66, pp. 1-40, 1982.

Longuet-Higgins, M.S.: On the Joint Distribution of Wave Periods and Amplitudes in a Random Wave Field, Proceedings of the Royal Society of London, Series A, 389, pp. 241-258, 1983.

Motora, S., Fujino, M., Fuwa, T.: On the Mechanism of Broaching-to Phenomena, Proceedings of the 2nd International Conference on Stability of Ships and Ocean Vehicles, Society of Naval Architects of Japan (Tokyo), pp. 535- 550, 1982.

Paroka, D. and N. Umeda: Capsizing Probability Prediction for a Large Passenger Ship in Irregular Beam Wind and Waves: Comparison of Analytical and Numerical Methods, Journal of Ship Research, 50, pp. 371-377, 2006.

Rutgersson, O. and Ottosson, P., Model Tests and Computer Simulations – An Effective Combination for Investigation of Broaching Phenomena, Transaction of the Society of Naval Architects and Marine Engineers, Vol. 95, pp. 263-281 1987.

Umeda, N.: Probabilistic Study on Surf-riding of a Ship in Irregular Following Seas, Proceedings of the 4th International Conference on Stability of Ships and Ocean Vehicle, Naples, Sept., pp.336-343, 1990.

Umeda, N. and M.R. Renilson : Wave Forces on a Ship Running in Quartering Seas - A Simplified Calculation Method -, Proceedings of the 11th Australian Fluid Mechanics Conference, Hobar, pp.363-366t, 1992a.

Umeda, N. and M.R. Renilson : Broaching - A Dynamic Analysis of Yaw Behaviour of a Vessel in a Following Sea, in Manoeuvring and Control of Marine Craft (Wilson,P.A. eds.), Computational Mechanics Publications (Southampton), pp.533-543, 1992b.

Umeda, N., A. Matsuda and M. Takagi: Model Experiment on Anti-Broaching Steering System, Journal of the Society of Naval Architects of Japan, 185, May, pp.41-48, 1999.

Umeda, N. and Hashimoto, H.: Recent Developments of Capsizing Prediction Techniques of Intact Ships Running in Waves, Proceedings of the 26th Symposium on Naval Hydrodynamics, Rome, 2006.

Umeda, N., Hori, M., Hashimoto, H.: Theoretical Prediction of Broaching in the Light of Local and Global Bifurcation Analysis, Proceedings of the 9th International Conference on Stability of Ships and Ocean Vehicles, Rio de Janeiro, 2006.

NOMENCLATURE

g	gravitational acceleration
GZ	righting arm
H	local wave height
I_{xx}	moment of inertia around the x-axis
I_{zz}	moment of inertia around the z-axis
J_{xx}	added moment of inertia around the x-axis
J_{zz}	added moment of inertia around the x-axis
k	wave number
K_p	derivative of roll moment with respect to roll rate
K_r	derivative of roll moment with respect to yaw rate
K_v	derivative of roll moment with respect to sway velocity
K_w	wave-induced roll moment
K_ϕ	derivative of roll moment with respect to heel angle
K_δ	derivative of roll moment with respect to rudder angle
m	ship mass
m_x	added mass in the x direction
m_y	added mass in the y direction
n	propeller revolution number
N_v	derivative of yaw moment with respect to sway velocity
N_r	derivative of yaw moment with respect to yaw rate
N_w	wave-induced yaw moment
N_ϕ	derivative of yaw moment with respect to heel angle
N_δ	derivative of yaw moment with respect to rudder angle
p	roll angular velocity
r	yaw angular velocity
R	ship resistance
T	wave period
T_P	propeller thrust
u	ship speed in the x direction
v	ship speed in the y direction
X_w	wave-induced surge force
Yr	derivative of sway force with respect to yaw rate
Y_v	derivative of sway force with respect to sway velocity
Y_δ	derivative of sway force with respect to rudder angle
Y_ϕ	derivative of yaw moment with respect to heel angle
Y_w	wave-induced sway force
z_H	height of centre of sway force due to lateral motions
α	propagation angle of element wave
δ	rudder angle
δ_{max}	limit of rudder angle
ρ	water density
ϕ	roll angle
χ	heading angle from the wave direction
ω	frequency of element wave

Non-linear Hydrodynamic Force Measurement System in Heavy Seas for Broaching Prediction

Akihiko, Matsuda,

National Research Institute of Fisheries Engineering, Japan

Hirotada, Hashimoto,

Osaka University, Japan

Tsutomu, Momoki,

National Research Institute of Fisheries Engineering, Japan

ABSTRACT

Mathematical models for capsizing prediction due to broaching have been developed by several researchers. However prediction accuracy of these models still remains in qualitative. In the previous research, the effect of heel-induced hydrodynamic forces in severe following waves with large heel angles up to 50 degrees was examined by captive model experiment for realizing quantitative prediction. However the previous measurement system, which fixes 6 degrees of freedom of ship model, requires many extra runs to obtain the correction coefficients of heave and pitch. Therefore we try to develop new measurement system, which fixes 4 degrees of freedom but allows heave and pitch motions to be free. Firstly, the comparison of measured results between ordinary towing and measurement system and the new system was conducted. Then nonlinear heel-dependent hydrodynamic forces and directly measured wave-exciting forces were measured in severe following and quartering seas.

KEYWORDS

New Measurement System, Heel-Induced Hydrodynamic Force, Wave-Exciting Force, Large heel angle, Heavy Seas, Broaching Prediction

INTRODUCTION

Nowadays, theoretical prediction of extreme motions in following and quartering seas is required not only for qualitative purposes but also for quantitative one towards direct stability assessment as an alternative route of IMO IS Code. The mathematical model for capsizing due to broaching, which is one of the great threats to ships running in following and quartering seas, has been developed by several researchers. However, prediction accuracy of these models is not in quantitative but in qualitative even now.

Although hydrodynamic forces in heeled condition in heavy seas could be important for broaching prediction, these effects had not been examined not only theoretically but also experimentally. For realizing quantitative prediction of capsizing due to broaching, the effect of nonlinear heel-induced hydrodynamic forces in severe following waves with the various heel angles up to 50 degrees was examined by the authors (Hashimoto et al., 2004) (Hashimoto et al., 2004). As a result, the nonlinear heel-induced hydrodynamic forces with respect to heel angle both in calm water and waves were reported and their effect on the numerical result was examined. However the

previous system, which fixes 6 degrees of freedom of ship model, requires many extra runs to obtain the correction coefficients of heave and pitch because exact running attitude in heavy seas with high forward speed cannot be estimated accurately, and the effect of the difference of running attitude on the measured result is significant.

Therefore we try to develop a new measurement system, which fixes 4 degrees of freedom but allows pitch and heave motions to be free as the more practical system.

NEW MEASUREMENT SYSTEM

Although the importance of heel-induced hydrodynamic forces on broaching prediction was pointed out (Renilson et al, 2000), it is difficult to do the model test in large heeled and severe wave conditions. Therefore, we developed a new measurement system to realise the measurement of heel-induced hydrodynamic forces even in severe waves with large heel angle. This system restricts surge, sway, yaw and roll but heave and pitch are in free. Photograph of the experimental setup is shown in Fig. 1.

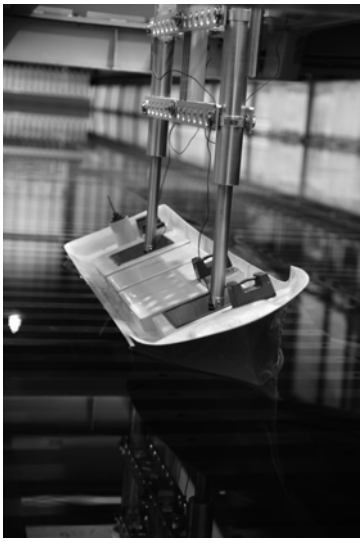

Fig. 1: New measurement system.

In this system, ship model is towed by two heaving rods. Heave and pitch motions are free and their values are measured by two potentiometers, respectively. Aft-rod can move in longitudinal to escape from the geometrical restriction due to large pitch motion. Surge and sway forces and yaw and roll moment are measured by a dynamometer located at the top of this system and above the centre of ship gravity.

EXPERIMENTAL RESULTS

The ship model used in this research is 1/25 scaled Japanese purse SEINER. Principal particulars are shown in Table 1.

Table 1 Principal particulars of the subject ship

Items	Values
length between perpendiculars: L_{pp}	34.5 m
breadth : B	7.60 m
depth : D	3.07 m
mean draught : d	2.65 m
block coefficient : C_b	0.597

Firstly practical resistance test with the new system was conducted with 0 degrees of heel. The measured sinkage, trim and resistance in calm water are shown in Figs. 2-3. In the figures, previous results with ordinary towing system, in which ship model is towed by a heaving road and pitch motion is in free with gimbals, are also shown. These figures indicate that there is small difference in sinkage and trim between the new and ordinary systems. This might be because the height of towing point is different. Measured resistance with 0 degrees of heel agrees well with existing results with an ordinary system. By utilising this new system, the resistance with large heel angles can be easily measured with no difficulty.

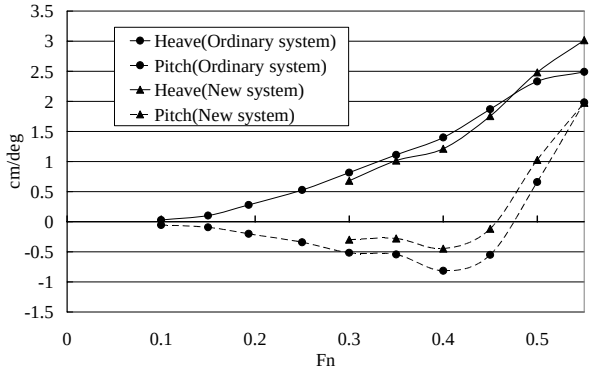

Fig. 2: Measured sinkage and trim in calm water.

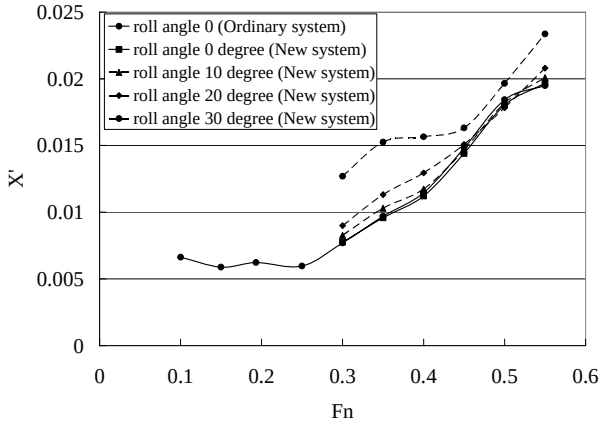

Fig. 3: Measured resistance with heel angles in calm water.

The experimental results of vertical motions in pure following seas are shown in Figs. 4-5, and the wave-exciting forces with 30 degrees of heel angle in quartering seas are shown in Figs. 5-6. Here wave length to ship length ratio, λ/L, is 1.5 and wave steepness, H/λ, is 1/10. These figures show that the new measurement system can measure surge and sway forces and yaw and roll moments even in severe quartering seas with large heel angle. These data could be useful for the validation of numerical codes for capsizing or large amplitude motion prediction.

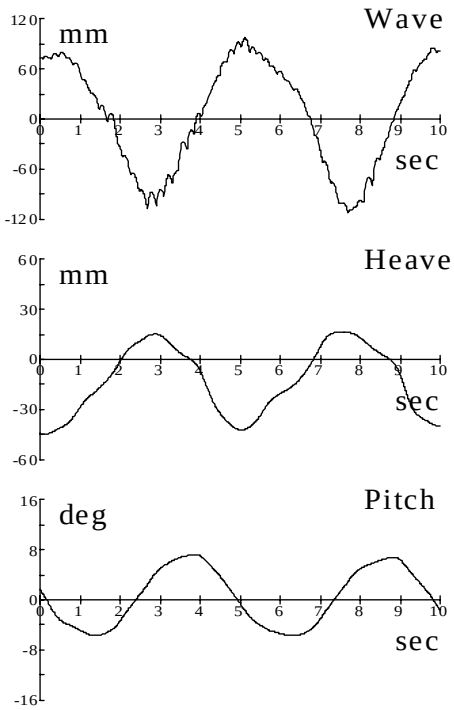

Fig. 4: Measured vertical motions and wave height with Fn=0.4, χ=0degrees, ϕ=0degrees

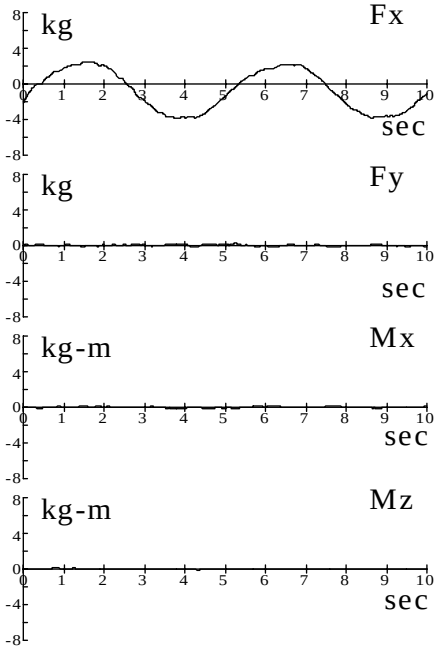

Fig. 5: Measured forces and moments with Fn=0.4, χ=0degrees, ϕ=0degrees

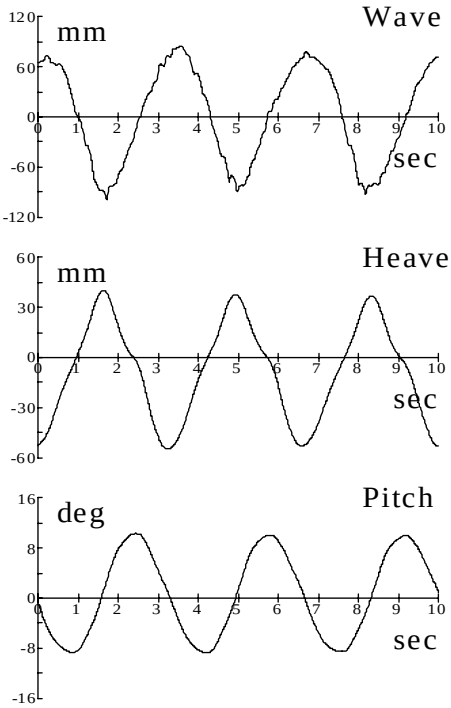

Fig. 6: Measured vertical motions and wave height with Fn=0.4, χ=30degrees, ϕ=30degrees

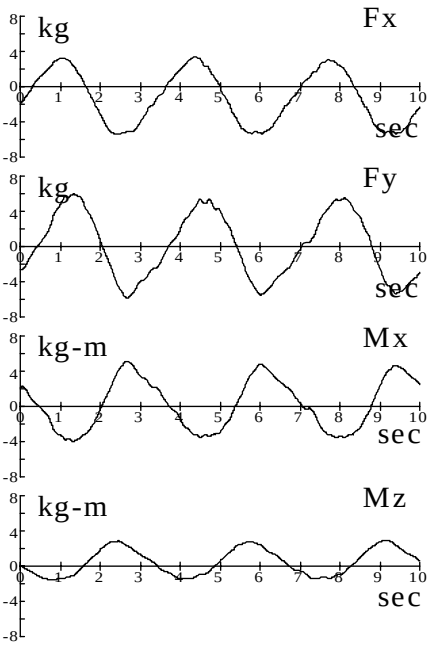

Fig. 7: Measured forces and moments with Fn=0.4, χ=30degrees, ϕ=30degrees

HEEL-INDUCED HYDRODYNAMIC FORCES AND MOMENTS WITH LRAGE HEEL ANGLE

Measured heel-induced hydrodynamic forces in calm water with the heel angles up to 30 degrees are show in Fig. 8. These forces are essential for quantitative broaching prediction. (Umeda and Hashimoto, 2007) Sway force has the linear relationship with heel angle. The nonlinearity of surge force, roll moment and yaw moment can be found particularly beyond 20 degrees of heel. This is because there is significant amount of water inflow into deck in that condition.

One example of roll moment variation with 30 degrees of heel in pure following seas is shown in Fig. 9. Here wave length to ship length ratio is 1.5. From the experimental result, roll moment increases as wave steepness increases around a wave crest, but it does not decrease around a wave trough. In high wave steepness, measured roll moment is not sinusoidal with encounter frequency.

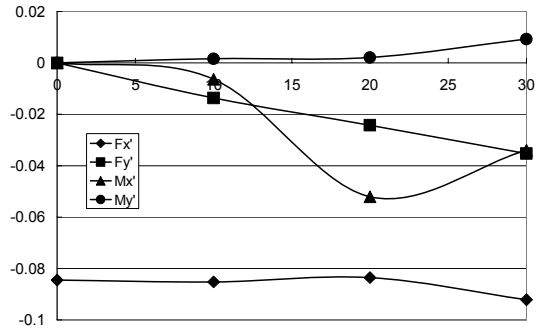

Fig. 8: Heel-induced hydrodynamic forces in calm water at Fn=0.4

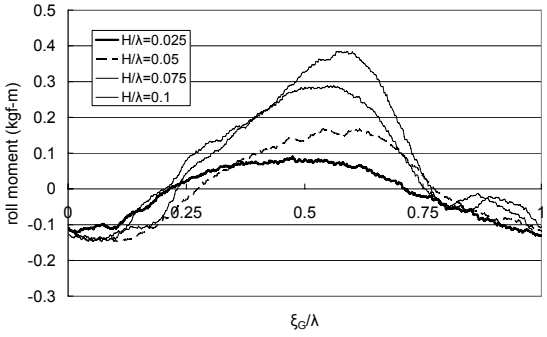

Fig. 9: Roll moment in following seas with 30 degrees of heel at Fn=0.4

CONCLUSIONS

Heel-induced hydrodynamic forces and wave-exciting forces in heavy seas were measured by the new measurement system. As a result, the following conclusions can be obtained:

1. The proposed new measurement system is applicable to measure non-linear hydrodynamic forces and moments with large heel angle even in severe following and quartering seas.
2. Heel-induced hydrodynamic surge force, roll moment and yaw moment in calm water have nonlinearity with respect to roll angle particularly beyond 20 degrees of heel angle.
3. Heel-induced roll moment in severe following seas was measured, and the characteristic of its variation was clarified.

Numerical simulation using measured non-linear heel-induced hydrodynamic forces and moments is planed to the next step.

ACKNOWLEDMENTS

This research was supported by a Grant-in Aid for Scientific Research of the Ministry of Education, Culture, Sports, Science and Technology of Japan (No. 18360426) and a Fundamental Research Developing Association for Shipbuilding and Offshore of the Shipbuilders' Association of Japan.

REFERENCES

Hashimoto, H., Umeda, N. and Matsuda, A. "Importance of Several Nonlinear Factors on Broaching Prediction" Journal of Marine Science and Technology, 9:2: 80-93, 2004

Hashimoto, H., Umeda, N. and Matsuda, A. "Broaching Prediction with Nonlinear Heel-Induced Hydrodynamic Forces Taken into Account", Proceedings of the 8th International Conference on Stability of Ships and Ocean Vehicles, pp.571-581, 2003

Renilson, M.R. and Manwarring, T. "An Investigation into Roll/Yaw Coupling and Its Effect on Vessel Motions in Following and Quartering Seas" Proceedings of the 7th International Conference on Stability and Ocean Vehicles, 452-459, 2000

Umeda, N. and Hashimoto, H. "Recent developments of capsizing prediction techniques of intact ships running in waves" 26th Symposium on Naval Hydrodynamics, 20

Using Full-Scale Capsizing Accidents for the Validation of Numerical Seakeeping Simulations

Florian Kluwe

Hamburg University of Technology (TUHH)

Stefan Krüger

Hamburg University of Technology (TUHH)

ABSTRACT

It has become obvious that modern ships suffer from problems related to their seakeeping-behaviour, which is mainly related to large amplitude roll motion in head and following seas. A state-of-the-art tool to address the phenomena connected to these stability accidents are numerical seakeeping simulations. The present document analyses a number of real capsizing accidents, which are related to poor stability in rough weather, showing that numerical simulations are suitable to identify safe and un-safe conditions clearly for specific ships. For this purpose various criteria assessing the intact stability of ships are applied, including a new one, which was developed at Hamburg University of Technology in the recent years.

KEYWORDS

Ship safety; parametric rolling; intact stability; capsizing; stability criteria; seakeeping performance;

INTRODUCTION

The last years have seen several intact-stability-accidents of ships, ranging from the loss of several containers to the total loss of the whole vessel due to capsizing. The causes often appeared to be related to poor seakeeping behaviour resulting in large amplitude roll motion. This generates the need for improved methods and tools, capable of predicting the seakeeping behaviour of ships sufficiently accurate in order to identify potential risks.

Numerical seakeeping simulations in the time domain are state-of-the-art tools to address the above mentioned needs. Hamburg University of Technology (TUHH) uses the code E4-ROLLS, which has been extensively validated by model tests within several BMBF (German Federal Ministry of Education and Research) founded projects. However, the possibilities in a towing tank are limited, for example due to the tank geometry (long crested waves only) and the limited duration of the test runs.

Therefore TUHH additionally follows a second, different approach to validate its seakeeping simulations. The bases for this methodology are real, full-scale accidents. A characteristic set of such accidents, all of them closely connected with the occurrence of large heeling angles in intact conditions, has been investigated for this purpose, including relevant effects such as cargo shift, extra heeling moments and water ingress.

The main aim of this analysis is to show whether the simulation code is capable to address the relevant hazards which lead to the above mentioned accident scenarios.

In the second stage of our investigations the intact stability of the ships was assessed in order to evaluate our new approach for an intact stability criterion, the Insufficient Stability Event Index (ISEI).

THE E4-ROLLS SIMULATION TOOL

The simulation code E4-ROLLS, based on the code developed by Kroeger (1987) and Petey (1988), was chosen to serve as basis for the evaluation of seakeeping related problems.. The code was validated and further enhanced by Cramer and Krueger (2005). The code considers all six degrees of freedom, whereas only two of them are treated non-linearly. Namely these are the roll motion and surge. All others are calculated by transfer functions, which make the code extremely fast. This enables us to calculate relatively long time series for a vast number of variations. The roll motion is simulated using equation (1].

$$\ddot{\varphi} = \left\{ \begin{array}{l} \sum M_{wind} + M_{sy} + M_{wave} + M_{Tank} - M_d - \\ m(g - \ddot{\zeta})h_s - I_{xz}\left[\left(\ddot{\vartheta} + \vartheta\dot{\varphi}^2\right)\sin\varphi - \left(\ddot{\psi} + \psi\dot{\varphi}^2\right)\cos\varphi\right] \end{array} \right\} / \quad (1)$$
$$I_{xx} - I_{xz}\left(\psi\sin\varphi + \vartheta\cos\varphi\right)$$

with

M_{wind}	Moment due to wind
M_{sy}	Moment due to sway and yaw motion
M_{wave}	Moments from radiation, diffraction and Froude-Krylow forces
M_{Tank}	Fluid shifting moment
M_d	Non-linear damping moment
φ, ϑ, ψ	Roll, pitch and yaw angle
m	Ship's mass
$\ddot{\zeta}$	Heave acceleration
h_s	Righting lever
I_{xx}, I_{xz}	Roll moment of inertia and mixed part

The current righting levers are determined by applying Grim's equivalent-wave concept as modified by Soeding (1982). This approach replaces the exact wave contour along the ship's hull by a simplified wave profile, which delivers similar righting levers as the exact solution. The coefficients of the equivalent wave are determined using a least squares approach.

Leaks and tanks can be taken into account as well for more detailed investigations. For this method the geometry of the respective tanks needs to be modelled. Once the geometry is known, the fluid movement within the tank can be calculated, using either a deep-water model or a shallow-water model depending on the tank's eigenfrequency. The deep-water model treats the water as a point mass concentrated in its current centre of gravity, assuming that the water surface is always an even plane. The shallow-water water model is implemented according to Petey (1985) .

THE INSUFFICIENT STABILITY EVENT INDEX (ISEI)

In the last years Hamburg University of Technology has developed a new probabilistic method, assessing the intact stability of ships in heavy seas. The methodology is based on the assessment of ship motions in heavy seas calculated by means of numerical seakeeping simulations in the time domain. All simulations are carried out in irregular, short crested waves, where the energy distribution is based on JONSWAP spectra.

In contradiction to existing criteria, it was decided to assess all possible scenarios that may lead to a dangerous situation with appropriate resolution. The new concept distinguishes between a ship being safe(0) or unsafe(1) in a specific operating condition, but it does not take into consideration the calculated up-crossing rates. This procedure was chosen due to two reasons: First it is relatively difficult to calculate up-crossing rates with sufficient reliability as extrapolation methods suffer from relatively large scatter and therefore are not well suited to serve as basis for a minimum stability requirement. Secondly real capsizing events are usually the result of very complex event chains which can not be taken fully into consideration for an intact stability criterion. Thus counting up-crossing rates would feign a precision of the criterion which is not met in reality.

Given an methodology, which is able to distinguish clearly between safe and unsafe conditions the total probability for a dangerous situation happening can be quantified by the insufficient stability event index (ISEI), which is defined by the following equation (see also Krueger and Kluwe (2006)):

$$ISEI = \int_{T_1=0}^{\infty} \int_{H_{1/3}=0}^{\infty} \int_{\mu=0}^{2\pi} \int_{v_s=v_{\min}}^{v_{\max}} p_{sea}(H_{1/3}, T_1) \cdot p_{dang}(H_{1/3}, T_1, \mu, v_s)\, dv_s\, d\mu\, dH_{1/3}\, dT_1 \quad (2)$$

Here p_{sea} denotes the probability of occurrence of a specific seastate defined by the significant wave height $H_{1/3}$ and the characteristic (peak) period T_1, whereas p_{dang} represents the probability for the actual loading condition leading to a dangerous situation under the condition of a specific seastate. The two-dimensional probability density function for the seastate is calculated from a scatter table presented by Soeding (2001). The failure probability p_{dang} is governed by the following relationship:

$$p_{dang}(H_{1/3}, T_1, \mu, v_s) = p_{fail}(H_{1/3}, T_1, \mu, v_s) \cdot p_{\mu}(\mu) \cdot p_v(v_s | H_{1/3}, T_1, \mu) \quad (3)$$

In this equation, $p_{\mu}(\mu)$ denotes the probability the ship is travelling at a course of μ-degrees relative to the dominating wave propagation. It is assumed that $p_{\mu}(\mu)$ is independent from the actual values of $H_{1/3}$ and T_1. $p_{\mu}(\mu)$ can be taken from full scale observations (see Krueger, Hinrichs, Kluwe and Billerbeck (2006)). Then $p_v(v_s | H_{1/3}, T_1, \mu)$ denotes the conditional probability that the ship is travelling at a speed of v_s knots. Not all speeds are physically possible in a specific situation. Krueger, Hinrichs, Kluwe and Billerbeck (2006) determine the maximum possible ship speed in the given environmental conditions at full engine output and the minimum speed at engine idle speed from systematic propulsion calculations. Within the range of possible speeds $[v_{min}, v_{max}]$ the probability of occurrence is assumed equally distributed as more accurate data are lacking.

The failure probability $p_{fail}(H_{1/3}, T_1, \mu, v_s)$ is determined from the time series of the numerical simulation by applying the Blume-criterion. In cases where the Blume-criterion does not deliver suitable results, typically due to large angles of vanishing stability, the occurrence of a certain maximum roll angle (e.g. 50°) may be taken into account simultaneously. The Blume criterion considers a ship as save if the following condition is met:

$$\overline{E}_R - 3s > 0 \quad (4)$$

Here $\overline{E}_R$ denotes the residual area below the lever arm curve, integrated from the largest roll angle observed during one simulation up to the point of vanishing stability, averaged over all runs. The symbol s represents the standard deviation of $\overline{E}_R$. Given the loading condition fulfills the Blume-Criterion in the actual situation, $p_{fail}(H_{1/3}, T_1, \mu, v_s)$ is set to 0, otherwise it is set to 1.

The criterion is aimed to prevent large roll amplitudes related to periodic stability variations in waves. Therefore our method explicitly treats head sea and following sea cases only, and therefore we restrict the contributing courses to a 45-degree sector of encounter angles, port and starboard in head and following seas. Consequently, it is then useful to split the ISEI in a head sea and a following sea index. The criterion in practice is calculated for a discrete number of operating conditions, leading to the following formulation of the criterion:

$$ISEI = ISEI_{following} + ISEI_{head} = \sum_{f,h} \left\{ \sum_{i=1}^{N_{T_1}} \sum_{j=j_{Bl}}^{N_{H_{1/3}}} \sum_{k=1}^{N_{\mu}} \sum_{l=1}^{N_v} \begin{pmatrix} p_{sea}(H_{1/3}(j), T_1(i)) \cdot \\ p_{\mu}(\mu(k)) \cdot \\ p_v(v(l) | H_{1/3}(j), T_1(i), \mu(k)) \end{pmatrix} \right\} \quad (5)$$

In the formula, the summation on the limiting wave heights starts at j_{Bl}, which is the smallest significant wave height for the given significant period T_1 where p_{fail} equals 1.

INVESTIGATION OF REAL CAPSIZE ACCIDENTS

TUHH currently analyses real capsizing accidents for two main purposes: First it is a second method, besides the model tests, to validate our numerical code by reconstruction of the environmental conditions during the accident. Secondly the accidents clearly define ships in “un-safe” conditions, which help us to define threshold values for the ISEI-concept.

The ships are each simulated with two different load cases: One representing the conditions during the accident and a second one assumed

to represent a safe condition. Simulations are carried out for both conditions. The resulting ISEI's are calculated demonstrating whether the new concept is able to distinguish between safe and un-safe loading conditions.

Besides the ISEI also other stability criteria were calculated for comparison. As it is not possible to present all of them within the frame of this paper we refer to the original literature.

The Capsizing of SS Fidamus (1950)

On January 31st, 1950, the 743 BRT vessel SS Fidamus capsized in heavy weather bound

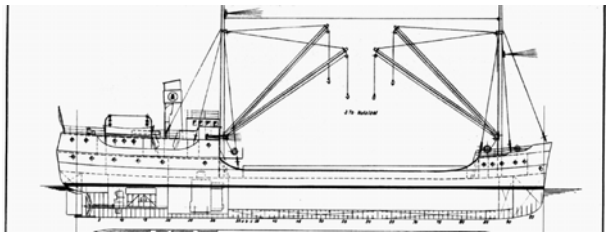

Fig.1: General Arrangement of SS Fidamus

from Wismar to Antwerp close to Langeoog, 54° N, 7° E. The vessel was loaded with ca. 900t potash (angle of repose ca. 35 Deg.). The vessel was travelling in following seas of ca. 40 m significant wave-length, $H_{1/3}$ was ca. 2.0 m and the vessel's speed was ca. 9.5 knots. The vessel suddenly heeled to more than 30 degrees and remained there with a steady list of ca. 35 to 40 degrees. Water ingress then lead to capsizing within 10 minutes according to Seeamt Bremerhaven (1950).

The floating condition prior to the accident could be reconstructed approximately as follows: The ship had a total displacement of ca. 1541 tons, resulting in a draft of 4.69m at the aft perpendicular (a.p.). The trim was 1.12m by stern. Interestingly enough the ship did not carry any ballast water, although this was strongly recommended in the stability booklet. The resulting righting levers are shown in Fig.2. The initial GM in still water conditions amounts ca. 0.30 m. Based on these lever arm curves we can conclude that, without any external heeling moment, the vessel would immediately heel to about 30 Degree if it stays long enough on the wave crest.

In an expertise made on behalf of Seeamt Bremerhaven, Kempf (1950) concluded that the vessel was travelling in a 1:1 following sea resonance, where the rolling period of the vessel (for small angles) was determined to 11.8 s by Kempf at an encounter period of 11.1s.

The numerical simulations, carried out with E4-ROLLS show that the vessel is permanently

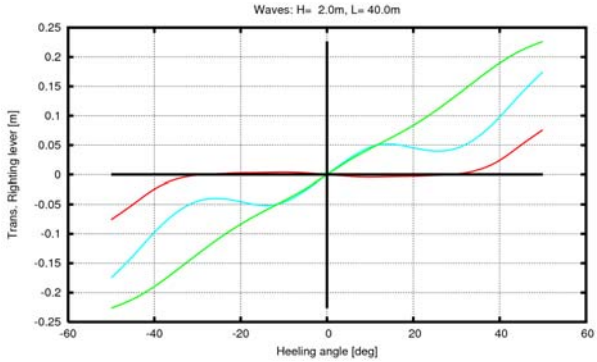

Fig.2: Lever arm curves for SS Fidamus
(cyan: still water, green: wave trough, red: wave crest)

rolling with a maximum angle of ca. 45 degree. As the static angle of vanishing stability in

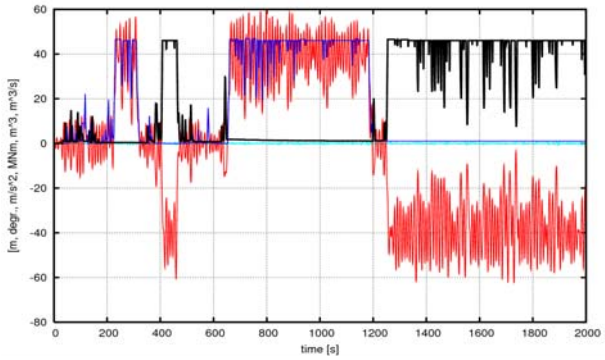

Fig.3: Simulated time series of SS Fidamus including entrapped water (blue: starboard side, black: port side). The red curve shows the roll angle (positive starboard)

still-water conditions is beyond 90 degree, it is theoretically not possible to capsize the vessel without any additional heeling moment. For the dynamically rolling vessel, additional water ingress is not necessary for the final capsizing. Another important aspect discussed already during the original investigations is, that a significant amount of water is entrapped between hatchway coaming and bulwark, which produces a sufficient heeling moment to keep the

ship at a steady list at around 40 degrees, as the time series in Fig.3 demonstrates clearly.

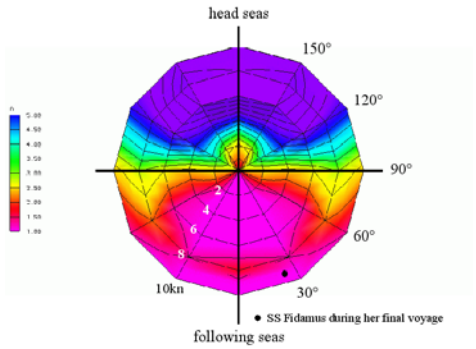

Fig.4: Polar diagram showing limiting wave heights with respect to a maximum roll angle of 40 degree. Significant wave length is 40 m

For nearly all situations the ship is travelling in following seas large heeling angles beyond 40° can be observed, as shown in Fig.4. It can be shown that the water between hatchway coaming and bulwark is sufficient to cause the final capsizing of the vessel.

Table 1: Results for different criteria in "safe" and "unsafe" loading condition for SS Fidamus

Criterion	GM=0.30 m	GM=0.50 m
Kastner/Roden Capsizing time [s]	487	2386618
Soeding Capsize Probability	0.25/Roll Cycle	0.1 - 0.7E-6 /year
Blume (Modified) E_R - 3 S	E_R = S = 0	1.772 mmRad
ISEI (direct)	0.20078	0.0008
Empirical Criteria		
Crest lever	< 0.05	> 0.05
Crest range	< 16 Deg	> 16 Deg.
Blume c- factor	none fulfilled	all fulfilled

Comparing the results for different intact stability criteria as presented in Table 1, it can clearly be seen that all criteria consider the case where the vessel did actually capsize as dangerous, whereas all criteria consider the 0.50m GM case as determined by the Kastner-Roden-criterion as clearly save. Additionally, it can be stated that a direct ISEI of 0.2 represents a condition, which has clearly proven to be unsafe, whereas an ISEI of 0.0008 represents a condition considered to be safe by all other criteria.

The Capsizing of MV Lohengrin (1963)

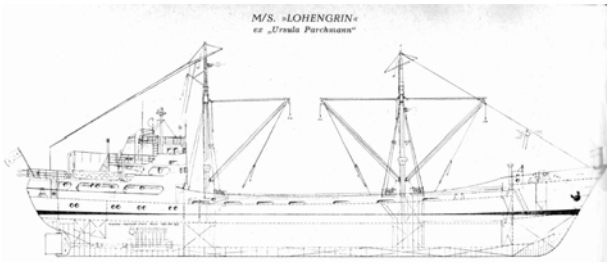

Fig.5: General Arrangement of MV Lohengrin (taken from Die deutsche Handelsflotte (1963))

On January 14th, 1950 the 955 BRT vessel MV Lohengrin capsized in heavy weather bound from Iggesund/Sweden to Kiel. The vessel was loaded with ca. 1195 t cellulose in bales. Half a year before the accident, the vessel was converted, which resulted in higher hatch coamings and an increased VCG of the cargo hold volume. Based on the information obtained from the Seeamt Flensburg (1964) the most probable floating condition at the time of the accident shows a draft of 4.69m at a.p. with a total displacement of ca. 2000 tons and an initial GM of 0.13 m. The resulting lever arm curves are shown in Fig.6. At the day of the accident the vessel entered the Kiel Fjord at about 14.00 hrs. The waves encountered the vessel from abaft. Significant wave period was ca. 6 seconds, the wave height was reported to be about 2 metres. At about 14.15 hrs the vessel heeled to 40-45 degree starboard side and remained there with a steady list of the same size. The ship finally capsized and sank ca. 1.5 hrs later.

Table 2: Results for different criteria in "safe" and "unsafe" loading condition for MV Lohengrin

Criterion	GM=0.131 m	GM=0.305 m
Kastner/Roden Capsizing time [s]	6024	-
Soeding Capsize Probability	-	0.4E-7/year
Blume (Modified) E_R - 3 S	-3.509 mmRad	51.9 mmRad
ISEI (direct)	0.18911	0.002
Empirical Criteria		
Crest lever	< 0.05	> 0.05
Crest range	< 16 Deg	> 16 Deg.
Blume c- factor	none fulfilled	all fulfilled

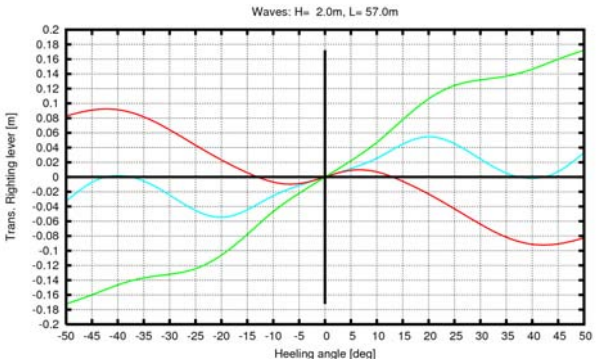

Fig.6: Lever arm curves for MV Lohengrin
(cyan: Stillwater, green: wave trough, red: wave crest)

The numerical simulations clearly show that the reason for the loss of MV Lohengrin can be consistently explained by insufficient stability and a pure loss on the crest situation. The stability at the time of the accident was even be low the recommended Rahola-criteria. As the deckhouse was weathertight the vessel could find an intermediate equilibrium while resting on the superstructures. This intermediate equilibrium is possible only if an additional heeling moment acts on the ship, for example due to cargo shift. Our investigations show that a shift of TCG of the cargo by 4cm would be enough to keep the vessel in the listed position. In general, in the given loading condition the vessel was theoretically unsafe in all following sea situations.

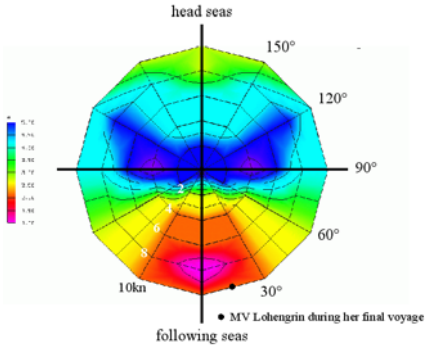

Fig.7: Polar diagram showing limiting wave heights with respect to the Blume-criterion. Significant wave length is 60 m

Again, comparing all criteria, the results are unique. All criteria consider the case where the vessel did actually capsize as dangerous. For the GM-value of 0.305m, which was selected from the simulations in artificially amplified waves, all criteria consider this case as safe.

Additionally, it can be stated that a direct ISEI of 0.189 represents a condition, which has clearly proven to be unsafe, whereas an ISEI of 0.002 represents a condition, which is considered to be safe by all criteria.

The Capsizing of SS Irene Oldendorff (1951)

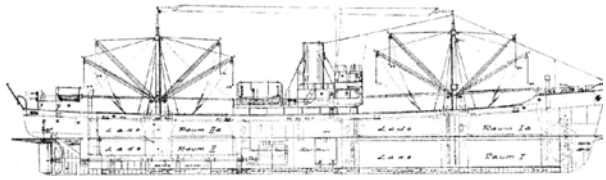

Fig.8: Side view of SS Irene Oldendorff

On December 31st, 1951, the vessel SS Irene Oldendorff capsized in heavy weather bound from Emden to Ystad in the Hubert Gat. The vessel was carrying ca. 2750 tons of coke, of which ca. 440 t has been carried on deck. The last known position of the vessel was close to buoy J/E 1 in the Hubert Gat. According to our findings based on data of the Seeamt Bremerhaven (1952) the vessel had a draft of 5.4 m a.p., trimmed 0.108 m by head at the beginning of the voyage (Emden Lock). This equals a displacement of 4575t.

Table 3: Results for different criteria in "safe" and "unsafe" loading condition for SS Irene Oldendorff

Criterion	**GM=0.14 m**	**GM=0.39 m**
Kastner/Roden Capsizing time [s]	13800	No capsize found
Soeding Capsize Probability	-	0.3E-6 for h>9m none for h<9m
Blume (Modified) E_R - 3 S	-64.0 mmRad	181.5 mmRad
ISEI (direct)	0.158	0.0011
Empirical Criteria		
Crest lever	0.008 < 0.05	> 0.05
Crest range	10 < 16 Deg	> 16 Deg.
Blume c- factor	none fulfilled	all fulfilled

The simulation-based analysis shows that the reason for the loss of SS Irene Oldendorff can be consistently explained as an intact stability accident due to the loss of stability in extreme weather conditions. The loss of stability in the particular situation can be clearly related to wa-

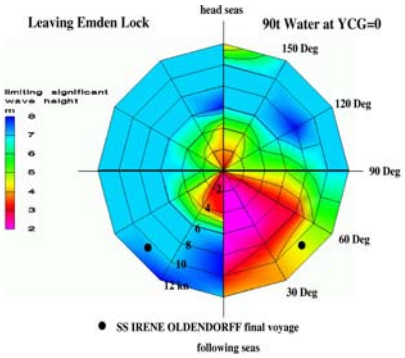

Fig.9: Polar Diagram showing limiting wave heights according to Blume criterion

ter entrapped in the coke deck cargo, which could not drain off fast enough through the freeing ports. The capsizing sequence most likely was as follows: Due to the low stability in wave crest conditions a large heeling angle must have occurred, shifting the vessel to an intermediate equilibrium at ca. 45°. Water ingress, cargo shift or both must then have lead to the final capsize.

The simulations have shown that capsizing is hardly possible for the stability the ship had, when she left Emden lock. This is clearly stated in the polar-diagram (Fig.9, left side) for the Emden Lock situation, where significant wave heights of ca. 7-8m are required to endanger the vessel. These extreme (significant) wave heights are hardly possible in the Hubert Gat. Assuming an amount of 90 tons water, entrapped in the coke, the polar-diagram changes significantly (Fig.9, right side). Now, the limiting wave height is shifted to much lower values of about 4-5 meters for the operating condition of the vessel.

Table 3 shows that all investigated criteria consider the case as dangerous, where the vessel did actually capsize. On the other hand all criteria consider the 0.39m-GM case as clearly save. Therefore the direct ISEI of 0.158 represents a condition, which has clearly proven to be unsafe, whereas an ISEI of 0.0011 represents a condition, which is considered to be safe by all criteria. All criteria except the C-factor and the Blume-criterion do not consider the situation at Emden lock as sufficiently safe where GM was ca. 0.20 m. This condition is related to an ISEI of 0.0139. The C-factor concept may suffer from the fact that the vessel is actually a Shelter Decker, which has large freeboard and may not be covered by the concept. Taking all findings into account, the SS Irene Oldendorff -accident can be regarded as a case, which did occur close to the limit that distinguishes a ship from being safe or unsafe.

The Capsizing of MV FINNBIRCH (2006)

On Wednesday, 1st of November 2006, the 8500 dwt RoRo-Ferry M/V FINNBIRCH (call sign SLNK) capsized in heavy weather in the Baltic Sea between the islands Gothland and Olland. At the time of the accident, the vessel was travelling south at an estimated course of abt. 190- 200 Degree. The vessel was loaded with trailers, of which a significant amount was stowed on the top deck (see). At the time of the accident, the weather wind was about 20-25m/s or BF9-10. The sea was rough with significant wave heights of abt. 5-6m, significant period about 8-8.5s. These data are obtained from hindcast sources.

Figure 10: MV Finrnbirch in intermediate floating condition

According to the observations of the master of M/V MARNEBORG, the vessel closest to the MV FINNBIRCH, who later coordinated the rescue operations the vessel was rolling significantly. At about 16:15 she heeled to about 50 degree. The vessel remained in that intermediate equilibrium floating condition for a while (see), until she finally capsized at about 19:37.

M/V FINNBIRCH was built in 1978. In 1979 the vessel was additionally equipped with side sponsons and in 1986 an additional weather deck was added. Both conversions have significantly affected the stability of the vessel.

The official accident investigation has not been finished yet, why no investigation report is available so far. Therefore, some assumptions have to be made with respect to the loading condition prior to the accident:

- The additional steel weight of the retrofitted top deck is ca. 250 tons.
- The top deck was fully loaded with 36 trailers according to . From this fact we conclude that also the other decks were almost fully loaded.
- The average trailer weight is assumed to be ca. 23.5 tons.

When M/V FINNBIRCH was delivered in 1979, no damage stability regulations were in force, which means that the stability of the vessel was governed by the relevant intact criteria.

The limiting intact stability criterion is most likely $h_{\min}(30°) \geq 0.20m$ for the vessel including the sponsons and the top deck. Our investigations show that, in case the top deck is fully loaded, the ship operates close to the intact stability limit. Taking all assumptions into account we obtain the following floating condition:

Table 4: Intact floating condition

Total Weight :	13686.000 t
Draft at A.P (moulded) :	6.843 m
Trim (pos. fwd) :	-0.078 m
Metacentric Height :	1.704 m

The computed righting levers in waves show practically no stability on the wave crest for a wave which comes close to the accident seastate (see).

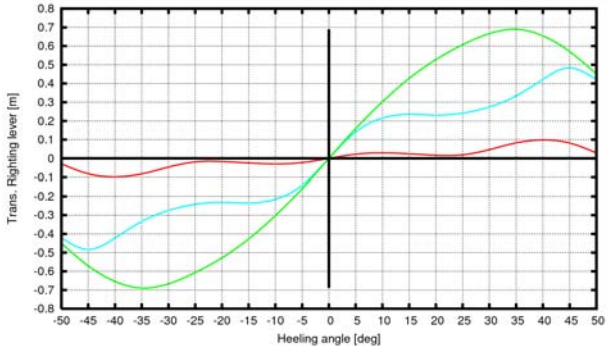

Figure 11: Lever arm curve of M/V Finnbirch

It is also important to underline the fact that the alterations of the initial GM in the sea state are substantial, which means that a lot of energy is introduced into the vessel by the sea state.

The speed of the vessel is assumed with 16 knots at an encounter angle of 30 degree. The results of the numerical simulation show that roll angles up to 40 Degree occur for situations when the wave height exceeds some threshold value and is at the same time in phase with the roll motion ().

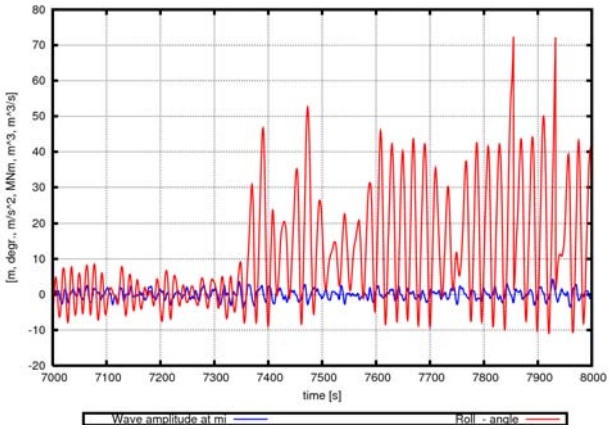

Figure 12: Simulated time series of the accident

shows a intermediate equilibrium floating condition of abt. 45-50 degree, which is only possible in case cargo has significantly shifted. Introducing this cargo shift into the simulation results in an intermediate equilibrium there as well (, 7350s onwards). In this phase, an additional cargo shift may have taken place or water may have entered the vessel, which has then lead to the final loss.

Our analysis indicates that the vessel was most probably travelling close to a 1:1 resonance condition at the time of the accident. In this context, it is interesting to note that the actual scenarios which lead to critical resonances could not be determined from the stillwater rolling period for small roll angles as the nonlinearity of the lever arm curve shifts the natural roll period significantly.

Concluded, it can be stated that the dynamic analysis has clearly shown that the reason for the loss of MV FINNBIRCH was most probably insufficient stability in a following sea scenario.

CONCLUSIONS

A selection of real capsizing accidents is investigated to follow two main goals. First these are used to further evaluate our numerical simulation code E4-ROLLS with respect to its capability to reproduce dangerous situations for ships in waves and its capability to predict the ship response in those situations with satisfying accuracy. Also more complex failure scenarios like cargo shift and entrapped water on deck are modelled for this purpose.

Secondly we use these accidents to assess the limiting boundaries, which separate the save and the un-save operating conditions of ships.

For this purpose TUHH has developed a new probabilistic intact stability criterion, called Insufficient Stability Event Index (ISEI).

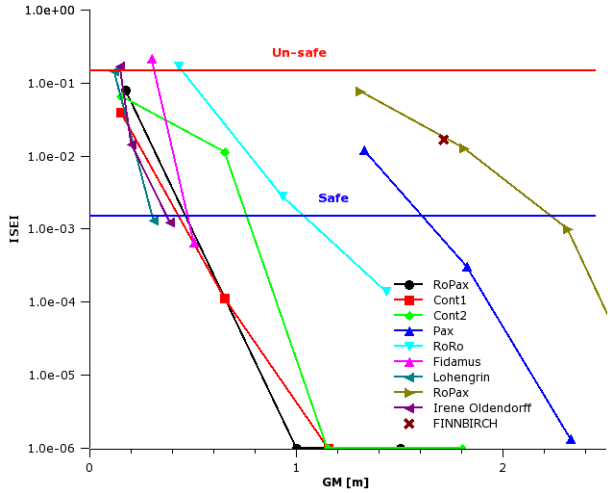

Figure 13: ISEI values for different ships

The new probabilistic concept takes into account the occurrence probabilities of seastate, course and ship-speed. The actual failure criterion for the ship in a specific operating condition is implemented via a “safe”/”unsafe”-decision based on the Blume-criterion and the maximum roll angle observed during the simulation.

In order to benchmark the new criterion, two loadcases were analysed for each of the investigated ships, one representing the failure condition and one assumed to be in the “safe” domain.

The results show that the concept is able to distinguish between safe and un-safe operating conditions clearly. shows the calculated ISEI-values for the investigated ships and a selection of modern vessels of different type. The “safe” and “un-safe”-boundaries are estimated values based on our findings. The picture demonstrates very clearly that typical modern ships, complying with all intact stability requirements in force, are critical, or even unsafe with respect to their stability. Therefore we can conclude that the current intact stability criteria are neither sufficient nor suitable to avoid accidents related to stability alterations in waves.

REFERENCES

Cramer, H. and Krueger S. (2005). “Numerical capsizing simulations and consequences for ship design”, Jahrbuch der Schiffbautechnischen Gesellschaft 2001, Springer, 2005

Die deutsche Handelsflotte (1962). “Pläne der Frachtschiffe über 300 BRT” Seehafen-Verlag

Kempf, G (1950). “Gutachten über die Ursachen, die zum Untergang des Frachtdampfers FIDAMUS geführt haben mögen.” Staatsarchiv Bremen

Kroeger, P. (1987). “Simulation der Rollbewegung von Schiffen”, Bericht, Nr.: 473, Institut für Schiffbau der Universität Hamburg

Krueger, S. and Kluwe, F. (2006). “Development of Dynamic Stability Criteria from Seakeeping Simulation.”, International Marine Design Conference (IMDC2006), Ann Arbor, Michigan, USA

Krueger, S. , Hinrichs, R., Kluwe F. and Billerbeck, H. (2006). “Towards the Development of Dynamic Stability Criteria” HANSA Maritime Journal, 10/2006, p.204

Petey, F (1985). “Berechnung der Flüssigkeitsbewegung in teilgefüllten Tanks und Leckräumen”, Schiffstechnik, Band 32

Petey, F (1988). “Ermittlung der Kentersicherheit lecker Schiffe im Seegang aus Bewegungssimulationen”, Bericht Nr.: 487, Institut für Schiffbau der Universität Hamburg

Seeamt Bremerhaven (1950). In seeamtlichen Untersuchungen über den Untergang des Frachtdampfers FIDAMUS. Staatsarchiv Bremen, 1950.

Seeamt Bremerhaven (1952). “Dampfer Irene Oldendorff aus Luebeck. UNTERGANG. SEEAMT BREMERHAVEN. 4. JUNI 1952.”, Staatsarchiv Bremen

Seeamt Flensburg (1964). „Frachtmotorschiff LOHENGRIN aus Bremen, KENTERUNFALL“,
Seeamt Flensburg, 22. Januar 1964, aus: Landesarchiv Schleswig- Holstein.

Soeding, H. (1982). “Leckstabilität im Seegang”, TU Hamburg-Harburg, Schriftenreihe Schiffbau, Report Nr. 429

Soeding, H. (2001). “Global Seaway Statistics”, TU Hamburg-Harburg, Schriftenreihe Schiffbau, Report Nr. 610

Session 6: Numerical prediction of intact stability

Session Chairman: Prof. Y.Ikeda Prof. M. Neves

1) O. M. El Moctar:

   “Prediction of Extreme Ship Responses Using Potential Flow and RANSE Codes“

2) L. Mc Cue, B. Campbell:

   “Approximation of ship equations of motion from time series data”

3) T. Katayama, M. Kotaki, Y. Ikeda:

   “A Study on the Characteristics of Roll Damping for Multi-hull Vessels”

4) C. Bassler, B. Campbell, W. Belknap, L. Mc Cue:

   “Dynamic Stability of Flared and Tumblehome Hull Forms in Waves”

Prediction of Extreme Ship Responses

Using Potential Flow and RANSE Codes

Ould M. El Moctar
Germanischer Lloyd

ABSTRACT

The paper presents numerical procedures to simulate ship seakeeping responses involving extreme motions and loads. Potential-flow codes are needed for a statistic/probabilistic long-term analysis of the ship's operation to define representative or most critical environmental conditions. Then a RANSE solver is employed to model highly nonlinear ship-wave interaction by solving the nonlinear rigid body six degrees of motion equations in the time domain. Extreme ship motions and wave-induced loads, including impact-related effects caused by slamming and green water on deck, can be computed simultaneously. Various applications for different ship types show the capability of the numerical simulations.

KEYWORDS

RANSE; ship motions; ship seakeeping

INTRODUCTION

For many seakeeping issues, seakeeping is determined as follows:

- Representation of the natural seaway as superposition of many regular (harmonic) waves
- Computation of the ship responses of interest in these harmonic waves

Addition of the reactions in all these harmonic waves to a total reaction (superposition)

This simplified linear approach is appropriate for many questions in ship seakeeping and frequently applied. The corresponding tool at Germanischer Lloyd (GL) is a 3-d Green function method (GFM). The advantage of this approach is that it is very fast and allows thus the investigation of many parameters (frequency, wave direction, ship speed, metacentric height, etc.). Computations become considerably more expensive if this simplification is not made. Non-linear computations are usually necessary for the treatment of extreme motions; here simulation in the time domain is the proper tools. Germanischer Lloyd uses nonlinear time-domain strip theory codes such as GL ROLLS and GL SIMBEL, Söding (1982), Pereira, (1988), Brunswig et al (2006). Methods that directly solve the Reynolds-averaged Navier-Stokes equations (RANSE), possibly including the two-phase flow of water and air, are better able to describe the physics associated with water on deck, viscous damping, 3d-effects etc. However, the computational effort for a three-dimensional RANSE method to simulate motions and loads on a ship at small, successive instances of time over a long time period appears beyond current computational capabilities

Combining intelligently potential flow methods with RANSE simulations allows exploiting the respective strengths of each approach, El Moctar et al. (2004, 2005). The approach starts with a potential flow code analysis to identify the most critical parameter combination for a ship response. Then a RANSE analysis determines the ship motions and loads.

This paper presents a numerical procedure based on the combined use of a boundary element method (BEM), a statistical analysis us-

ing random process theory and an extended RANSE solver to obtain the structural response of ships in a seaway. The BEM obtained the hydrodynamic data base, needed for a statistic/probabilistic long-term analysis of the ship's operation to obtain so-called equivalent regular design waves that represented design load conditions. The extended RANSE solver then obtained ship motions and the corresponding pressures distribution acting on the ship subject to these design wave conditions by solving the nonlinear rigid body six degrees of motion equations in the time domain. Wave-induced loads, including impact-related effects caused by slamming and green water on deck, were computed simultaneously. The resulting hydrodynamic pressures were transformed into nodal forces and became part of the input for the FE code.

The computational procedure has been applied to a large variety of ships, e.g. El Moctar et al. (2004, 2006), Some applications involving extreme responses are presented here.

THE EXTENDED RANSE SOLVER

The RANSE solver Comet implements interface-capturing techniques of the volume-of-fluid (VOF) type. The solution domain is subdivided into a finite number of control volumes that may be of arbitrary shape. The spatial distribution of each of the two fluids is obtained by solving an additional transport equation for the volume fraction of one of the fluids.

Fluid structure interaction effects were presently not fully accounted for. Except for the investigation of hull girder whipping, the ships were assumed to be rigid bodies. The fluid was assumed to be viscous and incompressible. The nonlinear ship motion equations were solved and coupled to the RANSE solver. The computational procedure comprised the following steps:

- The RANSE-solver computed the flow around a ship's hull, taking into account viscosity, turbulence, and deformation of the free surface.
- Hydro- and aerodynamic forces and moments acting on the ship were calculated by integrating the pressure and friction stresses over the ship's surface.

The nonlinear equations of the rigid body six degrees of freedom motions were solved in the time domain, taking account of all forces acting on the body. Integration yielded motions, accelerations, velocities, and translational and rotational displacements.

After updating the position of the ship and again computing the fluid flow for the new position and integrating over time, the trajectory of the ship was obtained.

The equations of motion were solved in the Newtonian reference frame (G,x,y,z) fixed with respect to the mean position of the ship. Its origin was located at the center of gravity of the ship, G. The coordinate transformation between the Newtonian and the ship-fixed local reference frame (G,ξ,η,ζ) was defined as follows:

$$\vec{x} = \vec{x}_G + S\vec{\xi}$$

where S denotes the transformation matrix and $\vec{\xi}$ the rotational position vector. The transformation matrix resulted from consecutive rotations about the vertical z-axis (yaw), the new transverse η-axis (pitch), and the new longitudinal ξ-axis (roll). The governing equations of motions are expressed as follows:

$$\vec{F} = m \cdot \ddot{\vec{x}}_G$$

$$\vec{M} = S\, I_L S^T \dot{\vec{\omega}} + \vec{\omega} \times S\, I_L S^T \vec{\omega}$$

where $\vec{F}$ denotes the resulting force vector, m the mass of the ship, $\ddot{\vec{x}}_G$ the translational acceleration vector of G, $\vec{M}$ the resulting moment vector with respect to G, I_L the inertia tensor of the ship about the axes of the ship-fixed (local) reference frame, and $\vec{\omega}$ the angular velocity vector. Integration in the time domain relied on the use of the so-called explicit trapezoidal method, Brunswig and El Moctar, 2004).

We validated motion predictions of the extended RANSE solver by comparing computations with experimental measurements obtained

from systematic model tests performed at the Hamburg Ship Model Basin (HSVA). These tests were carried out at a scale of 1:13, albeit not for a model of one of the ships investigated here, but for a 100 m motor yacht of 3600 t displacement. The favorable agreement between experimental measurements and RANSE computations validated the extended RANSE solver. Sample time histories of measured pitch , roll motion and vertical acceleration at the yacht's forward perpendicular (FP) are shown in Fig. 1 together with comparable results obtained from RANSE computations.

FLOW AND MOTION SIMULATION

The numerical volume grids surrounding the ships comprised typically between one and three million hexahedral control volumes. To avoid flow disturbances at outer grid boundaries, these boundaries were located one ship length ahead of the bow, two ship lengths aft of the stern, one ship length beneath the keel, and one ship length above the deck. This large domain of the mesh, especially above the deck, was necessary to allow large pitch motions in head waves. Near the ship hull and at the inlet boundary of the waves, grid density was high to resolve the wave, whereas at the outlet boundary of the waves, grid density was relatively course in order to dampen the waves. The innermost dimensionless cell thickness was chosen such that n+ = 100 on average. Figure 2 shows the numerical grid on the surface of the containership.

Front, side, bottom, and top flow boundaries were specified as inlets of known velocities and known void fraction distributions, thereby defining water and air regions. On the hull surface a no-slip condition was enforced on fluid velocities and the turbulent kinetic energy. The wake flow boundary was specified as a zero-gradient pressure boundary (hydrostatic pressure). All computations were performed using the RNG-k-ε turbulence model with wall functions. The time step size was chosen such that the Courant number was smaller than unity on average. Time step size was typically between 0.01 s. Ship motions were realized by moving the entire grid at each time step. Thus, all boundary conditions were newly computed at each time step.

Volume fractions and velocities that initialized the flow field arose from the superposition of ship speed and orbital particle velocities of the waves. Numerical diffusion caused by the course grid aft of the ships dampened the incident wave to such an extent that no significant wave reflection occurred at the outlet boundary.

Simulation of the flow fields continued until reaching a periodic solution. After a simulation time of two to five encounter periods, depending on ship motions, ship speed, and wave height, periodically converging solutions were obtained. For each time step up to ten outer iterations were needed.

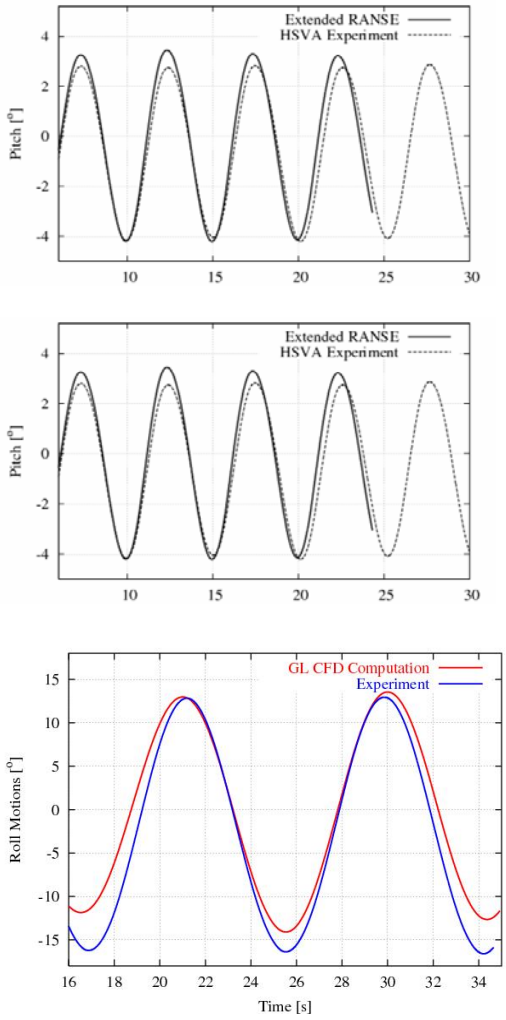

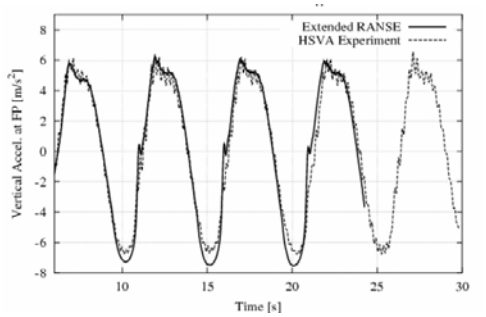

Fig. 1: Comparative time histories of pitch, roll motion and vertical acceleration at FP for a motor yacht in head and oblique regular waves

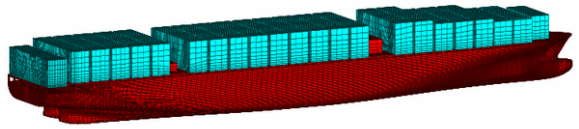

Fig. 2**:** Numerical grid on surface of the containership

LARGE POST-PANMAX CONTAINERSHIP

El Moctar et al. (2004, 2006) present in detail results of nonlinear seakeeping analyses for three hulls, with a focus on slamming and global loads. One of these hulls is a large modern Post-Panmax Containership. The sectional loads of a large modern Post-Panamax containership were computed for design wave conditions using RANSE and the frequency-domain panel code (GLPANEL). Non-linear corrections were applied to the GLPANEL computed loads.

The critical wave conditions selected represented worst case scenarios for midship vertical bending moment. Head wave conditions were rated most critical from the standpoint of slamming loads on the bow. However, because of the extreme stern overhang characteristic of modern containerships, stern wave conditions were also studied.

In heavy seas, the added resistance tends to result in voluntary or involuntary speed loss. Thus, both ships were analyzed advancing at reduced speeds. The exact speed loss was difficult to establish. Therefore, several reduced forward speeds were considered.

Table 1 shows main data of the containership and the design wave.

Wave-induced sectional loads were computed for the ship advancing at one-third and two-third forward speed in the design wave. For this particular case, the hull girder was subject to a vertical still-water sagging moment. Figures 3 to 6 depict the corresponding envelope curves of maximum and minimum vertical bending moments and shear forces at sections along the length of the ship. Results show that at one-third forward speed, sectional loads from RANSE compared favourably with sectional loads from GLPANEL. However, at two-third forward speed, bending moments as well as shear forces differed significantly in the bow region. These differences were caused by the effects of slamming at the bow and green water on deck, see Fig.7. As expected, these effects were more pronounced at higher forward speed. The results demonstrate the importance of accounting for the ship's forward speed when computing wave-induced sectional loads.

Table 1 : Principals particulars of Post-Panamx Containership

Length [m]	330
Width [m]	48
Draft [m]	12
Speed [kts]	27

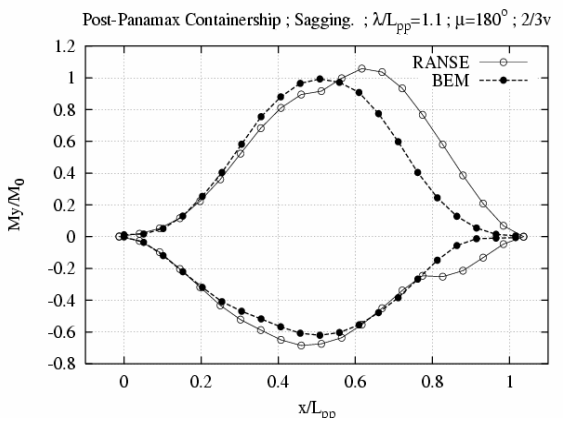

Fig.3: Envelopes of vertical bending moments for 2/3 ship speed at midship design wave condition

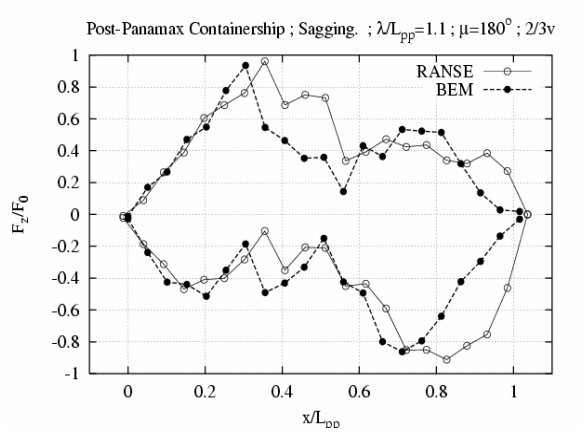

Fig.4: Envelopes of vertical shear forces for 2/3 ship speed at midship design wave condition

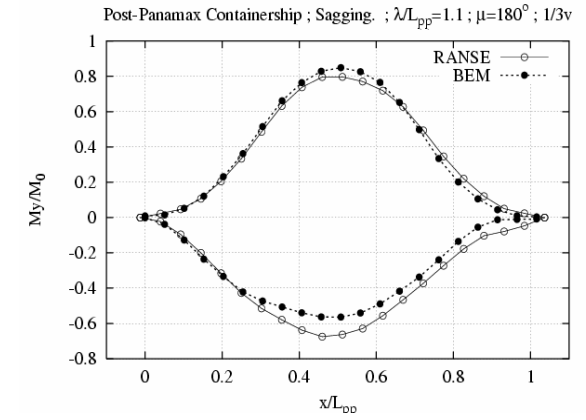

Fig.5: Envelopes of vertical bending moments for 1/3 ship speed at midship design wave condition

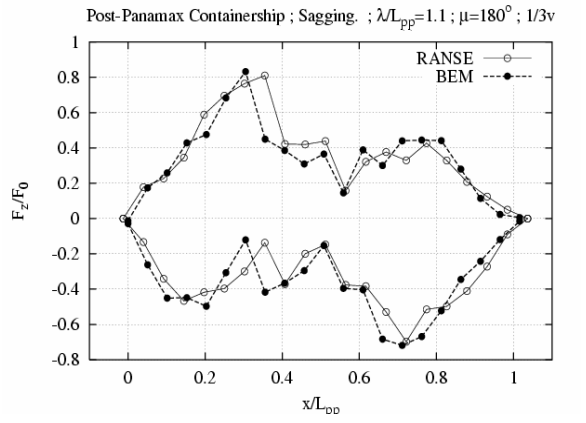

Fig.6: Envelopes of vertical shear forces for 1/3 ship speed at midship design wave condition

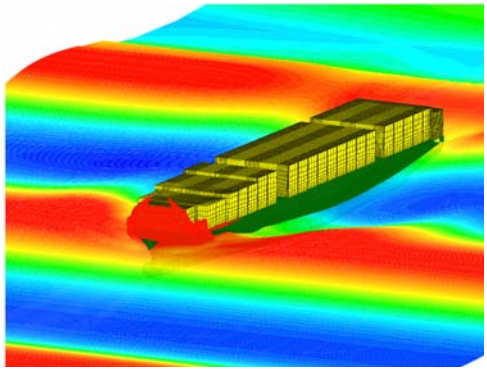

Fig.7: Water on deck of the containership

'ERTHRACE' TRIMARAN

EARTHRACE is a wavepiercing trimaran designed to break the world record for global circumnavigation using only renewable fuels. Circumnavigating the globe represents the world's longest marine race, spanning some 24,000 nautical miles. The current record stands at 75 days. Germanischer Lloyd was asked to assess the hydrodynamic loads and the ship motions. Figure 8 shows a pictorial representation of EARTHRACE, and Table 2 lists its principal particulars.

The unconventional shape of EARTHRACE represents a completely new design for which no rules are available. In addition, the vessel's extremely high service speed relative to its size (Froude number in access of 1.7) as well as its complex geometry made it necessary to account for forward speed effects and large (finite amplitude) waves. At sea, part of the ship's hull is likely to be completely immersed by waves, causing large amplitude highly nonlinear ship responses, and wave impact-related (slamming) loads had to be accounted for as well. This meant that standard potential flow based seakeeping analysis methods were unsuitable.

Screen shots of EARTHRACE in head and oblique waves, shown in Fig. 9 and pressure distributions, shown in Fig. 10, are typical samples of computed results.

Three cases that represent worst-case design scenarios were investigated. The first three cases determined design loads for the vessel advancing at 25 kts speed in waves of different

amplitude, period, and heading. These loads were later used as inputs for a structural analysis.

Figures 11 and 12 show typical time histories of computed results, here for case 1, examining the trimaran advancing at service speed of 25 knots in 5.0m high regular head waves. As seen in Fig. 11, maximum heave and pitch motions turned out to be 1.5m and 15°, respectively, and the corresponding maximum vertical acceleration reached values up to 2.25 times the acceleration of gravity. The corresponding hydrodynamic loads acting on one of the sponsons are shown in Fig. 12. These time histories revealed a typical characteristic of the vessel's motion behavior, namely, the response amplitude alternated between two values. This was the case although the amplitude of the incident wave train remained the same. Such highly nonlinear behavior occurred in large amplitude head waves. The ship's first encounter with such a large amplitude wave caused its entire foreship to be immersed into the surrounding water. The resulting initial conditions of the ship when it then headed into the following wave were not like those of the first wave and, consequently, the ship's response differed from the response caused by the first wave. This process more or less repeated itself during the next two wave amplitudes.

Cases 2 and 3 investigated the vessel's response in regular waves of lesser height and length, but again at the design speed of 25 knots. Motions, accelerations, and hydrodynamic loads were found to be less than for case 1. However, the largest hydrodynamic pressure occurred in oblique waves.

Fig. 8: The wavepiercing trimaran EARTHRACE

Table 2: Principal particulars of

EARTHRACE	
Displacement	24,900 kg
Length overall	23.9 m
Breadth at design waterline	7.9 m
Draft, full load	0.91 m
Service speed	25/50 kts

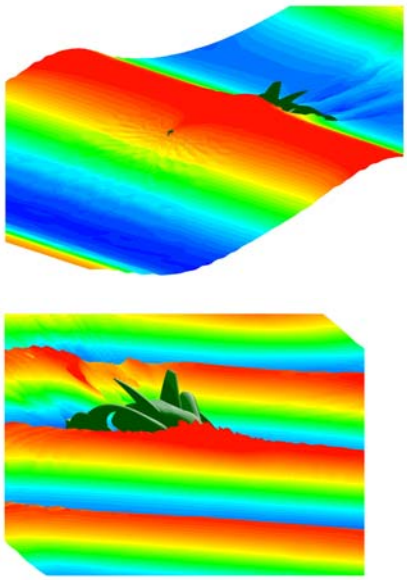

Fig.9: Trimaran in head and oblique regular waves

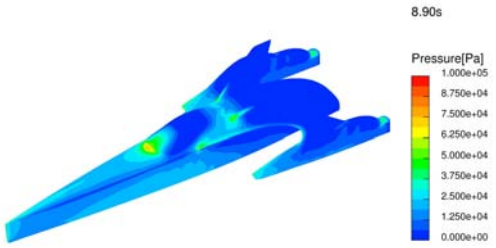

Fig.10: Pressure distribution on Trimaran

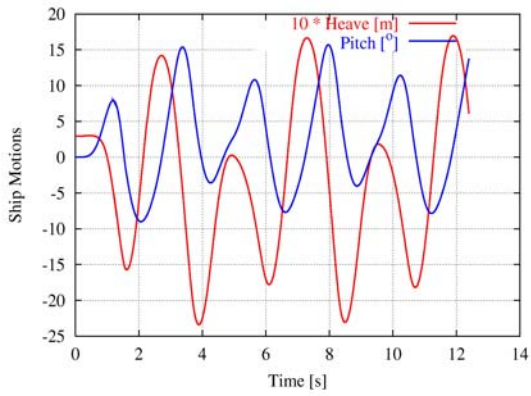

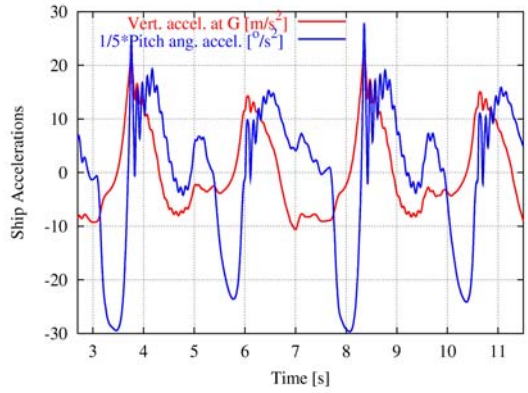

Fig.11: Motions and accelerations of EARTHRACE in 5.0m high head waves

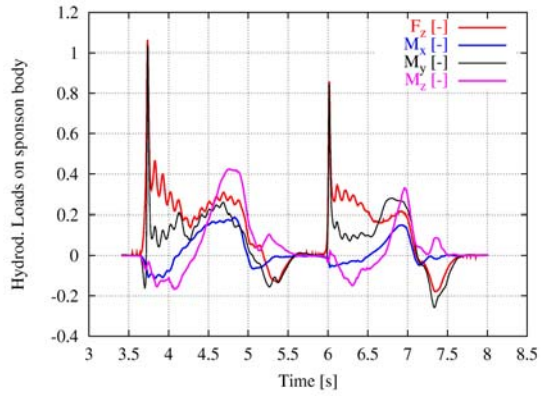

Fig.12: Normalized hydrodynamic forces on a sponson of EARTHRACE in 5.0m high head waves

CONCLUSIONS

Potential flow solvers remain useful in seakeeping analysis. However, for large ship motions (capsizing) and large loads (slamming), modern free-surface RANSE solvers offer superior simulation capability. Inclusion of green water on deck (or internal flooding) directly coupled to the global motions of the ship are feasible by now, with virtually no restrictions on ship or wave geometry. While the applications shown here focussed largely on loads on the ship, the same approach could be used for advanced capsizing simulations. For some time to come, such simulations will be restricted to a few service providers, as they require considerable resources in hardware, software and skill in using sophisticated programs for grid generation and simulation.

REFERENCES

Blume P., Ship Technology Research 26, Experimentally determined coefficients for effective roll damping and application to estimate extreme roll angles, 1979 (in German)

Brunswig J., El Moctar, O., 7th Numerical Towing Tank Symposium (NuTTS), Hamburg, Prediction of ship motions in waves using RANSE, 2004

Brunswig, J. Pereira, R., Kim, D-W. "Validation of parametric roll motion predictions for a modern containership design, Proc., 9th Int. Conf. on Stability of Ships and Ocean Vehicles STAB'2006", Proceedings of the International , Conference on Fast Sea Transportation (STAB), Rio, 2006

El Moctar O.M., Brehm A., Schellin T., 25th Symp. Naval Hydrodynamics, St. John's, Prediction of slamming loads for ship structural design using potential flow and RANSE codes, 2004a

El Moctar O.M., Schellin T., Priebe T., 26th Symposium on Naval Hydrodynamics, Rome, CFD and FE methods to predict wave loads and ship structural response, 2006

El Moctar, O., Brunswig, J. Brehm ,A., Schellinn, T.E. "Computation of Ship Motions in Waves and Slamming Loads for Fast Ships using RANSE", Proceedings of the International , Conference on Fast Sea Transportation (FAST), St. Petersburg, 2005

Pereira, R. (1988) Simulation nichtlinearer Seegangslasten, Schiffstechnik 35(4) 173-193

Papanikolaou A., Schellin T.E., J. Ship Technology Research Vol. 39, A three-dimensional panel method for motions and loads of ships with forward speed, pp.147-156, 1991

Söding, H. Leckstabilität im Seegang. Report No.429, Institut für Schiffbau, 1982

Approximation of ship equations of motion from time series data

Leigh McCue

Aerospace and Ocean Engineering, Virginia Tech

Bradley Campbell

Seakeeping Division, Hydromechanics Department,
Carderock Division, Naval Surface Warfare Center

ABSTRACT

In this work, ship equations of motion are approximated from numerically simulated test cases. Once approximated, the equations of motion can be used in an effort to predict future motions, to estimate the impact of initial conditions on an experimental data set, and to compare a broad range of experimentally based simulations to those from numerical/analytical models for validation purposes.

KEYWORDS

Capsizing; optimization; equations of motion

INTRODUCTION

Large amplitude ship motions represent complex, even chaotic phenomena. As part of the ongoing pursuit of techniques to evaluate, reconcile, and provide form to experimental data, the authors propose approximating the equations of motion based upon experimental time series. A recent effort towards approximating linearized coefficients as a function of forward speed for coupled heave-pitch ship motions from a numerically generated data series is discussed in Suleiman *et al.* (2000) employing the Eigensystem Realization Algorithm. Additionally, in Suleiman (2000), sway, roll, and yaw motions are considered as well as 5 DOF couplings of heave, pitch, sway, roll, and yaw. While the results using ERA prediction were strong for small amplitude motions, in higher sea states precision was lost. Nonlinear effects are considered separately in the special case when the ship is subjected to parametric resonance (Suleiman, 2000). The emphasis of the work presented herein is on large amplitude motions, primarily in the roll degree of freedom, where nonlinearities are prevalent. The motions are not constrained to any specified type of large amplitude rolling, such as parametric resonance.

Reconstructing equations of motion from data is discussed heavily in the complex systems literature. See for example Breeden and Hübler (1990), Cremers and Hübler (1987), Crutchfield and McNamara (1987), and Eisenhammer *et al.* (1991). While the specific details of different existing methods for approximating equations of motion from an experimental time series vary, all at their most fundamental level are predicated upon 'guessing' the form of equations, either composed of a sum of standard functions or some archetypical model, then optimizing the coefficients in the equations to best fit the experimental data.

For the case of vessel motions, a vast body of work exists describing the form of ship equations of motion ranging dramatically in complexity (Lewis, 1989; Bhattacharyya, 1978; Fossen, 1994; Lewandowski, 2004). In this paper a demonstration of concept is presented in which the authors work to approximate equations that fit artificially generated (*i.e.* through numerical simulation) 'experimental' data for single degree of freedom rolling and capsize of the *Edith Terkol* (Soliman & Thompson, 1991). The form of the approximated equations of motion are also taken to be represented by a single degree of freedom roll equation in which linear plus cubic terms are used for damping (Dalzell, 1978) and stiffness. Five unknown parameters are taken to be the damping and stiffness coefficients as well as the magnitude of forcing. The optimization procedure matches the 'experimental' data, accurately reproducing time series for small and large motions in addition to the roll/roll velocity safe basin.

SINGLE DEGREE OF FREEDOM DEMONSTRATION OF CONCEPT

As a numerical demonstration of concept, the single degree of freedom roll/roll velocity time series for the *Edith Terkol* was generated through integration of Equation 1 with parameters $b_1 = 0.0043$, $b_2 = 0.0225$, $c_1 = 0.384$, $c_2 = 0.1296$, $c_3 = 1.0368$, $c_4 = -4.059$, $c_5 = 2.4052$, and $\omega_e = 0.85 \cdot \omega_n = 0.85 \cdot 0.62 = 0.527$ (Soliman & Thompson, 1991).

$$\ddot{\phi} + b_1\dot{\phi} + b_2\left|\dot{\phi}\right|\dot{\phi} + c_1\phi + c_2\left|\phi\right|\phi + c_3\phi^3 + c_4\left|\phi\right|\phi^4 + c_5\phi^5 = F\sin\left(\omega_e t\right) \quad (1)$$

The output time series was then treated as though it were an unknown roll/roll-velocity "experimental" data set to which one wishes to approximately fit equations of motion. A simple, standard form of the roll equation of motion was assumed as given in Equation 2 where the subscripted letter *u* denotes an unknown. The only variable assumed to be explicitly known is the encounter frequency as that is comparatively trivial to approximate from a given data set. If necessary it is feasible to treat encounter frequency as an additional unknown at some computational cost.

$$\ddot{y} + b_{u1}\dot{y} + b_{u3}\dot{y}^3 + c_{u1}y + c_{u3}y^3 = F_u\sin\left(\omega_e t\right) \quad (2)$$

A Nelder-Mead simplex search is performed to minimize the distance between the phase-space output of the approximated equations of motion $< y, \dot{y} >$ and the "experimental" data $< \phi, \dot{\phi} >$, *i.e.* minimizing the function in Equation 3. The values of $< \phi, \dot{\phi} >_j$ are used as the initial conditions for the simulation to determine $< y, \dot{y} >_{j+1}$. Thus the coefficients for the approximated equations of motion are optimized over the entire time series via comparison of piecewise integrations. To avoid detecting an erroneous local minimum, each case was examined at a number of values for *N*. That is, while the length of a source time series is constant, the number of flow steps, *m* where *m* is the length of the time series divided by *N*, over which each piecewise integration was performed was varied to find a solution balancing local and long-time behavior of the system as well as computation time. For this reason the value deduced for each constant were considered both for ability to reproduce the experimental data, and physical relevance (*ie.* examination of roll damping and restoring arm curves).

$$\sum_{j=1}^{N}\left\| < y, \dot{y} >_j - < \phi, \dot{\phi} >_j \right\| \quad (3)$$

To begin, Equation 1 was used to generate 500 seconds of data with initial conditions $< \phi_0, \dot{\phi}_0 > = < 0,0 >$ and $F = 0.0195$. Using a Nelder-Mead search to optimize values for unknown coefficients in Equation 2 so as to minimize the summation in Equation 3 results in values: $b_{u1} = 0.0095$, $b_{u3} = -0.4445$, $c_{u1} = 0.4063$, $c_{u3} = 0.4209$, and $F_u = 0.0200$. Figure 1 shows the original time series, as generated

by integration of Equation 1 and the approximated time series, generated by integration of Equation 2 with the above optimized coefficients. The first 500 seconds of Figure 1 show that the approximated time series accurately reproduces the original source data. Equation 1 is then simulated for an additional 500 seconds and compared to the approximated Equation 2 to demonstrate that the steady state behavior of the system is also captured, that is, that behavior beyond the period used to optimize the unknown coefficients is reproduced by the approximated equations of motion.

Before assigning physical meaning to the approximated coefficients, one must carefully evaluate the limitations of the approximation. For example, the roll stiffness and damping curves bases upon the actual and approximated equations of motion are given in Figure 2. While the curves are fit quite well within the ranges of the incorporated source data, ie. roll from ±0.3 rad and roll velocity from ±0.15 rad/s, outside of these ranges agreement is poor. Indeed the asymptotic trends are distinctly non-physical with, for example, stiffness increasing infinitely with roll angle. By assessing the roll damping and stiffness curves one can glean a greater understanding of the range in which the approximated equations of motion are accurate and physically meaningful thus addressing the "cancellation" effect described by Suleiman (Suleiman, 2000) (in which Suleiman expresses concern that in this type of technique two incorrect parameters may have cancelling detrimental effects thus masking their inaccuracy). Additionally, through this method it is not the intention to state that the optimization has found the damping and stiffness coefficients for the system, rather that a set of coefficients have been found which accurately reproduce the input data series within a viable parameter range.

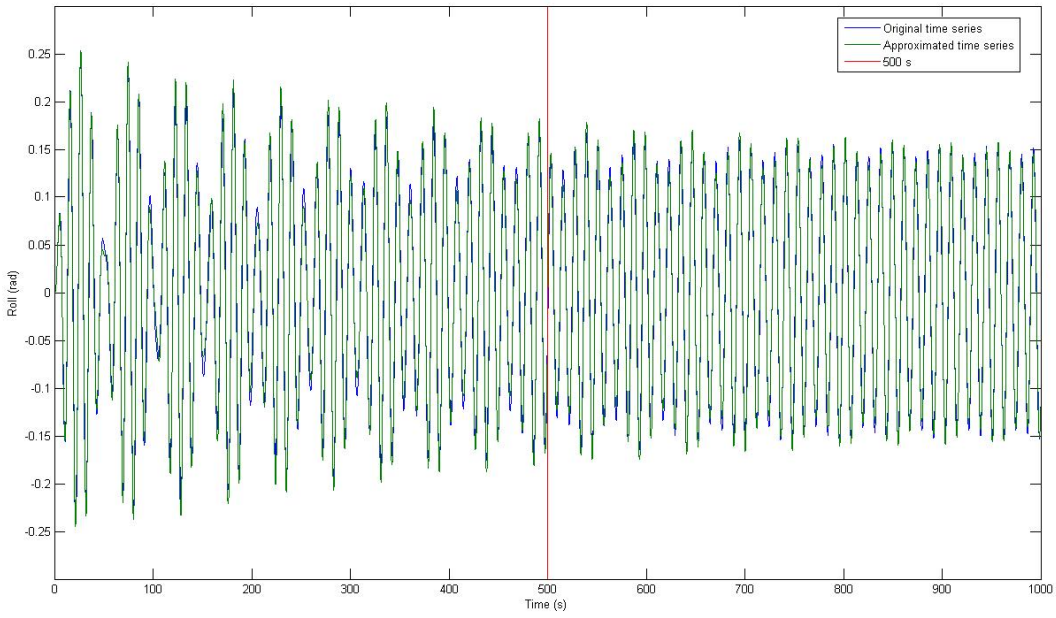

Figure 1: Original and approximated time series for roll/roll velocity initial conditions of < 0, 0 >. Initial 500 seconds of original data used to approximate coefficients of Equation 2 with subsequent 500 seconds demonstrating consistent prediction of steady state behavior.

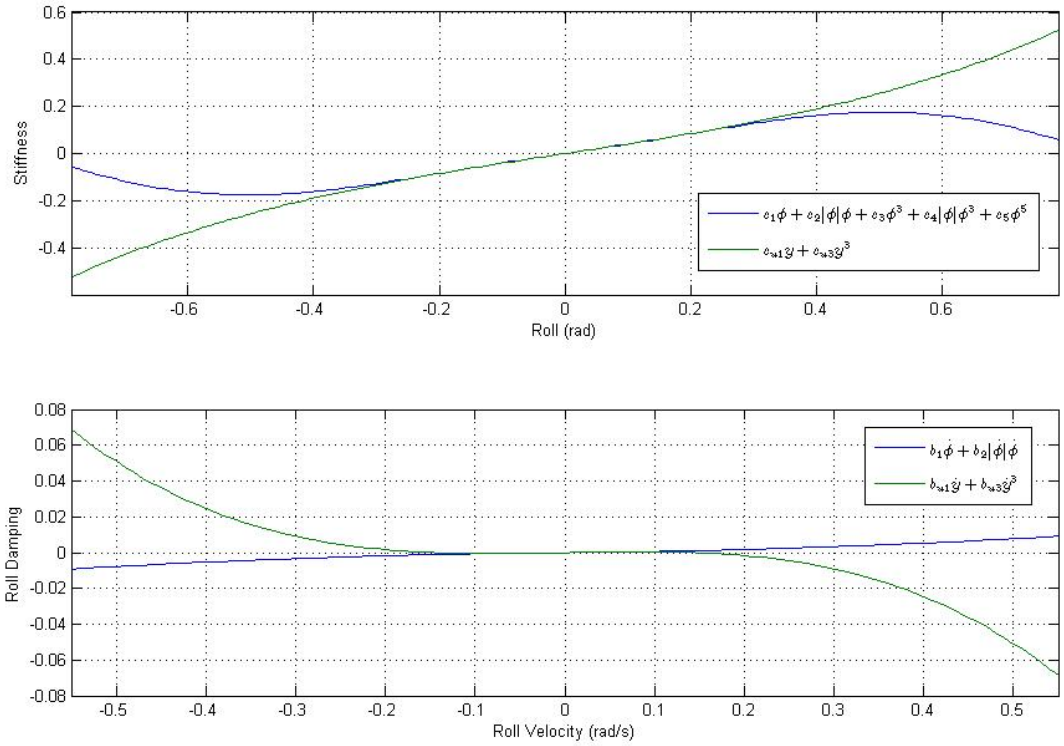

Figure 2: Comparison of original and approximated stiffness and roll damping curves for roll/roll velocity initial conditions of <0,0>.

If one begins at an initial condition leading to larger amplitude motions, the methodology is equally capable of replicating the desired time series while simultaneously capturing the expected roll stiffness and damping behavior over a larger parameter range. The same process described above was conducted for a time series generated from Equation 1 for initial conditions of < 0.4, 0 > for roll and roll velocity. When the optimization routine dictated by Equation 3 is run on Equation 2 the following coefficient values are found: $b_{u1} = 0.0060$, $b_{u3} = 0.0639$, $c_{u1} = 0.4344$, $c_{u3} = -0.2403$, and $F_u = 0.0200$. A comparison of the original and approximated roll time series is given in Figure 3. As with Figure 1 the approximate coefficients are based upon the first 500 seconds of data with the time from 500-1000s presented to show the appropriate capturing of steady state behavior in a quasi-predictive sense. A comparison of the original and approximated stuffiness and roll damping curves for this larger initial condition pairing is given in Figure 4. Intuitively, with the larger range of roll motion, damping and stiffness are accurately represented over a larger roll and roll velocity range than seen in Figure 2 which was based upon roll motions in a smaller region.

With this more accurate model of the restoring damping and stiffness force terms, other initial condition pairs can be simulated. For example, Figure 5 uses the coefficients found from the optimization routine based upon comparison to an original time series with initial roll and roll velocity of < 0.4, 0 > to simulate Equation 2 with initial conditions of < 0, 0 >. This simulation is compared to a time series generated from Equation 1 for the same <0, 0> initial condition pair. In general it is noted that roll motion is consistently underpredicted by as much as 4 degrees.

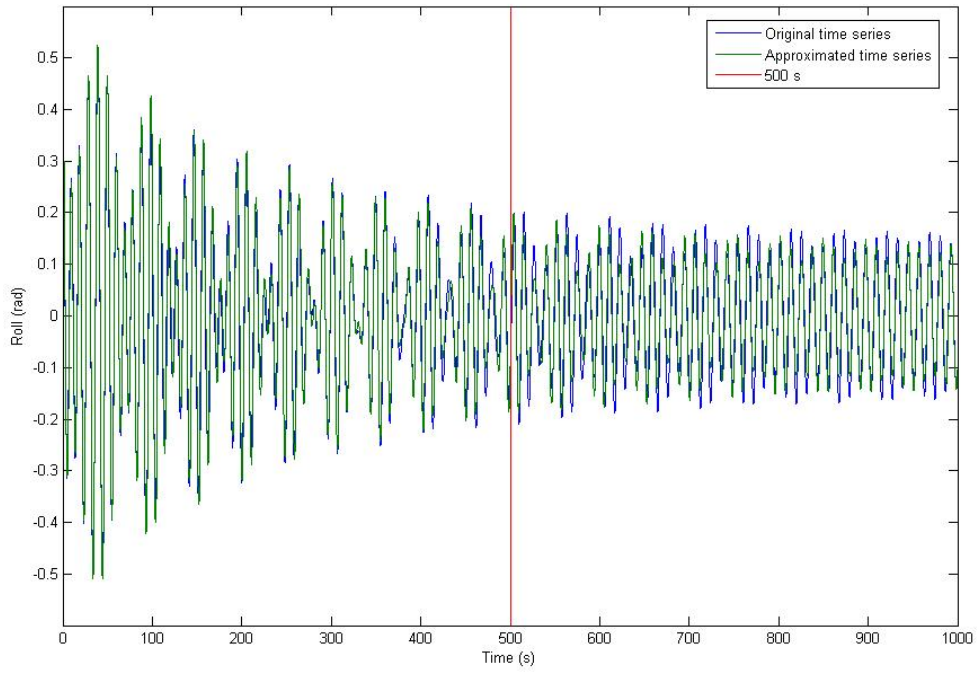

Figure 3: Original and approximated time series for roll/roll velocity initial conditions of < 0.4, 0 >. Initial 500 seconds of original data used to approximate coefficients of Equation 2 with subsequent 500 seconds demonstrating consistent prediction of steady state behavior.

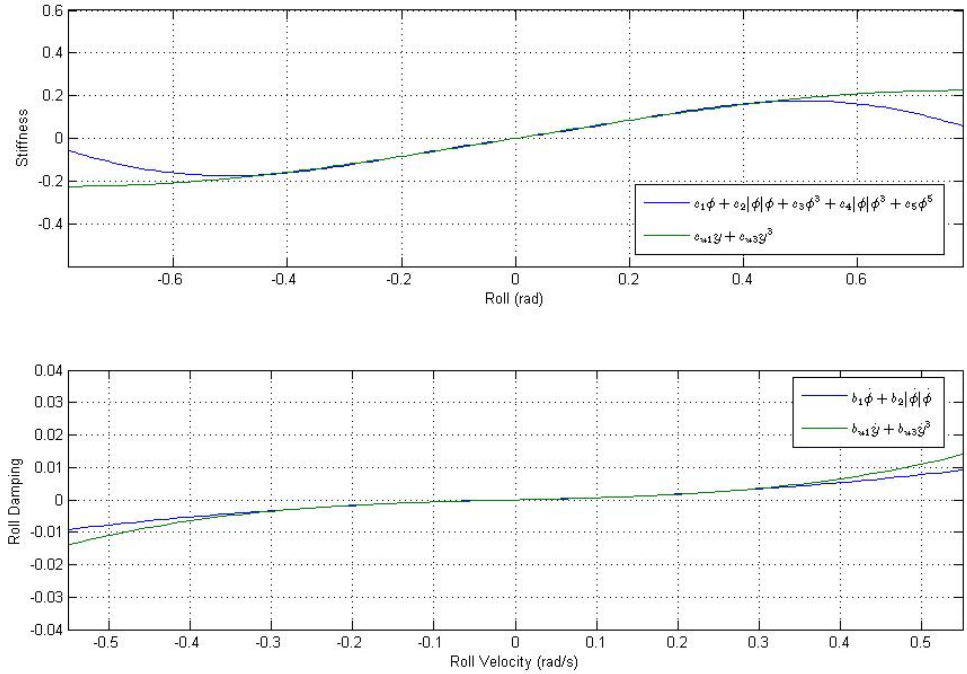

Figure 4: Comparison of original and approximated stiffness and roll damping curves for roll/roll velocity initial conditions of <0.4,0>.

If one uses simulated data near the separatrix between safe and unbounded motions which results in very large amplitude rolling, such as the roll/roll velocity initial conditions of <−0.4,−0.35 > a number of interesting findings arise. Specifically, while the estimated solution no longer accurately models small amplitude motions, it captures large amplitude motions as well as the safe basin with strong precision. To begin, consider Figure 6 which shows the original simulated time series for roll/roll velocity initial conditions of < −0.4,−0.35 > (top), < 0, 0 > (middle), < 0.4, 0 > (bottom). The equations of motion are approximated using 500 seconds of data with the initial conditions of < −0.4,−0.35 > to fit Equation 2 resulting in $b_{u1} = 0.0098$, $b_{u3} = 0.0388$, $c_{u1} = 0.5147$, $c_{u3} = -0.7052$, and $F_u = 0.0220$. The largest amplitude case is well replicated and projected for an additional 500 seconds. However, after the large amplitude transients diminish in the smaller amplitude cases, roll motion is consistently underpredicted. By comparing the actual and approximated stiffness and roll damping curves given in Figure 7 it is likely that this underprediction is due to overprediction of stiffness at small amplitudes. However, this large amplitude case does accurately capture the shape of both curves during initial large amplitude transients.

Figure 8 presents a safe basin generated via optimizing the unknown coefficients in Equation 2 to a time series generated from Equation 1 with initial conditions of <−0.4,−0.35 >. This non-capsize case on the separatrix between safe and bounded motions reproduces the original safe basin of the system governed by Equation 1 with high fidelity.

CONCLUSIONS

Noteworthy difficulties arise when attempting to apply this form of simplistic, brute-force approach to real data. Specifically, the number of unknowns and reasonable accuracy of the model become cumbersome when applied to realistic conditions. When applying this methodology to David Taylor Model 5514 data, it was quite apparent that idealizing the forcing as being at a single magnitude and frequency would result in inaccurate approximations to the actual case. Adding more forcing amplitude/frequency terms and/or more degrees of freedom results in an excessive number of unknowns for such a brute force optimization based approach.

In an on-board sense, to generate a simplified model for brief predictions of ship behavior, it is possible these difficulties could be overcome by idealizing the system as an oscillator with slowly varying coefficients. As such, a low-order model would be used for an optimal fit over short increments of time and continuously updated. In a similar vein, a neural-network could be used both to select an optimal model of the system and to predict motions. The work of Hess *et al.* has shown great promise for the use of recursive neural networks in maneuvering simulation (Hess *et al.*, 2006).

Clearly for the simplistic case presented above, in which the coefficients of the equation of motion are known, lower and/or different order approximations to the coefficients for Equation 2 could be generated with a least squares regression within some critical range of roll angles or roll velocities (Dalzell, 1978). However, it is a matter of intelligently determining an approximated form of equations of motion, appropriate time scale, and incorporating a sufficiently powerful optimization/determination method to extend this approach to actual experimental data. For example, to overcome the hurdles present with random waves, one might choose to provide an input of wave elevation whilst optimizing on remaining parameters. Alternatively, one might conclude that the truest necessity for predicting large motions is approximating only the next few roll cycles rather than an entire time series thus reducing the difficulty and time cost of an optimization routine.

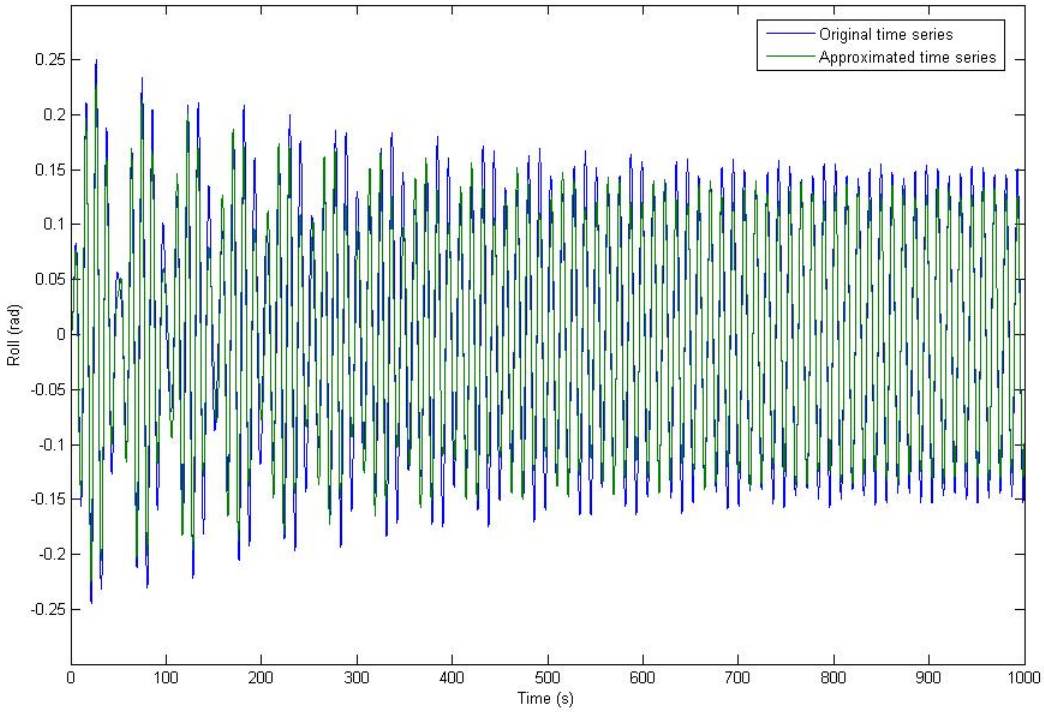

Figure 5: Original and approximated time series for roll/roll velocity initial conditions of < 0, 0 >. Approximated equations of motion generated from optimizing fit to time series data with initial conditions of < 0.4, 0 >.

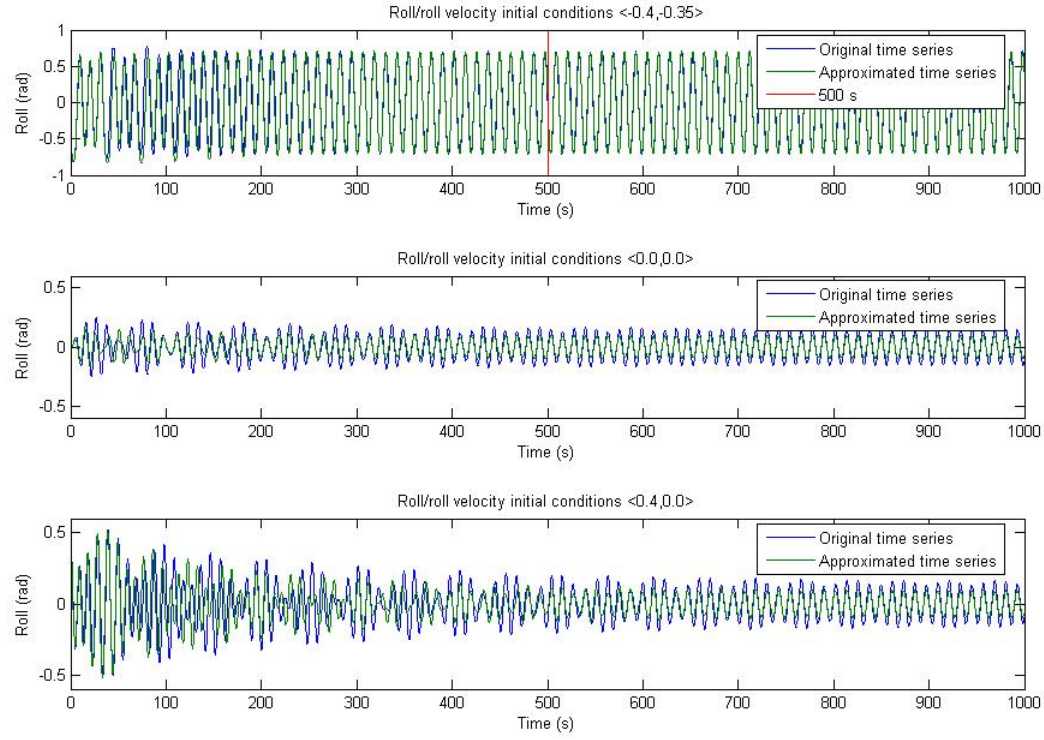

Figure 6: Original and approximated time series for roll/roll velocity initial conditions of < −0.4,−0.35 > (top), < 0, 0 > (middle), <0.4, 0 > (bottom). Approximated equations of motion generated from optimizing fit to timeseries data with initial conditions of <−0.4,−0.35 >.

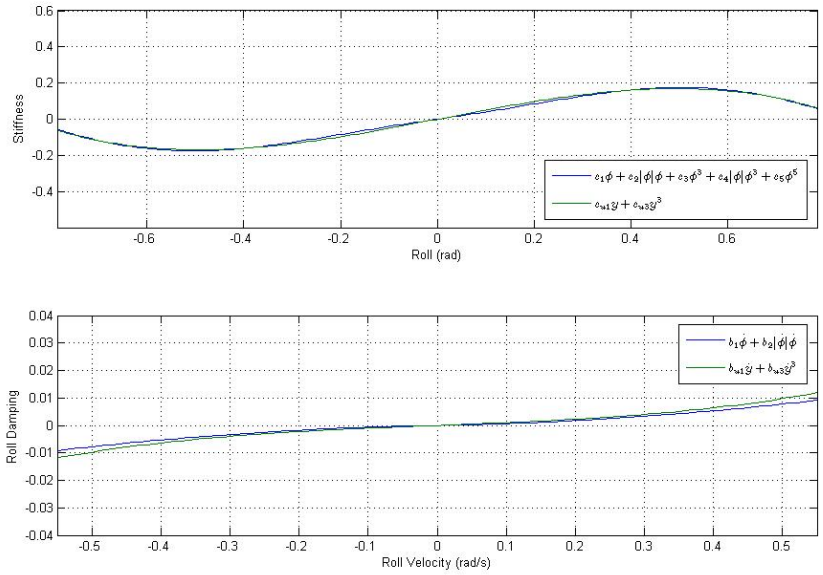

Figure 7: Comparison of original and approximated stiffness and roll damping curves for roll/roll velocity initial conditions of <−0.4,−0.35>.

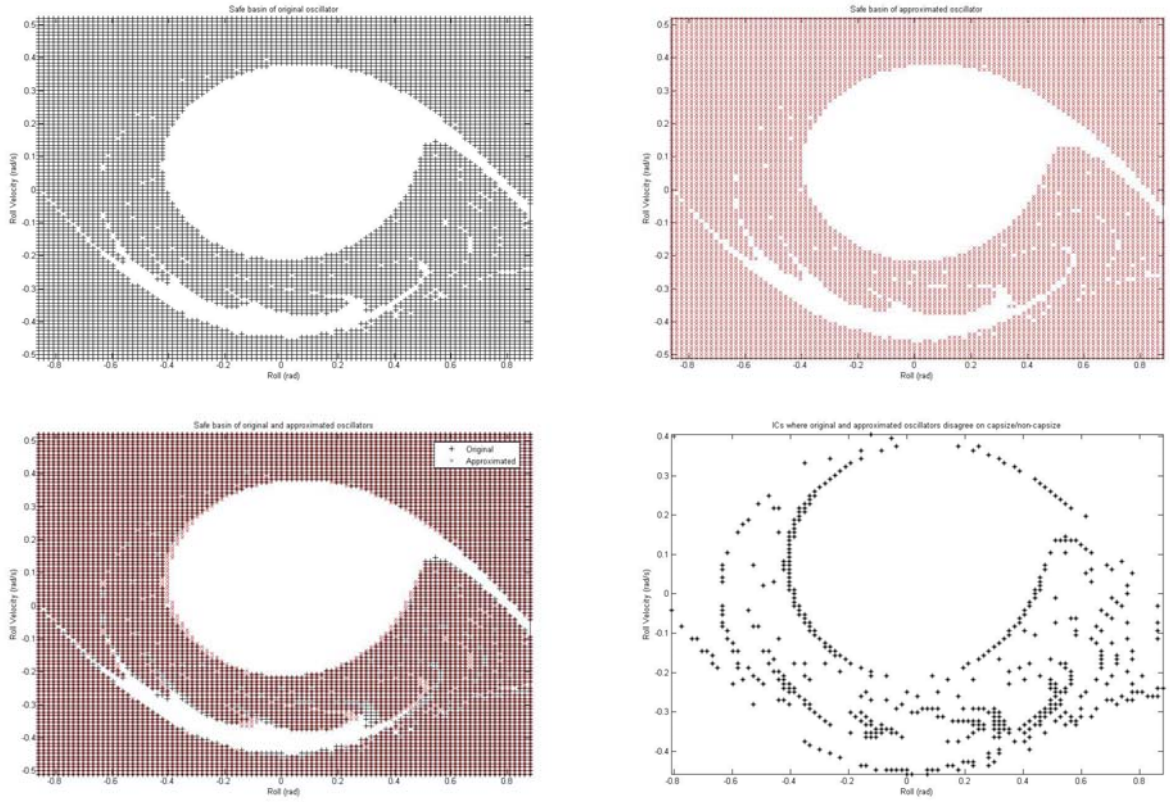

Figure 8: Safe basin for actual equations of motion Eq. 1 (upper left) and approximated equations of motion Eq. 2 (upper right). Both basins plotted together for comparison (lower left) and points in which the approximated and exact solutions disagree highlighted (lower right). Approximated equations of motion generated from optimizing fit to time series data with initial conditions of <−0.4,−0.35>.

ACKNOWLEDMENTS

The authors wish to acknowledge support from the ASEE-ONR Summer Faculty Research Program, and the Hydromechanics Department of the Carderock Division of the Naval Surface Warfare Center. This research was supported in part by funding from the DDG 1000 Phase IV Hull Form Program under Department of the Navy Prime Contract Number N00167-04-D-0004.

REFERENCES

Bhattacharyya, Rameswar. 1978. *Dynamics of marine vehicles*. John Wiley & Sons.

Breeden, Joseph L., & Hübler, Alfred. 1990. Reconstructing equations of motion from experimental data with unobserved variables. *Physical Review A*, **42**(10), 5817–5826.

Cremers, J., & Hübler, A. 1987. Construction of differential equations from experimental data. *Zeitschrift für Naturforschung A*, **42**, 797–802.

Crutchfield, James P., & McNamara, Bruce S. 1987. Equations of motion from a data series. *Complex Systems*, **1**, 417–452.

Dalzell, J.F. 1978. A note on the form of ship roll damping. *Journal of Ship Research*, **22**(3), 178–185.

Eisenhammer, T., Hübler, A., Packard, N., & Kelso, J.A.S. 1991. Modeling experimental time series with ordinary differential equations. *Biological Cybernetics*, **65**, 107–112.

Fossen, Thor I. 1994. *Guidance and control of ocean vehicles*. John Wiley & Sons.

Hess, D., Faller, W., Lee, J., Fu, T., & Ammeen, E. 2006. Ship maneuvering simulation in wind and waves: a nonlinear time-domain approach using recursive neural networks. *In: 26th Symposium on Naval Hydrodynamics.*

Lewandowski, Edward M. 2004. *The dynamics of marine craft*. World Scientific.

Lewis, Edward V. (ed). 1989. *Principles of Naval Architecture Second Revision. Vol. III*. Society of Naval Architects and Marine Engineers.

Soliman, M. S., & Thompson, J. M. T. 1991. Transient and steady state analysis of capsize phenomena. *Applied Ocean Research*, **13**(2).

Suleiman, Baha M. 2000 (December 11). *Identification of finite-degree-of-freedom models for ship motions*. Ph.D. thesis, Virginia Polytechnic Institute and State University, Blacksburg, Virginia.

Suleiman, B.M., Fahey, S. O'F., Nayfeh, A.H., & Hajj, M.R. 2000 (May 21-24). Identification of coefficients in coupled heave and pitch equations with forward speed effects. *In: EM 2000 14th Engineering Mechanics Conference*. ASCE, Autin, TX.

A Study on the Characteristics of Roll Damping of Multi-hull Vessels

Toru Katayama, Masanori Kotaki and Yoshiho Ikeda

Department of Marine System Engineering, Graduate School of Engineering,
Osaka Prefecture University

ABSTRACT

In this study, for a catamaran and a trimaran as multi-hull vessels, the characteristics of the roll damping are investigated experimentally. A free roll decay test and a forced roll motion test with and without forward speed are carried out. The results show that the roll damping of them is much larger than that of conventional mono-hull vessels, and the component created by side-hull accounts for a significant rate for trimaran. Especially, at the condition without forward speed, the interference of waves created by hulls are significant, the measured roll damping values by different experiments are different on the basis of different water surface condition created by hulls. Moreover, the simplified prediction method is proposed.

KEYWORDS

Catamaran, Trimaran, Roll damping, Wave making component, Eddy making component

INTRODUCTION

They are very important to understand the characteristics of the roll damping for any kind of vessels and to estimate it adequately, because it is significantly affect on the occurrence of parametric rolling, the amplitude of resonances and so on. However, it is very complicated to calculate the roll damping theoretically, because of significant viscous component depending on vortex shedding.

It is known that there is a prediction method of the roll damping proposed by Ikeda (one of authors) for conventional displacement type of mono-hull vessels, barge ships and a small hard chine fishing boat. It is composed of wave making, friction, transverse lift and eddy making prediction component those are developed with theoretically and experimentally backgrounds based on the hydrodynamic characteristics of the roll damping for the above-mentioned types of vessels. Therefore, it is difficult to apply the method to the resent vessels that have large different hull form from above-mentioned types of vessels.

In this study, for catamaran and trimaran as multi-hull vessels, the characteristics of the roll damping are investigated experimentally. And based on the results, the simplified prediction method is proposed.

MODELS

The photographs of two model ships are shown in Figs. 1 and 2, and their principle particulars are shown in Tables 1 and 2. The model of catamaran in Fig.1 is wave piercing type high-speed craft, and its loading conditions are decided by based on over-100m class wave piercing catamaran. On the other hand, the model of trimaran in Fig.2 is stabilized slender mono-hull type high-speed craft, and its distributions of displacement for main-hull and side-hulls are decided by based on a real high speed vehicle-passenger trimaran ferry.

Fig. 1: Model of catamaran.

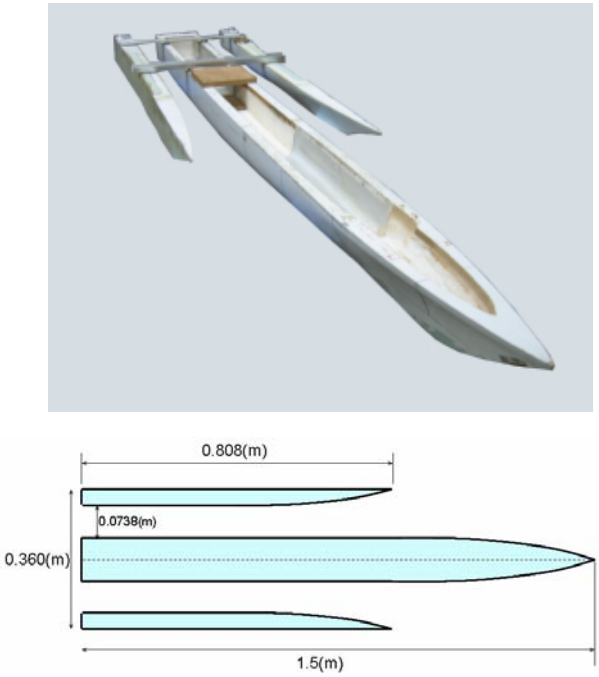

Fig. 2: Model of trimaran and its hull arrangement.

Table 1: Principal particulars of trimaran.

	main-hull	side-hull
L/B	12	10.2
L_{OA} (m)	1.5	0.888
L_{pp} (m)	1.42	0.808
breadth (m)	0.125	0.0874
depth (m)	0.1	0.07
draft (m)	0.037	0.012
displacement (N)	30.8	0.778×2
GM (m)	0.163	
T_n (sec)	1.04	

Table 2: Principal particulars of catamaran.

Scale	1/80
L_{OA} (m)	1.408
L_{PP} (m)	1.32
breadth(m)	0.38
depth (m)	0.07
draft (m)	0.04
displacement (N)	20.9×2
GM (m)	0.85
T_n (sec)	0.46

CHARACTERISTICS OF ROLL DAMPING WITHOUT FORWARD SPEED

In order to investigate the characteristics of roll damping of the models, at first, a free roll decay test is carried out without forward speed. In this test, for model, heaving, pitching, rolling, swaying and yawing are free, and it is initially heeled by fixing only rolling at arbitrary angle. From the condition with which model's attitude is balancing, motions are measured after freeing rolling.

The measured damping curves of rolling for each model are shown in Figs.3 and 4. The result for trimaran in Fig.3 seems to continuously damp, on the other hand, the result for catamaran in Fig.4 shows that the damping curve has some different periods and it damps irregularly.

Therefore, in this study, the results of the free roll decay test with catamaran, only the first swing is analyzed. And the results of the same test with trimaran are analysed for the first swing and other swings separately.

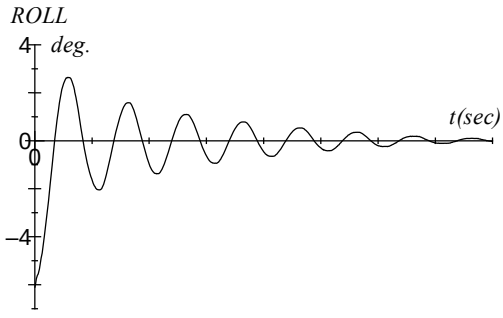

Fig. 3: Time histories of roll motion of the trimaran.

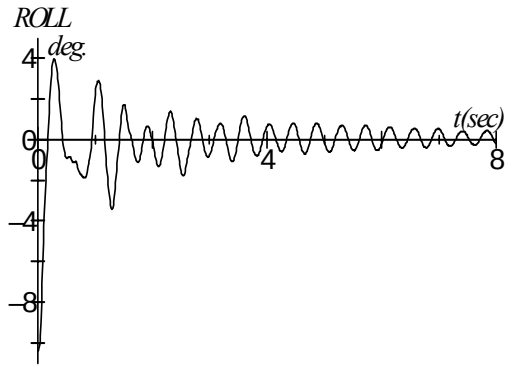

Fig. 4: Time histories of roll motion of the catamaran.

As another measurement of the roll damping, a forced roll motion test is also carried out. In the analysis, one degree of freedom of rolling motion equation is used, in which nonlinear terms are replaced by equivalent linear terms,

$$(I_{44} + a_{44})\ddot{\phi} + B_{44}\dot{\phi} + C_{44}\phi = M_R \qquad (1)$$

where (I_{44} + a_{44}), B_{44}, C_{44} and M_R denote the inartia term, damping term, restoring term and roll excitation moment, respectively. In this test, model is forced to sinusoidal rolling around the center of gravity as $\phi = \phi_a \sin \omega t$.

The measured roll moment is represented with Fourier series. Using the Fourier coefficient of the fundamental period for measured M_R, the amplitude M_{RF} in phase of roll angular velocity of measured M_R is obtained, and B_{44} is written as follows.

$$B_{44} = \frac{M_{RF}}{\phi_a \omega} \qquad (2)$$

where ω and ϕ_a are roll circular frequency and amplitude. The roll damping coefficient B_{44} can be represented by Bertin's N-coefficient on the condition that the energy losses of them in one period are equal,

$$B_{44} = 2g\rho\nabla \frac{GM\ \phi_a}{\pi\ \omega} N \qquad (3)$$

where ∇ is displacemental volume, and the unit of ϕ_a is degree. And B_{44} is non-dimensionalized as follow.

$$\hat{B}_{44} = \frac{B_{44}}{\rho\nabla B^2}\sqrt{\frac{B}{2g}} \qquad (4)$$

where B is breadth of vessel.

In Fig.5, the relative positions of the models to the water surface when the model has heel angle. In the free roll decay test, the initial heel angles, where hull of model is not exposed the air, are selected. And the experimental conditions in forced roll motion test are shown in Table 3.

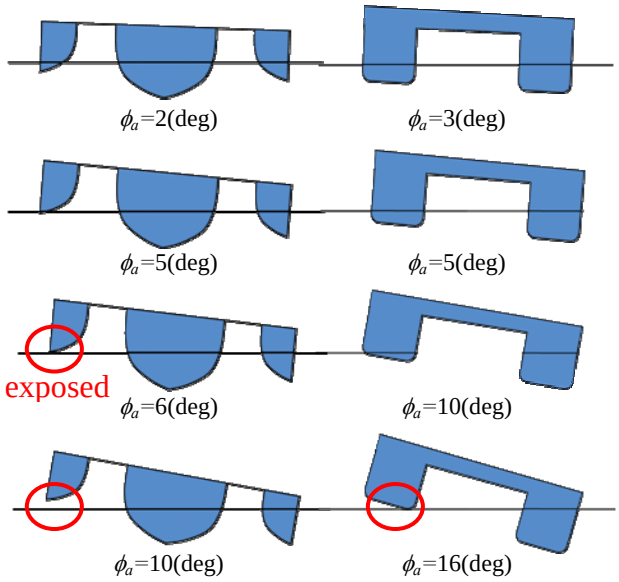

Fig. 5: Relative position of the heeling model to the water surface.

Table 3: Experimental conditions in forced roll motion test.

	trimaran	catamaran
center height of roll motion (m)	0.163	0.85
trim angle (deg)	0	0
forced rolling period: T (sec)	0.4, 0.8, 1.04, 1.3	0.3, 0.46, 0.7, 1.0
roll amplitude: ϕ_a (deg)	2, 5, 10	3, 5, 10

In Figs.6 ~ 9, B_{44} and N-coefficient for two models are shown. From the results of N-coefficient for both models in Figs.6 and 7, it is confirmed that their roll damping are sensuously large in comparison with it for common mono-hull vessels and the N_{10} is about 0.08. On the other hand, from the results of B_{44}, the effect of amplitude is observed. And, from Figs.8 and 9, the effect of roll period is also clearly found.

On the comparisons among different tests and analysis, quantitatively slightly different results are obtained. The results for trimaran show

that the results of the first swing of the free roll decay test indicate lager value than those of the other swing of the same test and the forced roll motion test. For the results for catamaran, the same tendency is also observed. As a reason of this, it is supposed that the free surface conditions in these tests are different and there is the disturbed water surface by previous swing excepting the results of the first swing of free roll decay test.

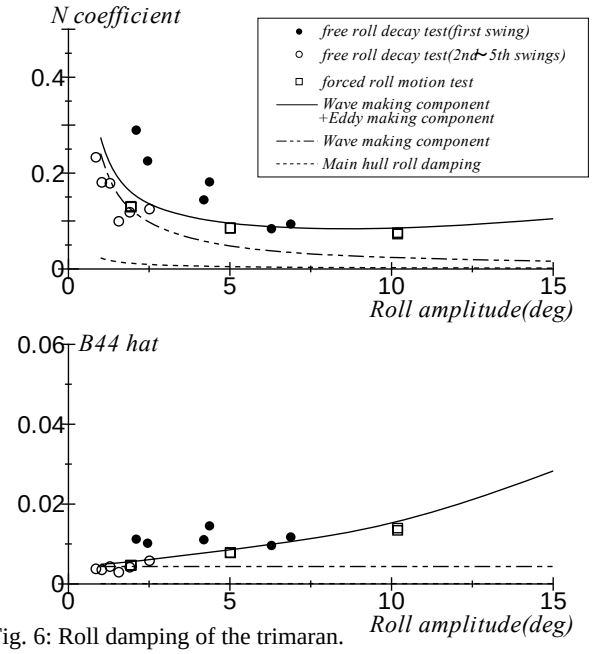

Fig. 6: Roll damping of the trimaran.

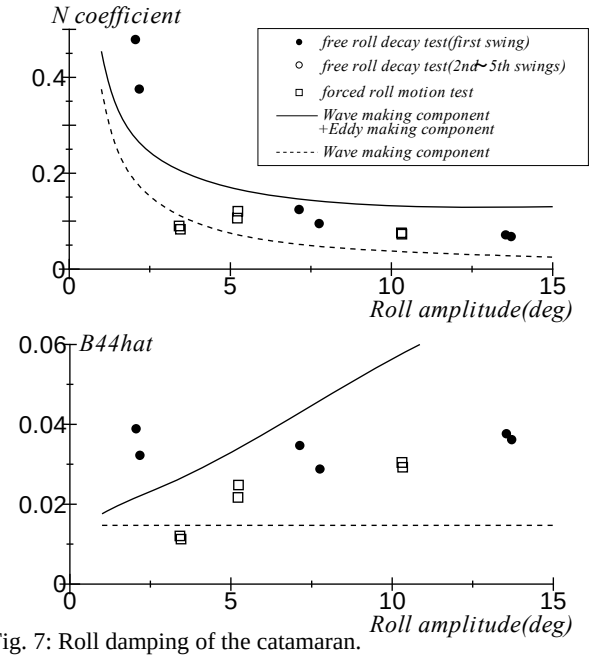

Fig. 7: Roll damping of the catamaran.

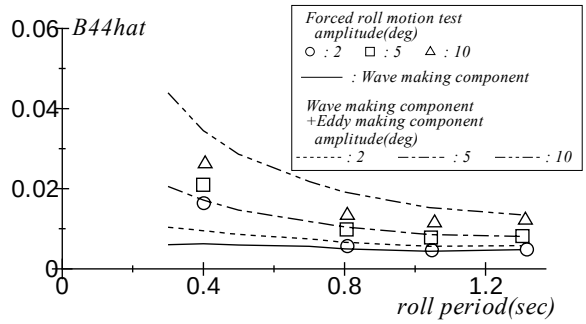

Fig. 8: Roll damping of the trimaran.

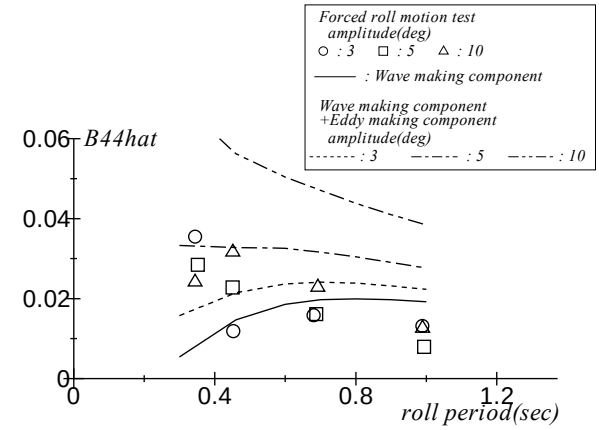

Fig. 9: Roll damping of the catamaran.

As reasons for the effect of amplitude on B_{44}, the nonlinearity of wave component caused by large amplitude motion, the interference of wave among hulls and the viscosity effects are occurred to. In Figs.8 and 9, the effect is also clearly observed for small amplitude. Therefore the viscosity component is considered in this study.

Fig.10 shows significant roll damping components acting on catamaran. One of them is the wave making component B_W which is created by the almost vertically oscillating demi-hull. This component can be roughly estimated by using the heave potential damping of demi-hull B_{33} as following equation.

$$B_W\dot{\phi} = B_W\omega\phi_a = 2l\ B_{33}\ l\omega\phi_a = 2l^2\ B_{33}\dot{\phi} \quad (4)$$

where l is the distance of demi-hull from the centre line shown in Fig.10. It is noted that the B_{43} is not include the interference of wave among hulls, in this study. Another component is the eddy making component and this component acts on the demi-hull moving

upward shown in Fig.10. This component can be expressed by using drag coefficient C_{DA}.

$$B_E\dot{\phi} = \frac{1}{2}\rho S C_{DA}(l\omega\phi_a)^2$$
$$\cong l^2\frac{8\omega\phi_a}{3\pi}\rho S C_{DA}(\omega\phi_a) \qquad (5)$$
$$= l^2\frac{8\omega\phi_a}{3\pi}\rho S C_{DA}\dot{\phi}$$

where ρ is density of fluid, S is hull projected area from below. In this study, C_{DA} is obtained from the data in Fig.11 and following equation.

$$C_{DA} = C_D - C_{DF} \qquad (6)$$

In Fig.11, C_D is the total drag coefficient of a 2-D section for a c/t, and C_{DF} and C_{DA} are the drag coefficients acting on forward-body and aft-body of the 2-D section, respectively. And C_{DF} is the drag coefficient at $c/t=\infty$. Moreover, C_{DA} is including roughly KC number effects by using the ratio of C_D for a KC number shown in Fig.12. In this study, KC number is assumed the following equation.

$$KC = \frac{2\pi l\phi_a}{\omega b}\left(Rn = \frac{2\pi l\phi_a d}{\nu}\right) \qquad (7)$$

where b is the breadth of cross section of demi-hull. For catamaran, the total roll damping is calculated by adding these two components. On the other hand, for trimaran, the total roll damping is calculated by adding these two components and the main-hull's roll damping calculated by Ikeda's prediction method[1].

In Figs.6 ~ 9, the estimated B_{44} is also shown as lines. The estimation can express the effects of roll amplitude and period for the trimaran, however, can not always for the catamaran. As one of reasons for the difference, it is supposed that the interference of waves among hulls is significant for the catamaran.

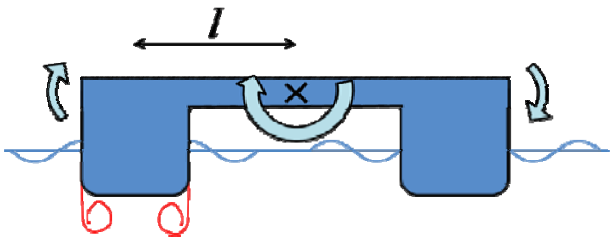

Fig. 10: Roll damping components for catamaran.

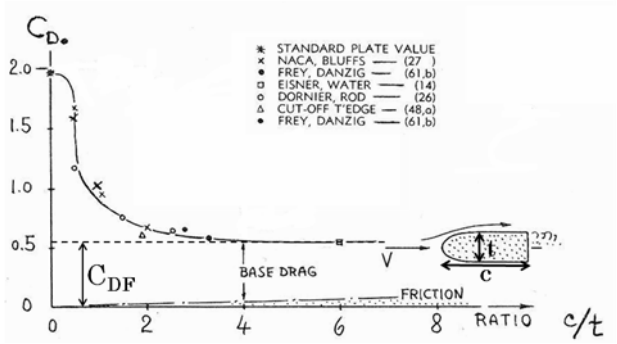

Fig. 11: Drag coefficients of 2-D section with several aspect ratio c to t. In this study, c is draft and t is breadth of demi-hull. (S. F. Hoerner, 1965)

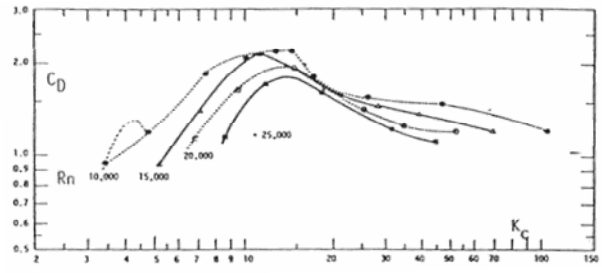

Fig. 12: KC number's effects of drag coefficient for cylinder. (Kuelegan G.H., Carpenter L.H., 1958)

CHARACTERISTICS OF ROLL DAMPING WITH FORWARD SPEED

In order to investigate the characteristic of the roll damping with forward speed, the forced roll motion test is carried out. In this test, the cases of forward speed are decided by based on the maximum speed of some real multi-hull high-speed craft. The experimental condition is shown in Table 4.

Table :4 Experimental conditions in forced roll motion test.

	trimaran	catamaran
Fn	0.148, 0.296 0.443, 0.591	0.136, 0.272 0.407, 0.543
trim angle (deg)	0	0
forced rolling period: T (sec)	0.4, 0.8 1.04, 1.3	0.3, 0.46 0.7, 1.0
roll amplitude: ϕ_a (deg)	2, 5, 10	3, 5, 10

In Figs.13 and 14, B_{44} for two models are shown, and their forced roll periods are their roll natural periods, respectively. For the results of the trimaran in Fig.13, the effect of forward speed on B_{44} is small. On the other hand, for the catamaran in Fig.14, the effect is significant.

In Figs.15 and 16, the effects of roll period on B_{44} for two models are shown, and their *Fn* are their service speed, respectively. The result of the trimaran in Fig.15 shows the same tendency as the results at *Fn*=0. On the other hand, the result of the catamaran in Fig.16 shows the different tendency from the results at *Fn*=0.

CONCLUSIONS

In this study, in order to investigate the characteristics of the roll damping for multi-hull vessel, the roll damping of a catamaran and a trimaran is measured. And Some conclusions can be remarked as follow.

1. In the result of free roll decay test, time histories of roll motion of the catamaran damp irregularly. This is caused by the interference of waves created by hulls.
2. The roll damping for the multi-hull has the effects of roll amplitude and period. The effects for the trimaran can be expressed by the eddy making component created by the demi-hull moving upward. However, it is not enough for the catamaran and it may be necessary to consider the interference of waves created by hulls.
3. The effect of forward speed on the roll damping for trimaran is small. On the other hand, the effect for the catamaran is significant, and the characteristics for the catamaran is different from that at *Fn*=0.

REFERENCES

Ikeda Y, Roll Damping, The 1th Symposium of Marine Dynamics Research Group, 1984, pp. 241-249

Motora S, Koyama T, Fujino M, Maeda H, Dynamics of Ships and Offshore Structures, 1997

S. F. Hoerner, FLUID-DYNAMIC DRAG, 1965

Kuelegan G.H., Carpenter L.H., Forces on Cylinders and Plates in an Oscillating Fluid, J. Res. Nat. Bur. Standard, LX No. 5, 1958, pp.423-440

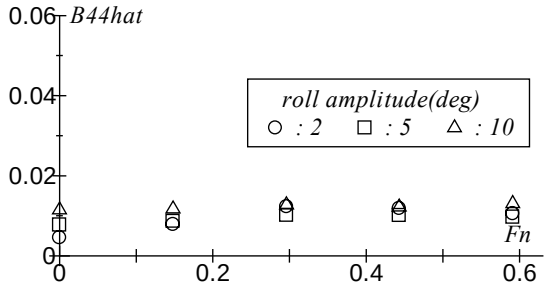

Fig.13: Roll damping of the trimaran at the roll natural period.

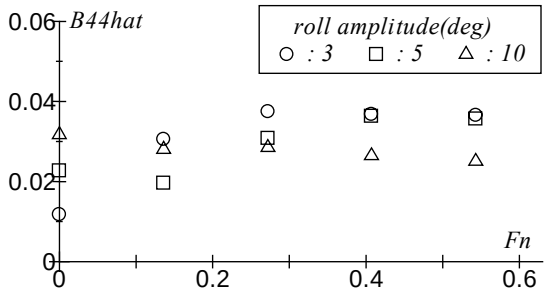

Fig.14: Roll damping of the catamaran at the roll natural period.

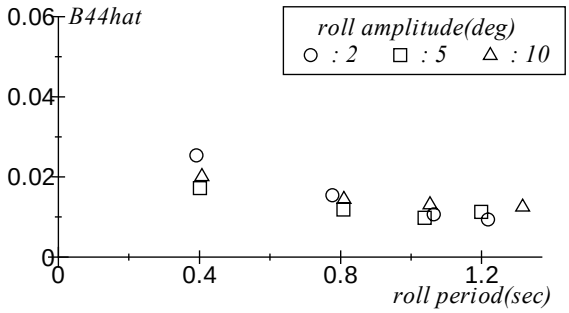

Fig. 15: Roll damping of the trimaran at *Fn*=0.591.

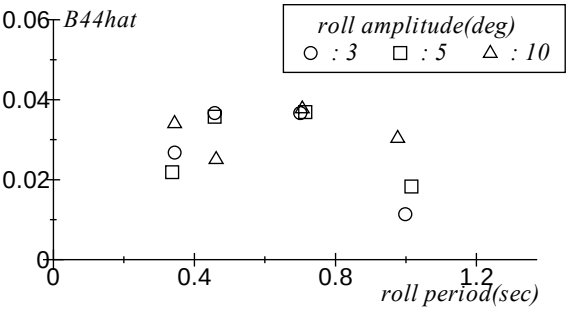

Fig. 16: Roll damping of the catamaran at *Fn*=0.543.

Dynamic Stability of Flared and Tumblehome Hull Forms in Waves

Christopher Bassler, *Seakeeping Division, Naval Surface Warfare Center, Carderock Division*

Andrew Peters, *QinetiQ*

Bradley Campbell, *Seakeeping Division, Naval Surface Warfare Center, Carderock Division*

William Belknap, *Seakeeping Division, Naval Surface Warfare Center, Carderock Division*

Leigh McCue, *Aerospace and Ocean Engineering, Virginia Tech*

ABSTRACT

A numerical seakeeping code was used to examine the influence of wave conditions, ship initial conditions, and ship operating parameters on dynamic stability events in regular and irregular waves, and assess variations in ultimate stability for changes in the center of gravity (KG) for two hull forms, flared and tumblehome. The results of this investigation aid in better understanding the influence of increased KG over the life-cycle of the ship, the ramifications of error in KG measurements, the required safety factor or error band in operator guidance, and the sensitivity of these variations to hull form geometry.

KEYWORDS

dynamic stability; capsize; broach; surfride; tumblehome; KG

INTRODUCTION

The increased desire for utilization of unconventional hull form designs necessitates improved understanding of the stability characteristics of these novel ship types. An essential component to ensuring the safety of these new ship types is a complete understanding of how stability performance for these vessels differs from conventional hulls. All vessels experience an increase in weight over the life-cycle of the ship, and often times this additional weight is placed on upper deck locations aboard a ship, leading to an increase in the height of the ship's center of gravity (KG). Understanding the sensitivity of this increase in KG for conventional and unconventional hull forms is necessary to accurately assess the safety of a ship.

In this study, a numerical seakeeping code, FREDYN 9.8, was used to examine the influence of wave conditions, ship initial conditions, and ship operating parameters on vessel capsize in regular and irregular waves, and determine the sensitivity of capsize to changes in the KG for two topside configurations. The investigation consisted of two parts, in regular and random seas, which were used to examine dynamic stability events and the interrelationship of KG and hull form geometry with various headings, speeds, and initial conditions.

MODEL GEOMETRY

The Office of Naval Research (ONR) Topside Series hull forms were designed for the purpose of providing a publicly available hull form which could be used to examine resulting differences from varying topside geometry, particularly for conventional and novel topside designs. The hulls feature a common naval combatant-type hull form below the design waterline. The above-waterline geometry consists of three topside configurations: wall-side (ONRWS), flared (ONRFL), and tumblehome (ONRTH). For this investigation the ONRFL and ONRTH hulls (Figures 1 and 2) were used to examine the impact of topside geometry on the risk of dynamic instability of a vessel in regular and random seas.

Fig. 1: ONR Topside Series Hull Forms- ONRFL (top) and ONRTH.

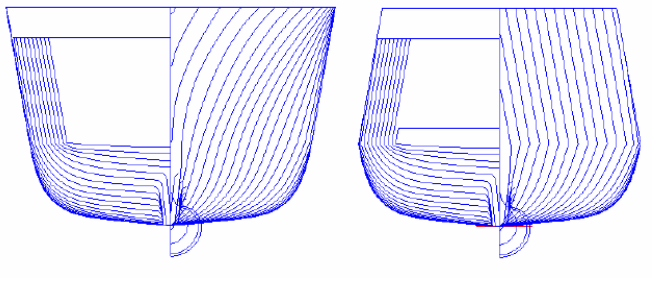

Fig. 2: Section View of ONRFL (left) and ONRTH.

Table 1: Ship Principle Dimensions for ONR Topside Series Hull Forms

Length	154 m
Beam	18.8 m
Draft	5.5 m
Displacement	8790 tonnes
LCB (aft of FP)	79.6 m
KM	9.74 m

NUMERICAL SIMULATIONS

Simulations of the ONRFL and ONRTH in regular and random seas were performed using FREDYN 9.8. FREDYN is a blended method maneuvering and seakeeping code (linear hydrodynamic forces, body-exact Froude-Krylov and hydrostatic forces) developed by the Cooperative Research Navies (McTaggart and de Kat). Computations were performed on Linux clusters at both NSWCCD and QinetiQ. Capsize and other dynamic stability events including broaching, mild-broaching, and surfriding, were investigated at incremental KG values (Table 2) in both regular and random seas. Radii of gyration were equal between both geometries and held constant across all KG values.

Table 2: ONRFL and ONRTH Numerical Loading Conditions

Hull Form*	KG (m)
ONRTH	*6.25*
ONRTH	*6.5*
ONRTH	*6.75*
ONRTH	*7*
ONRFL, ONRTH	7.25
ONRFL, ONRTH	7.75
ONRFL, ONRTH	8
ONRFL, ONRTH	8.25
ONRFL, ONRTH	8.5
ONRFL, ONRTH	8.75
ONRFL	*9*
ONRFL, ONRTH	9.25
ONRFL, ONRTH	9.5
ONRFL	*9.6*

* Italicized values indicate additional values included for the random seas study

Regular Seas

A systematic investigation of capsize was performed for varied ship roll/roll velocity initial conditions, at incremental KG values (Table 2), in stern-quartering seas. The study was conducted for a ship with constant forward speed in regular waves of varying steepness and for a constant wavelength to ship length ratio (Table 3). Simulations were performed for both the ONRFL and ONRTH hull forms.

Table 3: Regular Seas Input Parameters

Parameter	Value	Increment
Initial Roll	-88 to 88 deg	1 deg
Initial Roll Velocity	-50 to 50 deg/s	1 deg/s
Heading	45 deg	Constant
Speed (Fn)	0.3	Constant
Wavelength/Ship Length Ratio (λ/L)	1.25	Constant
Wave Height (m)	0, 6, 9, 12 to 20	3m, 1m
Wave Period (s)	11.104	Constant

Random Seas

A capsize sensitivity study was conducted for both the ONRFL and ONRTH with varied KGs (Table 2), speeds, and headings, in random seas. Twenty-five random wave seed 1800 second simulations were performed at each KG, in 15 degree heading increments for 7 speeds (Table 4) in each of the specified sea state 8 conditions (Table 5), resulting in 4200 total runs for each ship.

Table 4: Random Seas Input Parameters

Parameter	Value	Increment
Speeds	0 to 30 knots	5 knots
Heading	0 to 180 deg	15 deg

The ships were tested in sea state 8 conditions using a Bretschneider spectrum with 90 wave components. Three spectrum combinations were used, representing a most- probable sea state 8 condition (3), an intermediate case (2), and worst-case wave steepness conditions (1).

Table 5: Wave Conditions

Sea State 8 Condition	Significant Wave Height (m)	Modal Period (s)
1	9.0	10.4
2	11.5	15.0
3	11.5	16.4

Occurrences where dynamic stability event criteria (NSWCCD Seakeeping Department, 2003) were exceeded (Table 5), including capsize, broaching, mild-broaching, and surfriding, were recorded as a function of speed and heading.

Table 5: Definitions of Dynamic Stability Event Criteria

Event	Criteria
Capsize	Roll angle > 89 deg
Broach	Yaw angle > 30 deg Yaw Rate > 3 deg/s
Mild-Broach	Yaw angle > 15 deg
Surfride	V_g > 1.10* calm-water speed Pitch rate > 0.1 deg/s Yaw rate < 0.1 deg/s

RESULTS

Regular Seas

Integrity values, defined as the ratio of safe area, runs where capsize did not occur, to total area, the total number of runs, were utilized to examine changes in stability with increasing wave height for varying KG values. Integrity curves for KG values corresponding to realistic

vessel loading conditions are shown in Figures 2 and 3. The values shown were normalized to the integrity value of the ONRFL for KG=7.25 m in 0 m waves, corresponding to 1, enabling comparisons to be made between the two figures.

As utilized in this study, safe basins are plots of capsize based on a ship's initial conditions, initial roll angle vs initial roll velocity, in a given seaway. The white region indicates areas of safety, where the vessel did not capsize for the given initial conditions, and the dark region indicates areas of safety risk, where capsize did occur for the specified initial conditions.

In Figure 4, the ONRTH at the KG= 7.75m value, significant safe basin erosion occurred between the 12m wave height to 20 m wave height. For the ONRTH, the erosion of the safe basins occurred more rapidly for increasing KG values, as would be expected with a more unstable ship. The reduction of the integrity values, and corresponding degradation of the safe basins for regular waves of increasing heights, varied significantly for the ONRFL and ONRTH vessels.

Random Seas

The variation of the total number of capsizes for the 4200 total runs is shown over a range of KG values for all headings and speeds for both the ONRFL and ONRTH in three sea state 8 conditions (Figure 5).

For corresponding wave conditions, a significant difference can be observed between the flared and tumblehome hull forms, at similar KG values. For the worst-case sea state 8 conditions, the number of capsizes for a given KG value is much greater for the tumblehome topside when compared to the flare topside geometry. From this plot, it can be observed that the tumblehome topside requires about a 1m-1.5 m increase in KG (thus GM) to achieve a number of capsizes similar to the flared hull topside hull form.

The capsize risk increased for both topside configurations for worsening sea state 8 conditions. The capsize risk for the tumblehome geometry had a greater increase than the flared topside geometry over a smaller range of incremental KG values.

Comparison plots of twenty-five simulations of the ONRFL and ONRTH in the most probable sea state 8 conditions are shown for number of capsizes for varying KG values over a range of forward speeds for four headings: following, stern-quartering, beam and head seas (Figures 6-13).

As shown, the number of capsizes for the most-probable sea state 8 conditions increased drastically for the tumblehome topside for following, stern-quartering, beam and head seas. As expected, the capsize risk increased for both topside geometries with worsening sea state 8 conditions and with increasing forward speed. However the capsize risk for the tumblehome geometry had a greater increase for small increases in KG than the flared topside geometry.

Polar plots for capsize, broaching, mild-broach, and surfriding are shown for the 8.25m KG value in the most probable sea state 8 conditions (Figures 14 and 15).

A sharp increase in the number of capsizes for the tumblehome hull form occurred after the 8.25m KG value. The tumblehome topside travelling at moderate to high speeds in stern-quartering to near beam seas was observed to be the worst-case scenario for capsize from the polar plots. Similar risk susceptibilities for both the ONRFL and ONRTH were observed for broaching and mild-broaching. Broaching and mild-broach risk occurrence was observed to be worst at low speed, less than 5 knots, in bow-quartering and head seas, as well as stern-quartering seas. Mild-broach occurrence increased with increasing speed, and was observed up to 20 knots for both the ONRFL and ONRTH.

Surfriding occurrences were observed to be worst for following and near-following seas with continued risk at high speeds near a stern-quartering heading. Surfriding risk was slightly decreased for the tumblehome topside compared to the flared topside at the slower speeds and near stern-quartering seas.

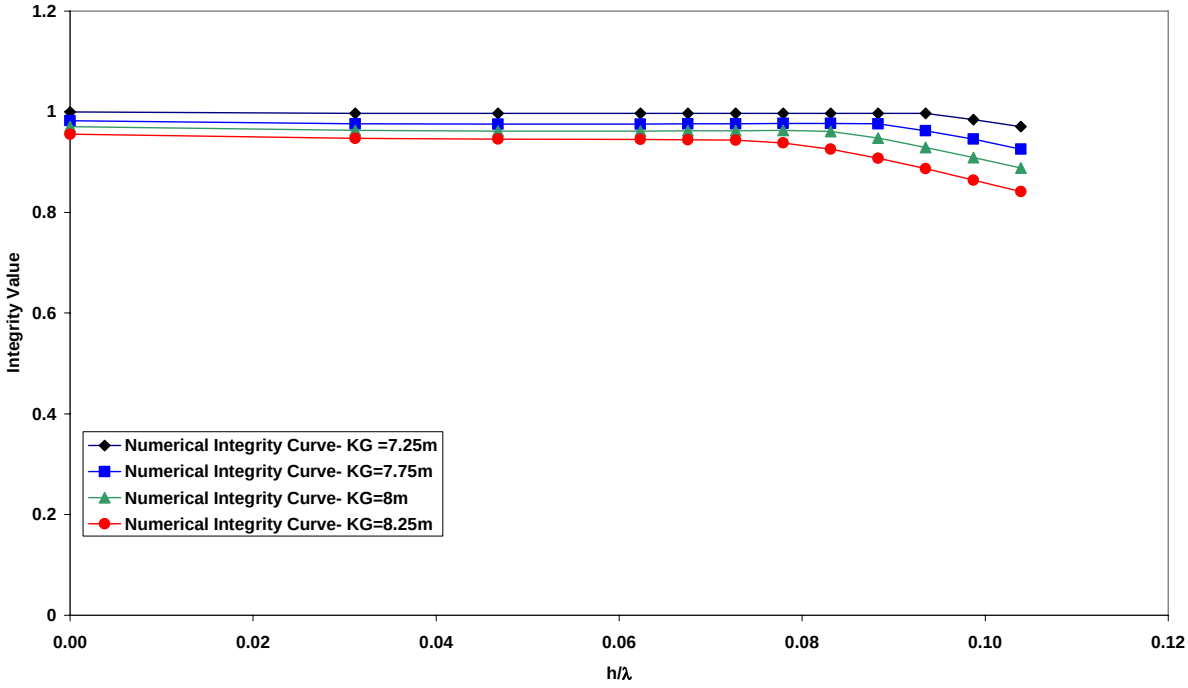

Fig. 2: Integrity Curves for ONRFL for various KGs at Fn=0.30, in stern quartering seas, λ/L=1.25

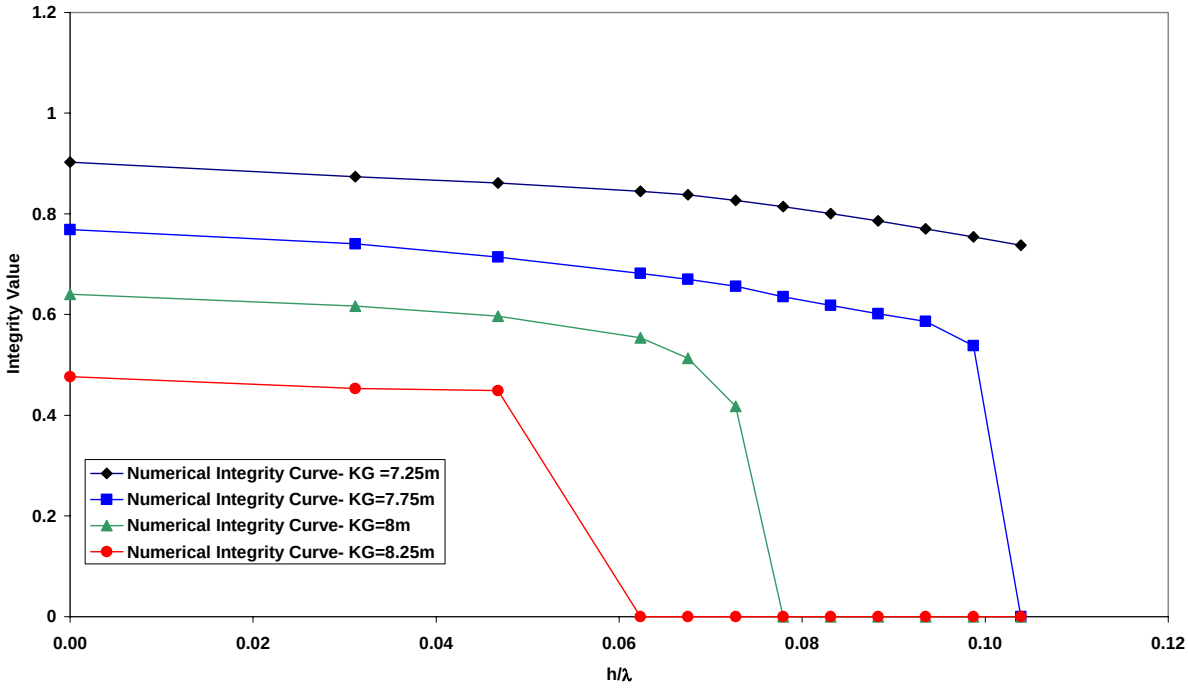

Fig. 3: Integrity Curves for ONRTH for various KGs at Fn=0.30, in stern quartering seas, λ/L=1.25

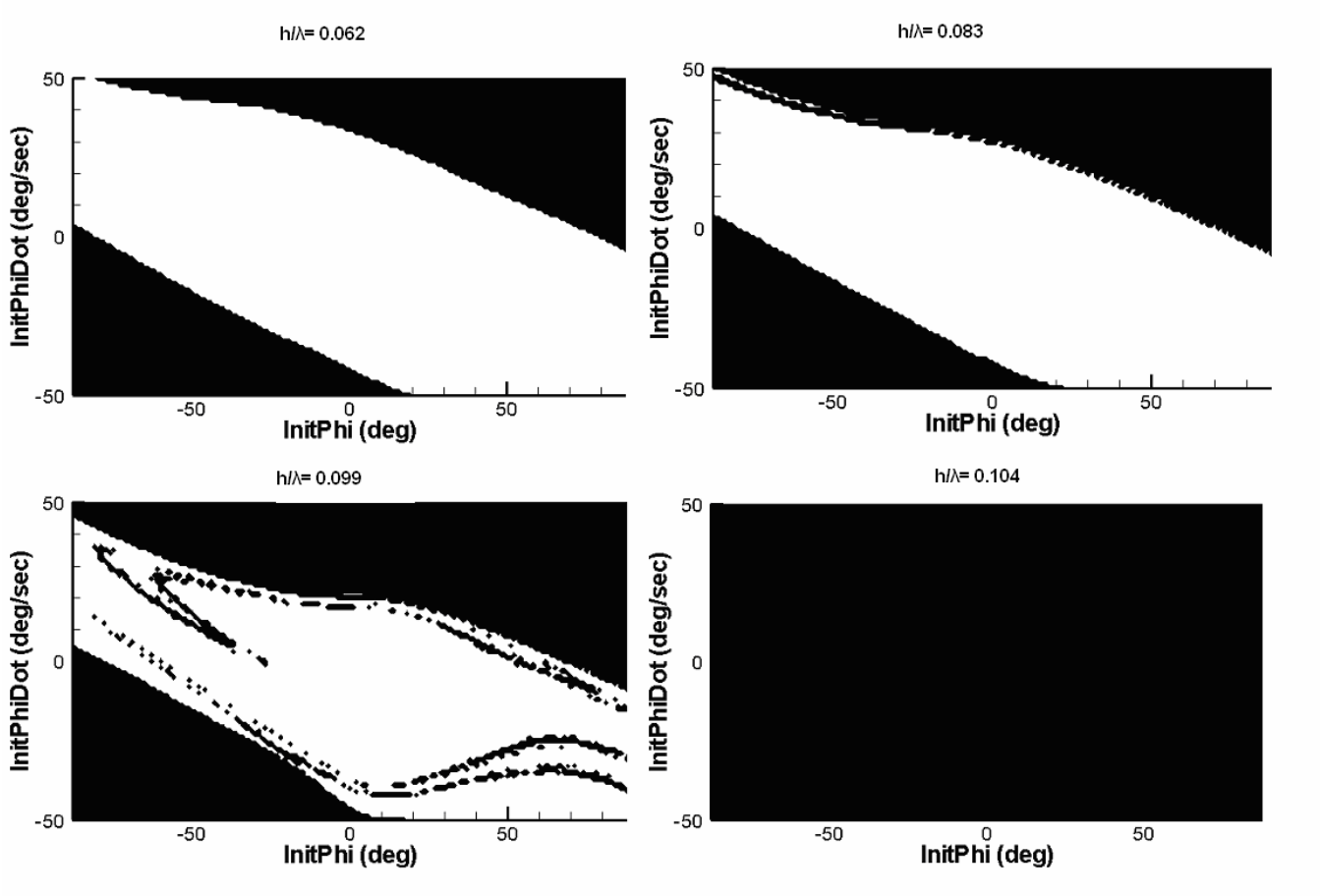

Fig. 4: Safe Basins (Initial Roll Angle vs Initial Roll Velocity) for ONRTH at KG=7.75m for four regular wave heights (h/λ).

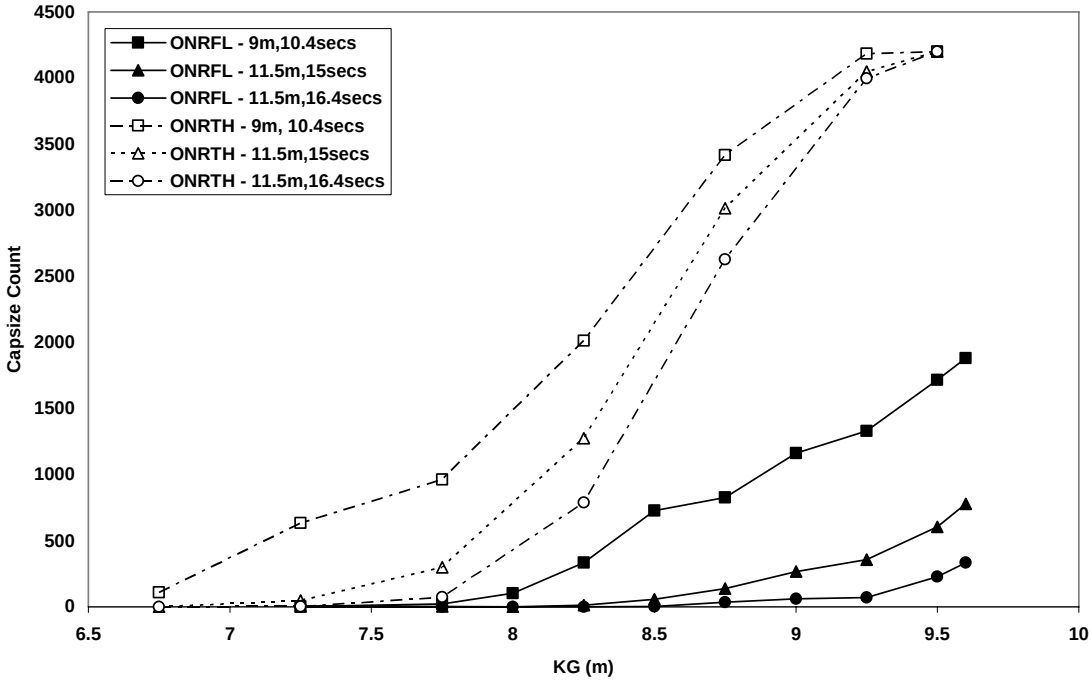

Fig. 5: Total Number of Capsizes vs KG for all ship headings and speeds, 4200 runs for each ship at each KG.

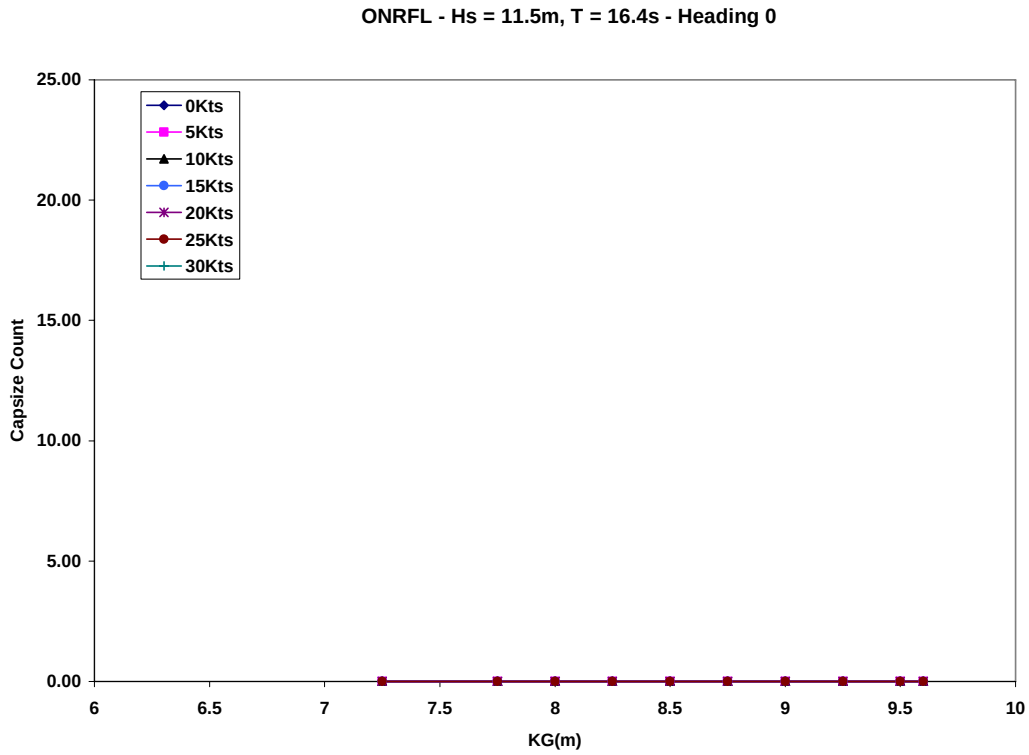

Fig. 6: Number of Capsizes vs KG for ONRFL, in following seas for Hs=11.5m, Tm=16.4 sec, at various forward speeds.

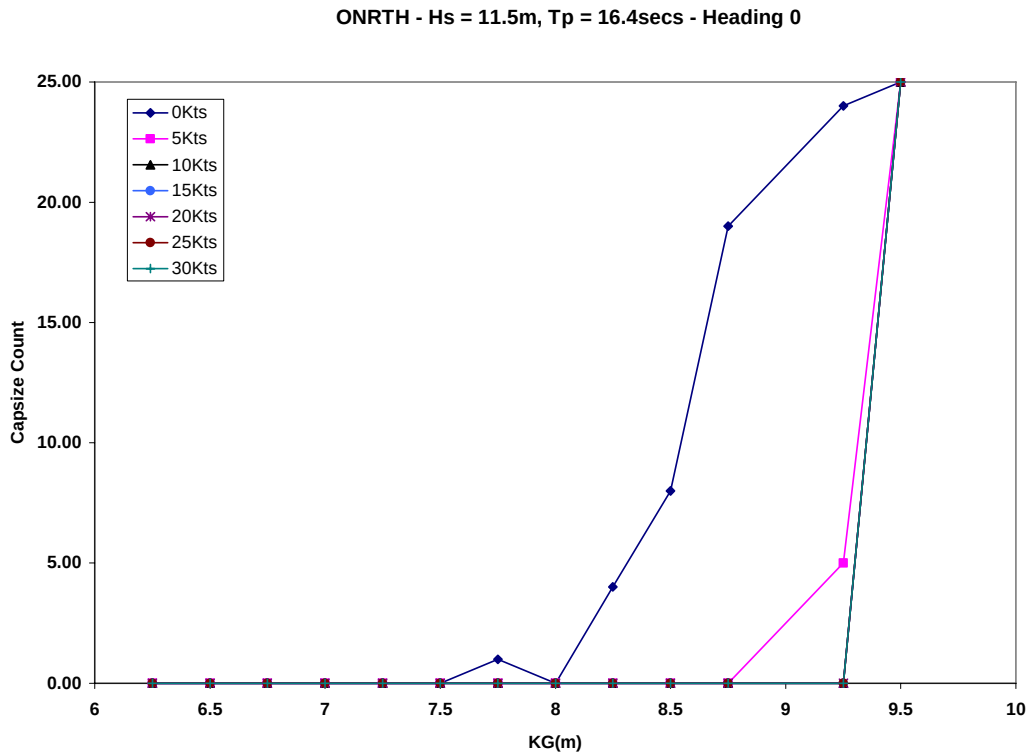

Fig. 7: Number of Capsizes vs KG for ONRTH, in following seas for Hs=11.5m, Tm=16.4 sec, at various forward speeds.

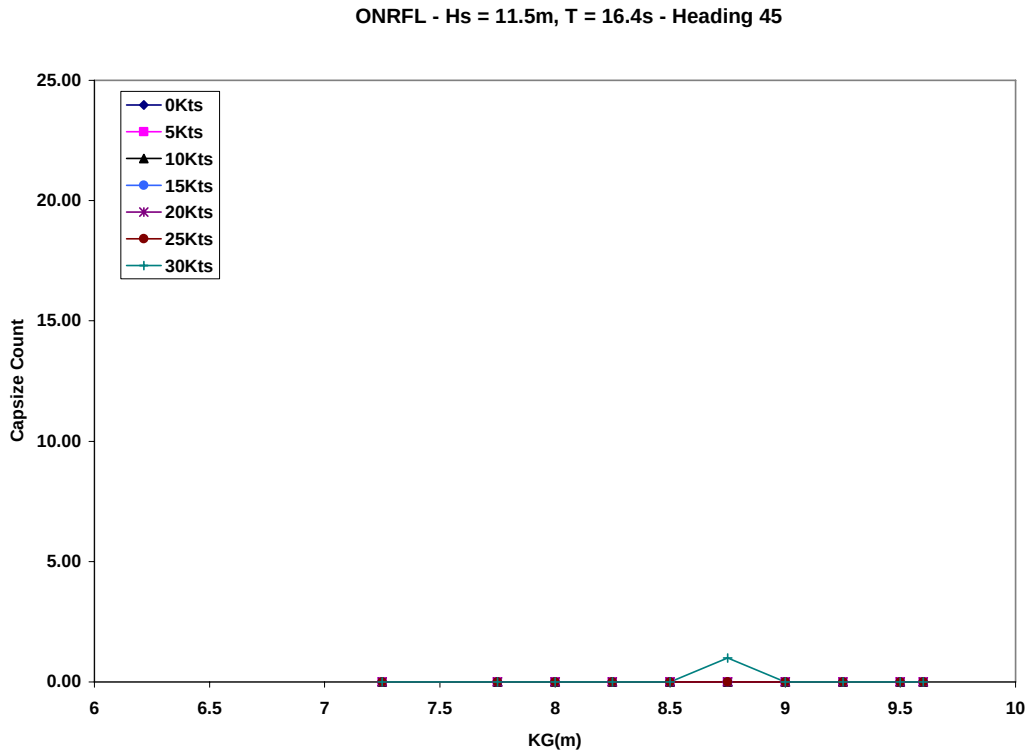

Fig. 8: Number of Capsizes vs KG for ONRFL, in stern-quartering seas for Hs=11.5m, Tm=16.4 sec, at various forward speeds.

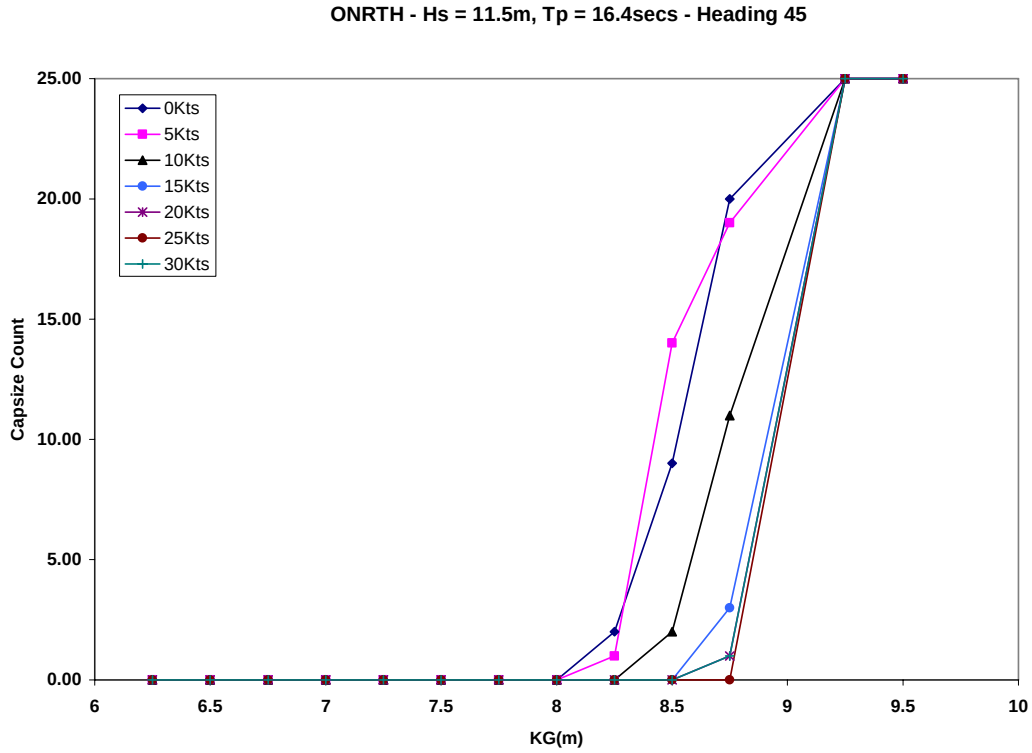

Fig. 9: Number of Capsizes vs KG for ONRTH, in stern-quartering seas for Hs=11.5m, Tm=16.4 sec, at various forward speeds.

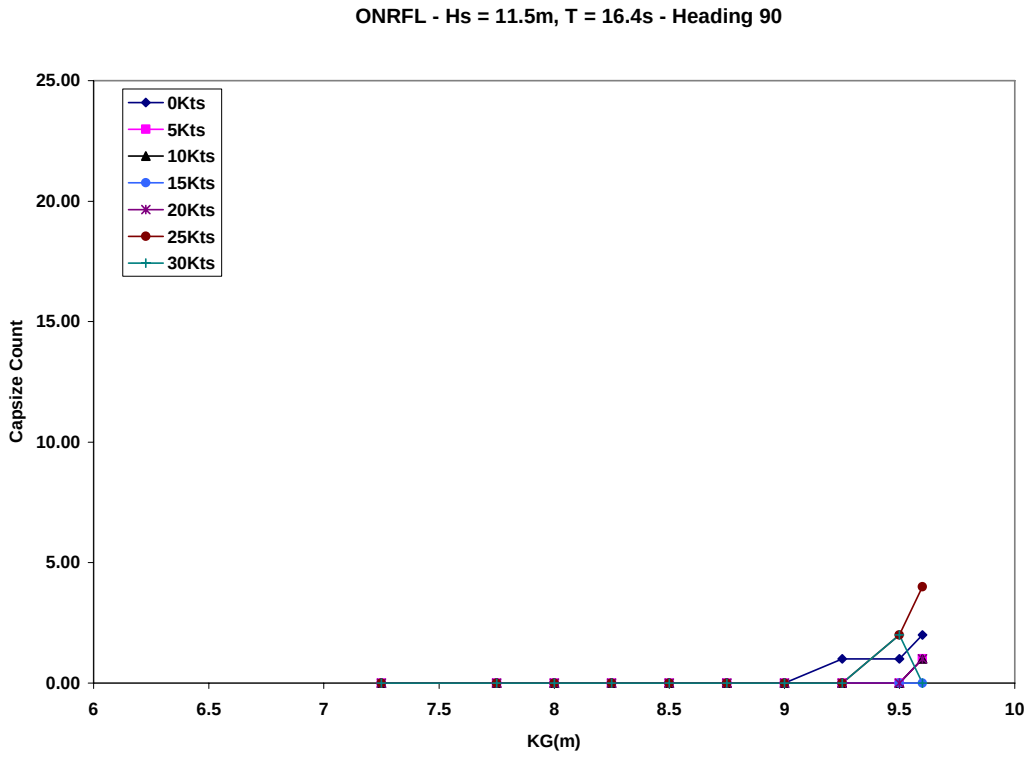

Fig. 10: Number of Capsizes vs KG for ONRFL, for 25 realizations for 1800s, in beam seas for Hs=11.5m, Tm=16.4 sec, at various forward speeds.

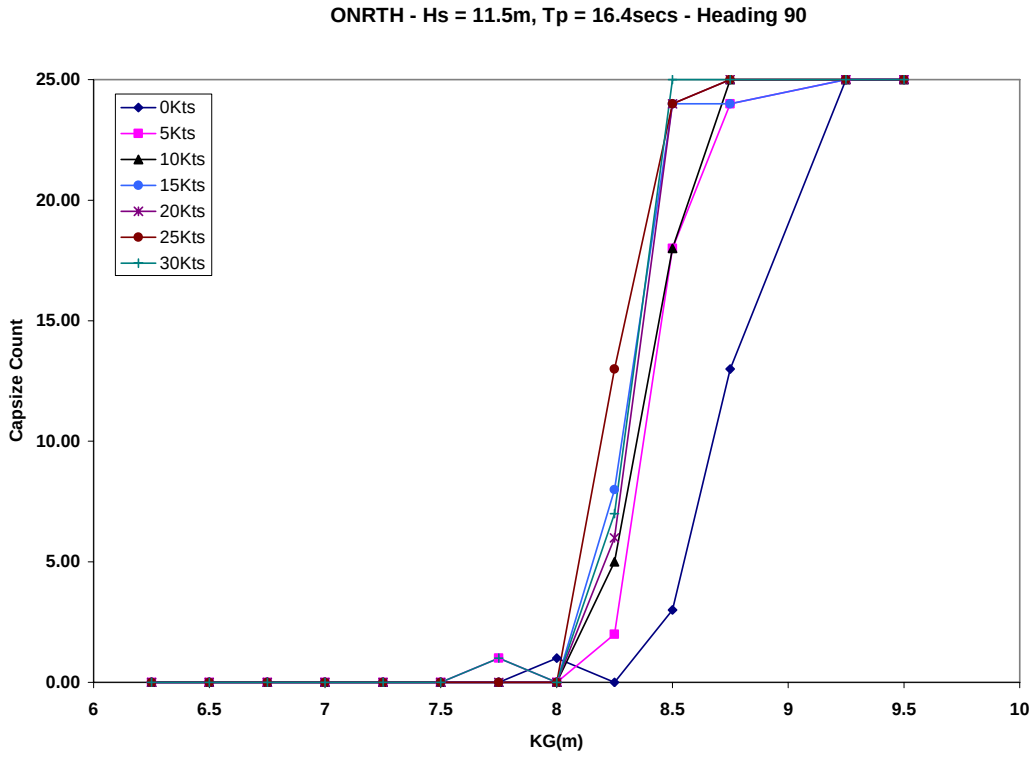

Fig. 11: Number of Capsizes vs KG for ONRTH, in beam seas for Hs=11.5m, Tm=16.4 sec, at various forward speeds.

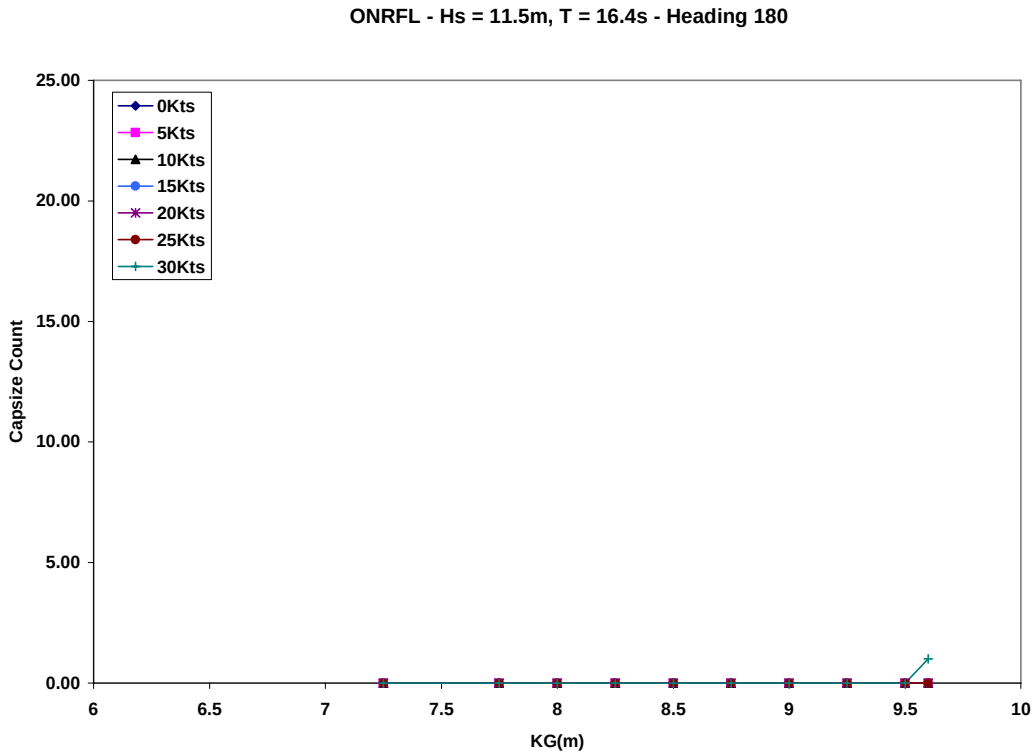

Fig. 12: Number of Capsizes vs KG for ONRFL, in head seas for Hs=11.5m, Tm=16.4 sec, at various forward speeds.

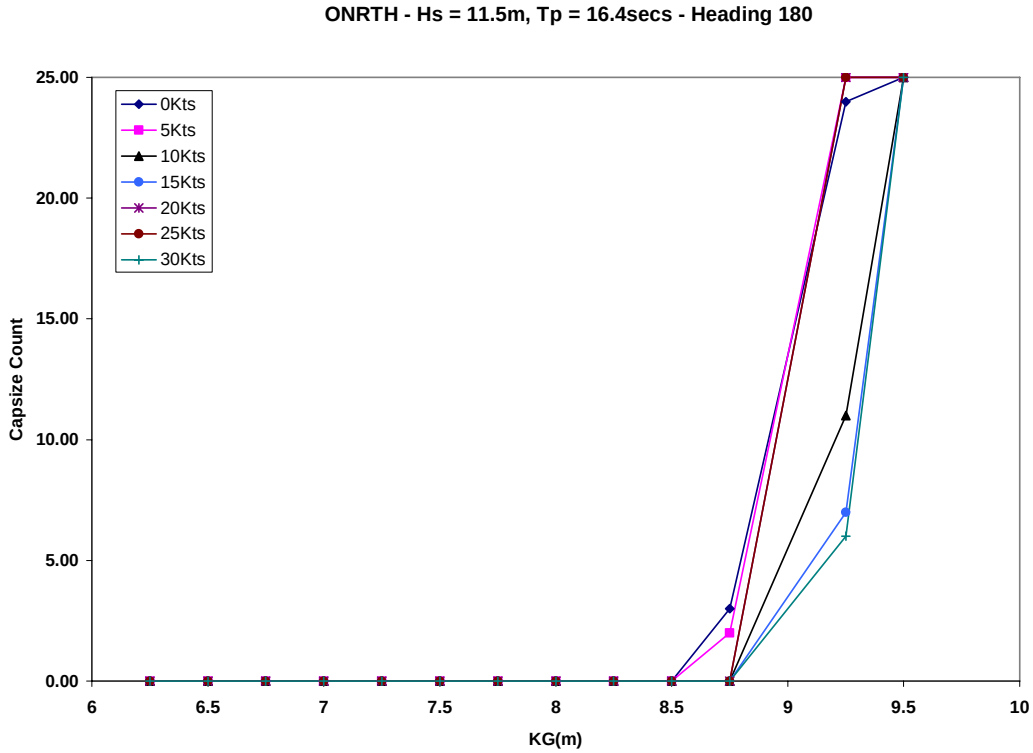

Fig. 13: Number of Capsizes vs KG for ONRTH, in head seas for Hs=11.5m, Tm=16.4 sec, at various forward speeds.

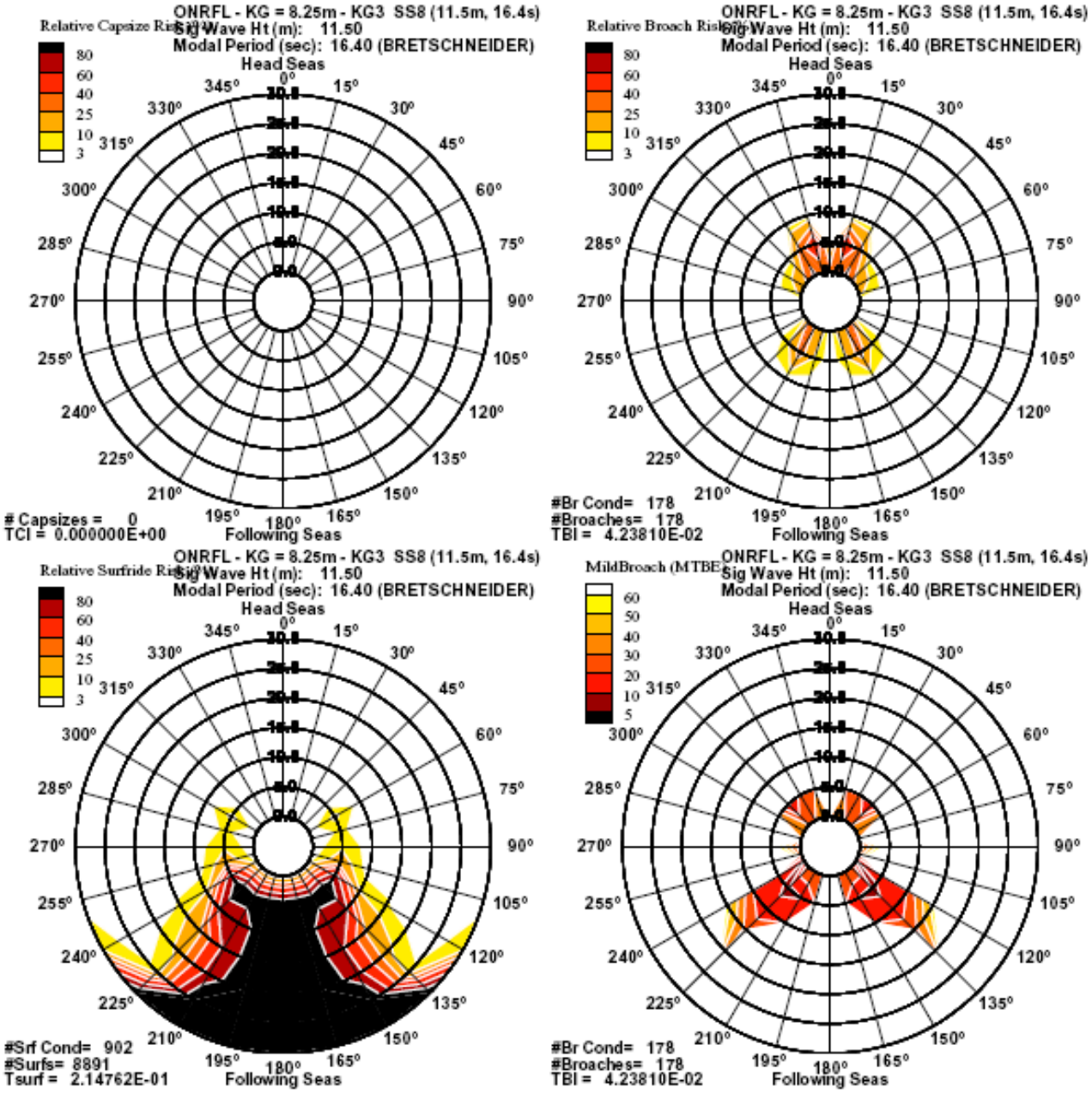

Fig. 14: Polar Plot of Capsize (top left), Broaches (top right), Mild-Broaches (bottom right), and Surfrides (bottom left) for ONRFL at KG=8.25 m, Hs=11.5m, Tm=16.4 sec

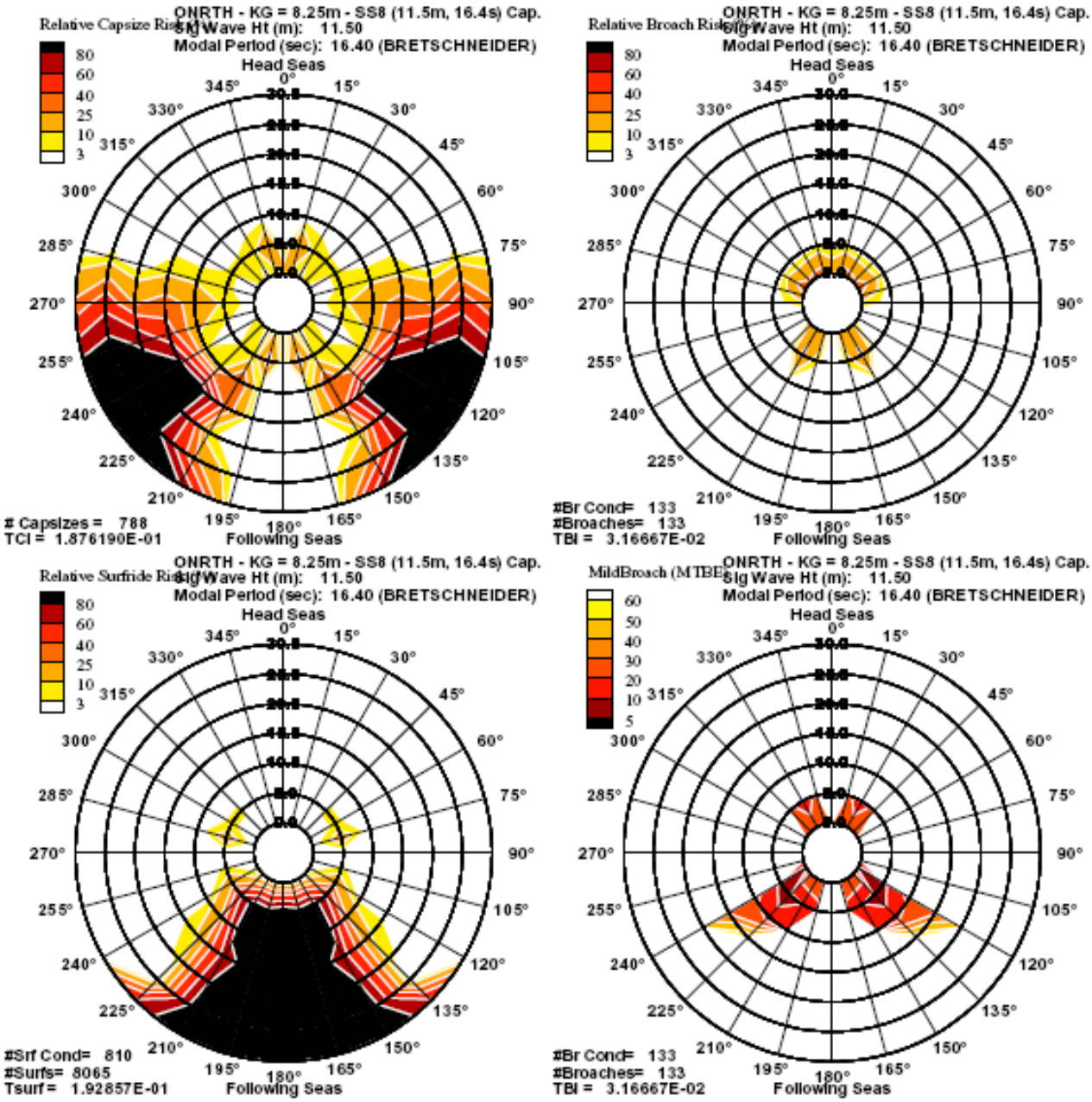

Fig. 15: Polar Plot of Capsize (top left), Broaches (top right), Mild-Broaches (bottom right), and Surfrides (bottom left) for ONRTH at KG=8.25 m, Hs=11.5m, Tm=16.4 sec

CONCLUSIONS

A numerical study was conducted using FREDYN 9.8 to examine dynamic stability risk in regular and random seas for varied topside geometries, flared and tumblehome.

From the regular seas investigation, drastic differences in capsize occurrence were observed for the ONRFL and ONRTH hull forms. Integrity curves and safe basins were used to assess the increase in capsize risk with increasing wave heights for varied KG values. Increasing wave heights, up to values of 1/10 wave steepness, lead to drastic reductions in the stability of the tumblehome topside hull form. For realistic loading conditions, even in steep waves, with large initial heel angles and roll rates, the flared topside had very few instance of capsize.

From the random seas investigation, a significant difference was observed for the capsize rate of the flared and tumblehome topside geometries. To achieve a similar, reduced number capsizes the GM of the tumblehome topside must be increased by 1-1.5m. Although decreasing the capsize risk for the tumblehome topside, this increase in GM would lead to a much stiffer ship and other safety considerations, such as accelerations on the crew members could be problematic.

As shown, the number of capsizes for the most-probable sea state 8 conditions increase drastically for the tumblehome topside for all headings. As expected, the capsize risk increased for both topside geometries with worsening sea state 8 conditions. However the capsize risk for the tumblehome geometry had a greater increase for small increases in KG than the flared topside geometry.

A sharp increase in the number of capsizes for the tumblehome hull form occurred after the 8.25m KG value. The tumblehome topside travelling at moderate to high speeds in stern-quartering to beam seas was observed to be the worst-case scenario for capsize from the polar plots. Similar risk susceptibilities were observed for broaching and mild-broaching. Surfriding occurrences were observed to be slightly decreased for the tumblehome hull form.

The results of this investigation provide a better understanding of the influence of increased KG over the life-cycle of the ship, the ramifications of error in KG measurements, the required safety factor or error band in operator guidance, and the sensitivity of these variations to hull form geometry. The results can be used for a preliminary assessment of the difference in dynamic stability, for a range of wave conditions, between varied topside geometry configurations. However, to accurately quantify the dynamic stability risk for different topside configurations, and establish the boundaries for these regions of vessel safety or risk with a high degree of confidence, additional experiments for the conditions outlined in this investigation should be conducted to validate the FREDYN results.

ACKNOWLEDMENTS

The authors would also like to express their appreciation for the support of the Hydromechanics Department of the Naval Surface Warfare Center, Carderock Division (NSWCCD).

REFERENCES

"Dynamic Stability Assessment Tools and Methodologies for New Monohull Displacement Surface Combatant Ships," Rev. 2. NSWCCD Seakeeping Department, 13 August, 2003.

McCue, L.S., Belknap, W., and Campbell, B., "Reconciling experimental and numerical data: techniques of nonlinear seakeeping code validation," *Marine Systems and Ocean Technology*, **2** (1-2), 2006, pp. 55-62. Originally presented at the 8th International Ship Stability Workshop, Istanbul, Turkey, October, 2005.

McTaggart, K., and de Kat, J.O. "Capsize Risk of intact frigates in irregular seas," *SNAME Transactions*, **108**, 2000, pp. 147-177.

Soliman, M.S., and Thompson, J.M.T., "Transient and steady state analysis of capsize phenomena," *Applied Ocean Research*, **13** (2), 1991, pp. 82-92.

Lee, Y.W., McCue, L.S., Obar, M., and Troesch, A., "Experimental and numerical investigation into the effects of initial conditions on a three degree of freedom capsize model," *Journal of Ship Research*, **50** (1), 2006, pp. 63-84.

Spyrou, K.J., & Thompson, J.M.T. "The nonlinear dynamics of ship motions: a field overview and some recent developments," *Philosophical Transactions of the Royal Society of London: Mathematical, Physical, and Engineering Sciences*, **358** (1771), 2000, pp. 1735-1760.

Thompson, J.M.T., "Designing against capsize in beam seas: recent advances and new insights," *App.l Mech. Rev.*, **50** (5), 1997, pp. 307-325.

Session 7: Probabilistic approach to damage stability and survivability assessment

Session Chairman: H. Bruhns ***Dr. P. Sames***

1) M. Gerigk:

   "Model of identification of events and accident scenarios for a method of risk and safety assessment of ships in damaged conditions"

2) M.Schreuder

   "HASARD Holistic Assessment of Ships Survivability and Risk after Damage"

3) A. Jasionowski, D. Vassalos:

   "SOLAS 2009 – Raising the Alarm

Model of identification of events and accident scenarios for a method of risk and safety assessment of ships in damaged conditions

Miroslaw Gerigk

Gdansk University of Technology

ABSTRACT

The paper regards some problems associated with identification of events and accident scenarios and modeling of risk for the alternative method of risk and safety assessment of ships in damaged conditions. The various problems associated with modeling the survivability of ships using a performance-oriented risk-based approach are considered. It is taken into account to apply the methodology within the decision making processes for either the design, operational or salvage-oriented purposes.

KEYWORDS

Ship safety, safety of ships in damaged conditions, safety assessment, risk analysis, ship design for safety, safe operation of ships.

INTRODUCTION

The paper presents some information on modelling the risk and safety assessment of ships in damaged conditions for the design, safe operation or salvage-oriented purposes. The research concerns development of an alternative performance-oriented risk-based method for assessment of safety of ships.

The current method of assessment of safety of ships in damaged conditions is based on the harmonized SOLAS Chapter II-1 Parts A, B and B-1, IMO (2005), IMO (2007). These regulations are prescriptive in their character and are based on the fully probabilistic and semi-probabilistic approaches to safety. Application of the requirements included in these regulations to certain types of ships e.g. large passenger vessels, Ro-Ro vessels or car-carriers may lead to insufficient level of ship safety or provide unnecessary design restrictions.

IMO has decided to improve the prescriptive regulations and create the sets of new rules based on the risk assessment technology. Such the rules should be directed towards satisfying the objectives. Between the standard design objectives the sufficient level of safety should be included. For the whole process of improving the rules IMO has recommended an application of the Formal Safety Assessment FSA methodology published as MSC Circ. 1023, IMO (1997, IMO (2002a). The proposed alternative method is a kind of performance-oriented risk-based analysis to be included in either the design operation processes with the reduction of risk and sufficient level of safety as an objective. The methodology adopted can easily be adopted for assessment of safety of undamaged ships as well as it very much depends on the problem (system) definition. In the paper the performance-oriented risk-based method of assessment of safety of ships in damaged conditions is briefly discussed because of limited space available. Some examples of assessment of safety using the method are presented. The detailed discussion regarding the method will be published by the Gdansk University of Technology later this year.

CURRENT METHOD OF ASSESSMENT OF SAFETY OF SHIPS IN DAMAGED CONDITIONS

The current method for safety assessment of ships in damaged conditions is based on the regulations included in the SOLAS Chapter II-I. Using this method the measure of safety of a ship in damaged conditions is the attained subdivision index "A". It is treated as the probability of survival of flooding any group of compartments. The basic design criterion is the condition as follows, IMO (2005), IMO (2007):

$$A > R \quad (1)$$

where:

A - attained subdivision index calculated, for the draughts d_s, d_p and d_l defined in regulation 2, according to the formula, IMO (2005):

$$A=\sum p_i s_i \quad (2)$$

p_i - probability that only the compartment or group of compartments under consideration may be flooded, as defined in regulation 7-1;

s_i - probability of survival after flooding the compartment or group of compartments under consideration, as defined in regulation 7-2;

R - required subdivision index.

The probabilities p_i and s_i are calculated according to the well known formulae accepted by IMO, IMO (2005), IMO (2007). The typical process of assessment of safety of ships in damaged conditions at the design stage or when the survivability of existing ships is considered is directed to satisfy the criteria (1). As an example the final results of survivability assessment for the 1100 TEU container ship can be introduced. The main data of this ship necessary to conduct the survivability assessment are as follows, Gdynia Shipyard (1999-2005):

-length between perpendiculars L_{BP}=145.00 m,

-subdivision length L_s=158.66 m,

-deepest subdivision draught d_s=10.20 m,

-light service draught d_l=7.56 m,

-lightweight = 6800.00 tonnes,

-coordinates of centre of gravity: LCG=58.10 m from A.P., VCG=11.10 m above B.P.

The calculations of the attained subdivision index "A" are connected with the large scale numerical calculations and they are time consuming. The final results of the probabilistic survivability assessment for the 1100 TEU container ship are as follows, Gdynia Shipyard (1999-2005), Gerigk (1999-2005), Gerigk (2005b), Gerigk (2006), Woznicki (2005):

$$A = \sum \Delta A_i = 0.52605 \quad (3)$$

$$R = 0.52510 \quad (4)$$

$$\text{Then } A>R \text{ as } 0.52605>0.52510 \quad (5)$$

Even if the criterion (1) is satisfied, by formulae (5), there are serious doubts if the ship could really be safe in operation. Of course, the optimisation of the attained subdivision index "A" can be applied to increase the safety of ships in damaged conditions. The optimisation may concern the optimisation of the so-called local safety indices. However these techniques should be considered as prescriptive as the method itself. Some example calculations associated with using these techniques were conducted at the University of Newcastle upon Tyne in 1991 by Gerigk and published in 1992, Sen et al. (1992).

PERFORMANCE-ORIENTED RISK-BASED DESIGN

As it was introduced by Vassalos, Skjong and the others, the risk-based design is a formalized design methodology that systematically

integrates the risk analysis in the design process with the prevention/reduction of risk embedded as a design objective, along standard design objectives. This methodology applies a holistic approach that links the risk prevention/reduction measures to ship performance and cost by using relevant tools to address ship design and operation, Vassalos et al. (2005a), Vassalos (2005b), Vassalos (2006), SSRC (2006), Skjong (2004), Skjong (2005), Skjong et al. (2006).

The following steps were introduced to be needed to identify the optimal design solution, SSRC (2006): set objectives, identify hazards and scenarios of accident, determine the risk, identify measures and means of preventing and reducing risk; select designs that meet objectives and select safety features and measures that are cost-effective, approve design solutions or change the design aspects.

A similar approach to assessment of safety of ships for design, safe operation and salvage has been applied for the method presented in the paper. The approach is similar but there are the differences in methods, models, solutions and details. The original structure of the method and proposed risk-based design system for assessment of safety of ships in damaged conditions is presented in Figure 1. Because of the limited space available in the paper more details regarding the method will be presented during the Workshop.

PROPOSED METHOD

The modern approach to ship safety is connected with combining the elements of system approach to safety and Formal Safety Assessment (FSA) methodology, IMO (1997), IMO (2002a). The major elements of the FSA methodology are as follows: hazard identification, risk analysis, risk control options, cost-benefit assessment, recommendations for decision making. The above steps have been combined with the modern ship design spiral, Gerigk (2005a), Gerigk (2005b), Gerigk (2006).

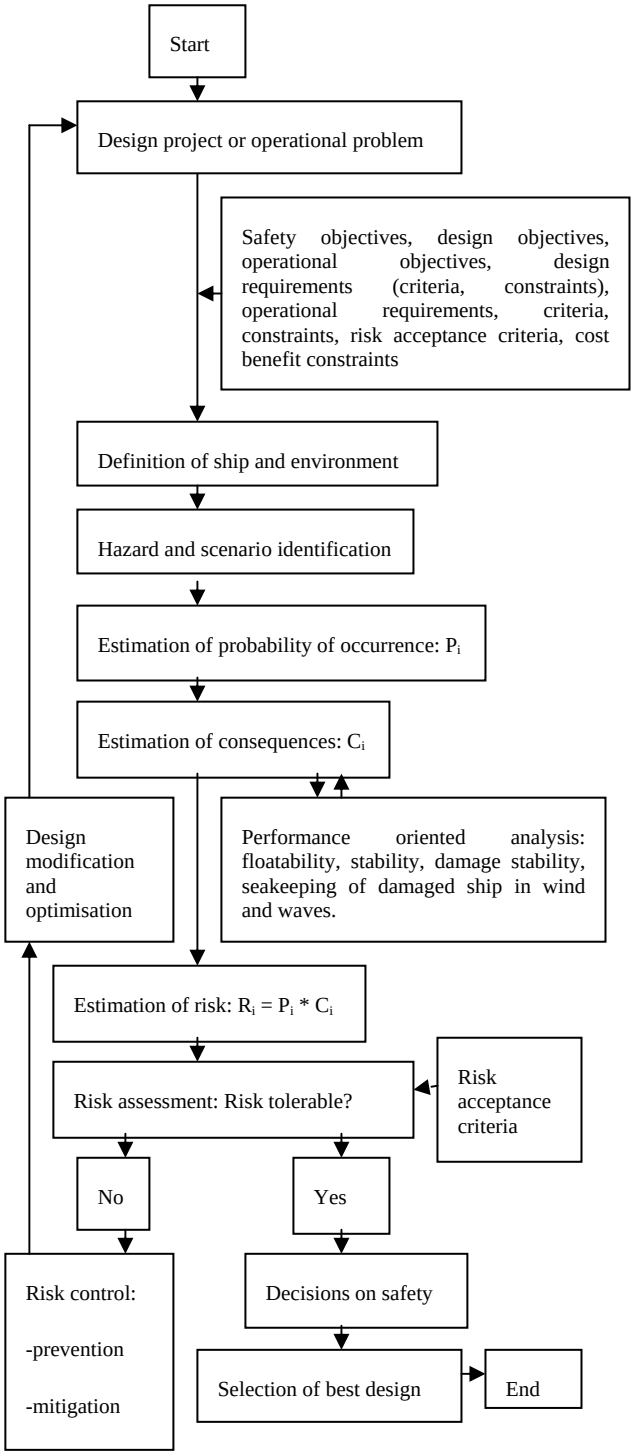

Fig. 1: Structure of the risk-based design system for assessment of safety of ships in damaged conditions.

The following methods have been used for the risk assessment including the hazard identification methods, frequency assessment methods, consequence assessment methods and risk evaluation methods, ABS (2000), Gerigk

(1999-2005): preliminary hazard analysis (PHA), preliminary risk analysis (PRA), what-if/checklist analysis, failure modes and effects analysis (FMEA), hazard and operability analysis (HAZOP), fault tree analysis (FTA), event tree analysis (ETA), relative ranking, coarse risk analysis (CRA), pareto analysis, change analysis, common cause failure analysis (CCFA) and human error analysis (HEA).

The risk reduction principle and main strategy adopted for the method was reducing the probability of consequences of accident, Grabowski et al. (2000), Gerigk (2005b), Gerigk (2006).

A method for assessment of safety of ships in damaged conditions is associated with solving a few problems regarding the naval architecture, ship hydromechanics and safety and it is novel to some extent. When preparing the method the global and technical approaches were used, Barker et al. (2000). The global approach mainly regards the problems associated with the development of risk assessment methodology. The technical approach concerns developing either the design, operational or salvage-oriented procedure including the structure of system (method), computational model, design requirements, criteria and constraints, library of analytical and numerical methods and library of application methods, Gerigk (2005a), Gerigk (2005b), Gerigk(2006). There are two approaches to risk management: bottom-up approach and top-down. For example, the top-down risk management methodology has been applied for design for safety. This approach should work in the environment of performance-based standards and help designing the ships against the hazards they will encounter during their operational life, Gerigk (1999-2005), Gerigk (2005a), Gerigk

$$R=P_c \times P_{c/fdpe} \times P_{c/fdpe/ns} \times P_{c/fdpe/ns/tts} \times C \quad (7)$$

(2005b).

MODELING RISK

The key issue when using the proposed method is to model the risk contribution tree for the risk assessment. Three categories of accidents which may potentially cause a damage to the ship were taken into account: collision, stranding and grounding. According to the statistics these categories are the main reasons of accidents at sea. They constitute about 53% of the whole number of accidents, Kobylinski (2001). The risk contribution trees for the collision, stranding and grounding were developed separately according to the general fault tree FTA and event tree ETA structures. The holistic approach to ship safety has been applied. According to this two major assumptions have been done. First assumption is that the system failures can be either the hardware, software, organizational or human failures. Second concerns the holistic risk model to be applied for assessment of safety of ships in damaged conditions. The Total Risk Management TRM approach should be

$$R_i = P_i \times C_i \quad (6)$$

implemented as a systematic and holistic approach that builds on the quantitative risk assessment and risk management. The risk associated with the different hazards and scenario development was estimated according to the well known general formulae:

where: P_i – probability of occurrence of a given hazard; C_i – consequences following the occurrence of the data hazard and scenario development, in terms of fatalities, injuries, property losses and damage to the environment.

The holistic risk model for the assessment of safety of ships in damaged conditions is as follows, Jasionowski et al. (2006), Skjong et al. (2006), Gerigk (2005b), Gerigk(2006):

where: P_c - probability of collision (hazard); $P_{c/fdpe}$ - probability of flooding having the ship hit from given direction at data position with given extent conditional on collision; $P_{c/fdpe/ns}$ - probability of not surviving conditional on having flooding when the ship is hit from given direction at data position with given extent conditional on collision; $P_{c/fdpe/ns/tts}$ - probability of given time to sink conditional on not surviving the conditional on having flooding when the ship is hit from given direction at data position with given extent conditional on collision; C - consequences regarding the fatalities, property (cargo, ship) and/or environment.

The risk model (7) is different from the model presented by Skjong et al. as it does not use the conditional probability of sinking given by the P_{sink}=1-A complement probability of the attained subdivision index "A", Skjong et al. (2006).

A good example of the risk and safety assessment according to the proposed method is the design analysis conducted for the container ship as follows:

-length between perpendiculars L_{BP}=163.00 m,

-subdivision length L_s=174.95 m,

-breadth B=26.50 m,

-deepest subdivision draught d_s=9.00 m,

-tonnage P_N=22286.00 DWT.

The hazards and scenarios concern flooding of the following damage zones (presented in Figure 2) due to collision: 1, 2, 3, 4, 5, 6, 7, 8, 9, 1+2, 2+3, 3+4, 4+5, 5+6, 6+7, 7+8, 8+9, 1+2+3, 2+3+4, 3+4+5, 4+5+6, 5+6+7, 6+7+8, 7+8+9.

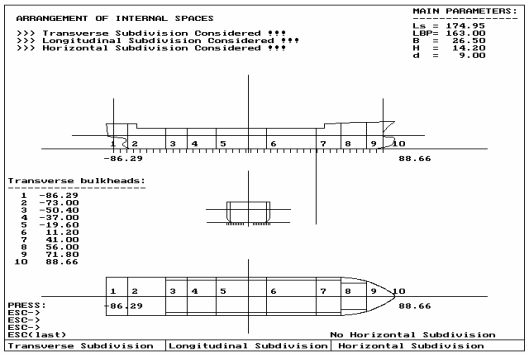

Fig. 2: Arrangement of internal spaces for a container ship, Gerigk (1999-2005), Gdynia Shipyard (1999-2005).

For calculation of the probabilities of occurrence including the uncertainties the Monte-Carlo techniques have been used to obtain the different scenarios, Gerigk (1999-2005), Woznicki (2005). In the case when the risk is estimated according to the formulae:

$$R_i = F_i \times C_i \qquad (8)$$

where: F_i – frequency of occurrence of a given hazard; C_i – consequences following the occurrence of the data hazard and scenario development, it is difficult to take the uncertainties into account or estimate.

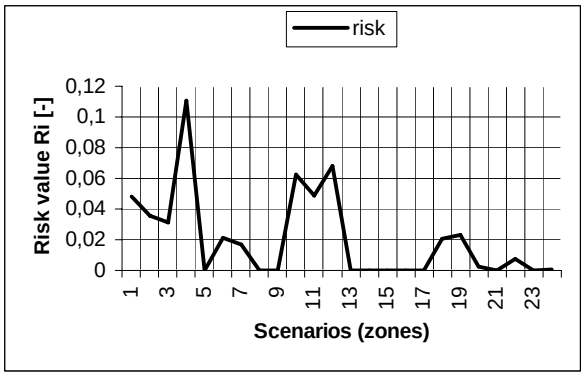

Fig. 3: An example distribution of the risk ($R_i = P_i * C_i$) values.

Simulating the P_i and C_i values using the Monte Carlo method the influence of different impacts (water on deck, wind, cargo shift) on safety of the ship can be taken into account. An example of the risk distribution ($R_i = P_i \times C_i$) in terms of surviving the collision is presented in Figure 3.

SHIP SALVAGE USING THE PROPOSED METHOD

In operation the factors affecting safety of a damaged ship may follow from three major sources: design (engineering), operation and management (ship management, safety management). The harmonized SOLAS Chapter II-1 is mainly related to design. The aspects connected with the operational and management issues are marginally underlined in these regulations. The other regulations better reflect the operation and management as well as the human factor.

Even if the current regulations are based on the probabilistic approach to safety they still are prescriptive in their nature. As indicated before, applying these regulations to certain types of ships the insufficient level of ship safety or unnecessary design restrictions can be observed. Despite many advantages from the ship design point of view the current regulations do not enable to conduct the safety analysis according to the complex sequence of real events which may occur at sea. Within the SOLAS based methodology the objective is survivability that is connected with estimation the attained subdivision index A and satisfying the criteria "A>=R". The index "A" may not reflect to the real level of safety of a damaged ship at sea. There is a problem if the results obtained during the performance-oriented investigations (using the physical and/or numerical simulations) can fully support the assessment of safety of a damaged ship in real sea conditions. Can the risk-based analysis guarantee that the risk level predicted at the design stage could be the same in ship operation. The assessment of safety of a damaged ship in operation requires a rapid modelling of situation. The proposed method enables to use the risk analysis as a salvage-oriented procedure which should be integrated with the risk control (prevention, reduction) embedded as the main objective. The risk analysis regards identifying all the possible hazards, describing all the possible scenarios development and calculating the risk (in terms of probabilities of hazard occurrence and consequences). It is followed by assessing the means of controlling (preventing, reducing, mitigating) the risk. The risk control options are the integrated parts of the method together with the decisions on safety. The multi-level safety assessment can be applied using the risk evaluation criteria.

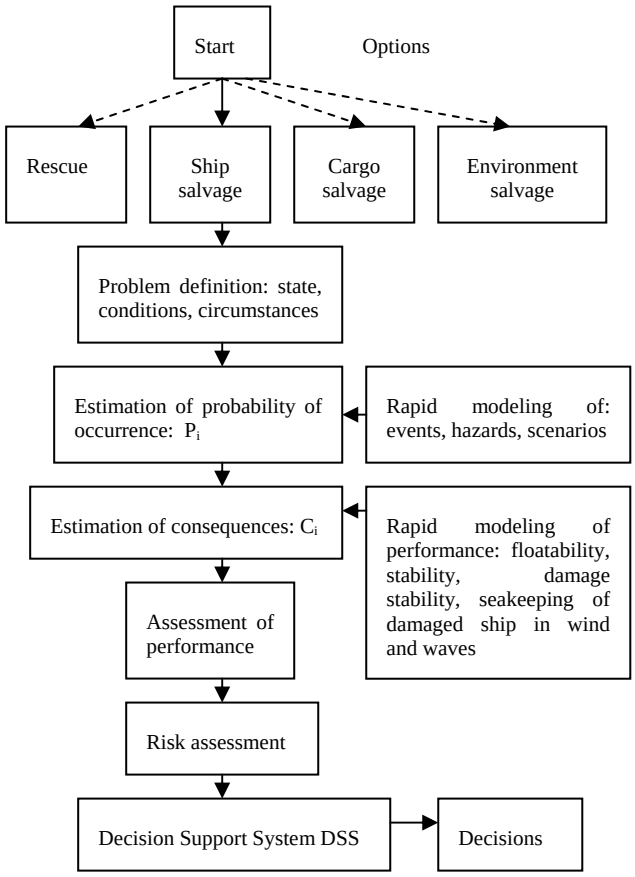

Fig. 4: Structure of the salvage-oriented method.

The main steps of the method as a salvage-oriented procedure are the hazard identification, hazard assessment, scenario development and risk assessment. The hazard and risk assessment are supported by modelling the uncertainties. The risk assessment can be done using the statistical method, analyst judgment, formal expert elicitation and Bayesian analysis.

The basic structure of the salvage-oriented method is presented in Figure 4. Despite of having the rapid modeling possibilities the most important feature for such the method is to have the components associated with the making decisions on safety. The modern

decision support tools for salvage purposes can be the fuzzy logic and neural-net techniques. Because of the limited space in the paper the further information on the salvage-oriented method will be presented during the Workshop.

CHALLENGES REGARDING FURTHER INVESTIGATIONS

Currently, there are a few problems under consideration regarding the safety of ships in damaged conditions which are associated with the existing prescriptive method included in the SOLAS Chapter II-1. The first problem concerns how to obtain the same level of safety for different types of ships. The second regards updating the statistical data for the p_i factor estimation. The next problem which can probably not be solved using the prescriptive approach is calculation of the s_i factor taking into account the possible hazards and scenarios.

The new formula for the s_i factor should include the components following from the fact that there are a few stages during the flooding process, IMO (2002b), Dudziak et al. (2001), Gerigk (1999-2005), Santos et al. (2005): creation of damage (stage 1), transient heel and intermediate flooding (stage 2), progressive flooding (stage 3), final stage (stage 4). During the above mentioned stages the internal and external impacts may appear according to the following: wind heeling moment, action of waves, ballast/cargo shift, crowding of people, launching life saving appliances, etc. The combinations of the above mentioned may create the sequences of events (scenarios) which are not taken into account within the current regulations. The alternative methods can be useful for developing the future regulations.

CONCLUSIONS

The performance-oriented risk-based method for assessment of safety of ships in damaged conditions is briefly presented in the paper. The current work regarding the method is associated with integrating the performance-oriented and risk-based analyses into the system introduced in Figure 1. The method uses the performance-oriented risk-based approach to safety. The risk analysis is based on the FSA methodology. The current research requires the further development of modelling the risk. The method can be implemented for the design, operational and salvage-oriented purposes.

ACKNOWLEDMENTS

The author would like to express his sincere gratitude to the Ministry of Science and Education, for the support to carry out the investigations on novel solutions for assessment of safety of ships, and Chair of Naval Architecture, Faculty of Ocean Engineering and Ship Technology, Gdansk University of Technology, for the scientific and research support.

REFERENCES

ABS document. 2000. Guidance notes on Risk Assessment Applications for the Marine and Offshore Oil and Gas Industries. American Bureau of Shipping, New York, June 2000.

Barker C.F., Arm P.E., Campbell C.B. 2000. Risk management in total system ship design. Naval Engineers Journal, July 2000.

Dudziak J. & Grzybowski P. 2001. Computer simulations of ship behaviour in waves according to the research activities of the Ship Research and Shipbuilding Centre in Gdansk. Proceedings of the 1st Summer School “Safety at Sea”, Chair of Ship Hydromechanics, Faculty of Ocean Engineering and Ship Technology, Gdansk University of Technology, Gdansk, 28-29th August 2001.

Gdynia Shipyard. 1999-2005. Design data of container ship of 1100 TEU. Internal report of Gdynia Shipyard, Gdynia 1999-2005.

Gerigk M. 1999-2005. Analysis of survivability of dry cargo ships. Internal reports of Gdansk University of Technology, Gdansk 1999-2005.

Gerigk M. 2005a. Safety assessment of Ships in Critical Conditions using a Knowledge-Based System for Design and Neural Network System. Proceedings of 4th

International Conference on Computer and IT Applications in the Maritime Industries COMPIT'2005, Hamburg, 8-11 May, 2005, ISBN 3-00-014981-3.

Gerigk M. 2005b. Challenges of modern assessment of safety of ships in critical conditions. BALKEMA – Proceedings and Monographs in Engineering, Water and Earth Sciences. Proceedings of the 12th International Congress of the International Maritime Association of the Mediterranean IMAM 2005, Volume 2, Lisboa, Portugal, 26-30 September 2005, Published by Taylor & Francis / Balkema, London / Leiden / New York / Philadelphia / Singapore, ISBN (Set): 0 415 39036 2.

Gerigk M. 2006. A method for assessing hazards, risks and safety of damaged ships at sea. BALKEMA – Proceedings and Monographs in Engineering, Water and Earth Sciences. Proceedings of the European Safety and Reliability Conference 2006 (ESREL 2006), Volume 3, Estoril, Portugal, 18-22 September 2006, Published by Taylor & Francis / Balkema, London / Leiden / New York / Philadelphia / Singapore, s. 2783-2790, bibliogr. 23 poz., 10 rys., ISBN (Set): 978-0-415-42315-1.

Grabowski M., Merrick J.R.W., Harrald J.R., Mazzuchi T.A., Dorp J.R. 2000. Risk modeling in distributed, large-scale systems. IEEE Transactions on Systems, Man, and Cybernetics – Part A: Systems and Humans, Vol. 30, No. 6, November 2000.

IMO. 1997. Interim guidelines for the application of Formal Safety Assessment (FSA) to the IMO rule - making process. MSC/Circ.829, MEPC/Circ.335, London, 17 November 1997.

IMO. 2002a. Guidelines for Formal Safety Assessment (FSA) for use in the IMO rule-making process. MSC/Circ.1023, MEPC/Circ.392, London, 5 April 2002.

IMO. 2002b. Development of Revised SOLAS Chapter II-1 Parts A, B and B-1, Investigations and proposed formulations for the factor "s": the probability of survival after flooding. SLF 45/3/3, London, 2002.

IMO. 2005. Report of the Maritime Safety Committee on Its Eightieth Session. MSC 80/24/Add.1, London, 2005.

IMO. 2007. http://www.imo.org.

Kobylinski L. 2001. Philosophy of safety at sea (in Polish). 1st International Workshop "Safety at Sea", Gdansk University of technology, Gdansk, August 2001.

Jasionowski A., Vassalos D. 2006. Coceptualising Risk. Proceedings of the 9th International Conference on Stability of Ships and Ocean Vehicles, Rio de Janeiro, 25-29 September 2006.

Santos, T.A. & Guedes Soares, C. 2005. Risk-based approach to the design of passenger Ro-Ro ships regarding damage stability. BALKEMA – Proceedings and Monographs in Engineering, Water and Earth Sciences. Proceedings of the 12th International Congress of the International Maritime Association of the Mediterranean IMAM 2005, Volume 2, Lisboa, Portugal, 26-30 September 2005, Published by Taylor & Francis / Balkema, London / Leiden / New York / Philadelphia / Singapore, ISBN (Set): 0 415 39036 2.

Sen P., Gerigk M. 1992. Some Aspects of a Knowledge-Based Expert System for Preliminary Ship Subdivision Design for Safety. Proceedings of the 5th International Symposium PRADS'92 on Practical Design of Ships and Mobile Units, Newcastle, May 1992, Edited by J.B.Caldwell and G.Ward, London, New York, Elsevier Applied Science, 1992.

Skjong R. 2004. Experience with Risk Based Decision Making in the Maritime Industry. SAFER EURORO II Workshop, Nantes, June 22, 2004.

Skjong R. 2005. Safety Assessment and Risk Acceptance Criteria. SAFER EURORO II Workshop, Glasgow, June 7, 2005.

Skjong R., Vanem E., Rusas S., Olufsen O. 2006. Holistic and Risk Based Approach to Collision Damage Stability of Passenger Ships. Proceedings of the 9th International Conference on Stability of Ships and Ocean Vehicles, Rio de Janeiro, 25-29 September 2006.

Stab 2000. 2000. Selected papers from the Proceedings of the 8th International Conference STAB 2003, Madrid, September 2003.

SSRC. 2006. http://www.ssrc.na-me.ac.uk.

Vassalos D., Konovessis D., Guarin L. 2005a. Fundamental concepts of risk-based ship design. Proceedings of the 12th International Congress of the International Maritime

Association of the Mediterranean (IMAM 2005): Maritime Transportation and Exploitation of Ocean and Coastal Resources, Lisboa, Portugal, 26-30 September 2005.

Vassalos D. 2005b. Risk Based Design – Concept, Methodology and Framework. Safer EuRoRo II Training Course, Glasgow, May 2005.

Vassalos D. 2006. Passenger Ship Safety: Containing the Risk. Marine Technology, Vol. 43, No. 4, October 2006, pp. 203-213.

Woznicki B. 2005. Parametric investigations of safety of ships in damaged conditions (M.Sc. thesis). Gdansk University of Technology, Faculty of Ocean Engineering and Ship Technology, Gdansk 2005.

HASARD

Holistic Assessment of Ship Survivability and Risk after Damage

Martin Schreuder

Chalmers University of Technology

ABSTRACT

This paper is an outline of the recently started research project HASARD. Some preliminary results are also presented.

HASARD is the acronym for Holistic Assessment of Ship Survivability and Risk after Damage. The project is funded by VINNOVA and by Lighthouse. HASARD is part of a coordinated European research program on maritime safety which is called SURSHIP – Survivability of ships.

KEYWORDS

HASARD, risk after damage

INTRODUCTION

A comprehensive calculation procedure useful for quantitative assessment of damaged ships survivability (incorporating structural collision resistance, structural stability and collapse (FEA), and time simulation of ship flooding and stability in waves) will be developed. The calculation procedure will be implemented in existing, modified, numerical simulation tools and it will be tested for a number of ship types/ship configurations and compared to existing model test data for validation.

Results from systematic simulations through this calculation procedure could be used in recommendations for future IMO rule making. It could also be used directly in a ship design process. Enhancement of the understanding of the physical processes involved in the chain of events following a collision between ships will also be obtained in the project.

The project constitutes two parts, structure and stability. Deliverables from the former will include among others phenomenological models which with satisfying reliability can mimic collapse and rupture phenomena in ship-ship collision simulations, and a methodology for estimation of the residual strength of a damaged ship structure. Deliverables of the latter will include among others further enhancement of the SIMCAP calculation tool, Schreuder (2005), and formulation of procedures which may quantify damaged ships ability to stay upright. These procedures are also proposed for use as a measure of the safety performance of e.g. Ro-Pax ferries.

The two parts of the project will work in close collaboration by exchange of information and results that will lead them towards a common aim: to develop a calculation procedure to become a useful tool for risk analysis (structural collapse

and ship stability) of the survivability of a collided and flooded ship.

AIMS AND OBJECTIVES

The main aim with the project is to outline a comprehensive calculation procedure which quantitatively can be used for assessment of damaged ships survivability, incorporating structural collision resistance, structural stability and collapse, and ship flooding and stability in waves. The main aim can be further refined as follows.

- **Structure perspective:**
  To increase knowledge and understanding of the consequences from collision impact on various side shell structures for various collision scenarios. Residual strength calculations for damaged structures will be carried out in order to make judgements of structural stability after collision. Necessary improvements and further developments of existing fracture/rupture criteria and phenomenological models have to be carried out.

- **Stability perspective:**
  To increase knowledge of the impact of different design solutions for e.g. passenger ships regarding the ability to keep also seriously damaged ships upright and prolong the available time for evacuation.

- **Structure and stability perspectives:**
  - To increase the knowledge of which physical phenomena that are relevant and must be involved in the assessment of the behaviour of damaged ships, and also how to incorporate them in numerical models in a comprehensive calculation procedure as proposed in this project.
  - To quantify the survivability of a ship subjected to different collision events. Here, various ships, collision scenarios, and sea state conditions will be accounted for.

APPROACH OF STABILITY PART

A tool called SIMCAP has been developed at the department for dynamic ship stability calculations. This prediction tool will be further developed to include arbitrary wave direction

and irregular wave effects on the damaged ship response, i.e. the possibility to evaluate any/general load situations will be added to the existing code. There will be a close collaboration with the structure part of the project, especially regarding properties of structural damages, damage scenarios, and damage patterns (e.g. projected area of damage) on the hull structure. Static stability analysis will be performed in a number of case studies to analyse and evaluate the risk of different design solutions for passenger ships regarding capsize. Procedures to quantify damaged ship's ability to stay upright will be studied incorporating structural collapse assessment provide by the structure part.

OUTLINE OF INTERACTION AND WORK FLOW BETWEEN STRUCTURE AND STABILITY PARTS OF THE PROJECT

It is crucial that geometry description and modelling of the ships under investigation in SURSHIP will be compatible with the tools and softwares used in the current project (or the opposite). In addition, the flow chart in Figure 1 is a schematic illustration of the work flow for the parts of the project and the interaction between them. Together, they outline a calculation procedure in accordance with to the aims of the main project.

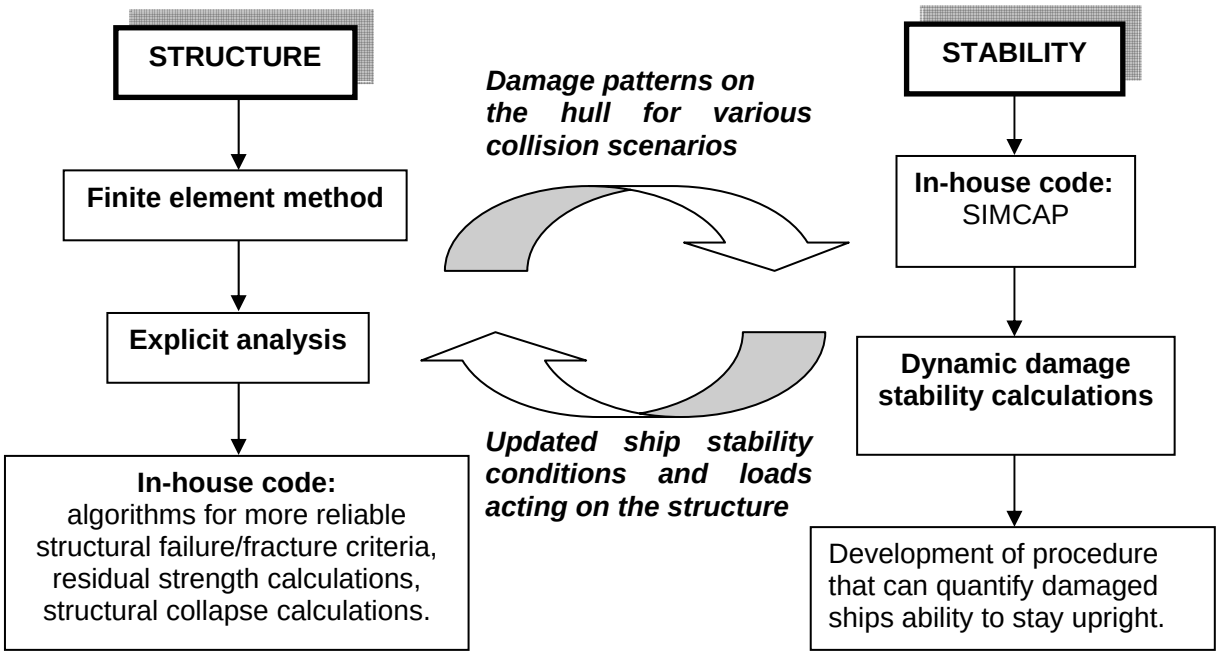

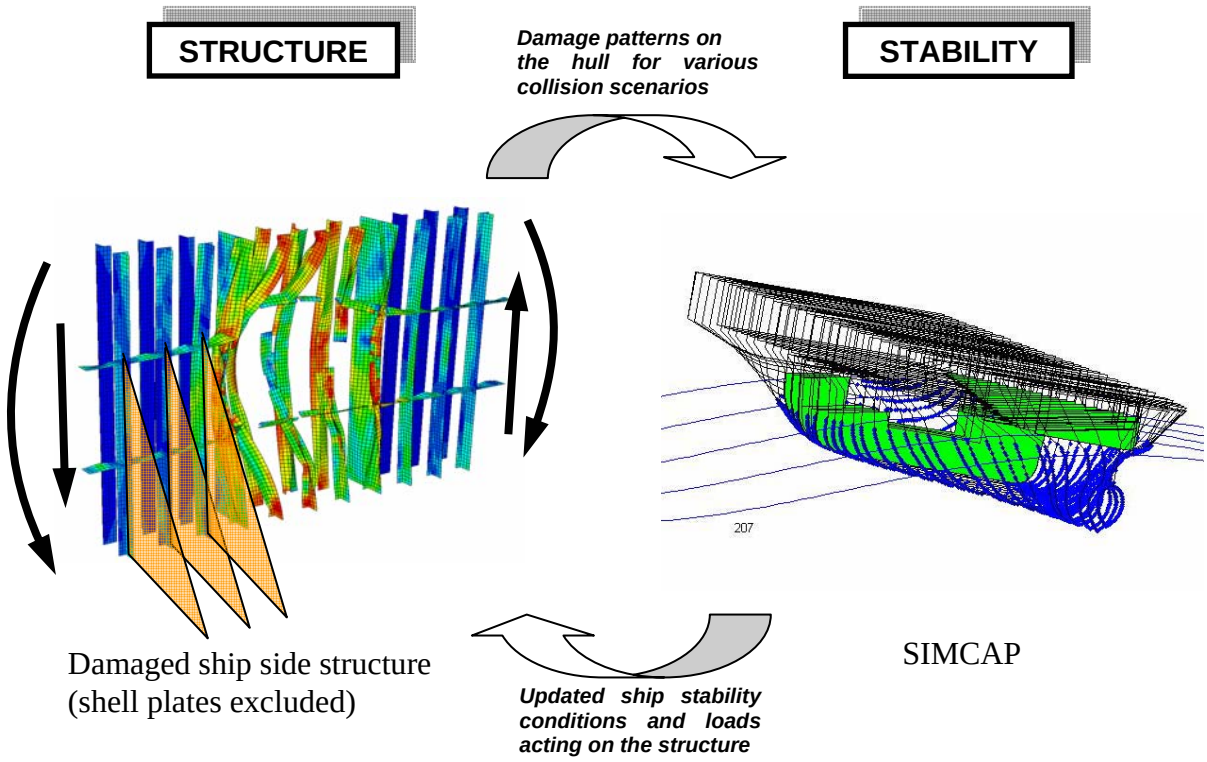

Figure 1**:** Schematic illustration of the work flow and interaction between the structure and stability parts of the project.

RESULTS AND IMPACT

- Further enhancement and validation of the existing SIMCAP numerical simulation tool.
  A preliminary result from development of the code is exemplified in Figure 2. Results also show capability of parametric roll resonance simulation.
- A comprehensive calculation procedure which quantitatively can be used for assessment of damaged ships survivability, incorporating structural collision resistance, structural stability and collapse, and ship flooding and stability in waves will be developed, see outline in Figure 1.
- New improved phenomenological models will be developed which with satisfying reliability can mimic structural collapse and rupture phenomena in ship-ship collision simulations even better in contrast to known models, methodologies and criteria found in the published literature. A methodology for estimation of the residual strength of a collided ship structure will be proposed.
- The impact of different design solutions regarding the ability to keep a damaged passenger ship upright also for large damages will be presented.
- Risk analyses of the survivability of a collided/damaged ship structure for various collision events will be investigated using the proposed calculation procedure.

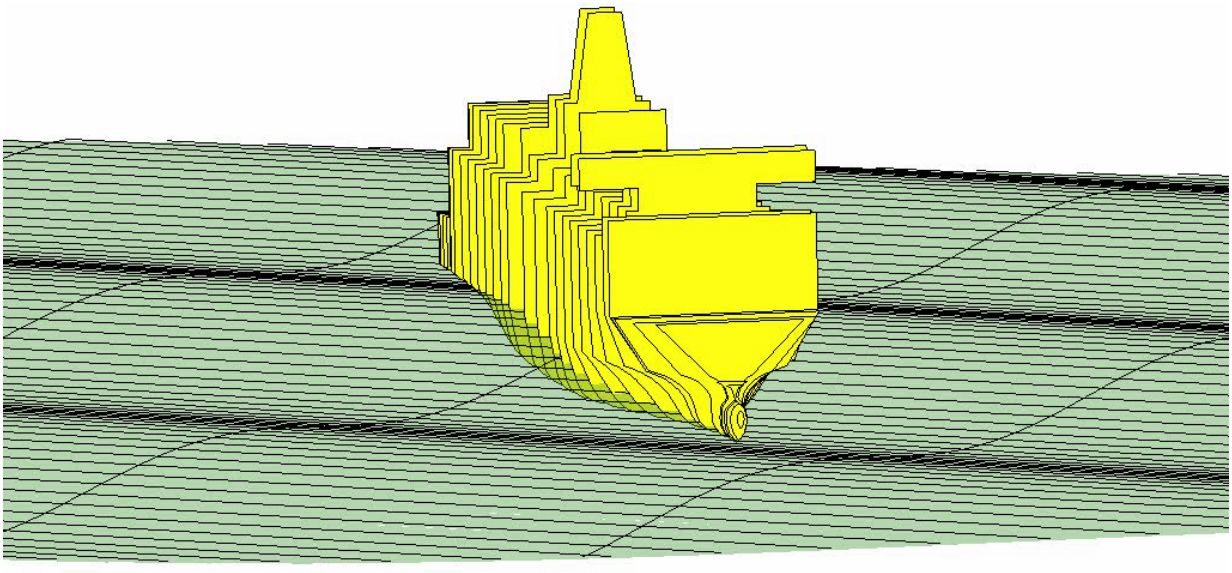

Figure 2**:** Snapshot from simulation in arbitrary wave direction

REFERENCE

Schreuder, 2005, “Time Simulation of the Behaviour of Damaged Ships in Waves”

Department of Shipping and Marine Technology, Chalmers, Göteborg, Sweden

Authors Data

Martin Schreuder, Chalmers University of Technology, P.O.Box 8873 SE-402 72 Göteborg, Sweden,
E-mail: martin.schreuder@chalmers.se

SOLAS 2009 – Raising the Alarm

Dracos Vassalos,

The Ship Stability Research Centre (SSRC), Dept of Naval Architecture and Marine Engineering, The Universities of Glasgow and Strathclyde, UK

Andrzej Jasionowski,
Safety at Sea Ltd (SaS), Glasgow, UK

ABSTRACT

In anticipation of the new harmonised probabilistic rules for damage stability being adopted in January 2009, a number of ship owners are opting to follow these rules in advance, somewhat hesitantly and reluctantly considering the general lack of experience and understanding but also the confusion that prevails. In this climate, the authors have found a fertile ground for introducing a methodology to deal optimally with this problem, deriving from the arsenal of tools and knowledge available at SSRC and SaS. As a result, the authors are involved in some way or other with many ships currently being designed in accordance with the new probabilistic rules for ship subdivision. This involvement has revealed a somewhat more serious problem with probabilistic damaged ship stability calculations, which is hidden in the detail of the rules, but one that matters most. This paper highlights this problem and recommends a way forward.

KEYWORDS

SOLAS 2009, damage survivability, probabilistic rules-based design

INTRODUCTORY INFORMATION FOR AUTHORS

Dracos Vassalos

Dracos Vassalos is Professor and Head of Department of Naval Architecture and Marine Engineering of the Universities of Glasgow and Strathclyde and the Director of SSRC, a world-leading centre of excellence on ship stability and safety. His life-long vocation has been to promote the use of scientific approaches in dealing with maritime safety and to create a critical mass in the research community by nurturing safety enhancement through innovation. He has lectured widely, published some 400 technical publications, won a string of prizes and awards, including some 100+ major research contracts totalling over £15M. Currently, Professor Vassalos is Chairman of the International Standing Committee of the "Design for Safety" Conference, a theme instigated and promulgated by SSRC and serves as member of the UK delegation to IMO for ship stability.

Andrzej Jasionowski

Andrzej Jasionowski graduated from the Technical University of Gdansk (MEng, 1997), and the University of Strathclyde (PhD, 2002). His current role involves being the Technical Manager of SSRC and a Director of Safety at Sea Ltd., an engineering consulting company offering specialist services to the maritime industry on ship stability and safety and on the design of knowledge-intensive, safety-critical ships. His main interests comprise ship hydrodynamics, damaged ship dynamics, stability, modern risk assessment, inductive inference, modelling uncertainty, numerical

algorithms development and the philosophy of safety. Andrzej Jasionowski is credited with a number of research awards and prizes and the publication of some 30 journals and conference papers.

INTRODUCTION

In January 2009, the new harmonised probabilistic rules for ship subdivision will become mandatory, initiating a new era in rule-making in the maritime industry in line with contemporary developments, understanding and expectations. This will be the culmination of more than 50 years of work, one of the longest gestation periods of any other safety regulation. Considering that this is indeed a step change in the way safety is being addressed and regulated, "taking our time" is well justified. However, the intention to provide a qualitative assessment of safety (a safety index) might have been enough at the time the probabilistic framework for damage stability was conceived (indeed for as recent as a few years ago) but this is not the case today. With the advent of Design for Safety and of Risk-Based Design, quantification of safety, consistently and accurately, is a prerequisite to treating safety as a design objective. This, in turn, entails that the level of detail in the method used to quantify safety carries a much bigger weight. With this in mind and in the knowledge that the Attained Index of Subdivision in the probabilistic rules is a weighted summation of survival factors, calculating survival factors consistently and accurately is paramount. Unfortunately, a close scrutiny of the work that led to the current formulation of the s-factor revealed that it is simply the result of a series of unjustified compromises, which inadvertently crept in during the rule-making process. In this formulation, due to be adopted in 17 months time, the s-factor derives from a regression analysis of only a filtered set of old cargo ships and as such it will be unsuitable even for this category of ships, considering the evolutionary changes in most cargo ship types. More importantly, recent research results indicate that, on the average, the formulation which is soon to be adopted seriously underestimates the inherent survivability of cruise ships whilst it drastically underestimates the survivability of Ro-Ro passenger ships. What is of crucial significance is that there is little consistency between the actual survivability of both these vessel types (the most safety-critical of ships) and that postulated by the currently proposed formulation. The problem does not end here: since this formulation was used to calculate the Index-A for a representative sample of various vessel types so as to evaluate the Required Index of Subdivision R (in principle, the safety level to be adopted), these results will also be in disarray. In short the proposed amendments SOLAS 2009 are in need of major re-evaluation!

This paper attempts to present these issues and in so doing to raise the alarm, hoping that in the time remaining no effort will be spared in ensuring that the best ever regulatory achievement in our industry will not fail to achieve it's aims before it gets started.

THE PROBABILISTIC CONCEPT OF SHIP SUBDIVISION

The first probabilistic rules for provision of stability after damage on passenger vessels, deriving from the work of Kurt Wendel on "Subdivision of Ships", [Wendel] were introduced in the late sixties as an alternative to the deterministic requirements of SOLAS '60. Subsequently and at about the same time as the 1974 SOLAS Convention was held, the International Maritime Organisation (IMO), published Assembly Resolution A.265 (VIII). The next major step in the development of damaged ship stability standards came in 1992 with the introduction of SOLAS part B-1 (Chapter II-1), containing a probabilistic standard for cargo vessels, using the same principles embodied in the 1974 regulations. This, in turn, necessitated launching at IMO the regulatory development of "Harmonisation of Damage Stability Provisions in SOLAS, based on the Probabilistic Concept of Survival" in the belief that this represented a more rational approach to addressing stability after damage.

In this state of affairs, the compelling need to understand the impact of the introduction of probabilistic damaged ship stability regulations in the design of cargo and passenger ships and the growing appreciation of deeply embedded problems in both the rules and the harmonisation process itself, provided the motivation for the adoption of an in-depth evaluation and re-engineering of the whole probabilistic framework through the EC-funded €4.5M, 3-year project HARDER [HARDER 2003]. The overriding goal of this project was to develop a rational procedure for probabilistic damaged ship stability assessment, addressing from first principles all relevant aspects and underlying physical phenomena for all types of ships and damage scenarios. In this respect, HARDER became an IMO vehicle carrying the major load of the rule-development process and fostering international collaboration at its best – a major factor contributing to the eventual success in achieving harmonisation and in proposing a workable framework for damaged ship stability calculations at the IMO SLF 47.

A stage has now been reached where the draft text of the major revision to the subdivision and damaged ship stability sections of SOLAS Chapter II-1 based on a probabilistic approach has been completed, following final amendments in January 2005 to Regulation 7-1 involving calculation of the "p" factor. The revised regulations were adopted in May 2005 by the IMO Maritime Safety Committee (MSC) and will be entering into force for new vessels with keels laid on or after 1 January 2009.

One of the fundamental assumptions of the probabilistic concept of the ship subdivision in the proposed regulations is that the ship under consideration is damaged, that is the hull is assumed breached and there is (large scale) flooding. This implies that the cause of the breach, the collision event with all the circumstances leading to its occurrence, are disregarded, and hence the interest focuses on the *conditional* probability of the loss of stability.

In other words, risk to life is assumed to be irrelevant on the likelihood of occurrence of a collision event that ends in hull breaching and flooding. For this reason, the regulations imply the same level of "safety" irrespective of the mode of operation that can e.g. take place in area of varying density of shipping (congestion of traffic), or indeed can be so different depending on ship type, or can involve vastly different consequences, etc, all of which might imply considerably different levels of actual risk. This said, all risk-related factors (e.g. size of ship, number of persons on board, life saving appliances arrangement, and so on) are meant to indirectly be accounted for by the Required Index of Subdivision, R. Summarizing, the probability of ship surviving collision damage is given by the Attained Index of Subdivision, A, and is required not to be lesser than the Required Index of Subdivision, R, as given by expression (1):

$$A = \sum_{j=1}^{J} \sum_{i=1}^{I} w_j \, . \, p_i s_{ji} \quad ; \quad \mathrm{A} > \mathrm{R} \qquad (1)$$

Where:

A/R Attained/Required Index of Subdivision

j loading condition (draught) under consideration

J number of loading conditions considered in the calculation of A (normally 3 draughts)

i represents each compartment or group of compartments under consideration

I set of all feasible flooding scenarios comprising single compartments or groups of adjacent compartments

w_j probability mass function of the loading conditions (draught)

p_i probability mass function of the extent of flooding (that the compartments under consideration are flooded)

s_{ij} probability of surviving the flooding of the group of compartment(s) "i", given loading (draft) conditions j occurred

The index A can thus be considered as the expected value of the "s-factor", with "p- and w-factors" being the respective likelihoods, reflected in worldwide ship collision statistics:

$$A = E(s) \qquad (2)$$

Consequently, (1-A) can be considered as the marginal probability of (sinking/capsize) in these scenarios, and as such it can be used for deriving the collision-related risk contribution, [Vassalos 2004].

The Required Index of Subdivision, R (derived principally from a regression on A-values of representative samples of existing ships) represents the "level of safety" associated with collision and flooding events that is deemed to be acceptable by society, in the sense that it is derived using ships that society considers fit for purpose, since they are in daily operation.

The new regulations represent a step change away from the current deterministic methods of assessing subdivision and damaged ship stability. Old concepts such as floodable length, criterion numeral, margin line, 1 and 2 compartment standards and the B/5 line will be disappearing.

With this in mind, there appears to be a gap in that, whilst development of the probabilistic regulations included extensive calculations on existing ships which had been designed to meet the current SOLAS regulations, little or no effort has been expended into designing new ships from scratch using the proposed regulations. However, attempting to fill this gap through research and though participation in a number of new building projects has revealed a more serious problem that affects the consistency and validity of the derived results and hence of the whole concept. These findings constitute the kernel of this paper and are described next, following a brief reminder on the derivation in project HARDER and the eventual adoption at IMO of the survival factor "s".

PROBABILITY OF SURVIVAL – "s-factor"

It has to be pointed out that despite the wide-raging investigation undertaken in HARDER, the survival factor "s" adopted in the new harmonised probabilistic rules designates simply the probability of a damaged vessel surviving the dynamic effects of waves once the vessel has reached final equilibrium, post-damage. All other pertinent factors and modes/stages of flooding are not accounted for. Moreover, whilst considering 7 ship models in the test programme [HARDER 2001], representing a range of different types, sizes and forms, namely: 3 Passenger ships (2 Ro-Ro's and one cruise liner) and 3 dry cargo ships (a Ro-Ro Cargo Ship, a Containership, and a Bulk Carrier - a Panamax Bulk Carrier was added later), the formulation for the s-factor focused on Ro-Ros and non-Ro-Ros. This categorisation derives primarily from the capsize mechanisms pertinent to these two categories.

Therefore, and without labouring the detail of the formulation (for which SSRC was responsible), the following two approaches were followed:

s-Factor for Low Freeboard Ro-Ro Ships

It was always the intention to base the survival factor for Ro-Ro ships on the SEM methodology, [Vassalos 1996]. In brief, the method statically develops the volume of water that will reduce the damage GZ curve to exactly zero and at the ensuing critical heel angle, θ, two parameters: h – the dynamic water head and f – the freeboard are calculated as shown in Figure 1.

The statistical relationship between parameters (h) and (f) and the significant wave height of the critical survivable sea state (H_S) is then established.

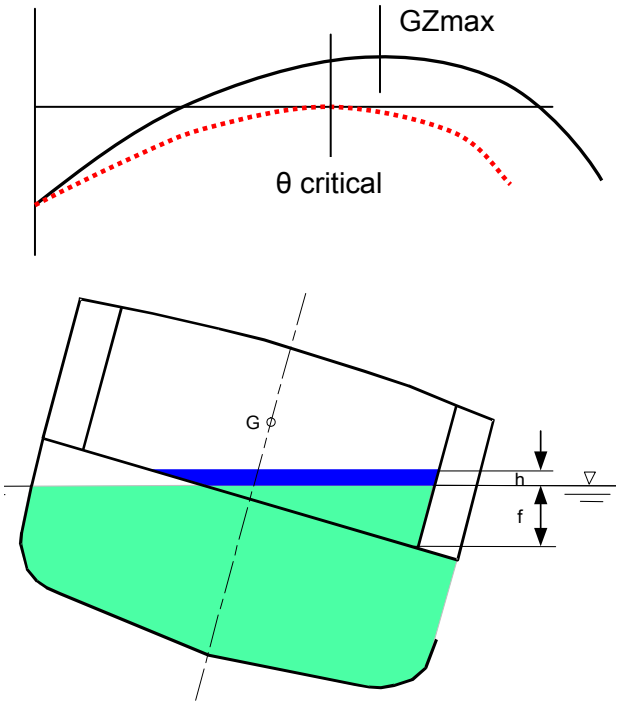

Figure 1: The SEM Methodology

Accounting finally for the likelihood of occurrence of this sea state at the time of casualty led to the following relationship (Figure 2):

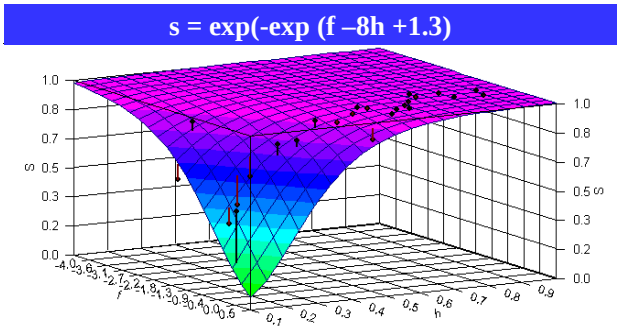

Figure 2: SEM-Based s-Factor for Ro-Ro Ships (25 Cases – 4 Ship Models)

s-Factor for non-Ro-Ro Ships

Having applied the SEM methodology to non-Ro-Ro ships and achieved what was considered unsatisfactory results, the focus shifted towards the more traditional damage stability criteria employing the use of properties of the GZ curve, such as GZ max, GZ Range, and GZ Area. In simple terms, the correlation of these three traditional parameters with the observed survival sea states from the non-Ro-Ro model tests was first established, shown here in Figures 3 to 5.

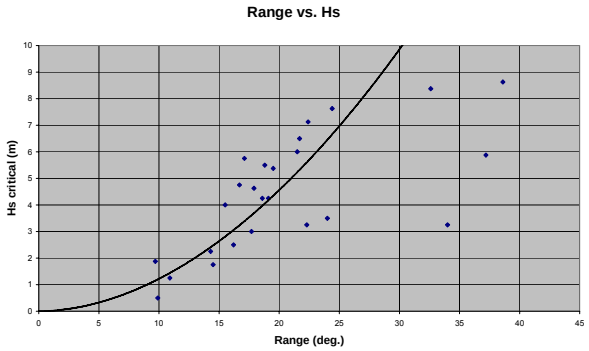

Figure 3: Regression of GZ range

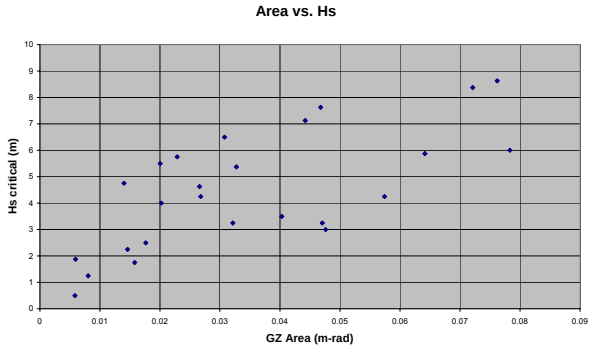

Figure 4: Regression of GZ area

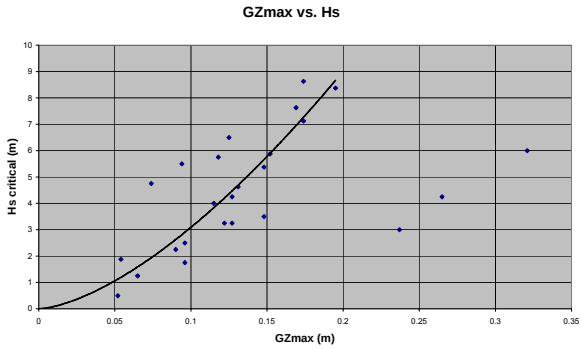

Figure 5: Regression of GZ max

A review of these results led to discarding the GZ area parameter due to apparent lack of correlation, with most points not falling naturally on the observed trends. Adopting finally an existing SLF format and with Hs limited to 4m, similar to Ro-Ro vessels, yielded the following final formulation (Figure 6):

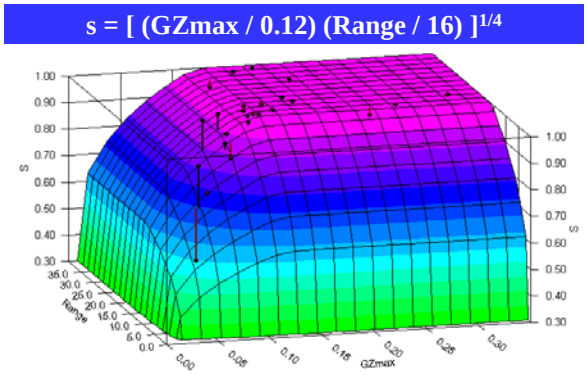

Figure 6: GZ-Based "s"-Factor for Conventional Ships (25 Cases – 3 Ship Models)

It may be noticed that 25 damage cases were used in the formulations described in the Figure 5 and another 25 damage cases in Figure 6. Thus, the whole data set used in project HARDER, and shown here in Figure 7, comprises 51 data points (the one point not accounted for relates to the cruise ship).

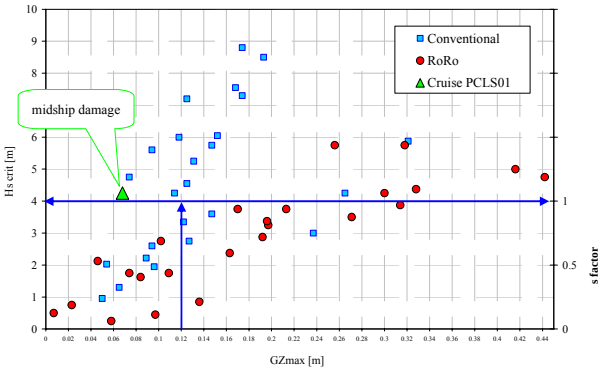

Figure 7: Data set of 51 measured points of survivability in the HARDER project

Based on the aforementioned developments the following points are noteworthy:

- The formulation for the survival factor in the new harmonised probabilistic regulations for damaged ship stability, due to be adopted in January 2009, is based solely on conventional cargo ships, Figure 6.
- The SEM methodology was never adopted; hence there is no formulation for the survival factor in SOLAS 2009 that could be applied to anything other than non-Ro-Ro ships.
- Examining also Figure 7, leads to some additional and even more disturbing observations:

  →The single result on the cruise ship, which was never used, shows that even with marginal static stability characteristics the vessel survives in sea states with Hs in excess of 4m. Several tests since then clearly demonstrate that the current formulation underestimates the survivability for cruise ships; as a general trend the bigger the vessel the larger the error!

  → On the other end of the spectrum, the formulation due to be adopted overestimates the survivability of Ro-Ro ships. In other words, survivability of Ro-Ro ships is lower than what the formulation implies.

Having made these sobering observations, there is yet another issue to consider: the development of the Required Index, R, for passenger ships. The original results, shown in Figure 8, represent the A-values calculated on the basis of the new formulation for a representative sample of ships.

Considering the arguments made above, it may justifiably be proposed that the observed trends simply reflect the oversight of the fact that the s-factors considered in the new harmonised rules had nothing to do with passenger ships.

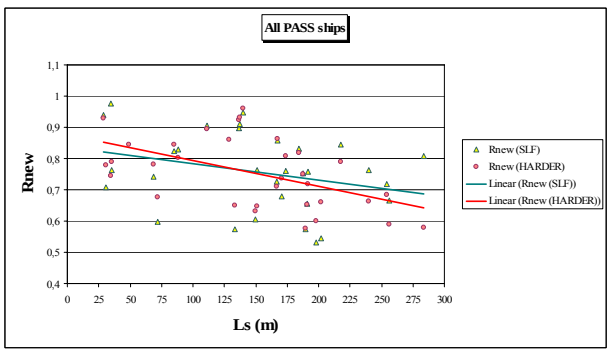

Figure 8: R_{new} for all passenger ships

Not realising this fact, rather than questioning the method of calculation, it was attempted

instead to make sense of the results at hand, using an approach questionable at best, which was surprisingly adopted by Member States at IMO; the tidal wave of the new probabilistic rules managed to push an excellent framework through the door but it seems that a series of questionable assumptions went though with it.

EMERGING EVIDENCE FOR RAISING THE ALARM ON SOLAS 2009

SAFENVSHIP Project

In the proposed formulation for the s-factor, described above, the still water GZ curve characteristics are calculated by assuming that the lowest-most spaces, within the damaged zone, flood instantly and that static balance between vessel mass, displaced water and floodwater describe fully the vessel stability.

To gain better understanding of the meaning of the above approximation and, in general, of the stability of modern passenger ships, a study was undertaken, [Jasionowski 2005], including probabilistic damaged ship stability calculations, numerical time-domain simulations and scaled-model tank testing of three cruise ship designs, considered representative of modern passenger ships. Figure 9 shows a sample result of the study. Altogether 33 different damage cases of the three vessels were investigated, chosen to provide a range of s-factors and distribution of damages along the whole length of the vessel; damage openings were chosen with a level of "high severity" in mind. Deriving from this study the following points are noteworthy:

- Of the 33 cases considered, 16 were found to lead to the vessel capsizing within two hours, sometimes rapidly. Of the 16 "capsizing" cases, 10 had an s-factor between 0 and 1, with some having s=1.0. Of the remaining 17 "surviving" cases, 7 had an s-factor equal to zero!
- The study demonstrates that traditional GZ-curve characteristics cannot adequately describe the behaviour (and hence the destiny) of a damaged ship with the complexity in watertight subdivision of internal spaces found on a typical cruise vessel, and consequently, that the formulation for the s-factor in its present form cannot meaningfully represent the average resistance of such ships to capsize when subjected to flooding, following collision damage. Another reason for this deficiency derives from explicitly neglecting the presence of multiple free surfaces (MFS effect), a phenomenon specific to ships with complex watertight subdivision, which substantially weakens or indeed leads to complete erosion of stability at any of the stages of flooding (this is a finding post-HARDER).

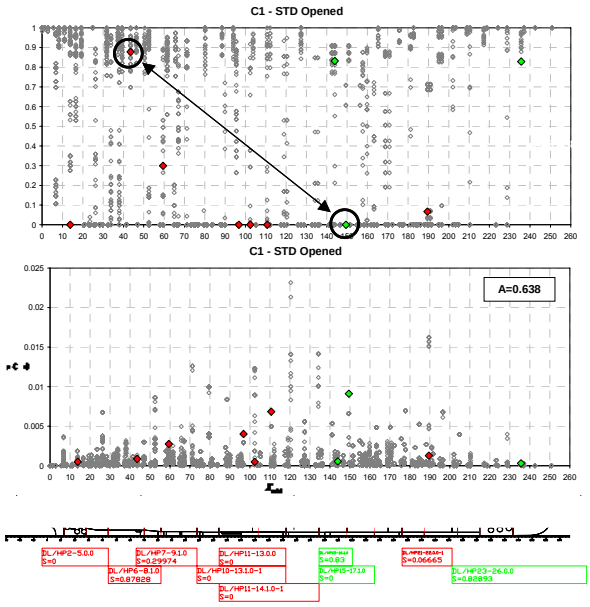

Figure 9: A map of "s" factors (upper plot) and the expression $p \cdot (1 - s)$, for all damage cases considered as a function of the damage locations. The red boxes in the lowest-most plot indicate cases where the ship capsized within 2 hours simulation time, whereas green boxes indicate survival cases

Newbuilding Design Experience

With the introduction of the new probabilistic rules, the dilemma of prescriptive SOLAS-minded designers must be overcome. Using an approach, known as **platform optimisation**, SSRC/SaS developed a fully automated optimisation process leading to ship designs with an acceptable level of flooding-related "risk" (i.e., compliance with statutory requirements) that can be optimised along with cost-effectiveness, functionality and

performance objectives. Alternatively, high survivability internal ship layouts can be developed, without deviating much from the current SOLAS practice, thus making it easier for ship designers to relate to the proposed procedure.

This procedure has been extended to address in full the damage survivability of a new building cruise and a RoPax vessels from first principles in a systematic and all embracing way, as explained in [Vassalos 2007].

Moreover, a direct link between Index-A and flooding-related risk contribution has been established, thus facilitating a better understanding of the meaning of all the factors involved and of their significance in affecting safety. This has also led to new evidence concerning the inconsistency and inaccuracy in the details of the new probabilistic rules, as summarised in Figure 10.

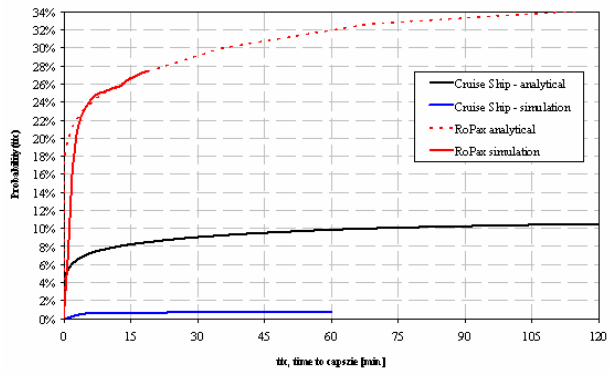

Figure 10: Cumulative probability distributions for time to capsize for a traditional Ro-Ro vessel and a large new building cruise ship. Deepest draft loading conditions.

The cumulative probability distributions for time to capsize, for the ships shown in Figure 10, are derived using two approaches: (a) an analytical expression based on the formulation of the new probabilistic rules, [Jasionowski 2006], and (b) a Monte Carlo time-domain simulation using 500 damage cases that represent the statistics of damage characteristics used in these rules. Both ships comply with the new rules. Moreover, as explained in [Vassalos 2007], the values of these distributions tend to 1-A within reasonable time period of several hours. Therefore, based on these results which seem to be typical for these groups of vessels, the following observations can be made:

- For the Ro-Ro vessel, [Jasionowski 2007], approximately one in three collision and flooding events would lead to capsize within an hour as inferred from either, analytical solution or numerical simulation (this is not a good standard!)
- Application of the new rules indicates that the cruise ship will follow a similar fate in approximately one every 10 events whilst using first-principles time-domain simulation tools the rate becomes approximately 1:100. This is a big difference!

This and other similar results have alerted the industry to the extent that a new investigation is being launched in an attempt to sort out the details in the new rules before they are adopted in January 2009, in the belief that the probabilistic rules constitute one of the most significant developments in the rule-making history of the maritime profession.

CONCLUSIONS

Based on the results and arguments presented in this paper the following conclusions can be drawn:

- The index A of new probabilistic rules on ship subdivision can be interpreted as a value that reflects the average survivability of a vessel following collision damage and flooding in a seaway. As such, an accurate calculation of the survival probability in these rules is of paramount importance.
- This being the case, there is new evidence emerging that indicates gross errors in the derivation of survival factors, demanding swift action by the profession to avert "embarrassment" on global scale.
- Such action is already being planned but it needs a wider participation to ensure that

results will be available on time to re-engineer a correct formulation before the new rules are enforced.

- More importantly, in the knowledge that the probabilistic rules are inconsistent and inaccurate, due care is needed in designing new (passenger) ships; in particular, the use of time-domain simulation tools or physical model tests must be fully exploited.

ACKNOWLEDMENTS

The financial support of the UK Maritime and Coastguard Agency and of the European Commission in the research undertaken is gratefully acknowledged. Special thanks are due to Royal Caribbean International and to Carnival for supporting this research.

REFERENCES

"HARDER - Harmonisation of Rules and Design Rationale", U Contact No. GDRB-CT-1998-00028, Final Technical Report, 31 July 2003

HARDER Task 3.1 – Main Report of Model Tests, Report Number 3-31-D-2001-13-1, 29/06/2001.

Jasionowski, A, "Survival Criteria For Large Passenger Ships", SAFENVSHIP Project, September 2005, Final Report, Safety at Sea Ltd

Vassalos, D Pawlowski, M and Turan, O, "A Theoretical Investigation on the Capsizal Resistance of Passenger/Ro-Ro Vessels and Proposal of Survival Criteria", Joint Northwest European Project, March 1996.

Vassalos, D: "A risk-based approach to probabilistic damage stability", 7th International Workshop on the Stability and Operational Safety of Ships, November 2004, Shanghai, China.

Vassalos, D: Risk-Based Design: Passenger Ships", SAFEDOR Mid-Term Conference, the Royal Institution of Naval Architects, Brussels, May 2007.

Wendel, K, "Subdivision of Ships", Diamond Jubilee International Meeting, New York, June 1968, pp 12-1 to 12-21.

Jasionowski, A, "Fast an accurate flooding prediction – analytical model", SAFEDOR, D2.1.3, November 2006.

Jasionowski, A, York, A, "Investigation Into The Safety Of Ro-Ro Passenger Ships Fitted With Long Lower Hold", UK MCA RP564, 10 July 2007, Draft Report MCRP04-RE-001-AJ, Safety at Sea Ltd.

Session 8: Intact capsize investigations

Session Chairman: A. Peters Prof. Perez-Rojas

1) L. Perez-Rojas, C. Lopez Pavon, F. Perez Arribas, A. Martin Landaluce:

   "On the Experimental Investigation on the Capsizing of Small Fishing Vessels"

2) Y. I. Nechaev, O. N. Petrov:

   "Control of Functioning Regimes of On-Board Intelli-gence Systems of Safety Monitoring"

3) A. B. Degtyyarev, Y. I. Nechaev:

   "Virtual Testbed for Marine Objects Behaviour Investigation"

On the Experimental Investigation on the Capsizing of Small Fishing Vessels

Luis Pérez Rojas
Carlos López Pavón
Francisco Pérez Arribas
Ainara Martín Landaluce

ETSIN Model Basin, UPM. Madrid (Spain)

ABSTRACT

The safety of seafarers and the protection of the marine environment can be enhanced by identifying the circumstances and causes of marine casualties and incidents.
The maritime accidents of the ships "O Bahía" and "Enrique el Morico" which took place in front of the Spanish coast in 2004 set up the beginning of the research presented in this paper. The purpose of it was to find how the ships sunk and if the stability regulations for this type of vessels are appropriate. To come to a conclusion, hydrodynamic tests for models of these two boats were carried out at the UPM and CEHIPAR model basins. The experiments methodology and results are here presented.
Free running tests have been performed in regular waves, with the models reproducing the accident's load condition but within regulation of watertightness. Wave steepness, vessels' asymmetry and inefficient water draining are considered relevant and influent parameters on capsizing.
It was nearly impossible to lead the models to capsizing, in spite of the rough conditions studied and the barely fulfilment of the stability criteria that these boats had at the accident. Only one of them overturned, and they are considered to be stable enough. The methodology developed in these tests is considered adequate to validate numerical calculations on capsizing

KEY WORDS

Capsizing, broaching, surf-riding, following and quartering seas.

INTRODUCTION

Seakeeping is a very difficult field to investigate where many aspects are not known enough. One of these aspects is how a ship reacts in following and quartering seas and more specifically how this can resolve on capsizing.

In the year 2004 some shipwrecks involving small fishing vessels occurred at the Spanish coast. As known, the commercial fishing industry is one of the most dangerous and deadly occupations in many countries, so the analysis of the casualties results helpful to determine the accident causes and prevent future sinkings. Two of the sunk boats have been considered for an investigation, with the intention of reproducing their capsizing. (Perez Rojas, 2003)

Those selected for the analysis were the "O Bahía" and the "Enrique el Morico".

The "O Bahía" is a purse seiner built in steel the year 1999. On June 2nd 2004, she sank at the waters near Sisargas Island on her way from Burela Port (Lugo) to Vigo estuary.

The "Enrique el Morico" is a long liner built in FRP the year 1999.On August 3rd 2004, she sank in front of Almeria's coast (South of Spain) due to two successive sea strokes.

The paper published in 2006 on the accidents of these fishing vessels (Perez Rojas, 2006), indicated that the load conditions at the accident, differed significantly from those considered in the "Stability Booklets". These results pointed out that the purse seiner did not fulfil the IMO stability criteria at the moment of the wreck and the long liner fulfilled them very slightly.

The IMO stability criteria are empirically developed with statistics of Northern European fishing vessels. In the last few years, some investigations have been carried out, trying to analyse if the fulfilment of these criteria results in real safety for capsizing or not. In this line of action, the article "Comparison of European and Asian Trawlers.-Stability in Seaways-" written by Umeda (2002), compares Japanese and European vessels from the viewpoint of the stability in seaways. As a result of difference of regulation for managing fishing efforts, hull forms of Asian fishing vessels are quite different from the European ones. European vessels under the regulations utilizing ship length are much wider and deeper than Japanese ones under the regulation utilizing gross tonnage. As the stability criteria were based on data from European vessels, in general, the Asian ones do not comply with them. The mentioned article concludes that the European fishing vessels, fulfilling the IMO stability criteria, are much safer than the Japanese ones, but they are easier to suffer broaching in quartering seas and parametric resonance in head seas.

The ships analysed in this paper are two quite representatives of the Spanish fishing vessels fleet. Nevertheless, there are important differences between the two boats, because they used to sail at very different zones. The boats could be considered typically Europeans vessels, but, in spite of this, they had many difficulties complying with the IMO stability criteria at the moment of the accident. Even so, this work points out that these boats do not suffer neither stability problems nor capsizing, even sailing in very harsh conditions. Only the "O Bahía" model turned over, but it was nearly impossible to reach this situation.

Previously to this work, experimental tests on capsizing were carried out at the CEHIPAR. A larger model of the "O Bahía" was used in these trials. These previous experiments were presented in 2006 (Maron, 2006) and suggested that a model made to a smaller scale was necessary to achieve capsizing.

According to these previous experiments (Maron, 2006), only regular waves have been studied due to the long time needed for the irregular wave experiments. The models have been studied in beam and longitudinal regular waves.

The "O Bahía" tests presented at this paper, are the development of those planned previously, that could not be performed due to the model scale.

Based on the previous experience obtained from the purse seiner results, the "Enrique el Morico" was tested in waves considerably higher than those assumed to be present at the time of the accident.

The report presented by Umeda at the 6th International Ship Stability Workshop (Umeda, 2002) shows that it is necessary to quantitatively predict capsizing, to systematically examine all factors relevant to capsizes in following and quartering seas. Efficient computer codes that could be very helpful in this issue are being developed rapidly, but the complexity of the involved phenomena and the high degree of nonlinearity in many characteristics together pose a formidable challenge that will require years of hard work. The Report of the Seakeeping Committee (ITTC, 1993) presents the need for model test data related to extreme wave

conditions that will provide the required information to validate simulation methods. These can consist of captive, partly captive and free running tests results. The results deduced from the experiments presented in this paper satisfy these requirements, and could be very useful for validation purposes.

MODEL DESCRIPTION

Ship Data

A model of each analysed ship was used to develop the experimental studies on the maritime accidents described before. The model of the ship “O Bahía” was made to scale 1:13.7 meanwhile the model of the ship “Enrique el Morico” was made to 1:13.5. The following figures show the general arrangement and body plans of the ships and some photographs of the models.

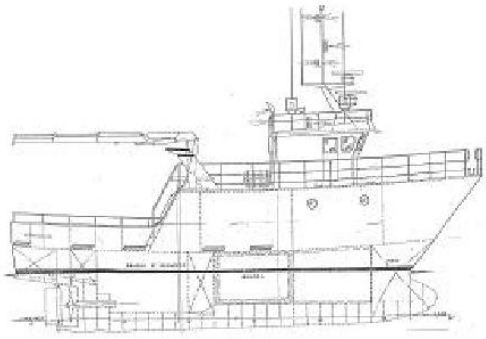

Fig. 1: "O Bahía” General Arrangement

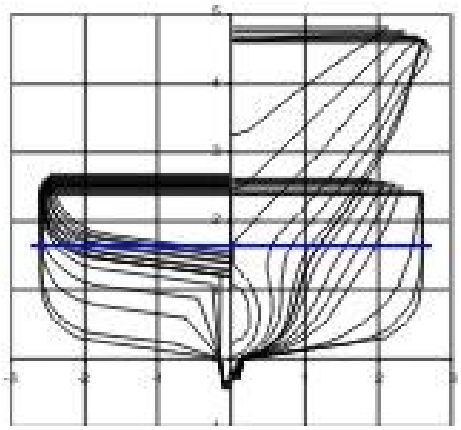

Fig. 2 :"O Bahía” Body Plan

Fig. 3 Model of the ship "O Bahía"

Fig. 4 Model of the ship " O Bahía"

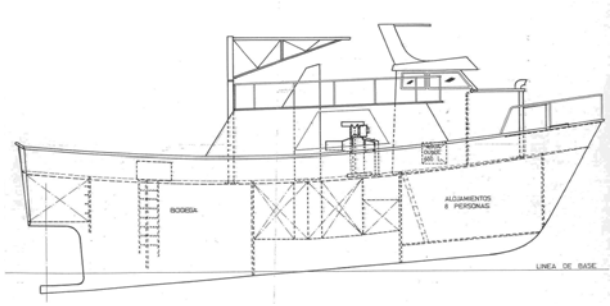

Fig. 5: “Enrique el Morico” General Arrangement

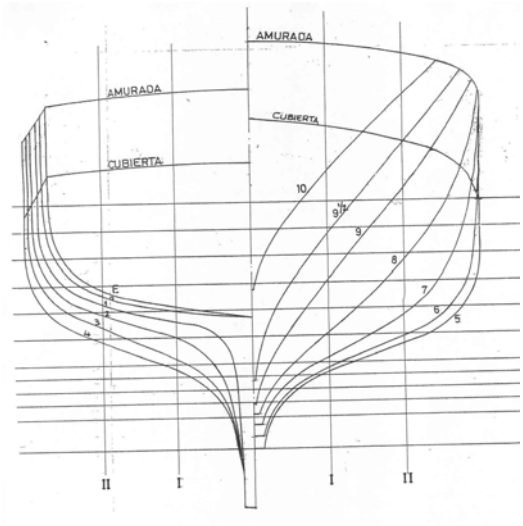

Fig. 6: “Enrique el Morico” Body Plan

Fig. 7: Model of the ship “Enrique el Morico”

Fig. 8 : Model of the ship “Enrique el Morico”

The following characteristics and load conditions are deduced from the accident reports:

Table 1 : Ships Characteristics

Ship	O Bahía	Enrique el Morico
Displacement (t)	74.20	39.05
Lpp (m)	13.50	13.80
Beam (m)	5.20	4.57
GM (m)	0.589	1.104
T (m)	1.63	1.78
TRIM (m)	0.45	0.11
Longitudinal gyradius (%B)	44.00	37.00
Transverse gyradius (%Lpp)	32.70	33.00
Pitching Period (s)	3.15	3.10
Rolling Period (s)	6.00	3.20

Model Construction and Fitting

The models were built in FRP, reproducing underwater hull and also superstructure.

The “O Bahía” model was provided with bulwark ports and their closures, which reproduced those in the shipwrecked vessel.

Detailed plans of “Enrique el Morico” boat were not available, so the information about the situation of the scuppers was obtained from a ship built in the same mould. The situations of the scuppers are supposed to be similar in both boats, as they were built at the same shipyard, and in the same mould.

Tests were carried out with all the openings closed, because the aim is to study the accident situations, but keeping the models within regulation conditions of watertightness, and without cargo movements.

They were loaded to reproduce the accident’s displacement. This done, the weights were moved fore and aft, to get longitudinal inertia, vertically to obtain proper GM, and crosswise to achieve transverse inertia.

Instrumentation

The models were provided with a gyrostabilized equipment composed of two stations communicated by radio link. The on-board station sent the measured data to the land station. The broadcast information was acceleration and angular position for each axis. The system can also be used as a 16 input/output channel control station. The rudder and the engine were servo-controlled by two of the mentioned channels.

Equipment main characteristics are:

- Maximum acceleration (vertically) 10 G
- Maximum angular velocity 300 º/s
- Angular position measurement resolution 0.05º
- Sampling Frequency 50 Hz
- Differential GPS

An ultrasonic device installed in the towing tank carriage was used to measure waves during the tests. The device main characteristics are:

- Range of measurement: 200-1300 mm

- Sampling frequency: 200 kHz
- Resolution: 0.18 mm

TESTS DESCRIPTION

Two groups of tests were accomplished for each model, first of them, at the ETSIN Model Basin, and the second group at the CEHIPAR Model Basin.

Tests at the ETSIN Model Basin.

Once the models were built and fitted, their velocity was calibrated. They were run at different velocities by changing the position of the potentiometer that controlled the engine. Velocity was measured when there was not relative motion between the vessel and the towing carriage.

The "O Bahía" was tested in longitudinal waves. The wave amplitude was the maximum possible at the facility (3.5 m and 5.5 s to real scale). Excessive rolling or manoeuvring difficulties were not noticed.

They were also tested in beam seas.

Tests at the "CEHIPAR Model Basin."

As said before, the tests for the "O Bahía" executed at the "CEHIPAR Model Basin" could be considered as a continuation of those completed previously for a model to a greater scale. These trials revealed the need of carrying on with the investigation, but using a smaller one, that would allow complying with the planned experiments, which could not have been completed because the wave generator limit had been reached.

Sea conditions at the moment of the accident were calculated by the CEDEX according to the data obtained by the Spanish Network of Buoys and the Spanish Meteorological Centre, and the studies on wave generation from the "Puertos del Estado" Institution. These studies suggested irregular seas with the following characteristics for each boat:

Table 2 : Waves Characteristics

Ship	O Bahia	Enrique el Morico
H (m)	2.7	1.3
T (s)	6.2	5

Previous studies in regular and irregular waves, (Maron, 2006), showed that the irregular waves did not lead the "O Bahía" to a situation that could be considered especially risky. These results denoted that the most interesting waves for the analysis were higher than those predicted for the moment of the accidents.

As a huge amount of tests was needed to obtain acceptable results in irregular seas, a deterministic study was selected, and the models were analysed in those regular waves that had a low but appreciable probability of appearance.

Other fact that also justified studying the phenomena in regular waves was that numerical simulations demonstrated that a big wave is usually accompanied by a previous and a following which have similar characteristics. Generally, the overturn is more frequent in regular waves.

Selected waves were steep and sometimes breaking waves. Test conditions were rougher than those at the accident. Although ships were loaded in the same way as at their accidents, cargo movements and water retention have been neglected at the experiment. The waves used when performing the experiments are presented at the following tables:

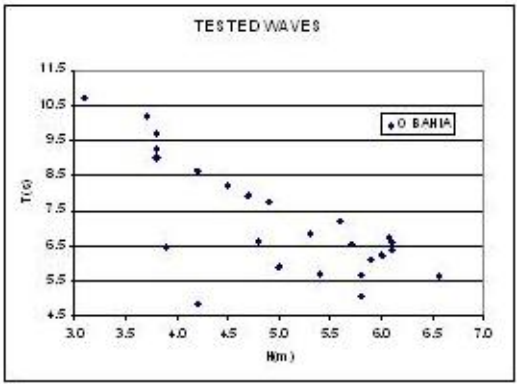

Fig. 9 : Tested waves for the model of the “O Bahía”

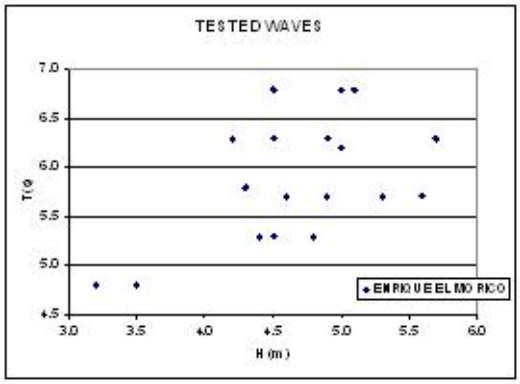

Fig. 10: Tested waves for the model of the “Enrique el Morico”

Tests Methodology

Tests started with each model stationary at the tank end. Waves with the theoretical amplitude and period were generated. The run commenced some waves after the first ones reached her. When the waves were considerably high, the test began with the boat heading the sea. Then, she bore away when the waves were regular, and the measuring began. Slalom courses, manually controlled were performed. The vessels sailed in quartering and following seas. An automatic regulation for the course was tried at the previous tests, in order to prevent any influence from the remote control skipper, but it was nearly impossible to maintain the course this way. For this reason a hand-operated heading control was selected.

The rudder was kept fixed during the tests, and only moved when the ship was near the walls of the basin. After setting a new course it was centered again.

The model course was modified at 20 m from the other tank end, and she sailed back to the department point, in head seas.

“O Bahía” and “Enrique el Morico” velocities during the tests were approximately 10 and 12 knots respectively.

As said before, the waves were measured during the tests using an ultrasonic device. The calibration wave was obtained at the same time as the experiments were carried out, in order to avoid other series of tests to make the calibration. So, for each test, real wave height and period was obtained.

A file containing time, acceleration and angular position for each axis was recorded for every run. Next, only the part where the ship was sailing in following and quartering seas was considered, neglecting the other situations. Trim data was corrected after every run, in order to refer this data to the water line. This correction was needed because the inertial unit was installed at its base trimmed. Yawing data was only used to know the beginning and the end of the run (that corresponded to appreciable variations in the heading), so this information was deleted once the data was analysed.

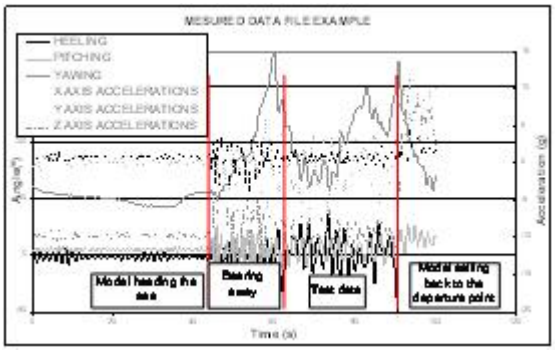

Fig. 11: Measured data during the tests

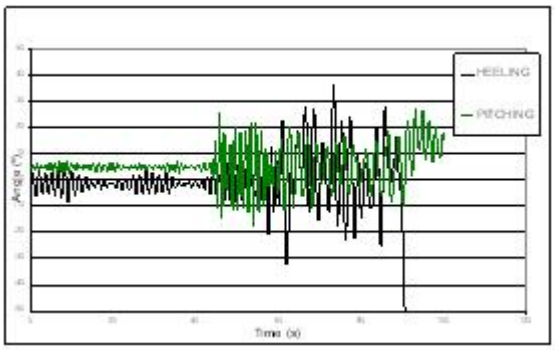

Fig. 12: Definitive data file

RESULTS

The maximum rolling and pitching data are here included for each model. These results have been deduced from the files mentioned above.

Table 3 : Results of the "Enrique el Morico" tests.

H (m)	T (s)	MAX. ROLLING ST (º)	MAX. ROLLING PT (º)	MAX. PITCHING (º)	MIN. PITCHING (º)
4.3	5.8	53.7	30.2	19.8	-26.7
4.9	5.7	34.8	38.5	18.4	-24.3
4.6	5.7	20.6	28.0	14.4	-17.2
5.3	5.7	20.6	28.0	14.4	-17.2
5.6	5.7	55.0	35.7	20.0	-23.2
4.2	6.3	28.1	27.8	14.8	-16.6
4.5	6.3	32.1	21.6	16.8	-21.2
4.9	6.3	37.8	35.0	18.4	-18.7
5.0	6.2	32.7	44.4	21.9	-24.6
5.7	6.3	54.0	43.7	29.4	-22.7
4.5	6.8	20.6	28.0	14.4	-17.2
5.0	6.8	19.1	19.7	17.4	-21.8
5.1	6.8	34.0	23.4	17.1	-20.4
5.0	6.8	21.4	28.9	19.6	-17.8
4.5	5.3	36.2	39.0	21.6	-21.8
4.8	5.3	41.6	39.3	24.2	-26.4
4.4	5.3	20.6	28.0	14.4	-17.2
3.2	4.8	32.1	36.9	23.0	-22.4
3.5	4.8	51.9	32.3	36.2	-12.9

The following table presents the data obtained from the “O Bahía” model tests. The results accompanied by an S or an F are those from the runs performed to a velocity lower or higher than the nominal one, respectively.

Table 4 : Results of the "O Bahía" tests

H (m)	T (s)		MAX. ROLLING ST (º)	MAX. ROLLING PT (º)	MAX. PITCHING (º)	MIN. PITCHING (º)
4.2	4.9		34.0	26.3	12.1	-10.8
5.8	5.1		CAPSIZING			
5.8	5.1	S	CAPSIZING			
5.8	5.1	F	CAPSIZING			
5.8	5.7		39.6	34.1	17.7	-15.4
6.6	5.6		26.4	34.4	12.7	-22.6
6.6	5.6	F	23.6	23.2	18.1	-20.2
5.4	5.7		34.8	35.2	13.4	-12.4
5.4	5.7	S	27.9	21.6	19.4	-18.9
5.0	5.9		15.0	23.4	21.7	-18.3
5.9	6.1		25.7	28.9	13.3	-11.9
6.0	6.3		28.6	26.5	13.5	-14.1
6.1	6.4		29.1	27.6	13.3	-18.4
3.9	6.5		22.5	20.5	8.1	-10.1
5.7	6.6		18.1	19.2	9.5	-12.2
6.1	6.6		16.0	16.7	10.7	-160.0
4.8	6.6		34.8	24.2	12.7	-12.2
6.1	6.8		22.5	20.6	12.2	-11.8
5.3	6.9		9.9	15.1	7.7	-9.3
5.6	7.2		17.9	16.9	7.1	-10.9
4.9	7.8		13.5	14.7	10.7	-8.3
4.7	7.9		6.8	13.0	4.9	-7.2
4.5	8.2		8.5	11.0	4.8	-6.5
4.2	8.6		7.4	7.9	7.5	-6.4
3.8	9.0		7.6	7.2	5.8	-5.5
3.8	9.3		6.9	7.8	5.5	-6.1
3.8	9.7		11.6	7.7	4.4	-5.2
3.7	10.2		4.4	6.1	4.7	-4.8
3.1	10.7		6.7	8.7	5.2	-3.6

Experimental data and information from the tests yield to the following results for the ship “O Bahía”:

When the vessel, without initial motion, sailed in beam seas, she suddenly headed into the waves without any rudder manoeuvring.

In head seas and with the engine stopped, she kept the bow to the waves.

The wave that turned over the model was a breaking wave. As recommended at Circ. 707, (IMO, 1997), the model was not only examined to the nominal velocity (10 knots), but also faster, and slower. The same wave

caused capsizing sailing either at the expected velocity or at a greater or lower velocity.

The most influent parameter on causing capsizing was the slope of the wave, as a high wave without a short period did not cause the overturn.

Water shipping by immersion of the stern and inefficient water draining are significant factors on capsizing. Difficulties to evacuate the shipped water were also shown at the previous experiments.

In the runs where capsizing occurred, the first wave heeled the ship dangerously. Therefore the working deck submerged, and then she did not have enough time to drain this water so the next wave caused the turn over.

“O Bahía” model always overturned on the port side. The asymmetry in the course of the shipped water seemed to be a determinant factor on capsizing, producing a complex composition of motions which endangered the ship.

She had problems maintaining the course, and started surf-riding, when the wave amplitude was considerably high.

“Enrique el Morico” model did not shipwreck, in spite of the rough conditions examined. She is considered to be stable enough.

When the long liner was tested in beam seas, without initial motion, she headed slightly into the waves.

Large heeling angles were reached sailing in following seas, but there were not stability problems. She surfed on the waves in following seas, making difficult keeping the course, but without water shipment. Broaching phenomenon appeared causing abrupt and sudden heading variations. Surf-riding phenomenon appeared during long periods when sailing in following and quartering seas. Fish handling area superstructure avoids water shipping during the surf-riding.

The tests preformed in regular waves, with the height and period corresponding to the acccidents’, did not cause any significant result for any boat.

CONCLUSIONS

Even though the harsh conditions proposed for the experiments, and the slightly fulfilment of the stability criteria, only the model of the “O Bahía” overturned.

Actually, the response to heavy seas of the two vessels can be considered adequate. The vessels did not capsize because of their seakeeping conditions, but due to other causes such as sailing with the openings not closed or in conditions where they were not perfectly watertight.

It is known that water shipping is a really important factor that can endanger the ship, and lead her to capsizing. The results obtained show that there was not water shipment in the long liner tests, due to her superstructure. Nevertheless, the water in the purse seiner´s deck, and her difficulties to drain it, caused large heeling angles, and sometimes the capsizing.

Deficient evacuation of shipped water is an influent factor on capsizing that should be further studied.

Broaching phenomena appeared in the “Enrique el Morico” tests, even though the length of the waves generated was bigger than the one that is considered to be the riskiest. For example, as it is shown in the book “Stability and Safety of Ships. Volume I” (Kobylinski , 2003), the range of danger of a ship sailing in following and quartering seas is one to two times the ship length. The length of the waves in our tests exceeded twice the ship length.

As it is mentioned in the Introduction, the "O Bahía" and the "Enrique el Morico" were built following European regulations and criteria, so they are fully representative European ships. However, the latter almost did not comply with the Stability criteria at the moment of the accident, which correspond to the studied situation; and more dangerously, the former did not comply with it.

In reference to the conclusions of the article "Comparison of European and Asian Trawlers.-Stability in Seaways"(Umeda,2002), which establish that European boats can suffer a situation of stable surf-ridding which ends with a broaching, the tests performed show this attitude in the "Enrique el Morico" experiment. ". Surprisingly, the results of the "O Bahía", fit in with the typical response of Asian boats. Even though, both ships have a more than good seakeeping.

The results of the experiments presented in this work show two boats with great difficulties in the fulfilment of the IMO stability criteria that do not capsize in the major part of the tests. This seems to suggest that the non-fulfilment of these stability criteria is not a synonym of danger for capsizing for the type of boats and waves considered in the experiment.

The data and results presented before (tables 3 and 4) represent useful information on the response of a vessel sailing in following and quartering seas when extreme wave conditions are considered. The methodology developed in the tests presented in this paper, and their results are considered adequate to validate numerical calculations on capsizing or prediction of extreme motions.

ACKNOWLEDMENT:

This work was supported by the Spanish Maritime Administration under a contract signed between Dirección General de la Marina Mercante and Universidad Politécnica de Madrid. The authors express their gratitude to the different students and other people involved in the work carried out by the Model Basin Research Group in the Escuela Técnica Superior de Ingenieros Navales. Specially, the authors would like to thank Jaime Moreu for his contribution to the investigation and the development of this paper.

REFERENCES

IMO, 1997, "Guidance to the Masters for avoiding dangerous situations in following and quartering seas." MSC/Circ.707

ITTC-1993 , 1993, "Report of the Seakiping Committee on Uncertainty Analysis And Vvalidation Procedures" Proceedings of the 20th International Towing Tank Conference.

ITTC-1993, 1993, "Discussion to the Seakeeping Committee On Experimental Investigation of Ship Dynamics in Extreme Waves." Proceedings of the 20th International Towing Tank Conference.

ITTC-1993 , 1993, "Discussion to the Report of The Seakeeping Committee on Model Tests For Validation of Extreme Motion Programmes" Proceedings of the 20th International Towing Tank Conference.

Kobylinski, L.K., Kastner S., 2003, "Stability and Safety of Ships. Volume I, Regulation and Operation. ". Series Editors R. Bhattacharayya & M.E. McCormick.

Maron, A., Carrillo, E., Valle, J., Prieto, M.E., Gutierrez, C., Taboada, M., 2006, "Investigation on the capsize of a small fishing vessel in following seas." Proceedings of the 9th International Conference on Stability of Ships and Ocean Vehicles.

Perez Rojas, L., Perez Arribas, F., Zamora, R. Guerrero y Pacheco, A., 2006, "On the accidents of smalls fishing vessels." Proceedings of the 9th International Conference on Stability of Ships and Ocean Vehicles.

Perez Rojas, L., Abad, R., Perez Arribas, F., Arias, C., 2003, "Some Experimental Results on the Stability of Fishing Vessels." Proceedings of the 8th International Conference on Stability of Ships and Ocean Vehicles.

Umeda, N., Iskandar, B.H., Hasimoto, H., Urano, S., Matsuda, A., , 2002, "Comparison of European and Asian Trawlers.-Stability in Seaways-." AP hydro.

Umeda and Peters. , 2002, "Recent Research Progress on Intact Stability in Following and Quartering Seas" Proceedings of the 6th International Conference on Stability of Ships and Ocean Vehicles.

Control of Functioning Regimes of On-Board Intelligence Systems of Safety Monitoring

Yury I. Nechaev,

State Marine Technical University, St.-Petersburg, Russia

Oleg N. Petrov,

State Marine Technical University, St.-Petersburg, Russia

ABSTRACT

The questions of the control of functioning regimes of onboard intelligence system in various operating conditions are discussed. The functioning regimes are developed with use of concept of a climatic spectrum of sea waves. Identification and control of making processes of oscillatory movement of a ship for non-standard (not regular and extreme) situations are carried out on the basis of methods of fuzzy logic. The basic attention is inverted on feature of behaviour of a ship at intensive external disturbance. The examples of modelling of rolling regimes of a ship at influence of packages of irregular waves are given. The rolling regimes are allocated at forming the attractor sets in the form of unstable limit cycles.

KEYWORDS

Fuzzy logic; safety monitoring; intelligence system; attractor; limit cycle; stability; rolling

PROPOUNDING

The problem complexity, the incompleteness and the uncertainty of the source information about behaviour of a ship and "Ship – Environment" system lead us to the necessity of development of computing technology that assures real-time data handling with the use of high-performance computing facilities. The basic role in this technology belongs to the data of dynamic measurements acting from sensors of onboard measuring system.

Let's discuss the discrete stochastically disturbed system with r-dimensional input space. At the point of time t system output are column vectors $\theta_t, \Psi_t, \ldots, \zeta_t$ of oscillatory movement parameters that determine the result of interaction of the dynamic object and environment in sea conditions. The measurements fix at the discrete points of time 1,2,3,…,t and define the trajectories of parameters that form informational vector in the range T:

$$J = \{\theta_t, \psi_t, ..., \zeta_t, ..., t \in [0, T]\}. \qquad (1)$$

If behaviour of the system is observed from the point of time 1 till the point of time t then vectors can be represented as

$$\begin{aligned} &\theta_t = [\theta(t), \theta(t-1), ..., \theta(1)]^T; \\ &\psi_t = [\psi(t), \psi(t-1), ..., \psi(1)]^T; \\ &... \\ &\zeta_t = [\zeta(t), \zeta(t-1), ..., \zeta(1)]^T, \end{aligned} \qquad (2)$$

where T is transposition operator.

It is necessary to hold the analysis of the situation and to construct the forecast function in the best way displaying the tendencies in change of components of an information vector (1) on the basis of data about

parameters $\theta_t,\Psi_t,\ldots,\ \zeta_t$. The critical ranges $\tau=\tau_{CR}$ within the limits of which safe operation of a ship is not provided can be found in the curves of ship oscillatory movement by assigning limiting values $\theta_t^*,\Psi_t^*,\ldots,\ \zeta_t^*$ of ship characteristics reasoning from maintenance of safety requirements:

$$\tau = \tau_{CR} \ when \ \theta(t_1) \geq \left|\theta^*\right|, \quad \psi(t_2) \geq \left|\psi^*\right|,\ldots,\zeta(t_n) \geq \left|\zeta^*\right|. \tag{3}$$

The features of ship behaviour at a various level of external disturbance are taken into consideration at the decision of a task on the basis of scenarios of storm development in the established operating conditions. The essential factors defining adverse modes of ship rolling are as a result established and the structure of mathematical model is formed.

SCENARIOS OF STORM DEVELOPMENT

The control of functioning regimes of intelligence system is carried out on the basis of mathematical modelling of extreme situations with the use of a climatic spectrum of sea waves (Lopatoukhin et al, 2000). The classification of frequency-directed spectra is presented in Fig. 1. The approach for typification of spectra of sea waves in frequency range on genetic set of patterns is used for modelling of weather scenarios so that the spectra of each type were geometrically similar and differed just by parameters of the corresponding various wave making conditions (Lopatoukhin et al, 2000). The essence of typification is in relating the records of wave ordinate $\zeta(t)$ to chop, wind wave or hybrid wave. Hence the genetic classification of spectral density of waves comes to typification by truncated or full spectrum moments and associated with them values. In that case any spectral density $S(\omega)$, that is a stochastic function as a result of the averaging, can be represented as a non-random function $S(\omega,\Xi)$ with the set of random parameters Ξ. The described in work (Lopatoukhin et al, 2000) procedure of classification of genetically similar spectra assures the classification of frequency-directed spectra of waves on the basis of on-site data and modelling calculations. These spectra are represented as:

$$S(\omega,\beta) = m_{00}\sum_{p=1}^{N}\gamma_p S_p(\omega,\beta \mid \omega_{\max},\beta_{\max})^{\sim} \tag{4}$$

$$\sum_{p=1}^{N}\gamma_p = 1$$

Here m_{00} is the zero moment of a spectrum (a dispersion of choppy surface), γ_p – the weight investment of each wave system into aggregate energy, ω_{max} – the frequencies of spectrum peaks and β_{max} – the corresponding directions of each wave system.

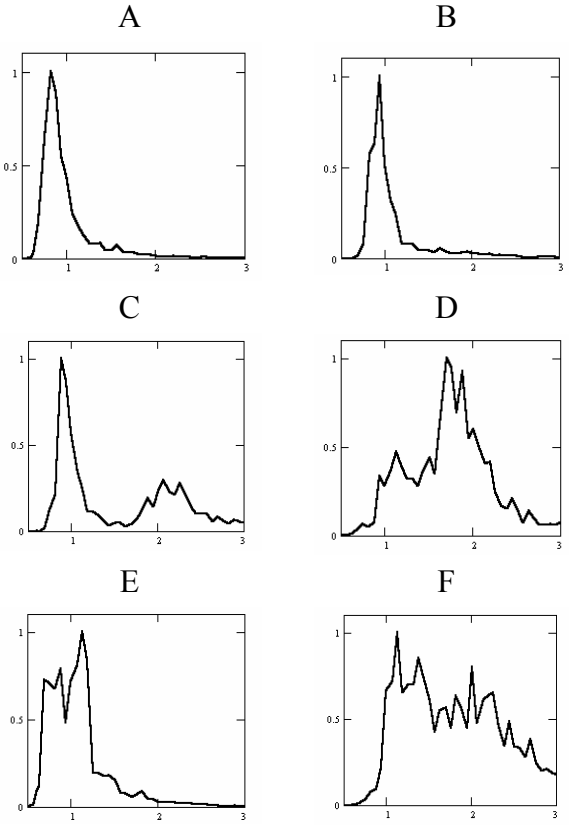

Fig. 1. Typical normalized spectra of sea waves: A – a chop; B – a wind wave; C – a hybrid wave with the split of systems and with the prevalence of a chop; D – a hybrid wave with the split of systems and with the prevalence of a wind wave; E – a hybrid wave without the split of systems and with the prevalence of a chop; F – a hybrid wave without the split of systems and with the prevalence of a wind wave. The vertical axis is the spectral density $S(\omega)/S_{max}$; the horizontal axis is the frequency ω, sec^{-1}.

This approach allows typifying each wave system using five parameters $\{\gamma_i, \omega_{maxi}, \beta_{maxi}, n, m\}$ (here n, m – parameters of spectrum shape).

The model of autoregression of moving average is used in modelling spacio-temporal field $\zeta_W(\vec{r},t)$ of choppy surface of sea waves (Fig. 3). This model is based on the representation of heaving process as a linear dynamic system of order N with the distributed parameters and stochastic input signal (Hayashi, 1968):

$$A[\vec{r},t]\cdot\zeta_W(\vec{r},t) = B[\vec{r},t]\cdot\varepsilon(\vec{r},t)$$

where

$$A[x,t] = \sum_{i=0}^{N} a_i \frac{\partial^i}{\partial t^i} + b_i \frac{\partial^i}{\partial \vec{r}^{\,i}}; \qquad (5)$$

$$B[x,t] = \sum_{j=0}^{M} c_j \frac{\partial^j}{\partial t^j} + d_i \frac{\partial^j}{\partial \vec{r}^{\,j}}$$

are linear differential operators with the autoregression coefficients (a_i,b_i) and the moving average (c_j,d_j), and $\varepsilon(\vec{r},t)$ is the field of centralized white noise with the unit variance.

Model parameters are identified by means of Yule-Walker equations using the spacio-temporal correlation function of the ordinates of waves

$$K_\varsigma(x,y,\tau) = \int_{-\infty}^{\infty}\int_{-\infty}^{\infty} E_\varsigma(u,v)\cos(xu + yv - \omega(u,v)\tau)\,du\,dv \qquad (6)$$

where $E_\zeta(u,v)$ is the energy spectrum in the plane of wave numbers (u,v). This spectrum is connected with the frequency-directed spectrum of waves $S_\zeta(\omega,\theta)=S_\zeta(\omega)Q(\omega,\theta)$ by means of dispersion relation $\omega = \omega(u,v)$ where ω is the frequency and θ is the corresponding direction.

CONTROL OF REGIME SYSTEM FUNCTIONING

The control of dynamics of a ship-environment interaction, danger levels of various disruptions in its behaviour and forming the corresponding criteria is carried out on the basis of methods and models that allow to formalize the range of deviation from the regime of normal operation and to estimate its safety. The information gathered in the process of intelligence system functioning takes on special significance during the solving of this task. Identification of mathematical models that describe non-standard (not regular and extreme) situations is carried out on the basis of statistical analysis of measuring data gained in the operating conditions and within the process of simulation of the ship-environment interaction. Time curves of the investigated processes are represented as (Anderson, 1971),(Kendal et al, 1976):

$$\Re(t_i) = F(t_i) + \Im(t_i) + S(t_i). \qquad (7)$$

Here $\Re(t_i)$ is interpreted as investigated processes $\zeta(t_i),\theta(t_i),\Psi(t_i)$; $F(t_i)$ is a slowly changing function of time $(\text{trend})_i$; $\Im(t_i)$ is the periodic (cyclic) component; $S(t_i)$ is the stochastic component:

$$S(t_i) = \xi(t_i) + \varepsilon(t_i). \qquad (8)$$

where $\xi(t_i)$ is the independent random sequence (noise) with the average of distribution $M[\xi(t_i)]=0$ and the dispersion $\sigma_\varepsilon^2(t_i)$; $\varepsilon(t_i)$ is a sequence of accidental events ("peaks") which represents irregular observations at the random points of time τ_i:

$$\varepsilon(t_i) = \begin{cases} A_i, & if \quad t_i = \tau \\ 0, & if \quad t_i \neq \tau \end{cases} \qquad (9)$$

Here A_i is amplitude of irregular observation considerably exceeding the swing of initial observation series. The sequence of irregular observations forms Poisson flow of events with the parameter λ.

Building of model (7) at experimental data handling comes to identification of analytic representation of each item. It is convenient to use fuzzy methods in the basis of the representation of intelligence system knowledge base as methods of estimation of allowable variation. When formalization of uncertainties the degree of conformity to the regime of normal operation assigns in the form of corresponding fuzzy sets and membership functions (Averkin et al, 1986),(Terano et al,

1983),(Zadeh, 1976). For example, when controlling the frequency of irregular data the estimation of Poisson flow density is used in the form of average frequency of events $\lambda=n_0/T_0$, where n_0 is the number of peaks during observing time T_0 and $\sigma^2(\lambda)=\lambda$. The true value of density lies within the ambit of $\lambda\pm1{,}96\lambda^{1/2}$ for 95% confidence interval and within the ambit of $\lambda\pm3\lambda^{1/2}$ for 99,9% confidence interval. These statistical estimations allow to reasonably soundly formalize the representation of fuzzy set $A=\{(x,\mu_\lambda(x))\}$ with the membership function $\mu_\lambda(x)$ assigning the measure of concordance of new density to the density previously determined in the process of information gathering during the operation of intelligence system. If the necessary degree of conformity is assigned as $\alpha\in[0,1]$, then the ambit of allowable variations of irregular data density can be determined. Within the ambit an observed density corresponds to a regime of normal operation. The situation where the new estimation of the investigated parameter λ exceeds the bounds of $\lambda\pm3\lambda^{1/2}$ may be interpreted as a complete unconformity to the previous state which leads to rebuilding of model and to establishing the reasons of meddling in the normal regime.

The degree of concordance between spectral characteristics and new observations of initial data is defined using a fuzzy set $B=\{(s,\mu(s))\}$ and a membership function $\mu(S)$ of the mean-square deviation of a noise term of new observations and a regime of normal operation with fixed deviation. The small values of membership function define the situation when virtually all peaks around the average represent the stochastic process $\xi(t)$ in (7). In that case the description of a cyclic component of the model $\Im(t_i)$ needs the inclusion of a number of harmonics into the estimating model. Another variant consisting in the increased swing of data oscillation around the average level is related with the necessity of recurring determination of $\xi(t)$ (Fig. 2). The choice of a degree of concordance $\alpha\in[0,1]$ determines the ambit of allowable variations of the investigated parameter S using the equation $\mu(S)=\alpha$. When $S\le S_\alpha$ the spectral characteristic remains changeless (Anderson, 1971),(Domrachev et al, 2006).

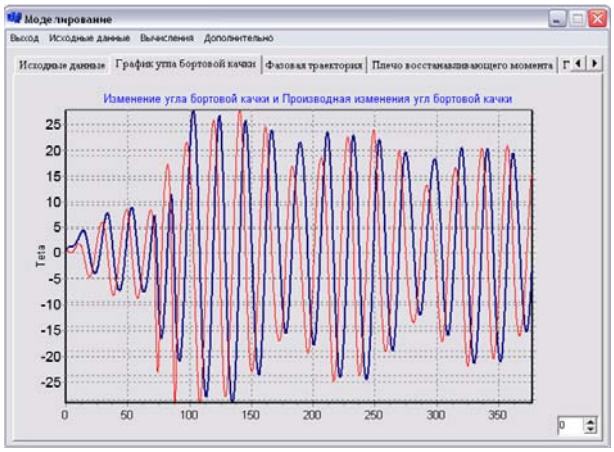

Fig.2. The origin of a considerable amplitude of oscillation as a result of an influence of the large single wave in the structure of random sea.

The reviewed situations of deviation from the regime of normal operation expect the presence of the required information to identification of the model parameters in new conditions. In the absence of new data about the components of forecasting model the work is carried out using an average value $\Re(t_i)^*$ and the mean-square deviation S in a short time after the warning about the inconsistency between the new data and the regime of normal operation. The registration data are considered as a sampling from the entire assembly with the average of distribution $\Re(t_i)^*$ and the dispersion S^2. Used estimations assume that the series of sequential observations is the entire assembly with the same parameter of dispersion S^2 but with new average of distribution. The average of distribution of new assembly is $(\Re(t_i)^* + b)$.

Two situations can be realized as a result of a sudden change with the value b. The first one characterizes by the presence of a sudden change and the situation that is not close to the limiting values ζ^*,θ^*,Ψ^*. In that case the conversion to the regime of current registration and data gathering is carried out in order to adjust the forecasting model. The second situation is close to the limiting values

ζ^*,θ^*,Ψ^* as a result of a sudden change. This situation is described below during the estimation of a danger level of system functioning. The analysis of probabilistic properties shows that the value |b| should exceed S in order to safely determine a sudden change with a confidence level of 0.99. This preliminary statistical estimation allows estimating the measure of concordance between the first situation and the "old" system state. The fuzzy set $C=\{(z,\mu_C(z))\}$ with the membership function $\mu_C(z)$ assigns the measure of unconformity between the new state z and the initial state z_0. The choice of an acceptable measure of unconformity $\alpha\in[0,1]$ allows determining the ambit of acceptable changes of the average level z from an equation $\mu_C(z)=\alpha$. Within the ambit the average value is supposed to be the same; there is no need to recalculate the forecasting model. The situation where the new estimation $z=z_0$ exceeds the bounds of $\Re(t_i)^*\pm 3S$ may be interpreted as a complete unconformity to the previous state which leads to rebuilding of model.

An expansion for the multidimensional case allows turning to the fuzzy estimation of concordance of the situation as a whole (Domrachev et al, 2006). The introduced fuzzy set $D=\{(x,s,z),\mu_D(x,s,z))\}, x>0,s>0,z>0$ is specified in the Cartesian product $X\times R\times Y$ with the membership function $\mu_D(x,s,z)$ of a point $(x,s,z)\in X\times R\times Y$. The resulting membership function is the composition of functions of individual fuzzy sets:

$$\mu_D(x,s,z)=\mu_\lambda(x)\wedge\mu(s)\wedge\mu_C(z)=$$
$$\min_{x,s,z}\{\mu_\lambda(x),\mu(s),\mu_C(z)\},\qquad(10)$$
$$\{x\in X, s\in R, z\in Y\}$$

The choice of measure of concordance $\alpha\in[0,1]$ allows controlling the preservation of normal regime of current data registration during the monitoring of alighting system using the equation (7). If $\mu_D(x,s,z)<\alpha$ then the return to the stage of learning with data analysis in corpore and of building of new forecasting model happens. Dangerous deviations from a stable system functioning are determined on the basis of field experience and analysis of influence on the quality of work of the system. Thus the monitoring is carried out by means of identification of mathematical model with the following control of normal regime parameters, lurking for moments of regime changing, correction and recalculation of the model and its parameters, monitoring the dangerous approach of the regimes to the conditions of loss of information.

SPECIALITY OF ROLLING REGIME

It is significant that the easiest way of solving the safety problems may be achieved during the design process through guaranteeing the rolling amplitudes not exceeding allowable values. At first glance, this approach seems tempting. Really, after achieving the conditions $\theta\le\theta^*,\Psi\le\Psi^*,\ldots,\zeta\le\zeta^*$ there is no need in building complex models and control system dynamics. But in practice, the situations with significant rolling amplitudes that cause disastrous effects may appear. One can't help but remember the tragedy with large container carrier (Nechaev, Dorogov, 2006), which was about 320 meters long. The phenomenon of parametric resonance under the influence of extreme wave packets was discovered as a result of this accident. This phenomenon became the topic of discussion at international conferences on safety for some years. Time curves and phase-plane portraits of oscillatory movement of the ship in an irregular head sea in parametric resonance regime under the influence of a large with a chop-like structure wave packet are shown in Fig. 3. As may be seen at the figure, the amplitude of parametric rolling in this situation increases fast and becomes stabilize around 30^o as a result of an influence of nonlinear effects.

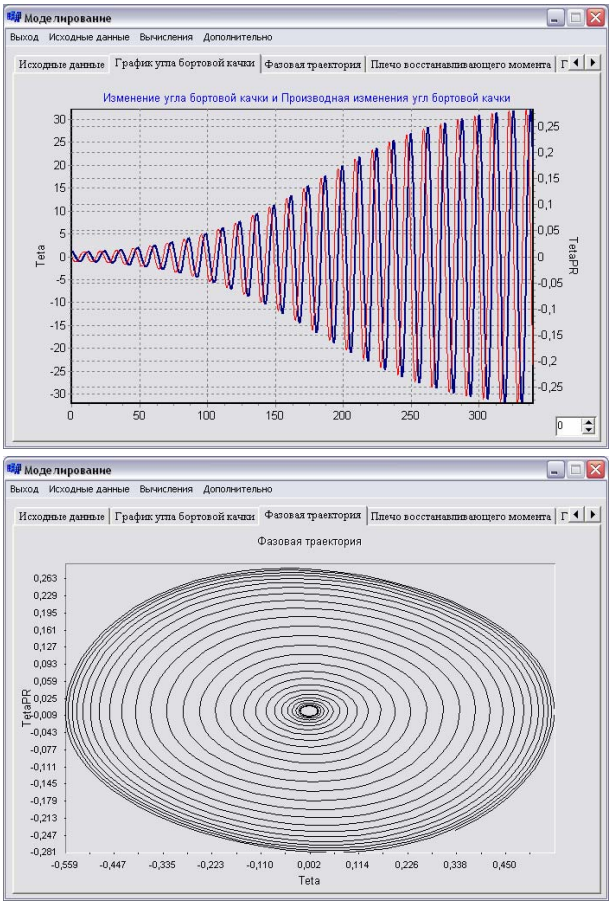

Fig.3. Time curves and phase-plane portrait of the parametric resonance regime during the rolling oscillation of dynamic object.

It is interesting to mention that pitching happens in a regime that is close to the principal resonance. Therefore pitching amplitude can achieve significant values as a result of intensive external disturbance. These values may exceed allowable angles of trim determined by the requirements of navigability. Modelling results of oscillatory movement in the pitching resonance regime are presented in Fig. 4.

The research results of ship oscillation features in the conditions of different structure of wave packets with the small amplitude of disturbance are represented in Fig. 5 (Nechaev, Petrov, 2006).

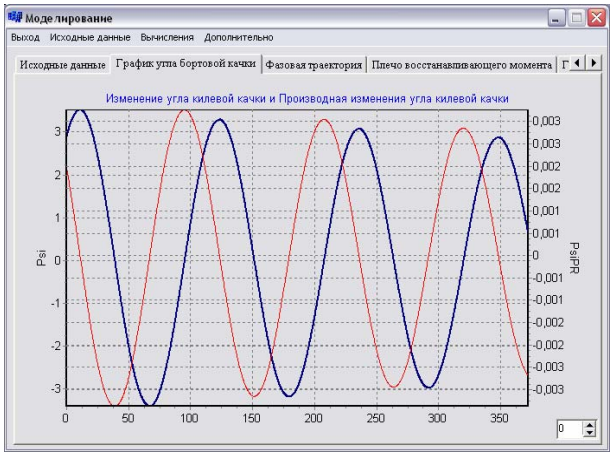

Fig.4. Time curves of the principal resonance regime ship during the pitching oscillation of ship.

Here the upper figures represent time curves of typical cases of oscillatory movement, the lower figures are the corresponding phase-plane portraits. Findings show the building of complex structures of rolling oscillatory regimes during the passing of wave packets. The feature of these structures consists in forming the attractor sets in the form of unstable limit cycles.

A

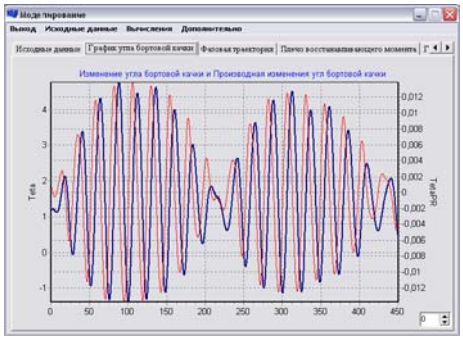

B

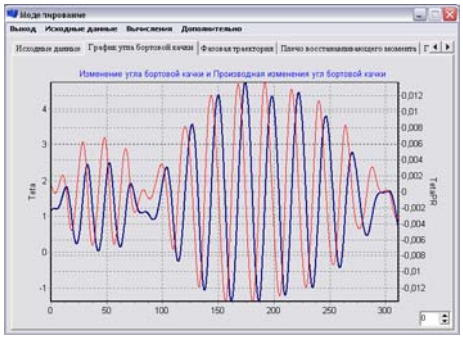

C

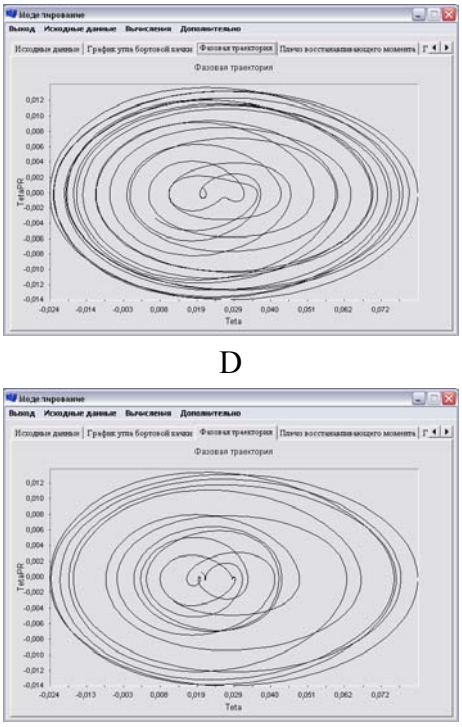

Fig.5. Forming the attractor sets under the influence of wave packets: A, C – time curves and phase-plane portraits under the influence of chop packets; B, D – time curves and phase-plane portraits of sequential influence of wave packets of various densities.

Buckling failure of cycle-attractor in the discussed one-parametric system happens by various scenarios. The interpretation of these scenarios is given in Fig. 6, 7. The easiest scenario is connected with the features of chop packet that forms the limit cycle characterized by amplitude stabilization as a result of nonlinear influence (Fig. 6A). This cycle appears in the area where the wave sequence in a packet exceeds the value $(h_w)_{CR}$ that forms the oscillatory regime with virtually constant amplitude θ_{max}. But the following height decreasing leads to breaking of stability conditions and the cycle disappears (Fig. 6B).

A more complex scenario is the collision with the unstable cycle (Fig. 7). In practice this situation happens much rarely and is characterized by the sequential wave packets consisting of waves with various densities. For instance the first packet with small height of resonance waves leads to forming the limit cycle of small amplitude, and the second one – of big amplitude. An initiation and a buckling failure of oscillatory regime ("the birth and the death of a cycle" by nomenclature of Andronov A.A. (1981)) are the result of the limitation of rolling resonance area in the relatively small range of intense oscillation during wave packets passing.

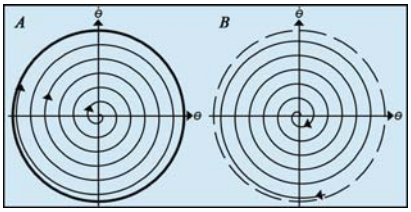

Fig.6. Forming (A is a birth and B is a death) of a limit cycle under the influence of wave sequence.

The indicated features of oscillatory movement should be taken into account during the control and forecast of ship behaviour in extreme situations connected with the execution of marine operations.

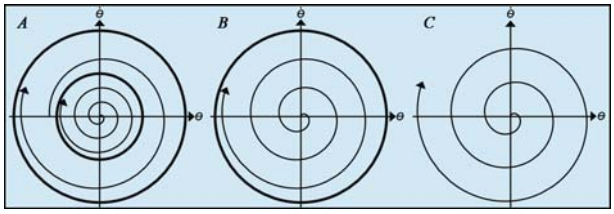

Fig.7. An initiation (A) and a buckling failure (B), (C) of the cycle.

It is interesting to mention that an evolution of parametric oscillations during the limit cycle forming appears more often in wave systems consisting of groups of almost regular waves. In that case initial conditions form by the large modulation depth of the parameter that plays a role of the multiplier of periodic function of the Mathieu equation (Hayashi, 1968). These conditions assure an overcoming of the "excitation threshold" of parametric resonance. As a result the initiation and evolution of parametric oscillations are registered even on the waves of relatively smaller steepness.

The comparison of the topology of phase space for nonlinear mathematical model and the topology of phase space for linearized mathematical model was made during the process of calculating experiment. Findings

show the practically impossibility of saving the phase streams which generate strange attractors and determinate chaos in the linearized systems.

CONCLUSION

The research allowed building the mathematical control model of the features of intelligence system functioning under the influence of various external disturbances determined by the scenarios of storm development. The modelling strategy is based on the notion of climatic spectrum of sea waves. An analysis of dynamics of a ship-environment interaction, danger levels of various disruptions in its behaviour and forming the corresponding criteria are carried out with the use of methods of uncertainty formalization on the basis of fuzzy logic.

Thus, a new paradigm of information processing in dynamic environment consists in the rational organisation of calculating technology. An inclusion of fuzzy models into the informational basis allowed widening the functional capabilities of calculating system and increasing the validity of taken decisions in extreme situations. The various scenarios of attractor sets initiation connected with the complex nonlinear interaction between the ship and an environment in the conditions of irregular waves were determined as a result of the analysis. The most typical scenario is forming the unstable limit cycle. The laws of phase path behaviour in the conditions of instability are assumed as a basis of the development of a dynamic knowledge base realizing the forecast and the interpretation of extreme situations in onboard real-time intelligence systems. The developed methods and algorithms of their realization can adapt to the varying external conditions and recognize the "templates" (cause-and-effect relations) of each process under control. This continuous self-instruction process allows the intelligence system to accumulate information on the interaction dynamics and to forecast the deviation of parameters from the regime (allowable) values.

REFERENCES

Anderson T.W. The statistical analysis of time series. – John Wiley and Sons, 1971.

Andronov A.A., Vitt S.,Chaikin S.E. Oscillation theory. Moscow. Science, 1981.

Averkin A.N, Batyrshin A.H., Blishun A.F.,Silov V.B., Tarasov V.B. Fuzzy models in the tasks control and artificial intelligence / Ed. D.A. Pospelov. Moscow. Science, 1986.

Domrachev V.G., Besrukavny D.S., Kalinina E.V., Retinskaya I.V., Skuratov A.K. Fuzzy models in the tasks of network traffic // Information technology. №3. 2006, p.p.2 – 10.

France W., Levadou M., Treakle T.W., Paulling J.R., Michel R.K., Moore K. An investigation of head-sea parametric rolling and its Influence on Container Lashing Systems // ANAME Annual Meeting 2001. Presentation, p.p.1 – 24.

Hayashi T. Nonlinear oscillations in physical systems. Moscow. Science, 1968.

Kendal M.,J.,Stevart A. Multimeasured statistical analysis and temporary rank. Moscow. Science, 1976.

Kosko B. Fuzzy systems as universal approximators // IEEE Transactions on Computers. – 1994. Vol.43. №11, p.p.1329-1333.

Lopatoukhin L.J., Rozhkov V.A., Ryabinin V.E., Swail V.R., Boukhanovsky A.V., Degtyarev A.B. Estimation of extreme wave heights. JCOMM Technical Report, WMO/TD. №1041, 2000.

Nechaev Yu.I. Principles of use measure tools in the onboard real times intelligence systems // Proceedings of national conference on artificial intelligence KII-96. Kasan. 1996. Vol.1, p.p.362-364.

Nechaev Yu.I. Neural network technology in the real time intelligence systems // Proceedings of 4-th national conference Neuroinformatics-2002. Moscow. 2002. Lecture on neuroinformatics. Part 1, p.p. 114-163.

Nechaev Yu.I., Petrov O.N. Forming of set attractor for research of dynamic of complex system in extreme situations // Proceedings of 4-th national conference "Control and information technology". St.-Petersburg. 2006, Vol.2, p.p.45-51.

Nechaev Yu.I., Dorogov A.Yu. Measurement technology and algorithms of the information transformation organization // Onboard intelligence systems. Part 2. Ships systems. Radiotechnic.2006, p.p. 13 – 22.

Terano T., Asai K, Sugeno M. Applied fuzzy systems. Moscow. Science, 1993.

Zadeh L. Linguistic variable conception and its application for decision fuzzy models, Moscow. Science, 1976.

Virtual Testbed for Marine Objects Behaviour Investigation

Alexander B. Degtyarev,

Applied Mathematics and Control Processes Faculty, St.Petersburg State University, Professor, St.Petersburg, Russia

Yury I. Nechaev,

Naval Architecture and Ocean Engineering Faculty, State Marine Technical University, Professor, St.Petersburg, Russia

ABSTRACT

Features of virtual testbed development for modelling of complex systems behaviour in various operation conditions are considered. Dynamic knowledge base of virtual testbed is developed on the basis of principles of information processing in multiprocessor computing environment with use fuzzy and neural network models, virtual reality and multiagent systems. Integration of various computer resources is carried out with the help of GRID technologies. Practical example of virtual testbed is shown.

KEYWORDS

Virtual testbed; mathematical modelling; GRID computing; problem solving environment.

INTRODUCTION

Design of complex technical objects and marine operations planning are result of complicated joint work of many various specialists. Traditional procedure of such work is long and requires carrying out of model or full scale experiments, calculations, variations, decision making. New information technology takes possibility to reduce terms of design, to develop virtual environment where specialists can carry out modelling, check many variants, to improve quality and complexity of result. Now it is possible to consider GRID technology as a tool that combine various resources and organizations in common recourse (in terms of GRID it names virtual organization) (see Foster, 2001). Such integration results in organization of problem solving environment.

Necessity of information technologies integration has arisen both in sphere of straight analysis of complex situations, and synthesis of models for situations simulation at decisions making. In problems of decision-making in safety navigation maintenance and aircrafts landings in sea conditions this integration is concretized both in development of complex systems modelling like «virtual testbed», and real time intelligent systems for monitoring and control of complex dynamic objects. At that «virtual testbed» concept in considered field is connected with development of new intellectual support tools. These tools are related with methods of decision-making in the worst-case and extreme situations.

VIRTUAL TESTBED CONCEPT

Modern transport objects (ship, airplane, helicopter, etc.) have reached such high level of

complexity and functionality, that mistakes made by operators can result in dangerous consequences. The operated object is more complex and the environment is more aggressive and unpredictable, the consequences of critical situations can be more serious. Therefore development of decision support systems with a view of monitoring and prevention of dangerous situations is urgent question now. Such systems have to be used in operators training to behaviour tactics in extreme situations.

The proposed concept defines organization of modelling control complex, as complicated multilevel intelligent system consisting of the following core components:

- hierarchies of imitating models specifying considered problem areas;
- hierarchies of analytical models giving simplified description of various parties of modelled phenomena;
- information system including DB and KB based on methods and models of AI;
- control systems and interfaces providing interaction of all system component and interactive work with operator.

"Virtual testbed" development represents complex multistage iterative process. The basic feature of this process consists in necessity to carry out coordination (at conceptual, algorithmic, information and program levels) of heterogeneous models describing various parties of functioning of investigated objects. Choice of admissible alternatives is based on compression of considered variants set by alternatives analysis in complex, especially in non-standard (supernumerary and extreme) situations. Concept of such analysis assumes that estimations of expenses for realization of obtained decisions (expenses for the charge of used resource) do not decrease and become more and more exact in process of admissible alternatives set narrowing. Thus it is considered that control processes by structural dynamics of system have multilevel, multistage and multifunctional character.

Functioning of system is carried out on the basis of a special firmware in accordance with the structure presented on Fig.1. (Bogdanov, et al, 2004, 2005)

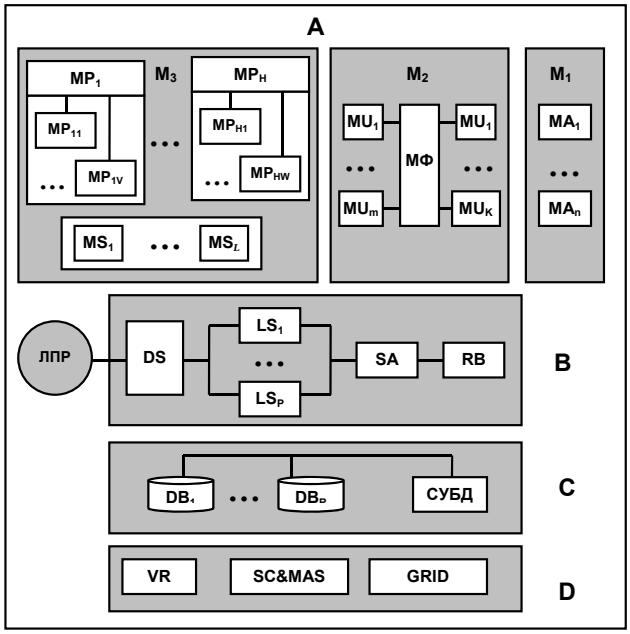

Fig. 1: Structure of virtual testbed: A is a block of models; B is a block of control and interpretation; C is a block of dataware; D is a block of information technologies; M_1 is a block of models for estimation of dynamic object (DO), navigation and operation situation; MA_i (i=1,…,n) are models for analysis of DO and environment behaviour; M_2 is a control models block; MΦ are models of central control and on-board systems functioning; MU_j (j=1,…,m) are control complex elements interaction; MU_k (k=1,…,K) are models of DO systems interaction; M_3 is a planning block; MP_h (h=1,…,H) is a block for long-term and operative planning by elements of virtual testbed; MP_{11} … MP_{1V} are long-term planning models; MP_{H1} … MP_{HW} are operative planning models; MS_l (l=1,…,L) are control models for component structures of virtual testbed; DS is dialog system for virtual testbed control; LS_p (p=1,…,P) are local control systems; SA is a block of scenarios and adaptation; RB is a block of practical recommendations; DB_r (r=1,…,R) are data bases about virtual testbed state, DO and environment; VR are virtual reality technologies; SC&MAC are soft computing and multiagent technologies; GRID is a technology for virtual testbed

COMPLEX MODELLING ENVIRONMENT

Complex modelling environment of a high degree of adaptability is based on use of multiagent systems (Gorodetsky, 1996), "soft

calculations" concept (Zadeh, 1994, Bogdanov et al., 2001) and real time systems (Degtyarev, 2003, On-board, 2006). It allows to involve in such environment additional resources. They could be both new computers, and various modelling environment elements (dynamic objects, information systems, sources of measuring information, etc.). Offered «virtual testbed» essentially differs from existing information systems and simulators and provides the complex problem decision.

Increase of complexity in situations estimation and forecast reliability at virtual testbed functioning is achieved with use of new approach to information processing based on development of "soft computing" concept. This approach is based on two theoretical principles allowing providing the rational organization of computing technology of parallel information processing in the problem of analysis and forecast of extreme situation development. Also it exploits the possibility to formalize information stream at realization of fuzzy inference models in multiprocessor computing environment (Nechaev, 2002).

Competition principle provides comparative analysis of results of situation estimation with the help of traditional algorithms and neural network models. Relevant procedures of parallel information processing reflect the process of virtual testbed functioning from the moment of the information inflow from measuring system up to procedure of inference and practical recommendations generation.

Principle of fuzzy information formalization in multiprocessor computing environment allows carrying out of parallel chains of fuzzy conclusions in continuously changing conditions of dynamics of object and environment. It uses also the possibilities to make programs for complex models of representation and processing of knowledge fuzzy system; to provide functioning of complex in real time; to cut down expenses on hardware development and to remove problems of parallelization of computing processes with essential irregularity characteristic for the integrated complexes

Realization of the above theoretical principles enables to increase efficiency of functioning of virtual testbed under continuously changing external conditions and dynamics of modelled objects and systems. The practical importance of information streams processing in real time is caused by aspiration to increase the speed of machine calculations by the way of computing algorithms parallelization and their realization on supercomputer platforms. Check of a correctness of control algorithms and decision-making is carried out by the formal way on the basis of the general requirements to algorithmic maintenance of the system. With reference to parallel algorithms of logic control the concept of correctness is connected with the specific properties of such algorithms as consistency, stability and a self-coordination.

Various approaches are used at the synthesis of algorithms for analysis and forecast of dynamic situations in virtual testbed. Among them the deterministic and stochastic approaches and the approach on the basis of principle of nonlinear self-organizing are most interesting. First two approaches assume presence of full information basis in initial data, i.e. all defining parameters and factors which are necessary for considering of the situation analysis and decision-making. The major principle of virtual testbed management is the principle of fast and proved reaction on a change of environmental situations. Thus, realization of the above principles of information processing at the analysis and synthesis of methods and models of virtual testbed functioning demands great volume of computing operations. These operations are connected with estimation and forecast of objects dynamics at various control strategies on the basis of mathematical modelling of situations with the subsequent formulation corresponding criteria estimations, alternatives analysis and decision-making.

GRID technologies play a very important role in "virtual testbed" concept realisation. They determine infrastructure development providing global integration of information and computation resources. Complicated modelling on remote supercomputers, joint visualisation of very large scientific data sets, distributed

processing for data analysis, linking of scientific tools with remote computers and archives are among GRID technologies.

Functioning as the virtual dynamic environment, GRID ensures end users functioning and applications performance as uniform computer system uniting not only separate systems, but organizations, various computer architectures and software also. Thus unlimited power, opportunity of teamwork and information access is offered to all users of GRID-network. Strategy of GRID-technologies at virtual testbed development allows to provide the following advantages:

- increase of efficiency of computing resources using of each organization and all other organizations providing functioning of the system;
- foundation of virtual organization (testbed) that work at joint problems allowing to use applications and data and providing reduction of aggregate computation value by the way of separate using and control of computer resources;
- possibility to work at big problems requiring huge computer power and permitting to joint computations, storages and other resources.

CHARACTERISTICS OF "VIRTUAL TESTBED" FUNCTIONING

Complex environment "virtual testbed" is complex informational object combining characteristics of corporate system and instrumental tool for high performance modelling. Reasoning from these base principles complex environment is assigned for decision of the following problems in real time:

- collecting and analysis of information about current DO and environment condition, remote monitoring of objects condition;
- estimation and coordination of joint functioning of DO and aircraft proceeding from current conditions;
- centralized decision-making support in DO control systems in complex, especially in non-standard (supernumerary and extreme) situations;
- computer modelling of possible scenarios of situations development with the purpose of optimum strategy choice;
- centralized control of completely automated (pilotless) technical means;
- data assimilation in dynamic databases.

Complex environment is distributed system uniting base information resources (server) and on-board systems of separate objects (client). Principle scheme of such environment organization is shown on Fig.2.

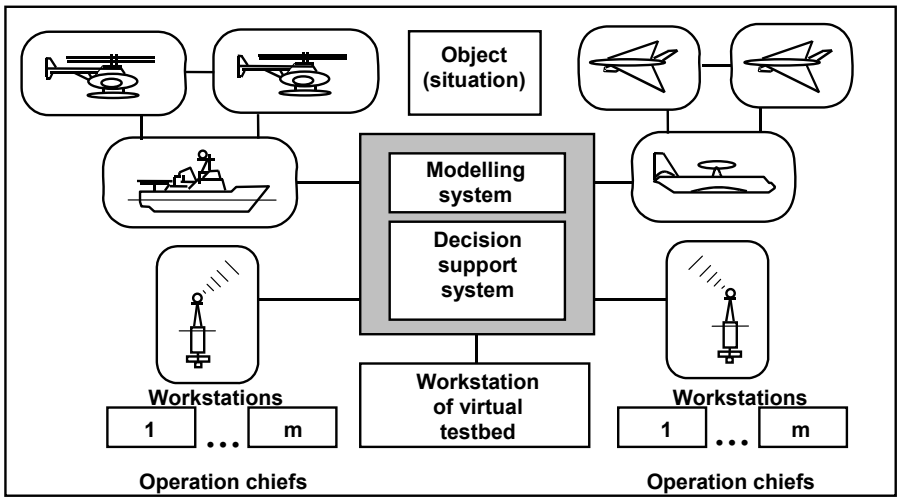

Fig.2. Principle scheme of complex environment organization

Here information streams (links) are considered as virtual (obtaining from modelling process) or real information sources about environment and control object state. In first case realization is full-scale simulator ("virtual testbed"), in second case it is complex system for monitoring and control of complicated technical objects and systems.

Server part of the complex environment is realized on multiprocessing computers. It allows to carry out basic operations on information reception and analysis from various sources, computer models of environment and DO, forecasting, scenarios generation and competing inference (Nechaev, 2002). Interaction with server part of the system is carried out by means of some workplaces. They include workstations of operators who are responsible for uninterrupted functioning of separate blocks during operation, and experts who are increase reliability of accepted decisions in especially important situations. Workstations with elements of virtual reality and cognitive graphics (Zenkin, 1991, Nechaev et al, 2002) are provided also. On these workstations all information obtained in environment is condensed. It is necessary for ground of decision-making by persons who control operation.

Strategy of general problem decision of virtual testbed functioning and set of corresponding procedures is based on the concept multiagent systems (MAS) (Gorodetsky, 1996)). It allows to carry out cooperation of users (operators of system) at collective performance of complex technical decisions. A set (community) of intellectual agents (IA) and their functions are defined in conformity with specially constructed decision trees – a tree of the purposes and a tree of estimation criteria. With the help of such trees which tops are corresponding macro procedures, algorithm of problem decision is mapped. Each such procedure is realized by special IA. As a result efficiency of complex functioning, validity of accepted decisions are increased.

Architecture of IA of considered distributed system can be developed within the frameworks of the general complex structure presented on Fig.3. Its realization as a part of the lower level is carried out in the form of classical MAS multilevel model. The top level of MAS represents a meta-level to which coordination of agents' activity of all system is assigned. This level realizes global strategy of complex problem decision in a view of general factors influencing on the result. Multilevel representation of IA knowledge simplifies their mapping to memory, repeated use and updating. Such levels are the following:

- level of subject domains knowledge and about initial conditions of problem decision where necessary knowledge of subject domain are reflected;
- level of cooperation rules knowledge and agents' interaction at the collective decision of a challenge;
- level of operating knowledge (here knowledge about procedures sequence decision control are contained);
- level of new knowledge generation, where rules of inference of new knowledge obtaining are presented.

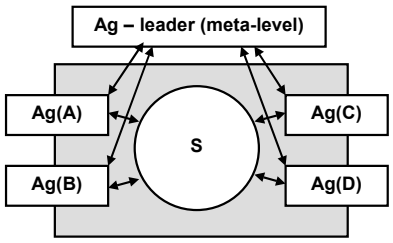

Fig.3 Typical scheme of MAS

The basic idea of agent functioning consists in the following. The agent "observes" environment and builds its model. Further the agent, using given strategy, transforms initial model to the model displaying modified environment. Comparing these two models the agent builds function which determines the purpose of its functioning. If the obtained estimation satisfies the agent, it realizes strategy which is presented by corresponding operation.

MAS focused on the decision of virtual testbed problem functioning is shown on Fig.3. Here S is environment of functioning, where agent Ag-leader determines meta-level of the system, and agents A – D are intended for decision of specific targets. Each of agents A – D depending on complexity of solved problem can contain a set of lower level agents.

SCENARIOS CONSTRUCTION AND ESTIMATION OF DECISIONS EFFICIENCY

The model «entity – association» is used in development of "virtual testbed" knowledge base (Maynika, 1981, On-board, 2006). Analysis of basic information objects allows to assign the following sets: S is scenarios set (contains scenario description and corresponding corrections in model's parameters); W is set of variants (concrete conditions described by information model); R is set of inferences (description of calculation results of concrete scenario for each variant); C is set of associations (they are entered for aggregation into semantic network of tuple {S, W, R}; these sets contain only references to copies of sets S, W, R).

In process of knowledge base filling by R-objects the semantic network is under construction. Frames realizing copies of sets S, W, R, C are located in network nodes. Frame of each type corresponds to one of sets S, W, R, C and includes set of this type frame copies: $S = \{S_i \mid i=0, \ldots, m\}$; $W = \{W_j \mid j =0, \ldots, n\}$; $R = \{R_i \mid i =0, \ldots, m\}$; $C = \{C_r \mid r =0, \ldots, k\}$.

Decision-making is carried out in conditions of uncertainty and time deficiency. Thus there is risk of wrong operator's actions. In this situation fuzzy models are used for intellectual operator support. Specificity of such models consists in use of fuzzy estimations $\mu(H)\in[0,1]$ and graph-interpretations allowing to relate formation of operator actions to combinatory problems on graphs. The area of admissible decisions in this case is determined by α-level of graph fuzziness which corresponds to fuzzy estimation $\mu(H)$. Giving by value $\mu(H)$, it is possible to determine constraint region, and then to search optimum decisions on graphs in this region (Maynika, 1981).

Mathematical model of decision-making in conditions of indeterminacy represents the ordered set $<X, Y, F(x,y)>$, where alternative $x\in X\subset R^n$ provides problem decision in conditions of indeterminacy $y\in Y\subset R^m$ in assumption that set of alternatives X, uncertainty set Y and criterion F(x,y) on direct product $X\times Y$ are known. Risk function $\Phi(x,y)$ is constructed using these data. Two-criterial problem of alternative $x\in X$ choice is considered in conditions of indeterminacy $<X, Y, \{F(x,y), \Phi(x,y)\}>$. Thus probably greater outcome F(x,y) is provided at smaller risk $\Phi(x,y)$ (Bogdanov et al, 2001, 2004, 2005).

Increase of estimation adequacy and situation forecast is reached with the help of dynamic measurements data and competing computing technologies. Analysis and forecast of events chains determined by various scenarios of extreme situations development are carried out on the basis of f mathematical modelling methods and neural network technologies. Scenarios formulation is carried out on the basis of forecast data by results of dynamic measurements of DO and environment parameters. Mathematical models and their factors are specified by results of measurements onboard of DO.

EXAMPLE OF "VIRTUAL TESTBED" FUNCTIONING

Concrete definition of theoretical principles incorporated in "virtual testbed" concept is considered on example of realization of unsinkability algorithms (grounding, shipwreck, ship collision, etc.). The sequence of operations which are carried out by "virtual testbed" at the decision of these problems is the following (Bogdanov et al., 2004, 2005, Boukhanovsky et al., 2001):

- modelling of wind, waves and ship motion; analysis of external excitation

characteristics and dynamics of "ship – environment" interaction;

- parameters determination for mathematical models correction (estimation of situation danger, forecast of its development);
- situation control and practical recommendations formulation during maintenance of buoyancy and stability of damaged ship.

This problem is solved on the basis of IS «Unsinkability». This module allows to realize continuous control of dynamics of damaged ship in various environment conditions. Software functioning is carried out in view of continuous change of damaged ship and environment dynamics on the basis of algorithms with a high degree of parallelism. It takes possibility to provide decision making for unsinkability maintain. Developed methodology allows to realize problem of control and forecast of emergency situation development in real time (Fig.4).

As a result of identification operation performance flooded compartment (group of compartments) pops up on the scheme (Fig.5). General dynamic characteristics defining current values of equilibrium angular of heal θ_0 and trim ψ_0, average draft ζ, and also metacentric height h and critical time interval τ_{CR} (limit time in extreme situation) are displayed in real time on the right side of the screen (Nechaev, 2002, Degtyarev, 2003). At achievement of any of these limiting characteristics (critical values) corresponding value is highlighted on red background on the screen.

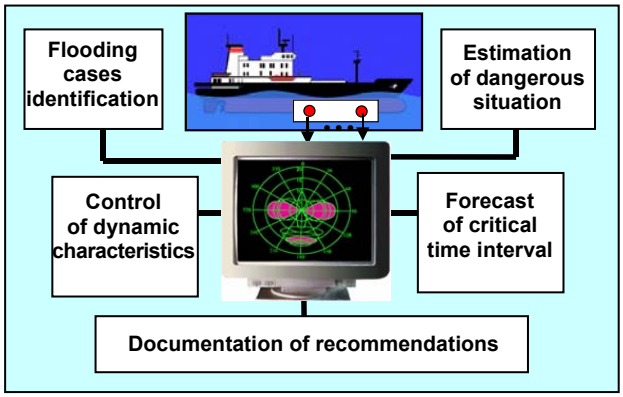

Fig.4. Information flow in IS "Unsinkability"

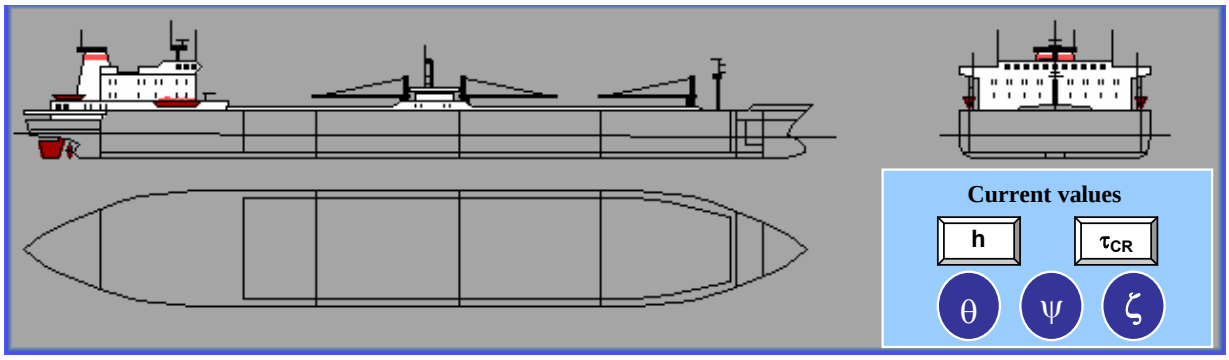

Fig.5 Scheme of ship's compartments (inboard profile)

Practical recommendations on survivability preservation of emergency vessel stand out at a special window together with the instruction of flooding character. Regarding «Estimation of situation danger» result of the first stage of inference functioning is displayed. Regarding «Situation identification. Practical recommendations» result of the second stage of inference functioning is displayed, namely prospective cause of current situation (accident) is set, and practical recommendations are offered. In case of good situation it is specified, that the considered situation does not represent danger and recommendations are reduced to maintenance of the accepted strategy of vessel control.

CONCLUSIONS

Current research permits to draw the following conclusions:

1. The concept of virtual testbed as complex high-level intellectual system is developed. This is high-availability system for complicated objects dynamic control in marine conditions.
2. Principles of dynamic knowledge base development are formulated. Fuzzy method for indeterminateness formalization, neural network and multi agent technologies, and virtual reality tools are used.
3. Organization of high performance calculations at analysis and forecast of dynamic situations development in the multiprocessor computing environment is proposed on the basis of GRID-technologies

Proposed intelligent technology will promote for increasing of taken decisions level and for development of high performance tools for information processing.

REFERENCES

Bogdanov A., Degtyarev A., Nechaev Yu. Fuzzy Logic Basis in High Performance Decision Support Systems. //in book "Computational Science - ICCS 2001", LNCS 2074, Springer, part II, pp.965-975.

Bogdanov A.V., Degtyarev A,B., Nechaev Yu.I. Problems of virtual testbed development for complicated dynamic objects modelling. //Proceedings of International conference “Supercomputer systems and its applications”, Minsk, 2004, pp.31-37 (in Russian)

Bogdanov A.V., Degtyarev A,B., Nechaev Yu.I. Parallel algorithms for virtual testbed // Proceedings of International conference CSIT-2005.Yerevan. Armenia.2005, pp.393-403.

Boukhanovsky A.V., Degtyarev A.B., Rozhkov V.A. Peculiarities of computer simulation and statistical representation of time–spatial metocean fields. LNCS 2073, Springer–Verlag, (2001), pp.463–472

Degtyarev A.B. Use of high performance computer technologies at the organization of onboard computing system // Proc. of the International conference STAB'2003, Madrid, 2003, pp.485-494

Foster, I., Kesselman, C. and Tuecke, S. The Anatomy of the Grid: Enabling Scalable Virtual Organizations. //International Journal of High Performance Computing Applications, 15 (3). 200-222. 2001.

Gorodetsky V.I. Multiagent systems: modern research condition and perspectives of application // News of artificial intelligence. 1996. №1,c.44-59. (in Russian)

Maynika E. Algorithms of optimization on network and graphs.– Moskow, Mir,1981. (in Russian)

Nechaev Yu.I. Mathematical modeling in on-board real-time intelligence systems // Proceedings of conference «Neuroinformatic-2002». Moscow.: MIFI. 2002. Lecture on neuroinformatic. Part 2, pp.119-179. (in Russian)

Nechaev Yu.I., Degtyarev A.B., Boukhanovsky A.V. Cognitive computer graphics in information interpolation in real time intelligence systems //in book "Computational Science-ICCS 2002", LNCS 2329, Springer, part I, 2002, pp.683-692

On-board intelligence systems. Part 2. Ship systems. – Moskow. Radiotechnik, 2006. (in Russian)

Winston P.N. Artificial intelligence. – Addison Wesley Publishing Company. USA.1993.

Zadeh L. Fuzzy logic, neural networks and soft computing // Commutation on the ASM-1994. Vol.37. №3, p.p.77-84.

Zenkin A.A. Cognitive computer graphic. – Moskow: Science, 1991 (in Russian)